WASHINGTON UNIVERSITY

Department of Mechanical, Aerospace, and Structural Engineering
School of Engineering and Applied Science

Dissertation Examination Committee:
Michael Swartwout, Chair
Ramesh Agarwal
Richard Axelbaum
Da-ren Chen
Raimo Hakkinen
Mark Jakiela
David Peters
Charles Svoboda

THE VORTEX FLAP

By

Brandon T. Buerge

A dissertation presented to the
Graduate School of Arts and Sciences
of Washington University in
Partial fulfillment of the
Requirements for the degree
of Doctor of Philosophy

August 2008

Saint Louis, Missouri

INFORMATION TO USERS

The quality of this reproduction is dependent upon the quality of the copy submitted. Broken or indistinct print, colored or poor quality illustrations and photographs, print bleed-through, substandard margins, and improper alignment can adversely affect reproduction.

In the unlikely event that the author did not send a complete manuscript and there are missing pages, these will be noted. Also, if unauthorized copyright material had to be removed, a note will indicate the deletion.

ProQuest LLC
789 E. Eisenhower Parkway
PO Box 1346
Ann Arbor, MI 48106-1346

Acknowledgments

Dr. Hakkinen helped me understand vorticity, boundary layers, and why planes *really* fly.

Gabriel Wade served as an excellent research assistant, helping with construction, experiment, and data processing.

Dr. Swartwout contributed advocacy, editing effort, penetrating insight, consistent guidance, and reliably witty banter.

Alden Buerge, Grandpa Blair, and Great-Grandpa Burke all contributed genetic material which bore a historically-verified disposition toward a love of airplanes.

Aaron and Justin Buerge worked hard to make, in part, the funding for this dissertation possible.

My wife endured an endless series of dissertation-related crises, and contributed emotional support as well as editing effort.

Table of Contents

Acknowledgments ..... **ii**

Table of Contents ..... **iii**

List of Figures ..... **vi**

Abstract of the Dissertation ..... **xvii**

1 Introduction **1**

1.1 Definition of the Peer Group 2

1.2 Basis for Evaluation 4

1.3 Contributions 5

1.4 Related Work 6

1.5 Dissertation Outline 9

2 Background **11**

2.1 Aerodynamic Considerations 16

2.1.1 Slot Effects 18

2.1.2 Vortex Shedding 21

2.2 The Peer Group of Trailing-Edge High-Lift Devices 28

3 Experimental Investigation **32**

3.1 Experimental Setup and Method 33

3.1.1 Wind tunnel 33

3.1.2 Force Balance 35

3.1.3 Model Construction and Operation 40

3.1.4 Wind Tunnel Doors 49

3.1.5 Data Acquisition System 52

3.1.6 Calibration 54

3.1.7 Testing Method 56
3.1.8 Kinematic Restrictions 57
3.2 Data Processing 58

4 Results 60
4.1 Dimensional analysis 60
4.2 Corrections to data 64
4.3 Results 75
4.3.1 Clark Y Airfoil Results 76
4.3.2 Rotating Cylinder Results 78
4.3.3 Vortex Flap results 84
4.4 Summary of experimental results 93
4.5 Application of Response Surface Methods: The Polynomial Curve Net 95
4.5.1 RSM Surface Plots 99
4.5.2 RSM Curve Plots 103
4.6 Potential Flow Analysis of the Vortex Flap 106
4.7 Pitching Moment of the Vortex Flap 117
4.8 Power Required to Drive the Vortex Flap 119

5 Discussion 124
5.1 Scale Effects 124
5.1.1 Fundamental Considerations 125
5.1.2 Scale Effect Corrections Applied to Results 131
5.1.3 Geometric and Configuration Effects 134
5.2 Comparison with Other Trailing-Edge High-Lift Devices 136
5.3 Discussion of Physical Phenomena of the Vortex Flap 142
5.4 Mission Analysis: Ship-borne Observation VTUAV 145

5.4.1 Modification of the Helio Courier 148
5.4.2 Analysis of Original and Modified Helio Courier for Mission 152
6 Conclusion 155
6.1 Review of Contributions 155
6.2 Significance of Findings 157
6.3 Future Work 158
Appendix A- Wind Tunnel Data Summary 169
Appendix B- Response Surface Method Results 198
Appendix C- Wind Tunnel Data Corrections 267
Appendix D- Efficiency of Circulation Generation 274
References 275

List of Figures

Figure 1-1. The configuration of the Vortex Flap 1
Figure 1-2. Estimated performance comparison for Vortex Flap and other high-lift devices. Adapted from Loftin (1985), Raymer (1999), Filiponne (2006), and Modi and Mokhtarian (1990). c' indicates flap chord; c indicates base airfoil chord. 4
Figure 2-1. Schematic of the trailing-edge high-lift devices in the peer group. Drawing by Brandon and Elizabeth Buerge. 30
Figure 3-1. An exterior and interior view of the wind tunnel test section used 34
Figure 3-2. Pitot-static tube installation in wind tunnel test section 35
Figure 3-3. Front view of force balance, base on bottom in white. Note foam that separates base from the plate. The bridge is in dark gray. 37
Figure 3-4. Picture of flexures used in force balance. Flexures in white, force transducers in silver and chrome. Bridge in gray, base and plate in white. 38
Figure 3-5. The force balance 'bridge.' The vertical masts bolt to the vertical face on each end of the bridge 39
Figure 3-6. Picture of the Clark Y airfoil model 41
Figure 3-7. Picture of the airfoil mounting clamps which permit the angle of attack adjustment 42
Figure 3-8. Picture from inside test section showing airfoil mounting 42
Figure 3-9. Two-bar arms and 'hands' used for airfoil mount support and movement 44
Figure 3-10. Single-belt transmission as seen from inside the test section 46
Figure 3-11. Pictures of 2" cylinder installed in the wind tunnel test section with a 3" fairing 47
Figure 3-12. Optical tachometer sensor and axle with reflective tape 49
Figure 3-13. Plexiglass wind tunnel door shown with wing directly behind cylinder. 51
Figure 3-14. View from inside the test section showing the typical cylinder clearance against the doors. 51

Figure 3-15. Force data acquisition schematic and photograph 53
Figure 3-16. Deadweight typical of those used to prevent transducer saturation 55
Figure 3-17. Testing method hierarchy 56
Figure 4-1. Thickness and body shape factor for each model 65
Figure 4-2. Volume of various tested model configurations 67
Figure 4-3. Solid blockage correction for various tested model configurations. 68
Figure 4-4. Velocity increment due to wake blockage for each model 70
Figure 4-5. Comparison of two methods for calculating the wake blockage correction. 72
Figure 4-6. Lift coefficient and angle of attack increment for models 73
Figure 4-7. Summary of wind tunnel correction parameters. 74
Figure 4-8. Clark Y wind tunnel results summary. 76
Figure 4-9. Cylinder only lift coefficient, drag coefficient, and L/D vs. SSR. 78
Figure 4-10. Comparison of data to that from NACA TN 209 79
Figure 4-11. Differences in performance compared to that of NACA TN 209. 81
Figure 4-12. Comparison of Reynolds number ranges with data from NACA TN 209. 83
Figure 4-13. Table of Vortex Flap position information. 85
Figure 4-14. Graphical depiction of Vortex Flap geometries tested. 86
4-15. Summary of data showing the influence of SSR on lift, drag, total lift increment, and L/D. 90
4-16. Summary of data showing effect of cylinder position on Vortex Flap performance. 91
4-17. Summary of data showing the influence of Reynolds number on lift, drag, and lift increment. 92
4-18. Summary of lift performance of the Vortex Flap 94
Figure 4-19. "Positions" as used in RSM plots. 97
Figure 4-20. RSM "Positions" compared to actual positions tested. 97
Figure 4-21. Lift surface plot for $\alpha = 0°$. 100

Figure 4-22. Drag surface plot for α = 0°. 100
Figure 4-23. Lift increment surface plot for α = 0°. 101
Figure 4-24. Lift surface plot for α = 5°. 101
Figure 4-25. Drag surface plot for α = 5°. 102
Figure 4-26. Lift surface plot for α = 5°. 102
Figure 4-27. Lift vs. SSR curve plot at each α for "Position 2." 103
Figure 4-28. Lift vs. α curve plot for each SSR at "Position 2." 104
Figure 4-29. Lift vs. SSR curves for each "Position" at α = 10°. 104
Figure 4-30. Lift vs. α curve plots for each "Position" at SSR=3. 105
Figure 4-31. Drawing of Bickley's model for a cylinder shedding vorticies in potential flow. Drawing by Brandon Buerge. 107
Figure 4-32. Drawing of Bickley's model of a rotating cylinder and the starting vortex in potential flow. Drawing by Brandon Buerge. 109
Figure 4-33. Drawing of the potential flow model and conformal mapping used for the rotating airfoil flap by Crabtree. Drawing by Brandon Buerge..... 111
Figure 4-34. Comparison of RSM and Potential Flow analysis results. 116
Figure 4-35. Position of flap axis of rotation relative to trailing edge. 118
Figure 5-1. Scale Effects on a Clark Y airfoil taken from NACA TR 502. 127
Figure 5-2. Normal, Super-critical, and Sub-critical Flow Over a Wing 129
Figure 5-3. Summary of application of scale effect adjustments to Vortex Flap data. 134
Figure 5-4. Summary of base airfoil data (see references below). 137
Figure 5-5. Summary of performance of passive trailing-edge high-lift devices (see references below)..... 137
Figure 5-6. Summary of power-assisted flaps and some high-lift systems (peer group in bold)..... 138
Figure 5-7. Summary of estimated performance of the Vortex Flap and other high-lift devices and systems..... 139
Figure 5-8. "Bonus" lift of the Vortex Flap. 142

Figure 5-9. Performance and Specifications of the U-10B Aircraft 149
Figure 5-10. Performance and Specifications of the new aircraft 151
Figure 5-11. Mission Analysis for U-10B and the modified Helio. 152
Figure 5-12. Payload vs. loiter time for modified Helio aircraft. 153
Figure 5-13. Relationship between gross takeoff weight and wind-over-deck required for VTOL. 154
Figure 6-1. Rotating cylinder with fairing. 161
Figure 6-2. Concept sketches of "scuppers" (top) and "gulleys." (bottom). 162
Figure 6-3. Picture of recirculating tufts on Clark Y during over-the-wing testing... 164
Figure 6-4. Vortex slat configurations. 165
Figure 6-5. Drawing of wing and nacelle of "poor man's tilt-rotor" showing force vectors. 167
Figure 6-6. Concept sketch of single-engine aircraft configuration for Vortex Flap. Bottom view (left) and side view (right). 168
Figure 6-7. Clark Y airfoil-only data in tabular form. 170
Figure 6-8. Cylinder-only data in tabular form. 172
Figure 6-9. Vortex Flap data in tabular form. 175
Figure 6-10. Data showing the influence of α on the lift of the Vortex Flap. 176
Figure 6-11. Data showing the influence of α on the lift of the Vortex Flap. 176
Figure 6-12. Data showing the influence of α on the lift of the Vortex Flap. 177
Figure 6-13. Data showing the influence of α on the drag of the Vortex Flap. 177
Figure 6-14. Data showing the influence of α on the drag of the Vortex Flap. 178
Figure 6-15. Data showing the influence of α on the drag of the Vortex Flap. 178
Figure 6-16. Data showing the influence of α on the L/D of the Vortex Flap. 179
Figure 6-17. Data showing the influence of α on the L/D of the Vortex Flap. 179
Figure 6-18. Data showing the influence of α on the L/D of the Vortex Flap. 180
Figure 6-19. Data showing the influence of α on the total lift increment of the Vortex Flap. 180

Figure 6-20. Data showing the influence of α on the total lift increment of the Vortex Flap. 181
Figure 6-21. Data showing the influence of α on the total lift increment of the Vortex Flap. 181
Figure 6-22. Data showing the influence of α on the rotational lift increment of the Vortex Flap. 182
Figure 6-23. Data showing the influence of α on the rotational lift increment of the Vortex Flap. 182
Figure 6-24. Data showing the influence of α on the rotational lift increment of the Vortex Flap. 183
Figure 6-25. Data showing effect of cylinder position on the lift of the Vortex Flap. 184
Figure 6-26. Data showing effect of cylinder position on the lift of the Vortex Flap. 185
Figure 6-27. Data showing effect of cylinder position on the lift of the Vortex Flap. 185
Figure 6-28. Data showing effect of cylinder position on the drag of the Vortex Flap. 186
Figure 6-29. Data showing effect of cylinder position on the drag of the Vortex Flap. 186
Figure 6-30. Data showing effect of cylinder position on the drag of the Vortex Flap. 187
Figure 6-31. Data showing effect of cylinder position on the L/D of the Vortex Flap. 187
Figure 6-32. Data showing effect of cylinder position on the L/D of the Vortex Flap. 188
Figure 6-33. Data showing effect of cylinder position on the L/D of the Vortex Flap. 188

Figure 6-34. Data showing effect of cylinder position on the total lift increment of the Vortex Flap. 189
Figure 6-35. Data showing effect of cylinder position on the total lift increment of the Vortex Flap. 189
Figure 6-36. Data showing effect of cylinder position on the total lift increment of the Vortex Flap. 190
Figure 6-37. Data showing the influence of Reynolds number on the lift of the vortex flap. 191
Figure 6-38. Data showing the influence of Reynolds number on the drag of the vortex flap. 192
Figure 6-39. Data showing the influence of Reynolds number on the L/D of the vortex flap. 192
Figure 6-40. Data showing the influence of Reynolds number on the total lift increment of the vortex flap. 193
Figure 6-41. Data showing the influence of Reynolds number on the lift of the vortex flap. 193
Figure 6-42. Data showing the influence of Reynolds number on the drag of the vortex flap. 194
Figure 6-43. Data showing the influence of Reynolds number on the L/D of the vortex flap. 194
Figure 6-44. Data showing the influence of Reynolds number on the total lift increment of the vortex flap. 195
Figure 6-45. Data showing the influence of Reynolds number on the lift of the vortex flap. 195
Figure 6-46. Data showing the influence of Reynolds number on the drag of the vortex flap. 196
Figure 6-47. Data showing the influence of Reynolds number on the L/D of the vortex flap. 196

Figure 6-48. Data showing the influence of Reynolds number on the total lift increment of the vortex flap. 197
Figure 6-49. Lift surface plot, SSR = 0. 198
Figure 6-50. Lift surface plot, SSR = 1. 199
Figure 6-51. Lift surface plot, SSR = 1.5. 199
Figure 6-52. Lift surface plot, SSR = 2. 200
Figure 6-53. Lift surface plot, SSR = 2.5. 200
Figure 6-54. Lift surface plot, SSR = 3. 201
Figure 6-55. Drag surface plot, SSR = 0. 201
Figure 6-56. Drag surface plot, SSR = 1. 202
Figure 6-57. Drag surface plot, SSR = 1.5. 202
Figure 6-58. Drag surface plot, SSR = 2.0. 203
Figure 6-59. Drag surface plot, SSR = 2.5. 203
Figure 6-60. Drag surface plot, SSR = 3. 204
Figure 6-61. Lift increment surface plot, SSR = 0. 204
Figure 6-62. Lift increment surface plot, SSR =1. 205
Figure 6-63. Lift increment surface plot, SSR = 1.5. 205
Figure 6-64. Lift increment surface plot, SSR = 2. 206
Figure 6-65. Lift increment surface plot, SSR = 2.5. 206
Figure 6-66. Lift increment surface plot, SSR = 3. 207
Figure 6-67. Lift surface plot, SSR = 0. 208
Figure 6-68. Lift surface plot, SSR = 1. 209
Figure 6-69. Lift surface plot, SSR = 1.5. 209
Figure 6-70. Lift surface plot, SSR = 2. 210
Figure 6-71. Lift surface plot, SSR = 2.5. 210
Figure 6-72. Lift surface plot, SSR = 3. 211
Figure 6-73. Drag surface plot, SSR = 0. 211
Figure 6-74. Drag surface plot, SSR = 1. 212
Figure 6-75. Drag surface plot, SSR = 1.5. 212

Figure 6-76. Drag surface plot, SSR = 2. 213
Figure 6-77. Drag surface plot SSR = 2.5. 213
Figure 6-78. Drag surface plot, SSR = 3. 214
Figure 6-79. Lift increment surface plot, SSR = 0. 214
Figure 6-80. Lift increment surface plot, SSR = 1. 215
Figure 6-81. Lift increment surface plot, SSR = 1.5. 215
Figure 6-82. Lift increment surface plot, SSR = 2. 216
Figure 6-83. Lift increment surface plot, SSR = 2.5. 216
Figure 6-84. Lift increment surface plot, SSR = 3. 217
Figure 6-85. Lift surface plot, SR = 0. 218
Figure 6-86. Lift surface plot, SSR = 1. 219
Figure 6-87. Lift surface plot, SSR = 1.5. 219
Figure 6-88. Lift surface plot, SSR = 2. 220
Figure 6-89. Lift surface plot, SSR = 2.5. 220
Figure 6-90. Drag surface plot, SSR = 0. 221
Figure 6-91. Drag surface plot, SSR = 1. 221
Figure 6-92. Drag surface plot, SSR = 1.5. 222
Figure 6-93. Drag surface plot, SSR = 2. 222
Figure 6-94. Drag surface plot, SSR = 2.5. 223
Figure 6-95. Drag surface plot, SSR = 3. 223
Figure 6-96. Lift increment surface plot, SSR = 0. 224
Figure 6-97. Lift increment surface plot, SSR = 1. 224
Figure 6-98. Lift increment surface plot, SSR = 1.5. 225
Figure 6-99. Lift increment surface plot, SSR = 2. 225
Figure 6-100. Lift increment surface plot, SSR = 2.5. 226
Figure 6-101. Lift increment surface plot, SSR = 3. 226
Figure 6-102. Lift curve plot, "Position 1." 227
Figure 6-103. Lift curve plot, "Position 2." 228
Figure 6-104. Lift curve plot, "Position 3." 228

Figure 6-105. Drag curve plot, "Position 1." 229
Figure 6-106. Drag curve plot, "Position 2." 229
Figure 6-107. Drag curve plot, "Position 3." 230
Figure 6-108. Lift increment curve plot, "Position 1." 230
Figure 6-109. Lift increment curve plot, "Position 2." 231
Figure 6-110. Lift increment curve plot, "Position 3." 231
Figure 6-111. Lift vs. α plot, "Position 1." 232
Figure 6-112. Lift vs. α plot, "Position 2." 233
Figure 6-113. Lift vs. α plot, "Position 3." 233
Figure 6-114. Drag vs. α plot, "Position 1." 234
Figure 6-115. Drag vs. α plot, "Position 2." 234
Figure 6-116. Drag vs. α plot, "Position 3." 235
Figure 6-117. Lift increment vs. α plot, "Position 1." 235
Figure 6-118. Lift increment vs. α plot, "Position 2." 236
Figure 6-119. Lift increment vs. α plot, "Position 3." 236
Figure 6-120. Lift vs. SSR curve plot, α = 0° 237
Figure 6-121. Lift vs. SSR curve plot, α = 5° 238
Figure 6-122. Lift vs. SSR curve plot, α = 10° 238
Figure 6-123. Drag vs. SSR curve plot, α = 0° 239
Figure 6-124. Drag vs. SSR curve plot, α = 5° 239
Figure 6-125. Drag vs. SSR curve plot, α = 10° 240
Figure 6-126. Lift increment vs. SSR curve plot, α = 0° 240
Figure 6-127. Lift increment vs. SSR curve plot, α = 5° 241
Figure 6-128. Lift increment vs. SSR curve plot, α = 10° 241
Figure 6-129. Lift vs. α curve plots, SSR = 0 242
Figure 6-130. Lift vs. α curve plots, SSR = 1 243
Figure 6-131. Lift vs. α curve plots, SSR = 1.5 243
Figure 6-132. Lift vs. α curve plots, SSR = 2 244
Figure 6-133. Lift vs. α curve plots, SSR = 2.5 244

Figure 6-134. Lift vs. α curve plots, SSR = 3 245
Figure 6-135. Drag vs. α curve plots, SSR = 0 245
Figure 6-136. Drag vs. α curve plots, SSR = 1 246
Figure 6-137. Drag vs. α curve plots, SSR = 1.5 246
Figure 6-138. Drag vs. α curve plots, SSR = 2 247
Figure 6-139. Drag vs. α curve plots, SSR = 2.5 247
Figure 6-140. Drag vs. α curve plots, SSR = 3 248
Figure 6-141. Lift increment vs. α curve plots, SSR = 0 248
Figure 6-142. Lift increment vs. α curve plots, SSR = 1 249
Figure 6-143. Lift increment vs. α curve plots, SSR = 1.5 249
Figure 6-144. Lift increment vs. α curve plots, SSR = 2 250
Figure 6-145. Lift increment vs. α curve plots, SSR = 2.5 250
Figure 6-146. Lift increment vs. α curve plots, SSR = 3 251
Figure 6-147. Cylinder positions tested 256
Figure 6-148. Lift vs. SSR 257
Figure 6-149. Lift vs. Vertical Position 258
Figure 6-150. Lift vs. Horizontal (chordwise) position 260
Figure 6-151. Surface generated for SSR = 0 261
Figure 6-152. Surface generated for SSR = 0 262
Figure 6-153. Surface generated for SSR = 1 263
Figure 6-154. Surface generated for SSR = 2 263
Figure 6-155. Surface generated by SSR = 3. 264
Figure 6-156. Surface generated at SSR = 4. 264
Figure 6-157. Surface generated at SSR = 5. 265
Figure 6-158. Surface generated by SSR = 6. 265
Figure 6-159. Corrected (left) and uncorrected (right) Lift vs. SSR graph. 267
Figure 6-160. Corrected (left) and uncorrected (right) Drag vs. SSR graph. 267
Figure 6-161. Corrected (left) and uncorrected (right) L/D vs. SSR graphs. 268
Figure 6-162. Corrected (left) and uncorrected (right) total lift increment graphs. ... 268

Figure 6-163. Corrected (left) and uncorrected (right) % lift increase vs. SSR graphs. 269
Figure 6-164. Corrected (left) and uncorrected (right) % lift increase vs. SSR graphs. 269
Figure 6-165. Corrected (left) and uncorrected (right) % increase in lift vs. SSR graphs. 270
Figure 6-166. Correction (left) and uncorrected (right) lift coefficient vs. angle of attack 270
Figure 6-167. Corrected (left) and uncorrected (right) drag coefficients vs. angle of attack 271
Figure 6-168. Corrected (top) and uncorrected (bottom) L/D vs. angle of attack 272
Figure 6-169. Corrected (left) and uncorrected (right) cylinder-only results 273
Figure 6-170. Efficiency of rotating cylinder as a generator of circulation, presented here as a function of SSR for various Reynolds numbers. 274

Abstract of the Dissertation

The Vortex Flap

By

Brandon T. Buerge

Doctor of Philosophy in Aerospace Engineering

Washington University in St. Louis, 2008

Professor Michael A. Swartwout, Chairman

The Vortex Flap is a new type of mechanically driven high-lift device consisting of a rotating cylinder placed underneath and near the trailing edge of an airfoil. Wind tunnel tests were designed and conducted in the Washington University Low-Speed Wind Tunnel. Wind tunnel tests indicate that the Vortex Flap produces notable lift coefficient increments and increases maximum lift coefficients, particularly for the low Reynolds number range tested. The best configurations of the configurations investigated (not necessarily optimal) produce lift increments of 300-900% at low-to-moderate angles of attack, and increase the maximum lift coefficient on the order of 200%. The large lift increments found, particularly at low angles of attack, underscore the ability to drive the airfoil to high lift coefficients even at low angles of attack, a potentially useful characteristic for certain flight maneuvers. Regions of fairly high L/D (on the order of 10) as well as low L/D performance were identified. The nondimensional cylinder rotation speed was found to be the most important

experimental parameter. Methods for correcting wind tunnel data were developed and outlined, and a Response Surface Method was applied to the corrected data for ease of interpretation. Performance comparisons between the Vortex Flap and other trailing-edge high-lift devices are included. To demonstrate the potential of the device, a Navy mission specification for a VTOL ship-borne UAV, currently filled by a rotary-wing aircraft, is analyzed using a hypothetical fixed wing aircraft and the Vortex Flap. It is demonstrated that, under certain reasonable wind-over-deck conditions, such an aircraft could hypothetically fill a VTOL mission.

1 Introduction

The "Vortex Flap" is proposed as a new trailing-edge high-lift device which increases the maximum lift of an airfoil. The Vortex Flap combines the relative mechanical simplicity of a rotating circular cylinder with the circulation-generating power of a rotating external flap (Crabtree 1960) to create a unique and powerful tool in the aircraft designer's trailing-edge high-lift device arsenal. The author led the effort to develop and test the Vortex Flap, and provides the following experimental investigation as evidence of its potential. Comparison with other high-lift devices and an investigation into applications are included.

The Vortex Flap is a trailing-edge high-lift device consisting of a mechanically driven spanwise rotating circular cylinder located below and near the trailing edge of a wing (see Figure 1-1). It has an independent boundary layer and is not a boundary-layer-control (BLC) device for the wing, and it does not utilize suction, blowing, or other pneumatic flow control schemes.

Figure 1-1. The configuration of the Vortex Flap

1.1 Definition of the Peer Group

The Vortex Flap, as presented here, is not proposed as a stand-alone high-lift system, but as one component of a hypothetical high-lift system which might incorporate leading-edge high-lift devices, or other high-lift components and features. To properly evaluate the Vortex Flap's merits, therefore, it should be considered in comparison with other trailing-edge high-lift devices. It should not be directly compared to complete multi-element systems or devices which function in a fundamentally different manner, such as slats, airfoils with pneumatic boundary layer control, or deflected slipstream aircraft.

An additional distinction must be made. The Vortex Flap is not a powered-lift device, but rather a power-assisted flap (Hoerner 1985). For the purposes of this discussion, a powered-lift device or aircraft is one in which a significant portion of the lift comes directly from the momentum of the exhaust of the powerplant or slipstream of the propeller, particularly as that slipstream interacts with high-lift devices, as in deflected slipstream and Upper Surface Blowing aircraft. A power-assisted flap is one which uses mechanical or pneumatic power primarily to control the flow, and where the direct momentum of any blowing or sucking does not contribute significantly to the overall lift. Examples of power-assisted flaps include rotating circular cylinder flaps of various configurations. The classification of blown flaps and circulation control wings varies according to the coefficient of momentum. At lower coefficients, they function

like power-assisted flaps; at higher coefficients, they function more like powered-lift devices. These types are excluded from the peer group.

Therefore, the appropriate peer group for the evaluation of the Vortex Flap consists of non-powered-lift trailing-edge high-lift devices, and also power-assisted flaps which are similar in function. Leading-edge devices, alone or as part of a high-lift system, are excluded. A complete list of the peer group considered in this paper follows:

- Non-power-assisted flaps and trailing edge devices
    - "Simple" flaps: plain, split, external
    - "Slotted" flaps: single, double, triple, and fowler
- Power-assisted "Mechanical" Flaps: Rotating cylinder flaps, trailing edge integrated rotating circular cylinder flaps, external rotating airfoil flap

Powered-lift devices and systems explicitly excluded from the peer group:

- Jet flaps
- Upper Surface Blowing aircraft
- Circulation Control airfoils
- Deflected slipstream aircraft

1.2 Basis for Evaluation

The Vortex Flap and its peers will be evaluated considering the typical functions of trailing-edge high-lift devices. A summary of the estimated performance potential of the Vortex Flap and some relevant high-lift devices and systems is presented in Figure 1-2.

Plain and split flaps	0.9	1
Fowler	1.3c'/c	2
Double Slotted Flaps	1.6c'/c	3
Triple Slotted Flaps	1.9c'/c	4
Rotating Cylinder Flap	2	5
Rotating Airfoil Flap	3.2	4
Moving Surface Boundary Layer Control (leading and trailing edge cylinders)	2.7	5
Vortex Flap	3.1	4
Typical Modern High-Lift System (Triple-Slotted Flaps and Slats)	3.8	5
Vortex Flap plus Slat and Plain Flap (hypothetical configuration)	5	6

Figure 1-2. Estimated performance comparison for Vortex Flap and other high-lift devices. Adapted from Loftin (1985), Raymer (1999), Filiponne (2006), and Modi and Mokhtarian (1990). c' indicates flap chord; c indicates base airfoil chord.

The Vortex Flap will be shown to have unmatched lift-enhancing capability within its peer group, with low power demands, but at the cost of significant drag and pitching moment. The lift increment and the ability to control the lift increment precisely over a wide range of angles of attack offer intriguing possibilities for improved maneuverability and control in low speed flight. Also, there is a range of operation which permits significant lift enhancement while maintaining a moderate L/D.

1.3 Contributions

The author claims the following contributions:

- The first application of a rotating circular cylinder in combination with an airfoil which does not function as a boundary layer control device (Modi 1997).
- The first application of a rotating circular which constitutes a multi-element system per the definition of A. M. O. Smith (Smith 1974).
- The first rotating external flap design which addresses some of the vibration and likely power consumption issues associated with the only other rotating external flap design to date (Crabtree 1960).
- An experimental investigation, which demonstrates the effectiveness and potential usefulness of the Vortex Flap, including the development and application of suitable wind tunnel corrections.

- The most effective lift-generating single-rotating-circular-cylinder configuration found to date.
- A simplification of Response Surface Methods which does not require the development of a single polynomial in order to generate meaningful response surfaces (Box and Draper 1987).
- The demonstration of hypothetical utility in a Mission Analysis.
- A compelling program for future research based on the results of this investigation.

1.4 Related Work

There are three devices in particular which merit mentioning for direct comparison with the Vortex Flap. They are:

1. The use of a rotating cylinder embedded in a flap as investigated by NASA in the 1960's. This was a flap integrated into the leading edge of the flap with no appreciable gap (Kohlman 1981) and underwent flight and full-scale wind tunnel testing on a modified Bronco YOV-10A. The traditional sharp trailing edge remains.

2. The use of a rotating circular cylinder *in place* of a flap at the trailing edge (Hoerner1985 and Modi and Mokhtarian 1990). There is no traditional sharp trailing edge.
3. A rotating external airfoil flap, as investigated in Germany during WWII and by the British in the 1950's (Crabtree1960).

The rotating cylinder flap (1) is worth mentioning given the extensive flight testing and the use of a rotating cylinder, but the data are difficult to use for direct comparison because the configuration was tested on a powered-lift aircraft. The rotating cylinder flap was found to be mechanically simple, to take a relatively small amount of power to operate, and to enhance significantly the lifting capabilities of the aircraft. The aircraft was modified with the flaps, but the control system was not sufficiently powerful to allow full advantage to be taken of the rotating cylinder flaps. In this particular application, the rotating cylinder served to inject momentum into the boundary layer and keep the flow attached on the top of the deflected flap. Wind tunnel data are available for very similar configurations, and these data will be used for the evaluation of this particular type of device.

The use of a rotating circular cylinder in place of a trailing edge flap (2) was investigated in Germany in the 1940's , in Britain in the 1950's (Crabtree 1960), and in the United States in the 1990's (Modi 1997). The results, not to mention the persistence of the concept in intriguing researchers, suggest that this is a powerful

approach. However, more lift can be generated if the single cylinder is relocated to other locations on the wing. As such, this particular configuration has never matured, but will be included for comparison.

The closest functional relative of the Vortex Flap, the rotating external airfoil flap (3) was investigated only once in Germany in the 1940's. While extremely effective, more effective than either (1) or (2) in increasing lift, the power required to turn the flap is considerably higher than that required for a comparable rotating circular cylinder (Crabtree 1960). Also, the lift is a periodic function of flap rotation, causing vibration which probably makes this alternative impractical (Lugt and Ohring 1977, E. H. Smith 1971).

None of these three approaches have seen implementation on any non-research aircraft. The most successful to date is arguably (1), but the installation on the YOV-10A Bronco was the last aircraft to fly with rotating circular cylinder flaps. The Vortex Flap picks up where these three devices left off by addressing some of the major weaknesses which have prevented the implementation of these devices. The location of the Vortex Flap allows it to be the most effective location for a single-rotating cylinder installation on or around an airfoil, by generating the largest lift increment of any of the devices discussed when adjusted for scale and wind tunnel effects. The smooth surface of the cylinder minimizes the power requirements. Further, there is no aerodynamic vibration associated with the rotation of the cylinder.

1.5 Dissertation Outline

The object of this dissertation is to present the reader with credible evidence of the claimed contributions. In order to do this task thoroughly, every aspect of the investigation must be revisited. The dissertation began as a broad theoretical consideration of the role of vortices in fluid force and motion. Gradually, the notion of using cylinders as part of a high-lift system became compelling. Ultimately an experimental investigation (portions of which merit revisiting in the future) was conceived and implemented which gradually narrowed to this present configuration through experimentation. Thus, it is important to investigate the context of the Vortex Flap by examining the historical and developmental context of both traditional trailing-edge high-lift devices, and rotating cylinders as high-lift devices. The process of designing the experiments, both in terms of the meaningful parameters, and the experiment rig itself, was rather complicated and required a great deal of attention. The brute-force experimental configuration optimization highlighted the relatively narrow set of parameters that are outlined here. It was hoped that some useful application might be found for these results, and the product of that search is outlined in the Mission Analysis and Future Work sections.

Section two develops the background of trailing-edge high-lift devices, and outlines the remainder of the peer group for eventual comparison to the Vortex Flap. Section three outlines the experimental work. Section four presents the results of the

experimental investigation, including a dimensional analysis, an outline of the wind tunnel corrections applied to the data, and an application of Response Surface Methods to the data to ease interpretation and comparison. Section five compares the experimentally obtained results to the peer group performance after adjusting for Reynolds number effects and analyzes the hypothetical application of the Vortex Flap to a Helio Courier fixed wing aircraft for a US Navy ship-borne VTOL UAV mission. Section six draws conclusions from the data and suggests future work.

2 Background

Trailing-edge high-lift devices and high-lift devices in general have been the object of a great deal of research since aerodynamics became a stand-alone science in the 1910's. Necessitated by the ever-higher wing loading demanded by progressively faster aircraft, the trailing-edge high-lift device is generally a pilot-controlled device which permits the geometry of the airfoil to be changed in order to improve performance or control the direction of the aircraft (Abbott). Note well that while the purpose of this section is to develop a body of evidence for comparison, for brevity most graphics are found in the Addendum Appendix C, and in the original sources (Abbot and Von Doenhoff 1959, Ames 1940, Cahill 1949, Critzos, Heyson, and Boswinkle 1955, Deckert, Koenig, and Wieberg 1966, Hoerner and Borst 1985, Jacobs 1939, Lowry 1941, Munk 1927, Omar, Zierten, Hahn, Szpiro and Mahal 1973, Ou and Burns 1991, Platt 1935, Reid 1924, Schuldenfried 1942, Selig, Donovan and Fraser 1989, Silverstein 1935, Tolumaru and Dimotakis 1993, Weick 1932, Wenzinger and Harris 1940).

The trailing-edge high-lift device called the Vortex Flap is a part of that small trickle in aeronautical history which combines the curiosity surrounding the Magnus effect, and the ever-present drive to increase the lifting capacity of wings. Within this small trickle there are three streams of work. In the first, a rotating cylinder is embedded in

the primary airfoil, and functions as boundary layer control in a manner similar to pneumatic blowing. In the second, the rotating devices (regardless of cross-section) is external to the primary airfoil and functions to increase the lift through the direct generation of circulation, as well as, perhaps, through some physical interaction with the primary airfoil. In the third, lift is enhanced by somehow 'trapping' a free vortex (rather than a mechanically-generated vortex) above an airfoil, which has been argued by some to enhance lift at very high angles of attack (Cox 1973). The investigations of Reid of the American NACA in the 1920's and of Dr. Kuchemann in Germany during WWII were probably the first systematic investigations into finding a useful combination of spanwise rotating devices and fixed airfoils (Crabtree 1960, Reid 1924).

Reid's investigation, of the first branch above, placed a mechanically driven rotating cylinder in the leading edge of a fairing. Results were mediocre due primarily to mechanical and aerodynamic shortcomings of the chosen model. This branch continued into the 1960's NASA conducted wind-tunnel and flight tests, on a device apparently developed originally by Alvarez Calderon, which combined an embedded rotating cylinder with a single-slotted double-hinged flap and slat, placing the rotating cylinder at the junction between the wing and the flap (Calderon 1960, Cook and Hickey 1975). The modified YOV-10A Bronco, which was the deflected-slipstream aircraft used as a testbed for this technology, ultimately achieved an in-flight $C_{L,max}$ of 4.3. Interest in what Modi called "Moving Surface Boundary-Layer Control"

prompted tests on a variety of configurations of single and double rotating cylinders embedded in Joukowski airfoils at the leading and trailing edges, as well as protruding from the upper surfaces in the early 1990's (Modi and Mokhtarian 1990). Even more recently, embedded rotating cylinders have drawn attention as potential control effectors for UAV's (Wood and Bauer 1999).

Dr. Kuchemann's work, of the second branch, allowed the external flap of an NACA 23015 airfoil to rotate about its spanwise axis (Crabtree 1960). Very significant lift was achieved, at the cost of substantial drag, pitching moment and power to rotate the flap. It must be presumed also that vibration with such a rotating device must have been significant owing to the periodic shedding of vortices from the sharp edges of the rotating external airfoil flap, which calls in to question the practicality of such a device in any real application (Lugt and Ohring 1977). Aside from the present investigation, this is the only work in which a spanwise external rotating device has been seriously investigated.

The final branch found its genesis in the controversial claims of Witold Kasper, a Boeing engineer who in the 1960's designed ultra-light aircraft which he claimed trapped large free vortices above the wing at very high angles of attack, eventually spawning a fleet of "Kasperwing" aircraft that can still be found at airshows today. Initial wind tunnel investigations were not as fruitful; however, significant numerical effort was expended which demonstrated that, if such a flow could be generated, it

would indeed enhance lift a great deal (Kurpa 1977, Walton 1974, Saffman and Sheffield 1977, Saffman and Tanveer 1984, Chow, Chen, and Huang 1986). Efforts at step-induced free vortices has shown some promise, but not on the order originally claimed by Kasper (Finnaish and Witherspoon 1998). Other methods have been attempted to generate and sustain this elusive free vortex, but have met with more frustration than fruition (Rossow 1978, Sunderland 1976).

It was in the claims of Kasper, however, that the present investigation found its inspiration. It was thought that if a mechanically generated vortex were placed above an airfoil, by means of a rotating cylinder, that some of the beneficial effects demonstrated numerically by others might be experimentally and reliably demonstrable. An investigation was designed which was, in effect, a mechanical optimization investigation to find promising configurations of a rotating circular cylinder near an airfoil. The initial focus was on configurations placing the cylinder above the primary airfoil, but serendipitously, some under-the-wing configurations were investigated, and those are the subject of the present paper. The author hopes to return to the other configurations in a future project.

The particular under-the-wing configuration chosen here places the Vortex Flap squarely in the second stream, and identifies the Vortex Flap as the direct functional descendant of the work of Dr. Kuchemann outlined by Crabtree. Crabtree's major contribution to the branch was to catalog Kuchemann's work and to develop a

convenient potential flow analysis equally applicable to the Vortex Flap and to the rotating external airfoil flap it was intended to model.

The broader developmental history of passive high-lift devices in general has been steadier, and more practically fruitful. An outline of the basic evolution of the most common high-lift devices in use today, adapted from Anderson's "A History of Aerodynamics," follows (Anderson 1997):

- 1908- Henry Farman develops the first conventional control flap, wherein a flush-mounted integral portion of the trailing edge of the wing was allowed to move up and down independently of the wings, to allow lateral control and avoid infringing the patented 'wing-warping' technology that was the state of the art at the time.
- 1914- The Royal Aircraft Factory simultaneously deflects both control flaps down to gain a net increase in lift.
- 1917- G. V. Lachmann, a young German pilot, first conceives of a spanwise slot near the leading edge. A patent application is rejected on grounds that slots would not work.
- 1920- Handley Page verified the effectiveness of slots in wind tunnel tests, which were corroborated by tests conducted by Prandtl at Gottingen.
- 1920-1922- Handley Page combines a slot and a flap to create the slotted flap.
- 1920- Orville Wright and J. M. H. Jacobs invent the split flap.

- 1924- Harlan D. Fowler, conducting self-funded research, invented the Fowler flap in which the flap not only deflected downward, but moved downstream, thus increasing the wing area as well as the wing camber.
- 1933- The Douglas DC-3 becomes the first mass-produced aircraft to use split flaps.
- 1937- The Lockheed 14 becomes the first production aircraft to use Fowler flaps.
- 1937- G. Pegna of Piaggio aircraft (modern-day producer of the Piaggio Avanti) invents the double-slotted flap, which found essentially immediate application.
- 1960's- Boeing uses the triple-slotted Fowler flap on the 727, essentially representing the pinnacle of passive trailing-edge high-lift device design.

Several of the flap configurations mentioned above are shown in Figure 2-1.

2.1 Aerodynamic Considerations

Passive trailing-edge high-lift devices increase lift by some or all of three means: increase in effective camber, increase in wing area, and the use of slots. While the first two are well understood and widely accepted even in the popular aviation literature, a fundamental misunderstanding of the function of the slot in lift enhancement persists even among industry professionals (Whittley 1993, Woodward and Dean 1993). As

the Vortex Flap includes a slot in its basic configuration, an accurate understanding of this third means is desired. A brief review of the basics will aid this discussion.

While debate remains between the "Newtonian" and "Bernoullian" explanations of the creation of lift, the author asserts that this is a false dichotomy. While the Newtonian perspective describes lift as the reaction force created when an air mass is accelerated opposite the direction of lift, the Bernouillians insist that the lift is the result of a pressure distribution caused by relatively different velocities above and below the wing. The author submits that the derivation of Bernoulli's equation from Newton's Second Law demonstrates the common physical underpinnings of these two perspectives, and suggests simply that they are two physical expressions of the same basic process, stated thus:

> A lifting device creates lift as it influences the surrounding air (by its shape, orientation, or other means) to cause it to accelerate in the direction opposite of the resultant lift force; as air is a fluid, this acceleration is communicated through the flow and indeed actualized by a pressure distribution which causes the flow to accelerate in that direction, and this distribution is reflected in a relatively higher/lower pressure below/above the airfoil.

On these grounds, it can be recognized that a passive translating wing generates lift more or less effectively depending on how well it can 'turn the air down' as it passes. It stands to basic physical reason that the more curved (cambered) the wing is, the more effective the wing will be at turning the air. The motion of the typical flap creates a bend in the wing which has exactly this effect. The influence of a larger wing area needs even less justification, as it should be immediately recognized that the lift force is created in a manner that is proportional to the size of the wing. Thus, any increase in wing area should result in some roughly proportional increase in lift, and this is the basic advantage of a Fowler flap over a simple slotted flap.

2.1.1 Slot Effects

The reason typically given for the addition of "slots," either in the form of a slotted leading edge or a slotted flap, is that the slot allows the flow of high-pressure air from below the wing to accelerate through the slot, re-energize the boundary layer above the wing, and prevent flow separation which normally occurs and reduces the effectiveness with which the wing can turn the air down (Abbot and Doenhoff 1959). Thus the slot has been considered a boundary-layer control device. This understanding was held as correct until A. M. O. Smith's classic 1972 paper "Aerodynamics of High-Lift Airfoil Systems" (Smith 1972) presented a "clear and comprehensive insight into the fundamentals of a multi-element foil" (Whittley 1993) which explicitly counters

the boundary-layer-control hypothesis. Smith's explanation will be outlined below and proposed as the "correct" explanation, but it should be mentioned that the prior explanation persists with alarming ubiquity in popular and quasi-technical literature today. For an example, see (Smith 1992). While explicitly excluding low Reynolds number effects, A. M. O. Smith outlines five primary functions of slots, paraphrased here:

1. Slat Effect: The circulation on the upwind element reduces the velocity in the vicinity of the leading edge of the downwind, reducing the severity of the low-pressure peak normally found near the leading edge of an airfoil. The effect is not primarily to increase lift at a fixed angle of attack, but rather to delay flow separation to a higher angle of attack.
2. Circulation Effect: The presence of the downwind element creates a region of high-velocity flow which is inclined to the mean camber line of the upwind element near the trailing edge of the upwind element. This requires an increase in circulation around the upwind element to satisfy the Kutta condition in the presence of the downstream element.
3. Dumping Effect: The region of high velocity induced by the downstream element reduces the adverse pressure gradient which the boundary layer on the upstream must contend with as it approaches the trailing edge, thus alleviating some of the flow separation that might otherwise occur.

4. Off-The-Surface Pressure Recovery: As implied above, the boundary layer of the upwind elements is 'discharged' at a velocity much higher than free stream. This wake is then free to decelerate to free stream velocity without being in contact with the surface of any element, generally a more efficient process allowing superior pressure recovery when compared to decelerating in contact with a surface.

5. Fresh Boundary Layer Effect: This is perhaps the effect closest to that implied by previous and erroneous understandings; each new downstream element forms a new boundary layer at its leading edge, and this new, thin boundary layer is better able to remain attached in the presence of adverse pressure gradients, reducing flow separation and increasing lift on the downstream element.

Power-assisted flaps function in a slightly different manner, depending on the device. The rotating cylinder flap functions as a boundary layer control device which permits the flow to remain attached to even a very highly deflected flap (see Addendum Figure 5 or Kohlman 1981). This permits the wing to develop more circulation, or 'turn the air down' more effectively. The trailing edge rotating cylinder flap is similar, but more directly 'pumps' the air around the trailing edge itself (Hoerner and Borst 1985), rather than modifying the flow around a separate flap. This 'pumping' action deflects the flow in a manner similar to any deflected flap, and contributes directly to the

circulation of the wing. The rotating external airfoil flap uses two mechanisms. The first is the direct generation of circulation through the Magnus effect of the rotating airfoil itself. The second is the influence of the rotating airfoil on the primary airfoil in a manner analogous to a slotted flap, as outlined above. It is not immediately clear what influence the 'periodic' nature of the flow around the rotating external airfoil flap has on each of the five "slot" effects outlined earlier.

In a manner similar to the rotating external airfoil flap, the Vortex Flap does not operate directly on the boundary layer of the airfoil. While all five "slot" effects are present for the vortex flap (particularly if one is willing, at times, to consider the airfoil as a 'slat' for the rotating cylinder), the 'circulation' and 'dumping' effects most clearly explain the beneficial effect of the presence of the stationary rotating cylinder, and these appear to be intensified when the cylinder rotates.

2.1.2 Vortex Shedding

The chief shortcoming of the use of a blunt body, like a circular cylinder, as a high-lift device lies in the nature of the wake, which normally involves shedding vortices which produce fluctuating forces on the body and a high mean drag (Zdravkovich 1997). The nature of the flow around a circular cylinder is remarkably complicated, given the simple geometry, and highly dependent on the Reynolds number, surface

roughness, the presence of vortex suppression devices, proximity to other objects, and rotation.

Stationary Circular Cylinder

The flow around a stationary circular cylinder has been parsed more and more precisely into narrow Reynolds number ranges as investigations have uncovered the staggering complexity of the flow. Most generally, there is the divide between sub- and super-critical flow, which divides the generally higher and lower drag ranges, respectively. Depending on the flow conditions, this break is taken to occur at around 3-4 x 10^5 where a shift from a primarily laminar boundary layer to a turbulent boundary layer produces a dramatic narrowing of the wake, and consequent drop in drag coefficient (Hoerner 1992). Additional investigation into this transition reveals that the critical range contains its own unique flow characteristics (Bearman 1969). High Reynolds number testing also shows a transcritical range that appears at very high Reynolds numbers, and is thought to be the "terminal" condition as Reynolds number increases to infinity (Jones, Cincotta, and Walker 1969 and Roshko 1961). Finally, Zdravkovich subdivides even these ranges in a multi-volume treatment of the flow around circular cylinders (Zdravkovich 1997 and Zdravkovich 2003), providing no less than fifteen distinct ranges characterized by Reynolds number, and the precise nature and location of the transition from laminar to turbulent flow. Over these ranges,

the mean and fluctuating lift and drag coefficients vary by an order of magnitude, so the precise definition of the flow range for operation cannot be overestimated. While alternately increasing and decreasing in severity, it appears that increasing Reynolds number offers no final solution to the vortex shedding problem, as can be witnessed even in the wakes of islands and mountains.

For the present investigation, the Reynolds number based on cylinder diameter varied from 15,000-80,000 placing the experiments firmly in the subcritical, and more precisely, transition-in-shear-layer-3 or upper subcritical regime (Zdravkovich 1997). This is sufficiently high to escape the very high drag coefficients found at low Reynolds number, but well above the minimum drag coefficient, which is found in the supercritical or transition-in-boundary-layer-3 regime (Zdravkovich 1997). For a smooth cylinder, this minimum varies from around 0.23-0.40 (Achenbach 1971, Bearman 1969, Hoerner 1992). The coincident small lift fluctuations that exist in the TrBL3 regime make it desirable for operation. The narrow upper subcritical range in which the present investigation was largely conducted contains lift and drag fluctuations that are dramatically more severe than even the neighboring regimes, exceeding lift fluctuations over most Reynolds numbers by an order of magnitude (Zdravkovich 1997).

A great many schemes have been devised to address the vortex shedding and high drag characteristics of circular cylinders. Though the vortex shedding appears to be the primary source of drag on a circular cylinder (Bickley 1928, Zdravkovich 1981), and suppressing the vortex shedding generally reduces the degree of force fluctuation, some means of suppression increase the mean drag even while reducing the force fluctuations. These schemes include strakes of all kinds, shrouds (Zdravkovich 1981), splitter plates (Hoerner 1992, Apelt, West, and Szewczyk 1973, Apelt and West 1975), surface roughness (Fage and Warsap 1930, Achenback 1971), grooves and dimples (Lim and Lee 2002, Bearman and Harvey 1993), fins (Zaida et al 2005), transverse motions (Li and Aubry 2003), rotational oscillations (Tokumaru and Dimotakis 1991), radial vibrations (Oualli et al 2004) and even separate control cylinders (Dipankar, Sengupta, and Talla 2007).

An additional complication is the effect of the presence of an airfoil near the cylinder. The aerodynamic loading on the stationary cylinder is dramatically affected by the airfoil. The relative position is very important, with positions directly in the wake of the wing holding a particular disadvantage in terms of fluctuating lift (Zhang, Huang and Zhou 2005). For the present investigation, the primary airfoil is thought to operate in a super-critical flow regime and to not have significant vortex shedding, with the cylinder generating most force fluctuations. The location of the Vortex Flap below the airfoil wake helps to mitigate additional lift fluctuation. The forces were not measured

on the wing and cylinder separately, however, so only fluctuations in the combined system can be observed in this investigation.

Given the unique requirements of the Vortex Flap, namely, that it also be able to rotate, that it not produce excessive vibration, that it has a reasonable power consumption, that there be a suitable cruise configuration, and that there be a suitable high-lift configuration, most vortex suppression methods can be immediately dismissed as impractical. The two most obvious and practical methods of addressing these issues are to retract the stationary cylinder, or to streamline the cylinder with an afterbody, removing the blunt-body nature of the wake.

Rotating Cylinder

Conveniently, the most vexing problem outlined in the previous section, vortex shedding and the attendant forces, is largely resolved by cylinder rotation (Zdravkovich 1997). In particular, when considering the ratio between the peripheral speed and the free stream velocity (referred to as the Surface-Speed-Ratio or SSR, see Section 4), the following can be stated (Diaz et al 1983):

SSR = 0:	Represents the limiting case of a stationary cylinder
0 < SSR < 1:	Vortex shedding still dominant
1 < SSR < 2:	Vortex shedding diminishes rapidly, wake narrows
SSR > 2:	Vortex shedding ceases

Simply rotating the cylinder appears to be the easiest way to resolve the vortex shedding issue. It should be mentioned that some numerical investigations at very low Reynolds numbers predict a second band of vortex shedding around SSR = 4.5 (Mittal and Kumar 2003), but the author expects that this band is unique to very low Reynolds numbers and laminar flow.

A rotating cylinder generates lift by the well-known Magnus effect. There has been some debate, however, as to the maximum limit of lift that can be generated by

rotation of a cylinder in uniform flow. Prandtl derived the maximum lift coefficient on a rotating cylinder as 4π or about 12.6, arguing that the circulation could not be increased beyond the circulation produced at a theoretical SSR = 4, when the stagnation points in a potential flow will have merged at the bottom of the rotating cylinder (Prandtl 1926, Zhradkovich 2003). While some experimental results have demonstrated that this limit can be exceeded (Tokumaru and Dimotakis 1993), the point remains that the flow begins to fundamentally change at around SSR = 4 as the cylinder begins to entrain flow (Diaz 1983) and that the rate of lift increase with increasing SSR begins to fall off at SSR > 4 (Chew, Cheng and Luo 1995, Hoerner 1992).

The high mean drag expected of a stationary cylinder in the subcritical regime is somewhat reduced by rotation for $0.5 < SSR < 2$, but then increases to a value greater than for the stationary cylinder at higher SSR (Zdravkovich 2003). One possible means to reduce the drag on the rotating cylinder could be to install coaxial discs along the length of the cylinder. Tests conducted by Thom found that, at least in the laminar range, the presence of the discs drove the drag to zero at SSR = 4, and generated a thrust for higher SSR, which peaked at $C_D = -1$ at SSR = 7 (Zdravkovich 2003). This would require additional investigation to ensure that the mechanism responsible for the drag reduction continued across other flow regimes, but holds

tremendous potential for the Vortex Flap. The thrust presumably comes at the cost of increased power consumption required to turn the rotating cylinder.

2.2 The Peer Group of Trailing-Edge High-Lift Devices

The peer group is identified, grouped, and described. For extensive performance information for the peer group, see Section 5.2, the Addendum, and the sources outlined in Section 2.0. For a pictorial representation, see Figure 2-1.

1. Simple flaps
    a. Plain flaps: Often used as control surfaces, the rear portion of the wing is hinged, increasing camber, lift and drag.
    b. Split flaps: The trailing edge splits, leaving a blunt edge which creates drag, and also resulting in an increase in lift due to an increase in camber.
2. Slotted flaps
    a. Single-slotted flaps: A single slot between the primary airfoil and the flap enhances the lift over that of the plain flap.

b. Fowler flaps: The flap translates downstream as well as pivoting, increasing the area and camber, and usually creating a slot which enhances the lift.

c. Double-slotted flaps: Same as single-slotted flap above, except that the flap itself is also slotted. Often combined with a Fowler-type action.

3. Mechanically-assisted flaps

a. Rotating cylinder trailing edge flap: The trailing edge is cut off short and replaced with a rotating cylinder. Lift is generated by a direct "pumping" action (Hoerner and Borst 1985).

b. Rotating cylinder flap: A rotating cylinder is installed at the junction of the primary airfoil and flap. The cylinder injects momentum into the boundary layer and prevents flow separation on the flap.

c. Rotating external airfoil flap: An external flap is caused to rotate near and underneath the trailing edge of the airfoil.

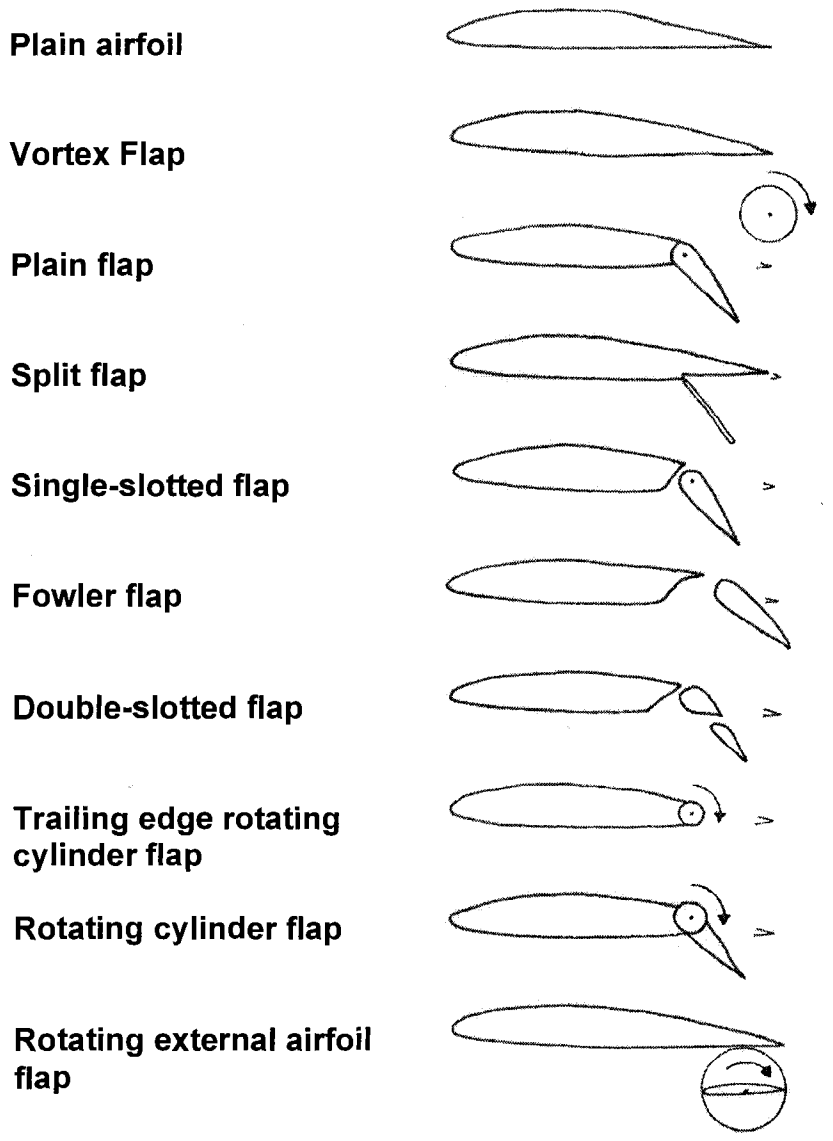

Figure 2-1. Schematic of the trailing-edge high-lift devices in the peer group. Drawing by Brandon and Elizabeth Buerge.

The widest and most monolithic body of data available for high-lift devices was generated by the NACA and NASA. It is relied upon here heavily. Though the peer group is carefully delineated, data for the most directly comparable configurations is

not always available, and substitutions have been made. For example, no data are available for the rotating cylinder flap except in combination with an unusual single-slotted double-flap of unusually large chord, and a large leading edge flap, so these data are included with the caveat that it is not directly comparable. Also, for the sake of comparison, the data for a double-slotted Fowler flap in combination with a leading edge slat from a more modern investigation than the bulk of the original research done by the NACA are included in the summary. So, too, are the data for a leading-edge rotating cylinder and for an airfoil equipped with leading- and trailing-edge rotating cylinders simultaneously, even though these configurations are not in the peer group.

The rotating external airfoil flap bears the strongest functional resemblance to the Vortex Flap. The lift results are very similar, and the ratio of rotating airfoil chord to main airfoil chord is very similar to the ratio of cylinder diameter to airfoil chord in the Vortex Flap testing. While obviously effective in generating lift, drag is considerable, and there is presumably a great deal of vibration associated with the periodic shedding of vortices from the sharp edges (Hoerner and Borst 1985 and Lugt 1979). Some effort was expended to determine the 'ideal' position behind the wing (Crabtree 1960).

3 Experimental Investigation

An experimental wind-tunnel investigation was designed. A common airfoil and a mechanically driven rotating circular cylinder were tested. It was considered desirable that the Reynolds numbers obtained be as high as possible to more accurately reflect what might be expected of a full-scale Vortex Flap. The investigation included the maximum possible range of physical parameters given the constraints of the available equipment. Since the optimal parameters were unknown at the outset, the tests were designed to systematically explore the design space.

The input variables of greatest interest were the rotational speed of the cylinder, free stream velocity, position relative to the wing, and angle of attack. Different positions relative to the wing were investigated, varying both in vertical and horizontal distance from the trailing edge. The output variables of greatest interest were lift, drag, and pitching moment. In order to simplify the interpretation of the results, the wind-tunnel model was designed to approximate two-dimensional flow by extending from wall to wall with a constant cross section. The Clark Y airfoil was selected due to the large body of available experimental data over a wide range of Reynolds numbers.

3.1 Experimental Setup and Method

In this section, the basic experimental approach, design and fabrication of the test setup, and data analysis procedure are outlined.

3.1.1 Wind tunnel

The tests were conducted in Washington University in St. Louis' Fluid Mechanics Laboratory low-turbulence wind tunnel (see Figure 3-1). An open-return induced-draft design, the tunnel has an unusually large 16-to-1 contraction ratio with a honeycomb flow straightener and two layers of screen. These features serve to render the wind tunnel very low turbulence for a tunnel of its type. The test section is 24" x 24" in cross section, roughly five feet long, with three Plexiglas doors for access and viewing. The fan is an eight blade wooden fan driven by a 3-phase 40 kW electric motor, capable of driving the tunnel to just above 200 feet per second. The wind tunnel is equipped with a data acquisition system for airspeed. The pitot-static probe was positioned about two feet upstream of the model and well clear of the wind tunnel boundary layer. The pitot-static probe was connected to a Validyne pressure differential electronic force transducer, which fed into a voltmeter and into the data analysis program in a PC computer. Once calibrated according to local conditions, the airspeed data acquisition system is manually triggered to take 250 readings over the

course of five seconds, and then the mean value is produced as the airspeed at that point. Care must be taken that the airspeed is stabilized prior to triggering the system.

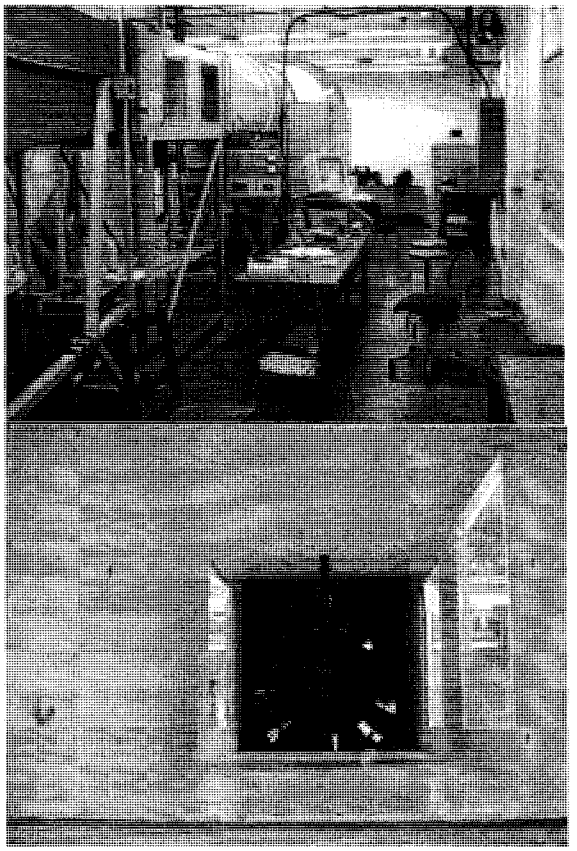

Figure 3-1. An exterior and interior view of the wind tunnel test section used

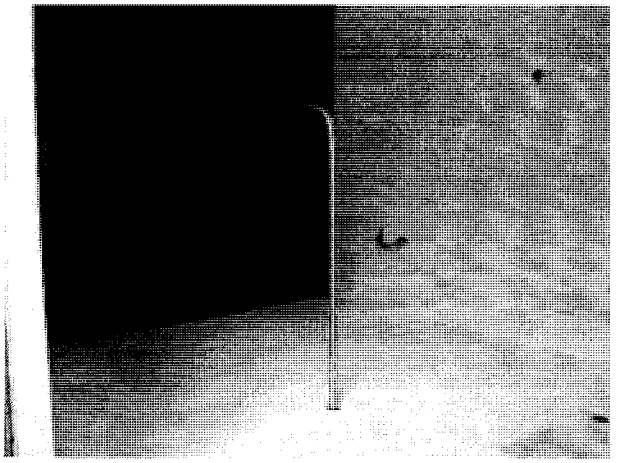

Figure 3-2. Pitot-static tube installation in wind tunnel test section

3.1.2 Force Balance

The biggest single obstacle to conducting the wind tunnel testing was the absence of a suitable force balance. The tests were 2-D so the balance only needed to measure lift, drag, and moment in one plane. This substantially simplified the design. It needed to be sufficiently strong to support a rather heavy model which could create substantial mechanical vibration. It was known that the model would run from wall to wall inside the test section, which made the use of a sting balance impossible. Two methods were available. One was to construct a force balance which would support the model through the test section walls on both sides. Alternatively, an array of pressure taps and a pitot rake could be used to measure the pressure distributions on the top and bottom of the tunnel and the velocity distribution behind the model, thus allowing the lift and drag to be calculated. However, substantial flow separation was expected

during testing which would have made the latter method inaccurate. It was decided to design and construct a custom force balance.

It was expected that the rig supporting the model and drive system, as well as the model itself, would be rather heavy. A balance had to be devised which provided sufficient strength, while not interfering with the accurate measurement of the forces on the model. Eventually a design was chosen in which the base of the force balance (Figure 3-3) rested on top of the wind tunnel test section, just above the desired model location. Resting on top of the base was a plate to which four flexures were attached (Figure 3-4) in a configuration which would allow lift, drag, and moment to be measured directly and independently. The flexures were milled from solid aluminum, tested, and re-milled until they offered sufficiently low resistance to motion perpendicular to their line of force. Double flexures where selected for redundancy in the event that fatigue caused a failure. The three vertical transducers to measure lift and moment (two of the vertical transducers were located at the same x position, so there were only two vertical forces in the frame of reference of the x-y plane). The single horizontal force transducer was located on the center line of the rig and measured drag. The flexures allowed the very slight motion necessary for the horizontal and vertical flexures to function independently. This fidelity was confirmed through extensive testing and calibration (see "Calibration" Section 3.1.6).

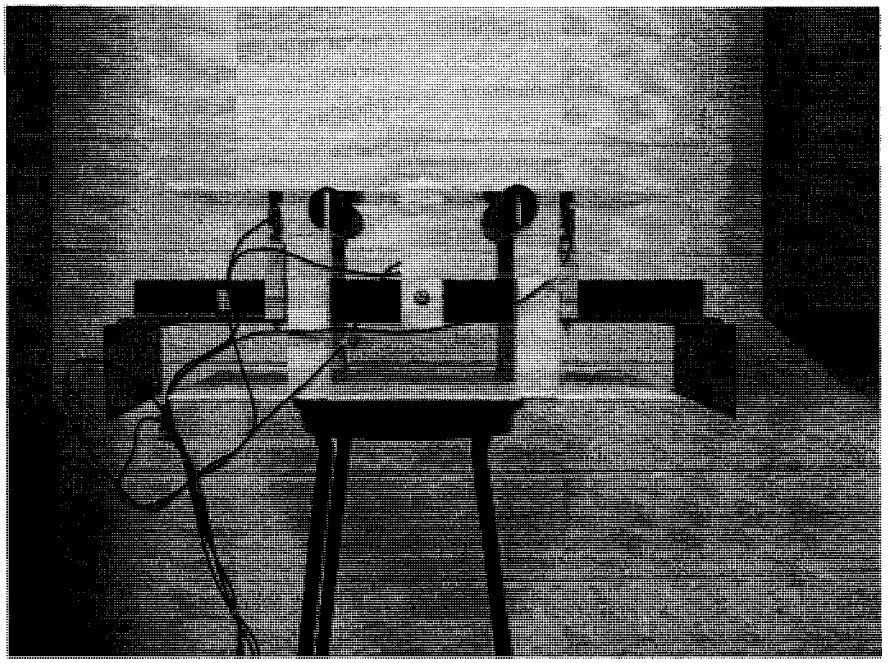

Figure 3-3. Front view of force balance, base on bottom in white. Note foam that separates base from the plate. The bridge is in dark gray.

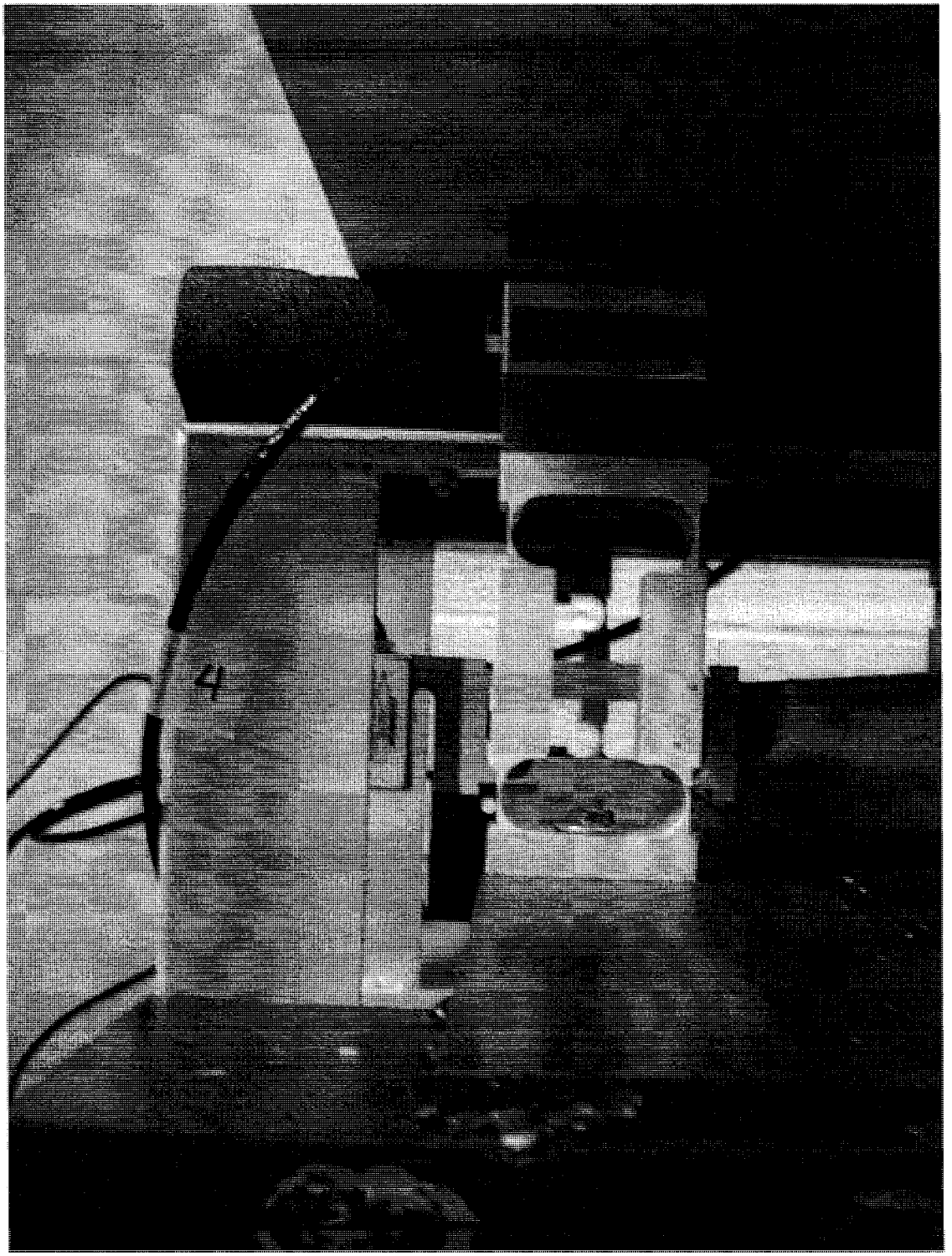

Figure 3-4. Picture of flexures used in force balance. Flexures in white, force transducers in silver and chrome. Bridge in gray, base and plate in white.

Suspended from the four force transducers and flexures was the backbone of the model support which came to be called the 'bridge' (see Figure 3-5). The bridge connected the support structures on either side of the tunnel. On either end of the bridge was a vertical plate to which the support masts for the cylinder and the arms for the airfoil were bolted.

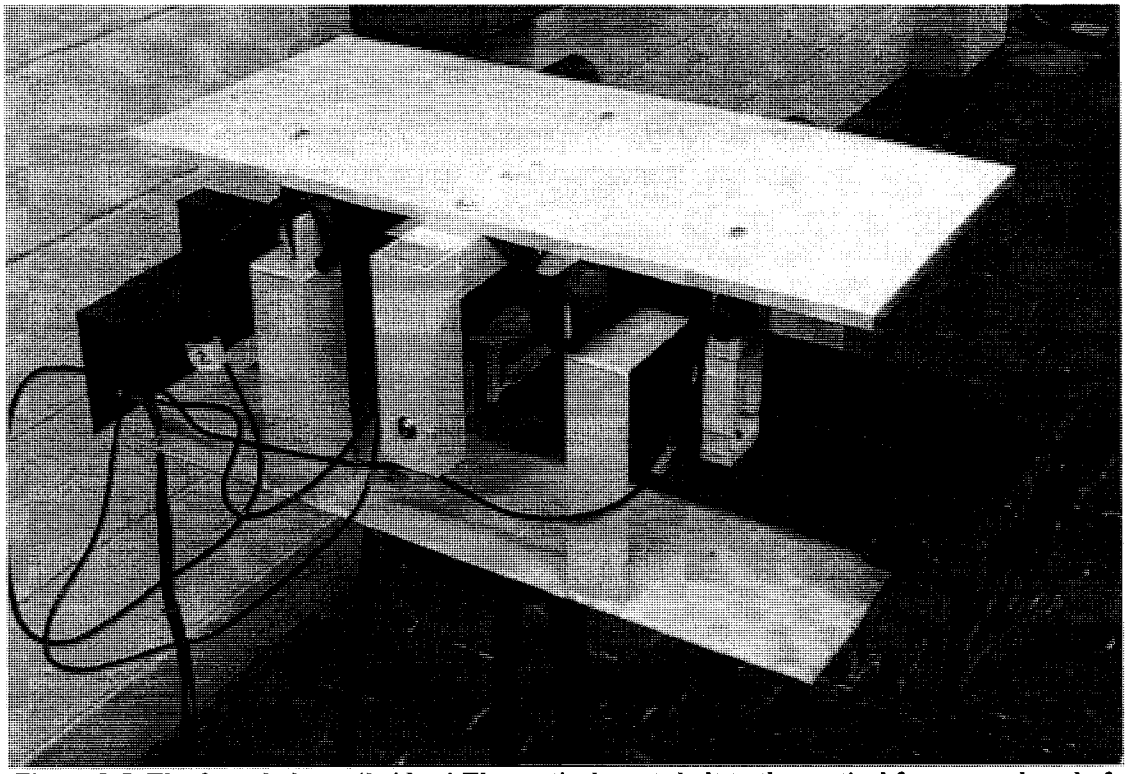

Figure 3-5. The force balance 'bridge.' The vertical masts bolt to the vertical face on each end of the bridge.

Complicating the measurement of forces were the wires which powered the cylinder drive motor and the wires which powered and read the force transducer outputs. Care was taken to bundle all of these wires together (ten in all) and run them to a fixed point on the tunnel test section in such a manner as not to interfere with the motion of

the force balance. The weight and stiffness of the wires themselves was accounted for during calibration.

3.1.3 Model Construction and Operation

In order to maximize the Reynolds numbers available during testing, the model was made as large as possible given the wind tunnel constraints. The Clark Y airfoil chord was 7.5 inches, the span was 24 inches, and it was fashioned by hand from balsa, basswood, and aluminum using paper templates that had been adjusted to the proper size (see Figure 3-6). The airfoil was as wide as possible without mechanically interfering with the walls of the tunnel. The airfoil was mounted on ½" diameter aluminum rods which penetrated the test section doors and clamped into the force balance on either side. This permitted the angle of attack to be adjusted manually (see Figure 3-7) and allowed the wing to be adjusted laterally for clearance against the wind tunnel doors (Figure 3-8). The angle of attack was measured manually against the chord line by means of a digital leveling yard stick. The slope of the wind tunnel itself was taken into account during these measurements, as well as the difference between the flat bottom of the airfoil and the actual chord line.

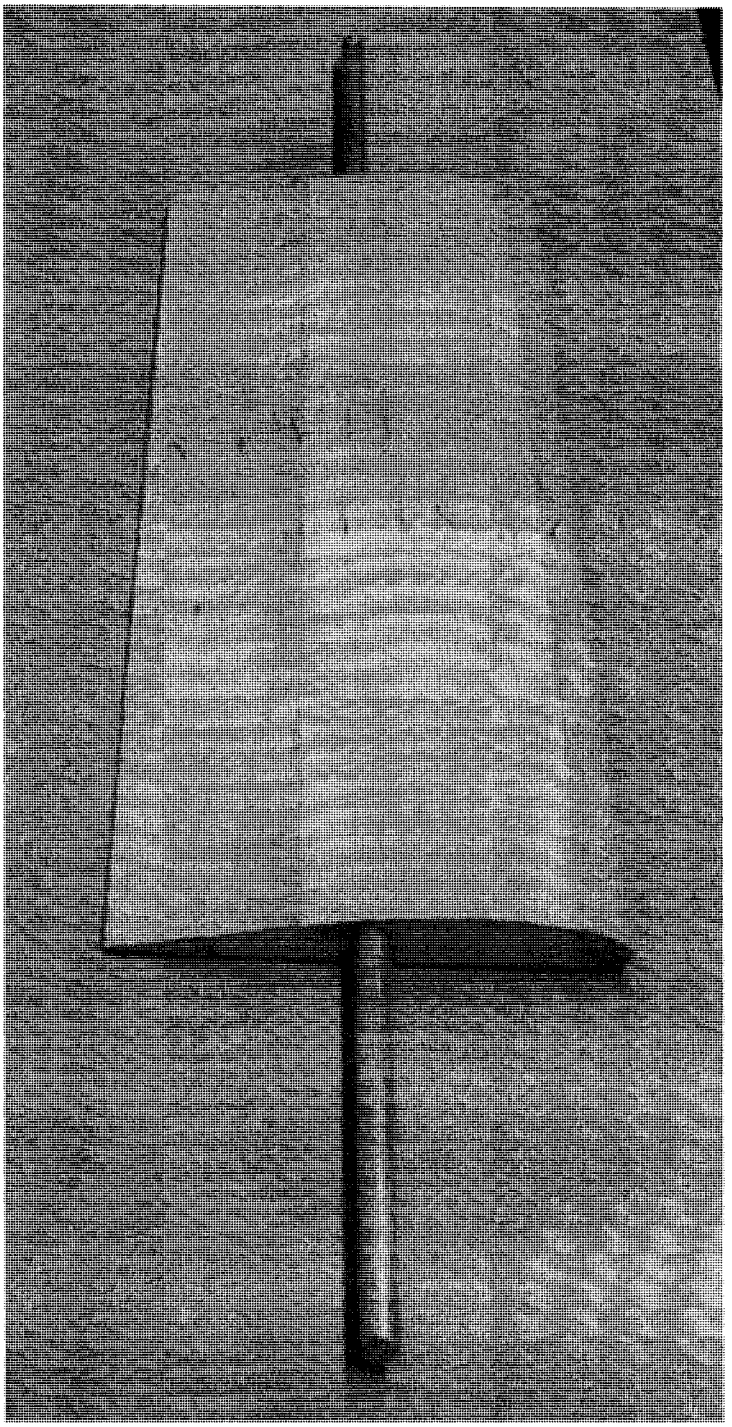

Figure 3-6. Picture of the Clark Y airfoil model

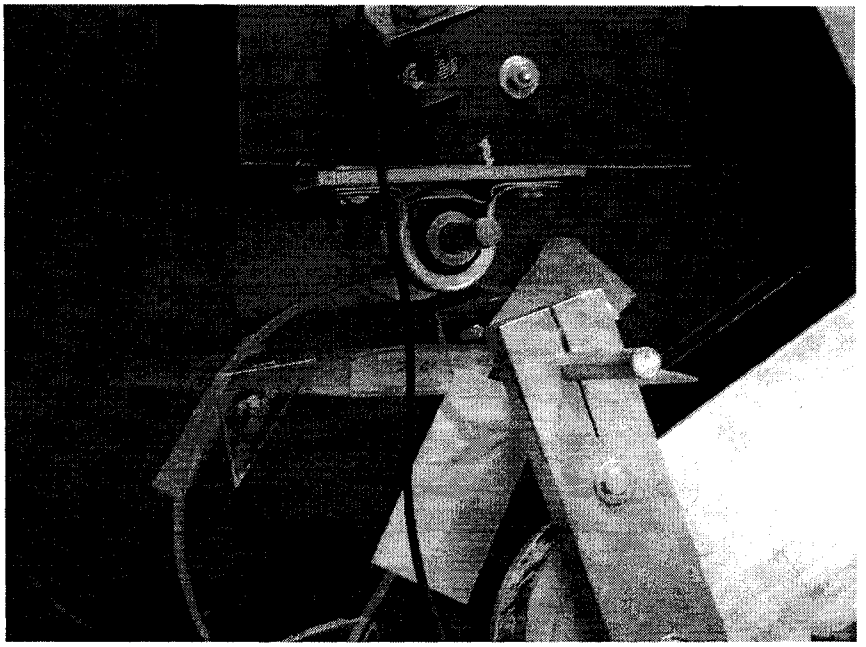

Figure 3-7. Picture of the airfoil mounting clamps which permit the angle of attack adjustment

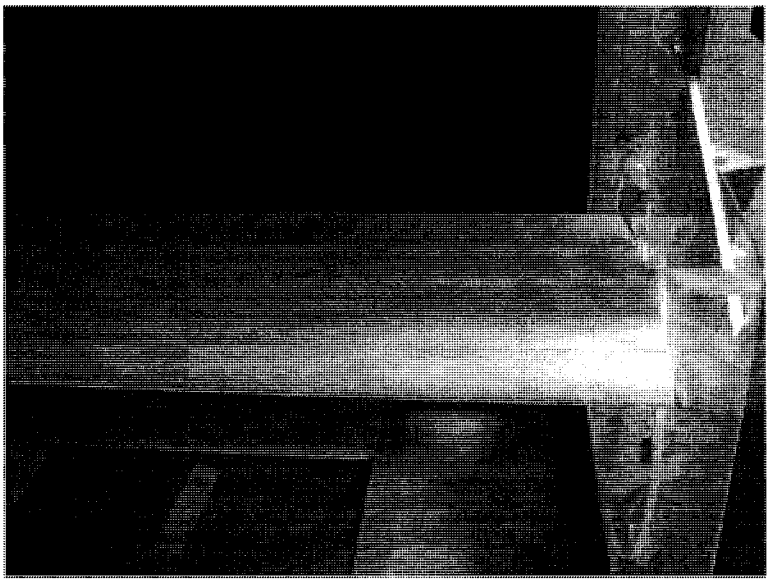

Figure 3-8. Picture from inside test section showing airfoil mounting

To test the effect of cylinder position relative to the airfoil, it was necessary that at least one of the two items be adjustable, both vertically and horizontally. The weight and mechanical complexity of the cylinder and drive system made the airfoil the obvious choice. Therefore, provision was made in the design of the force balance that would allow the airfoil to be moved up and down as well as fore and aft. The two airfoil clamps, one on each side, were mounted on two-bar arms which permitted a wide range of motion (see Figure 3-9). The procedure for adjusting the position of the wing required two people, one on each side. First all the bolts were loosened, then the arm was held in approximate position while the 'shoulder' 'elbow' and 'wrist' bolts were made just snug, which allowed for fine adjustments before final tightening. The angle of attack could be adjusted much more simply, requiring the loosening of only the 'hand grip' bolts. Care was taken during testing to see that the arms which held the airfoil had not shifted. For the handful of times that shift occurred out of thousands of runs, the test was repeated.

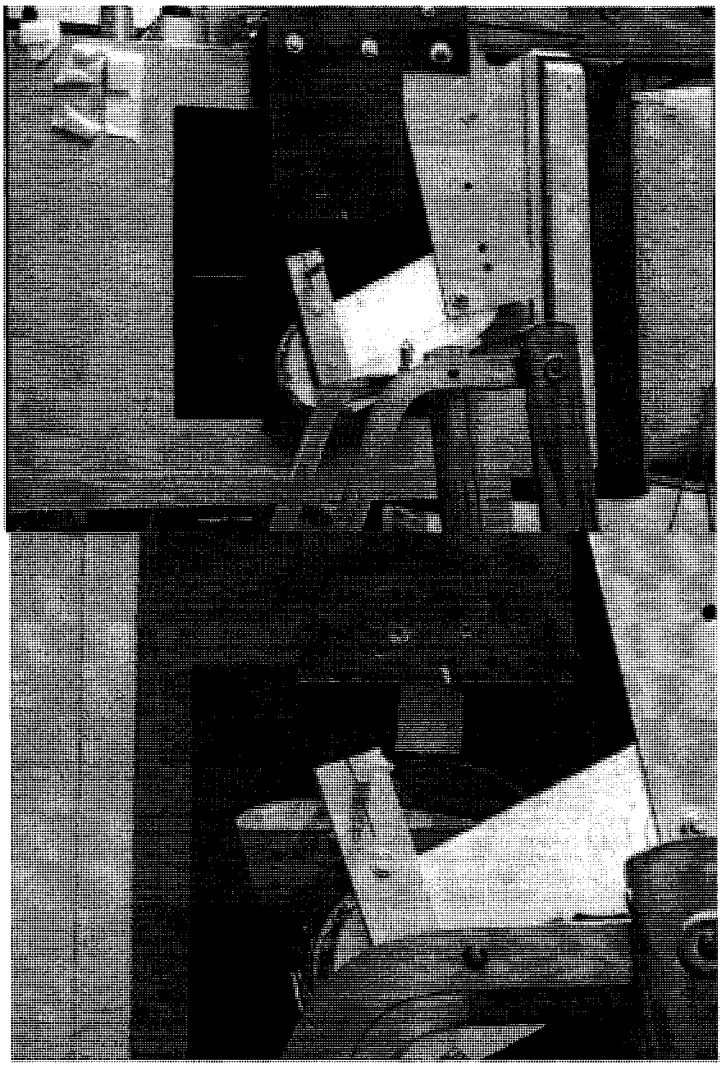

Figure 3-9. Two-bar arms and 'hands' used for airfoil mount support and movement

The rotating cylinder was mounted to two permanently fixed vertical masts, separate from the airfoil arms. One mast held the 1/3 horsepower 24 Volt DC Dayton motor which was used to drive the cylinder, as well as the custom-built single speed belt drive transmission (see Figure 3-10). It was estimated that the cylinder would need to turn as fast as 30,000 RPM, requiring a transmission. The transmission consisted of only two pulleys, a 9" diameter cast iron balanced drive pulley fixed directly to the

motor shaft, and a 2.5" aluminum pulley fixed directly to the rotating cylinder axle, and a V-belt. Instead of using an idler pulley and adding resistance to the system, the belt tension was adjusted using spacers underneath the cylinder ball bearing mounts. A great deal of experimentation was required to find a belt which would function at the higher speeds. The belts and pulleys were designed for a belt speed in the range of 1,000-4,000 feet per minute, and were being pushed to well over 15,000. At very high speed, often the V-belt would 'flip' over in the groove as the inertial forces became very high, and this caused a large increase in resistance. Finally a deep-groove belt was located through the Brewer Machine & Gear Co. that functioned well for most of the tests. The cylinder rotated on standard mounted sealed ball bearings (rated for roughly 3,000 RPM) which had been modified for the unusually high speeds (ball bearings designed for 30,000+ RPM were unavailable). Testing showed that the bearings would overheat above 10,000 RPM. It was deduced that the packing grease was actually causing friction and heat build up at high RPM. The seals were removed; the viscous packing grease was eliminated and replaced with a low-viscosity aerosol lubricant, ACF-50, and the resistance decreased dramatically. The bearings were lubricated regularly, and only two bearings failed during many hours of testing.

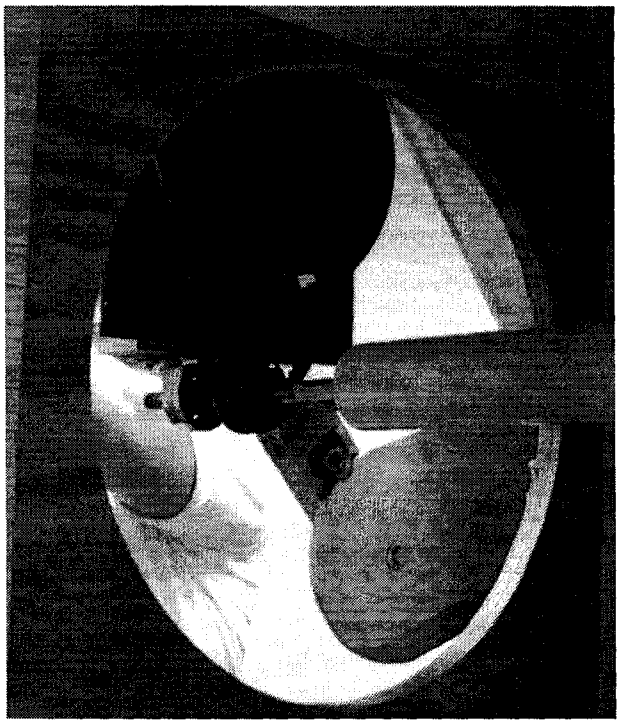

Figure 3-10. Single-belt transmission as seen from inside the test section

The 2" diameter cylinder was made of solid aluminum. The cylinder was 24" long and fitted with turned, ground, and polished ½ inch diameter steel rod axles which penetrated the wind tunnel doors in the same manner as the airfoil mounting rods (see Figure 3-11). Because it was thought that thin aluminum rod axles might fatigue and fail during operation it was decided to fit the steel axles for safety. The holes were drilled and bored on a lathe with as much precision as possible to maintain balance. A set screw arrangement would not have permitted a centered axle, so the steel axles were interference-fitted into the cylinder. The cylinder was heated to near melting temperature with an acetylene torch, and the steel rod was cooled to below freezing, and was driven in to the cylinder with a sledge hammer. Then the axles were

'adjusted' while the cylinder turned to make them as straight as possible. Ultimately, the cylinder ran smoothly as high as 40,000 RPM in testing, and the design and fabrication techniques were considered successful. A great deal of effort was expended to make 1" diameter and ½" diameter cylinders operate smoothly, but those efforts were ultimately unsuccessful. It appeared that the natural frequency of those cylinders was considerably less than for the 2" cylinder, and could be excited during the tests, making it impossible to operate safely. It was decided to go-ahead with only the 2" cylinder.

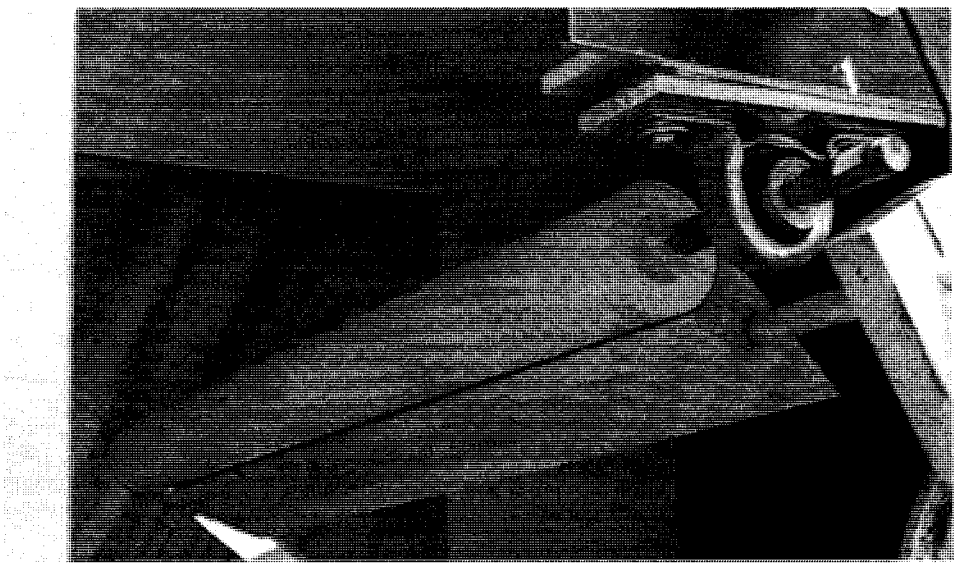

Figure 3-11. Pictures of 2" cylinder installed in the wind tunnel test section with a 3" fairing

The drive motor was powered by four Shenzen-Mastech DC Power Supplies, capable of providing as much as 600 Watts each at 30 Volts and 20 Amps. Depending on loading, the drive motor could be either current or voltage constrained, that so the

power supplies were re-wired in parallel, series, or dual-parallel-dual-series depending on the test being conducted. The motor was driven using up to 60 Volts and 40 Amps, and was monitored to prevent overheating, which never became an issue. Motor RPM was controlled by adjusting the output voltage of the power supplies. Generally, as the motor RPM would increase, the speed would be adjusted using only one power supply until it was saturated, and then the next power supply in series would be used to control the motor and so on. A great deal of heat was generated during operation of the power supplies, and one failed during testing.

The RPM was read directly on the cylinder shaft by an optical sensor and reflective tape (see Figure 3-12) which was connected to a Monarch Instrument Panel Tachometer. The complete model and support structure weighed over 70 pounds.

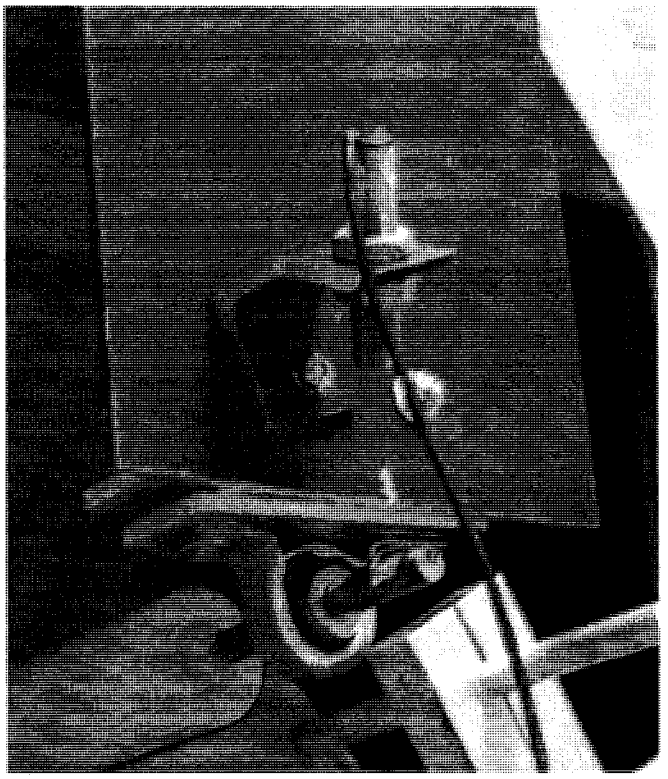

Figure 3-12. Optical tachometer sensor and axle with reflective tape

3.1.4 Wind Tunnel Doors

Perhaps the single most perplexing problem encountered during the operation of the wind tunnel balance/model system was determining how to support the airfoil and drive the cylinder through the test section doors, while avoiding any mechanical interference which would compromise the data, providing a smooth surface inside the test section, providing as tight a seal as possible, and while accommodating wide and regularly changing model geometries. Another problem was that the force balance itself would prevent opening or closing hinged doors.

After a set of prototype doors were constructed, a design was settled on. It fit in the spaces left by the existing doors which were removed, could be installed and removed at any time, and accommodated the model through the full desired range of motion. Each door was a four piece design (see Figure 3-13). The outer two pieces filled in the door leaving only a circle, in to which the inner two pieces could be inserted. The inner pieces fit together leaving a slot, which allowed the cylinder drive shaft through the center of the circle, and by rotating the inner two pieces the slot could accommodate the airfoil support shaft through any location within the azimuthal range of motion of the slot. One door was made of plywood and the other machined from solid Plexiglas to retain visibility. The doors were shimmed to avoid mechanical interference with the model (see Figure 3-14), and once the doors and models were in position, the larger gaps were sealed with masking tape to minimize leakage.

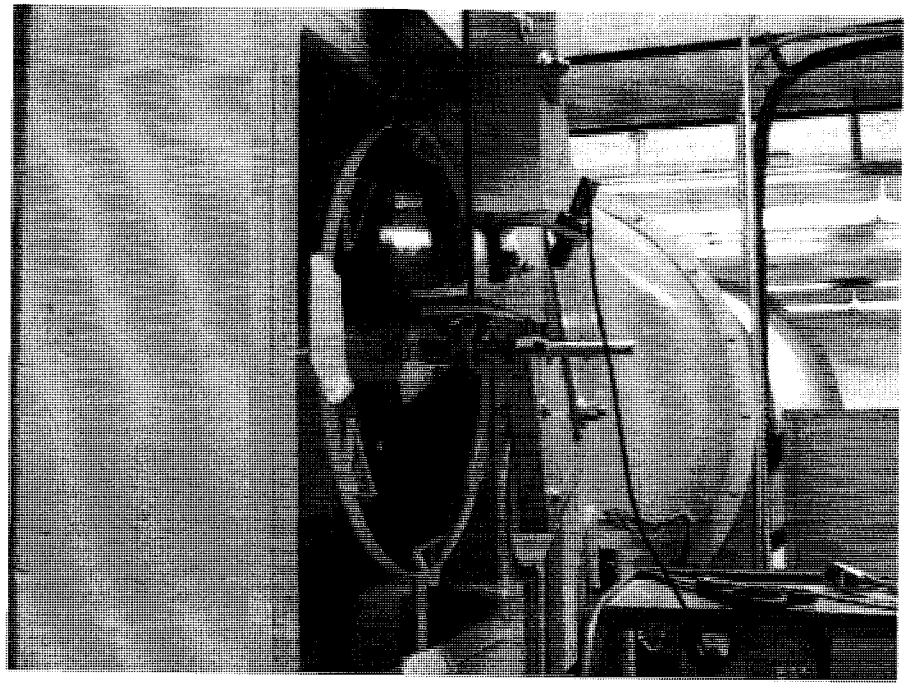

Figure 3-13. Plexiglass wind tunnel door shown with wing directly behind cylinder

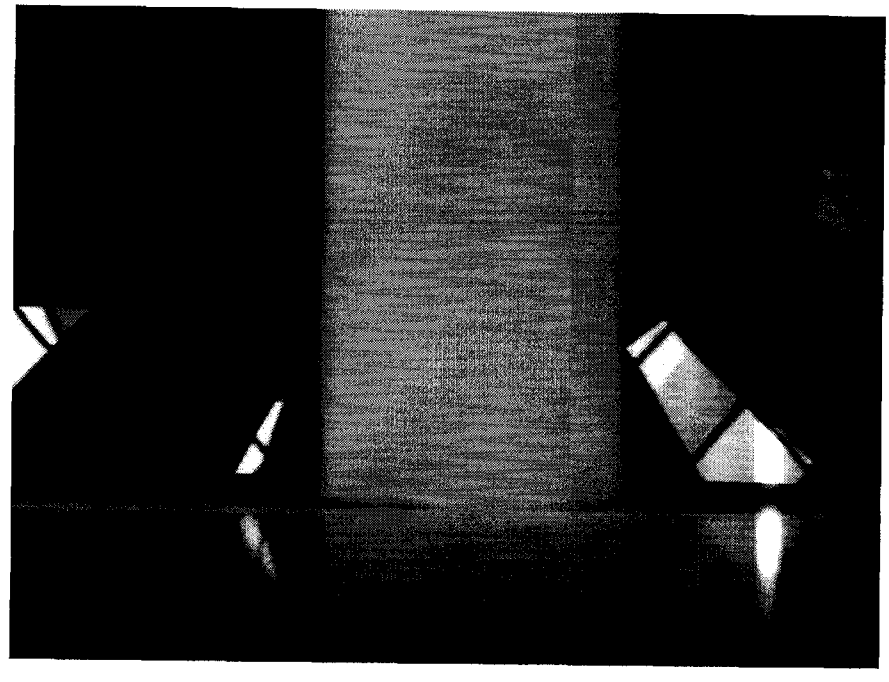

Figure 3-14. View from inside the test section showing the typical cylinder clearance against the doors.

3.1.5 Data Acquisition System

The force transducers were Model LCCA-50 high-accuracy S-beam load cells from Omega Engineering, Inc. with a 50 pound capacity and 0.037% full scale accuracy. The load cells were excited by a high precision 10V power supply. The transducer outputs were fed into an Inet-100HC A/D box to convert analog signals from the transducers to digital signals. The signals from the Inet-100HC were fed into an Inet-230 PC card controller installed in a laptop computer (see Figure 3-15). Software allowed the transducers to be set up and calibrated from the laptop, and made provisions for the data to be read and saved in an Excel spreadsheet format. The equipment had the capacity to take readings from the transducers at 1000 Hz, and for these tests was set to collect readings for two seconds.

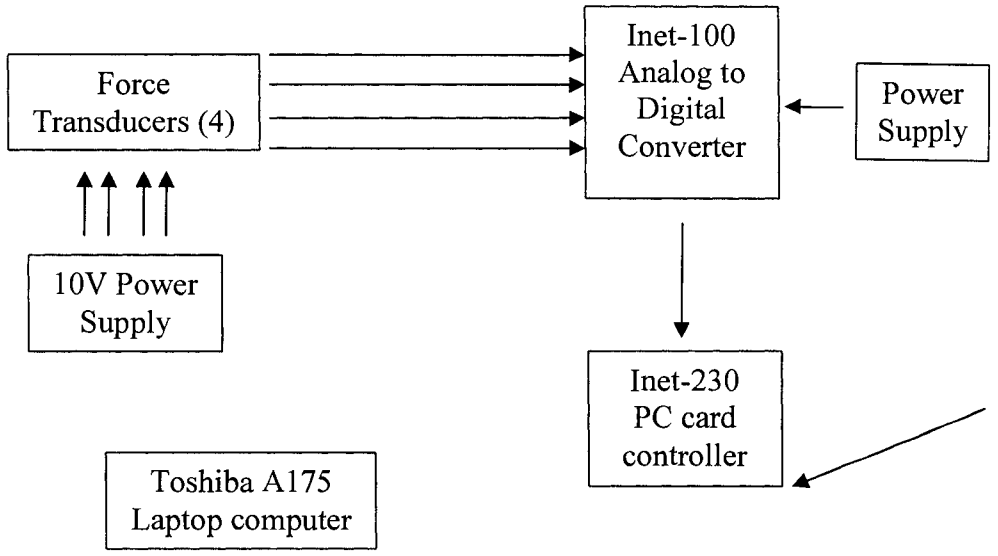

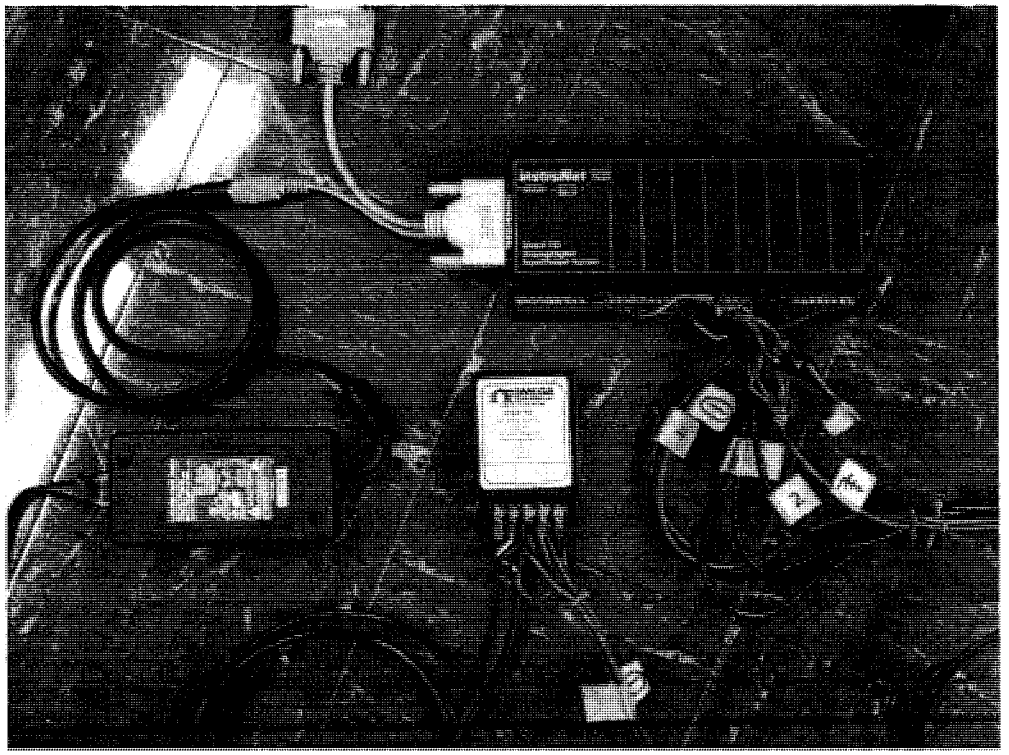

Figure 3-15. Force data acquisition schematic and photograph

3.1.6 Calibration

Calibration was done with consideration given to the anticipated loads for the test. For light loads, precision weights of various masses were hung in sequence from the center of the rotating cylinder for lift. For drag, a string was wrapped around the center of the cylinder and run over a pulley to apply the force horizontally to the cylinder. The flexures performed very well in separating the lift and drag forces. After construction, it was realized that the double-flexure design did not accurately transmit moments and rendered any attempts to calculate pitching moment inaccurate. As a result, the tests produced only lift and drag forces.

For moderate forces (10-20 pounds), some hunks of metal were weighed on a triple-beam balance and used in the manner described above to provide sufficient force to the balance for calibration. For large forces, care had to be taken not to saturate the force transducers. The model was mounted upside down for many of the tests to eliminate mechanical interference between the airfoil support arms and the cylinder drive shaft. Often a large deadweight was fastened to shift the center of mass of the rig away from the saturating sensor (see Figure 3-16). To calibrate for these tests, reams of paper were weighed and marked, then stacked on top of the 'bridge.' Care was taken to apply the load near the plane of the rotating cylinder, and near the center of the test section. Often more than 10 reams (50 pounds) were required to sufficiently calibrate the very large lift generated by the Vortex Flap during testing.

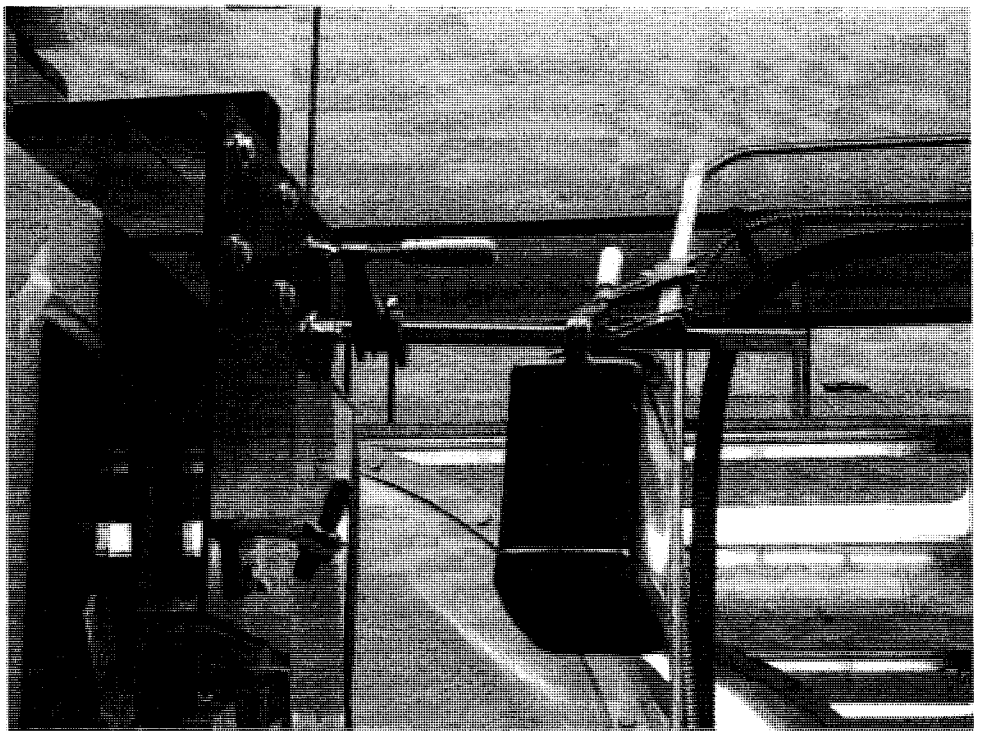

Figure 3-16. Deadweight typical of those used to prevent transducer saturation

This type of thorough calibration was conducted at least twice per day at the open and close of testing, and more frequently in cases where the model configuration was substantially changed. However, given the variable geometry of the airfoil supports, the center of mass of the rig often shifted between tests, and it was necessary to take a set of 'tare' data before every single group of tests and again afterward. This procedure allowed any sensor drift or mechanical creep to be detected. It was a rare occurrence, but a few tests were conducted more than once because of unacceptable mechanical creep or sensor drift. No attempt was made to explicitly calibrate the rig in

pitching moment; the double flexure design does not permit the accurate sensing of pitching moment..

3.1.7 Testing Method

It was desirable to conduct the tests over a range which included the highest possible Reynolds numbers coupled with the highest possible surface-speed-ratios (SSR, the ratio of the linear velocity of a point on the surface of the cylinder to the free stream velocity). Due to limitations on cylinder diameter and maximum RPM, the upper range of available Reynolds number and SSR was constrained.

To cover the widest possible range of parameters as quickly as possible, a testing hierarchy was devised. The most time consuming variables to change were changed least often, and the least time consuming variables to change were changed most often. The variables were changed according to the following hierarchy (Figure 3-17), from least to most frequent:

Basic Configuration→Airfoil position→Angle of Attack→Cylinder RPM→Air speed

Figure 3-17. Testing method hierarchy

A variety of basic configurations were tested, including cylinder only, Clark Y airfoil only, cylinder with flat plate, and cylinder with fairing. Also, some tests were run with a smaller cylinder at lower RPM, but a complete set was impossible.

3.1.8 Kinematic Restrictions

The airfoil and cylinder were supported separately, and their motion was not kinematically coupled. The wing position was set by the position of the wing support rod, located at the ½ chord point, and the cylinder drive shaft. The positions were set by measuring the center-to-center distances both vertically and horizontally. From that position, the wing was rotated through a range of angles of attack, usually 0, 5, and 10 degrees. However, since the cylinder did not rotate with the wing, the position of the cylinder relative to the wing changed when the angle of attack was changed. So, for example, the gap between the surface of the cylinder and the underside of the wing might vary considerably over the range of tested angles of attack in a given airfoil position.

To determine the performance of the wing-cylinder combination in a constant position relative to one another as the airfoil rotates through the range of angles of attack, it is necessary to interpolate the closest available data points from different position runs that occurred at similar wind tunnel speeds and cylinder RPM. Adjusting the position of the wing as well as the airfoil angle of attack between each test run would have unacceptably impeded the testing process, and since the optimum position was not known beforehand, this approach was considered acceptable. Ultimately, a Response

Surface Method approach was devised and used to ease the interpretation of the results of this testing approach.

The maximum RPM available on an extended basis was in the low twenty-thousands. Above this and bearing overheating became a concern. The cylinder RPM was usually set at 0, 5, 10, 15, 20, and 25,000 in sequence. Each of these RPM was run through the entire range of wind tunnel speeds, usually 0, 40, 60, 80, and sometimes 100 feet per second. It was expected from previous literature review that the range of interesting SSR would probably stretch from zero to six or eight. Due to cylinder RPM constraints, the upper range of SSR was not available at the upper range of wind tunnel speeds, so testing was only rarely conducted above 100 fps. Increasing the cylinder diameter was considered undesirable because of wind tunnel blockage effects, and the ratio of cylinder diameter to wing chord was at the upper limit of the desired range with the 2" cylinder. At these speeds, load cell saturation was also a concern.

3.2 Data Processing

Each testing point (a combination of a particular configuration, airfoil position, angle of attack, cylinder RPM, and air speed) produced 2,000 samples from each of the four load transducers in an Excel spreadsheet format. The data were examined early on to determine that the sample rate was sufficient to capture all of the significant vibration that the rig was experiencing, and cylinder vibration was easy to identify.

To condense the data to a single point, a simple average of the samples was calculated. This output, when compared to the 'tare' data for that group of runs (a group consisted of the entire range of wind tunnel speeds and cylinder RPM, but no other parameters were varied within the group) produced the net lift, drag, and moment for that testing point. These data were entered into a master spreadsheet for processing. The calibration data for each day were used to adjust the readings, and the 'tare' data taken at the beginning and end of each run were double checked to ensure that only acceptable drift had occurred. Possible sources of error include:

- Mechanical interference between the model and the wind tunnel
- Slippage of airfoil support arms
- Sensor drift
- Typographical error (much of the data processing was done by hand)
- Fabrication errors render the model an imperfect representation of the airfoil

4 Results

In this section, a comprehensive overview of the results of the wind tunnel investigation is presented. First, a dimensional analysis is presented which identifies the most important nondimensional parameters relevant to this investigation. Next is a discussion of the necessary adjustments and corrections that need to be made to the raw data. Following are the results, first in uncorrected and then in corrected form. The results are given a Response Surface Method treatment and presentation. Finally, the results are compared with the theoretical predictions of a potential flow analysis. Two things are evident from these results:

1) The Vortex Flap provides significant increases in lift.
2) The Vortex Flap provides a significant range of lift coefficient at a fixed angle of attack.

4.1 Dimensional analysis

To place the results of these experiments in proper context with respect to other experiments as well as full scale aircraft, it is necessary to nondimensionalize the results. The Buckingham Pi Theorem was applied to generate an appropriate list of nondimensional parameters for these experiments. The treatment of Munson, Young, and Okiishi (Munson, Young, and Okiishi 1998) was generally followed, and resulted in the following four Pi terms, for each system geometry:

Surface Speed Ratio (SSR):

The SSR is the ratio of the tangential velocity of a point on the surface of the rotating cylinder to the free stream velocity. The SSR serves to nondimensionalize the cylinder rotation speed, and is described by the following formula:

$$SSR = \frac{r\omega}{V} \tag{4.1}$$

Reynolds Number (Re):

The Reynolds number is the ratio of inertial fluid forces to viscous forces in the fluid medium. This serves to nondimensionalize the velocity and scale of the model, and is described by the following formula (Anderson 2001):

$$\mathrm{Re} = \frac{\rho V D}{\mu} \tag{4.2}$$

Coefficient of Lift (C_L):

The coefficient of lift nondimensionalizes lift, allowing the relative lifting effectiveness of a lifting surface or section to be compared to others. The coefficient of lift is described by:

$$C_L = \frac{L}{\left(\frac{1}{2}\right)\rho V^2 A} \tag{4.3}$$

Coefficient of Drag (C_D):

The coefficient of drag nondimensionalizes drag, allowing the relative drag of a surface or body to be compared to others. The coefficient of drag is described by:

$$C_D = \frac{D}{\left(\frac{1}{2}\right)\rho V^2 A} \tag{4.4}$$

The appropriate area to be used in the calculation of the lift and drag coefficients for an airfoil section is generally accepted as the wing area (chord multiplied by span). The addition of variable geometry devices complicates this somewhat. In the case where the deployment of a trailing-edge high-lift device increases the wing area, the coefficients can be calculated either on the basis of the original wing area or the wing area with the device deployed. The data can be presented either way, and of course the difference will be a simple factor equal to the ratio of areas.

When the data are presented with the coefficients calculated on the basis of the undeployed wing area, it gives the impression that the trailing edge devices are even more effective than they would appear were the data presented on the basis of the increased area. This presentation is still germane, however, because the typical intended application is to a particular full-scale vehicle, and allows one to observe the increase of lift or drag that the device would provide the aircraft when deployed. The

coefficients based on the increased post-deployment wing area are sometimes referred to as 'transformed' and would require the reader to account for the increase in area as well as any increase in coefficient in order to interpret the data properly (Hoerner and Borst 1985).

For permanently deployed external flaps, it is reasonable to include the area of the flap as a part of the total wing area, which is analogous to the 'transformed' values above. However, in the case of the vortex flap, it is not at all certain that the cylinder would be permanently deployed. In fact, given the large drag associated with a large rotating cylinder, it is very likely that such a device would be retracted during cruise operations. As such, it seems reasonable to use the airfoil area alone as the reference wing area. In this paper, coefficients will be calculated with the airfoil area alone as the basis, except when otherwise noted.

The lift increment due to deployment of the Vortex Flap will also be calculated and presented. For the purposes of this paper, the deployment can be thought of in two stages. First, the stationary cylinder is placed in position behind and underneath the wing. This location produces a significant change in lift and drag due largely to the circulation effect. Second, as the cylinder begins to rotate, the lift and drag change according to the SSR.

The lift increment can be calculated two ways. One incorporates the entire effect of the Vortex Flap. The second isolates the effect of the rotation of the Vortex Flap from the effect of the presence of the stationary cylinder. The first lift increment calculated is $\Delta C_{L,total}$ and is calculated by comparing the lift coefficient of the wing with the deployed vortex flap with the lift coefficient of the airfoil alone at the same angle of attack. The second lift increment calculated is $\Delta C_{L,rotation}$ and is calculated by comparing the lift coefficient of the wing with the deployed vortex flap with the lift coefficient of the wing with the deployed, but stationary, vortex flap.

4.2 Corrections to data

The test was designed to be as two dimensional as possible, with the exception of small clearances required to prevent mechanical interference, and the test section boundary layer itself. There is a great deal of variation to account for when processing and interpreting the data from a wind tunnel investigation. The treatment chosen is not comprehensive, but contains the corrections most relevant to the Vortex Flap investigation. The treatment of Barlow (Barlow 1999) and Thom (Thom 1943) is generally followed here.

Horizontal buoyancy

The growth of the boundary layer on the test section walls causes the flow to be gradually 'squeezed' as it progresses through the test section. For incompressible flow, this has the effect of causing the air to accelerate, creating a static pressure gradient in the tunnel which tends to 'draw' the model down the tunnel. The total drag increment in a tunnel with a constant gradient is

$$D_B = \frac{1}{2}\pi\lambda_2 t^2 p' \qquad \text{lb/ft span} \tag{4.5}$$

Where t is the body thickness and λ_2 is the body shape factor. In the case of the airfoil and cylinder together, the thickness is taken to be the thickness if the cylinder and airfoil simply added together. Figure 4-1 contains the relevant information for this correction.

Model	Thickness t (feet)	Body shape factor
Airfoil	0.073125	4.2
Cylinder	0.1667	1
Airfoil and cylinder	0.2398	2

Figure 4-1. Thickness and body shape factor for each model

Horizontal buoyancy effects are pronounced for bodies with significant length and volume such as nacelles and fuselages. For the configurations tested, the correction should be insignificant, particularly for an airfoil and unswept spanwise cylinder. The effect of horizontal buoyancy is to draw the model downstream, artificially increasing the measured drag; thus, not making this correction will only make the performance estimates based on data from this investigation more conservative. Since the static pressure gradient information needed for this correction is not readily available, and neglecting this correction does not artificially improve the perceived performance, this correction will not be applied to the data.

Solid Blockage

For approximately incompressible flow, continuity requires that the presence of the model in the test section act to constrict the flow around the model, causing the local velocity to increase somewhat compared to the 'free' stream velocity in the test section. This increase causes the lift and drag to be higher than in the free stream, and must be accounted for as an incremental increase in the velocity used to calculate the relevant coefficients. Following the treatment of Thom (Thom 1943)

$$\frac{\Delta V}{V_u} = \varepsilon_{sb} = \frac{K(Volume))}{(BH)^{3/2}\left(\sqrt{1-M^2}\right)^n} \tag{4.6}$$

where V_u is the uncorrected velocity, $K = 0.63$, *Volume* refers to the model volume, B is the test section width, H is the test section height, M is approximately zero, and $n = 3$. The volume of the various model configurations are tabulated in figure 4-2.

Model configuration	*Volume (ft^3)*
Plate	0.013021
Clark Y	0.063984
Cylinder	0.043633
Plate + Cylinder	0.056654
Clark Y + Cylinder	0.107617

Figure 4-2. Volume of various tested model configurations

The effect of this correction will be to increase the effective dynamic pressure used to calculate the lift and drag coefficients, and thus reduce the values of the coefficients themselves. The solid blockage correction for each configuration is tabulated in figure 4-3.

Model Configuration	ε_{sb}
Plate	*0.001025*
Clark Y	*0.005039*
Cylinder	*0.003436*
Plate + Cylinder	*0.004462*
Clark Y + Cylinder	*0.008475*

Figure 4-3. Solid blockage correction for various tested model configurations.

Wake Blockage

The thickness of the model wake itself will have a constricting effect similar to the presence of the model, causing the velocity outside the wake in the test section to be higher. This velocity increase results in decreased pressure downstream of the model, which creates a pressure gradient and adds a velocity increment at the model. The solid blockage effect for a typical streamlined body can be calculated as (Barlow 1999)

$$\varepsilon_{wb} = \frac{\Delta V}{V_u} = \frac{c/h}{4} c_{du} \tag{4.7}$$

Where c is the model chord, h is the test section height, and c_{du} is the uncorrected section drag coefficient. The calculation for the airfoil + cylinder configuration is complicated somewhat by the presence of two bodies with generally distinct wakes, as well as the blunt-body character of the cylinder. Thom suggests a more complicated

expression which generally approximates the expression given above, but which varies significantly for a blunt body. This expression is

$$\varepsilon_{wb} = \frac{C_D c}{H}\left\{\frac{1}{4} + \frac{3}{16}\sqrt{\frac{\mu c}{H}} - \frac{\pi}{36}\frac{c}{H}\right\} \tag{4.8}$$

Where C_D measured drag coefficient, c is the chord. H is the test section height, μ is about 0.1 for an airfoil and 10 for a circular cylinder. Calculating the wake blockage for either the airfoil or the cylinder individually is a simple matter.

For the combined configuration, the equation must be modified somewhat from the form presented in the literature. If the drag force on the cylinder and airfoil were measured separately, the blockage corrections could simply be added together in the form of equation 4.8. However, the combined drag for both components is the only information available, so the author proposes the equation be written

$$\varepsilon_{wb} = \frac{C_D{}^* c^*}{H}\left\{\frac{1}{4} + \left[\frac{3}{16}\sqrt{\frac{\mu_a c_a}{H}} - \frac{\pi}{36}\frac{c_a}{H}\right] + \left[\frac{3}{16}\sqrt{\frac{\mu_c c_c}{H}} - \frac{\pi}{36}\frac{c_c}{H}\right]\right\} \tag{4.9}$$

where

$C_D{}^*$ = total measured drag coefficient, calculated based on the airfoil area

c^* = chord used for calculating $C_D{}^*$

H = test section height

subscript a denotes an airfoil parameter

subscript c denotes a cylinder parameter

which produces the corrections listed in figure 4-4.

Model	ε_{wb}
Airfoil (plate or Clark Y)	$0.079961 * C_D{}^*$
Cylinder	$0.034491 * C_D{}^*$
Airfoil and cylinder	$0.131177 * C_D{}^*$

Figure 4-4. Velocity increment due to wake blockage for each model

The size of the wake is physically correlated to the amount of drag, so it is logical that the wake blockage correction is a direct function of the drag coefficient. The correction is relatively minor, on the order of just a few percent, for a broad range of drag coefficients. However, when large-scale flow separation causes the drag coefficient to be on the order of 1, the wake blockage correction is on the order of tens of percent, and has a substantial depressive effect on the corrected values of lift and drag coefficient.

It should be noted that an alternative approach for the bluff body and stalled airfoil cases exists, put forth by Maskell (Maskell 1963). With some derivation, it can be written in the form

$$\varepsilon_{wb} = \frac{\epsilon c C_D}{2w} \tag{4.10}$$

For the combined cylinder and airfoil configuration

$\epsilon = 1$

c = chord of airfoil

w = width of tunnel

This correction is explicitly for bodies with extreme separated flow, but results in corrections only slightly more conservative than found above. A comparison follows in figure 4-5.

Configuration	*Thom-Buerge*	*Maskell*
Airfoil + cylinder	$0.13118*C_D$	$0.15625*C_D$

Figure 4-5. Comparison of two methods for calculating the wake blockage correction.

It is the opinion of the author that the former correction is sufficient for this investigation. The Maskell correction does not reflect the hybrid nature of the model, with both blunt and streamlined forms. As a result, the Maskell correction is thought too aggressive in the extreme cases, particularly when the drag coefficient exceeds 1.5. The data calculated using the Maskell correction does not make physical sense within the context of the larger body of data by suggesting, for example, that the drag in extreme cases would decrease with increasing SSR. It is likely that this correction is too sever, and artificially depresses the lift coefficient obtained in these cases. The author questions the utility of the Thom-Buerge in these extreme cases as well, but the correction is less severe.

Streamline Curvature

In a manner analogous to the effect of the ground on a landing aircraft, the floor and ceiling of the test section prevent the streamlines from deflecting normally, which artificially increases the lift and pitching moment at a given angle of attack. Note that the effect on a 3-D test would be to reduce the induced drag as well, but there is no

induced drag to be reduced in a 2-D flow. The effect on lift is relatively small and can be calculated as (noting that the author has corrected a sign error in the text of (Barlow 1999))

$$\Delta c_{l,sc} = -\sigma c_l \tag{4.11}$$

$$\Delta \alpha_{sc} = \frac{\sigma c_l}{2\pi} \tag{4.12}$$

where

$$\sigma = \frac{\pi^2}{48}\left(\frac{c}{h}\right)^2 \tag{4.13}$$

so for these models

Model	*Lift coefficient increment*	*Angle of attack increment (radians)*
Airfoil	$0.02008*C_L$	$0.0031196*\alpha$
Cylinder	$0.001428*C_L$	$0.000227*\alpha$
Airfoil and cylinder	$0.02008*C_L$	$0.0031196*\alpha$

Figure 4-6. Lift coefficient and angle of attack increment for models

Summary of Corrections

The corrected values for angle of attack, lift coefficient, and drag coefficient can be calculated as follows.

$$\alpha = \alpha_u + \frac{\sigma c_l}{2\pi} \tag{4.14}$$

$$c_l = c_{l,u}\left(1 - \sigma - \varepsilon_{sb} - \varepsilon_{wb}\right) \tag{4.15}$$

$$c_d = c_{d,u}\left(1 - 3\varepsilon_{sb} - 2\varepsilon_{wb}\right) \tag{4.16}$$

$$\sigma = \frac{\pi^2}{48}\left(\frac{c}{h}\right)^2 \tag{4.17}$$

These can be calculated using the parameters summarized in the figure 4-7. Sample calculations showed that the corrected angle of attack was within the precision of the original measurements, so the uncorrected angle of attack was used in all figures.

Model	*Chord (in.)*	σ	ε_{sb}	ε_{wb}
Plate	7.5	0.02008	0.001025	0.079961*C_D
Clark Y	7.5	0.02008	0.005039	0.079961*C_D
Cylinder	2.0	0.001428	0.003436	0.034491*C_D
Plate + cylinder	7.5	0.032117*	0.004462	0.131177*C_D
Clark Y + cylinder	7.5	0.032117*	0.008475	0.131177*C_D

**calculated using the combined chord = 9.5" to make the corrections conservative*

Figure 4-7. Summary of wind tunnel correction parameters.

4.3 Results

Following are the data from the wind tunnel investigation. Only a small fraction of the tests performed are plotted here, and a great deal of experimentation was done with cylinder positions above the airfoil, rather than below. The initial results from the above-the-wing work suggest that additional investigation may be justified (see Appendix B for a more in-depth discussion). For the purpose of this paper, only the results from the below-wing trailing-edge high-lift device configuration will be presented and discussed. The full results for the Vortex Flap are presented in Appendix A.

First the data from the Clark Y airfoil tests are presented to verify the validity of the general wind tunnel results and to establish a baseline from which to calculate the performance of the Vortex Flap. Second, the results of the cylinder-only testing are presented. Finally, a summary of the Clark Y plus cylinder data is presented. For a more comprehensive collection of data, and full-size graphs, see Appendix A.

4.3.1 Clark Y Airfoil Results

The performance of the Clark Y airfoil model is presented in figure 4-8.

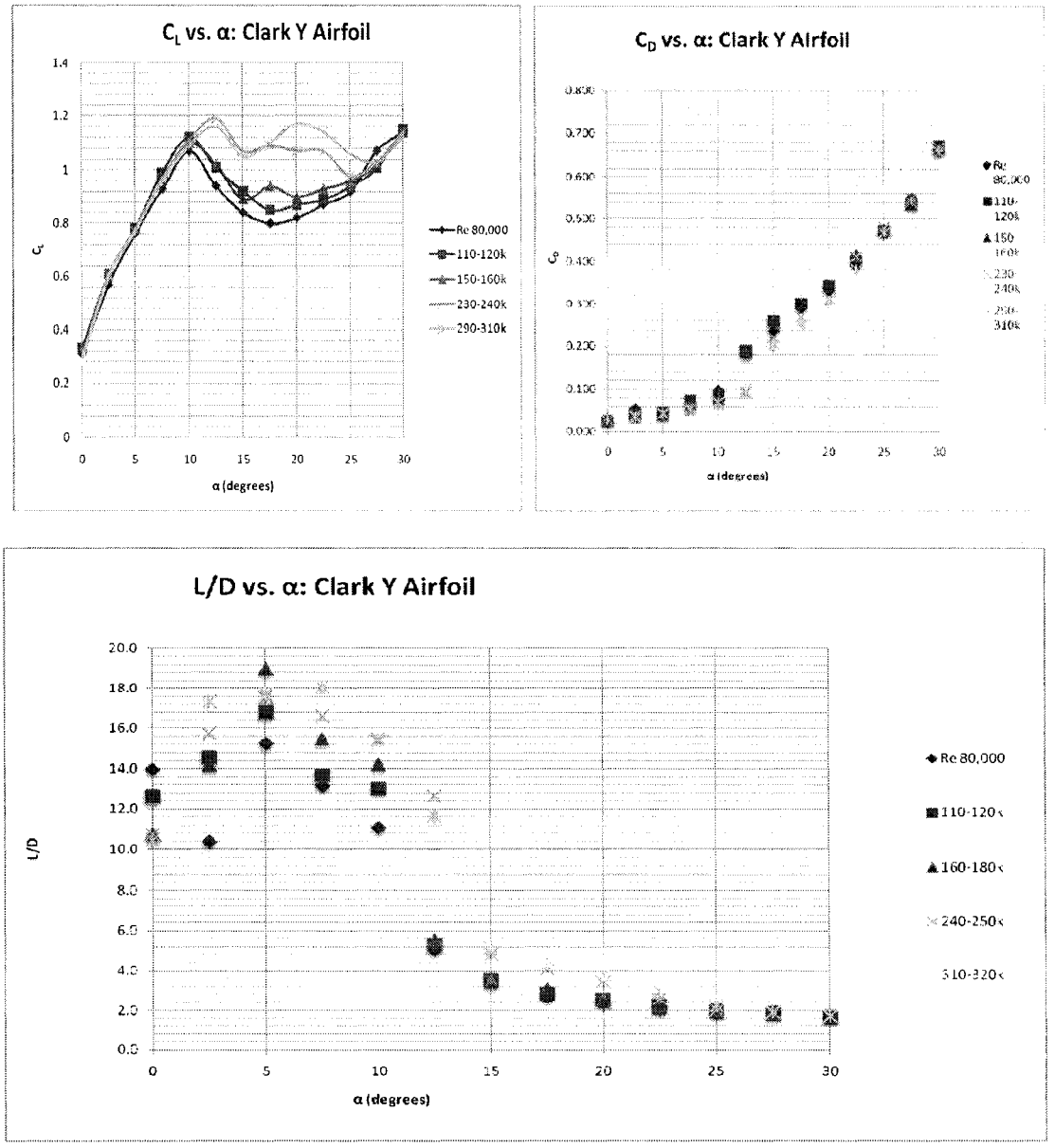

Figure 4-8. Clark Y wind tunnel results summary.

The angle of attack range presented for the airfoil exceeds the range for the Vortex Flap configuration by a factor of three. There are two reasons for including these data. The first is that the expected effect of the cylinder was to increase the circulation around the airfoil, making it behave as if it were operating at a higher angle of attack, so the data were included so reasonable expectations could be developed as to the behavior in this range. The second is to verify that the wind tunnel corrections affected the data in a reasonable manner, and the wind tunnel corrections only become significant at the higher angles of attack for the Clark Y airfoil. See Appendix C for a comparison with "uncorrected" values.

No two tunnels ever produce identical data even for equivalent tests. Further, the model produced for this investigation is not identical to the models produced for other investigations, and being hand-made, does not reproduce with complete fidelity the intended airfoil section. The results of similar tests, then, must be used to verify the general acceptability of the data for this investigation, and not the ability of the investigation to reproduce exactly another test. Given the inconsistencies inherent in different wind tunnel investigations, the data obtained compared well with those available from other tests (see Selig, Fraser, and Donovan 1989 and Simons 2002). Note that the "second rise" in lift evident in the data obtained is normal behavior and mirrors closely similar behavior obtained at very high angles of attack shown in other investigations (Critzos, Heyson and Boswinkle 1955).

4.3.2 Rotating Cylinder Results

Figure 4-9 shows the wind tunnel results for the rotating cylinder.

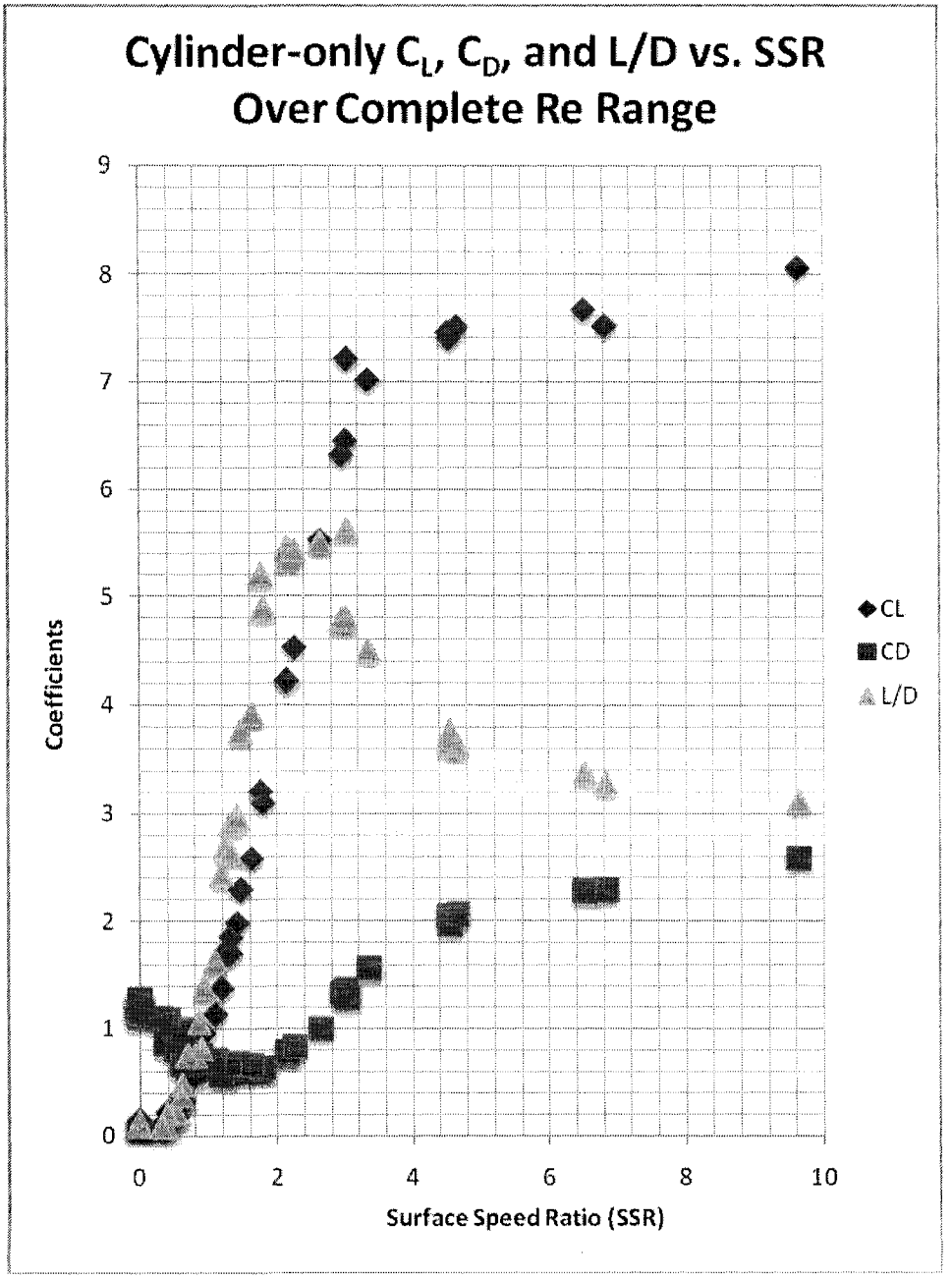

Figure 4-9. Cylinder only lift coefficient, drag coefficient, and L/D vs. SSR.

The Reynolds number range for these tests was 20,000-150,000. The tests at higher SSR were conducted at lower Reynolds numbers, in general (see figure 4-12). Data widely available in the literature are drawn from a relatively small number of original sources. The most complete, and most often cited, tests were reported in NACA Technical Note No. 209, and those data are re-plotted in figure 4-10. These tests were conducted in a Reynolds number range of 50,000-118,000 (estimated by the author) and in a manner also reflected in figure 4-11; the higher SSR tests were conducted at lower Reynolds numbers. There were no apparent wind tunnel corrections applied to the data.

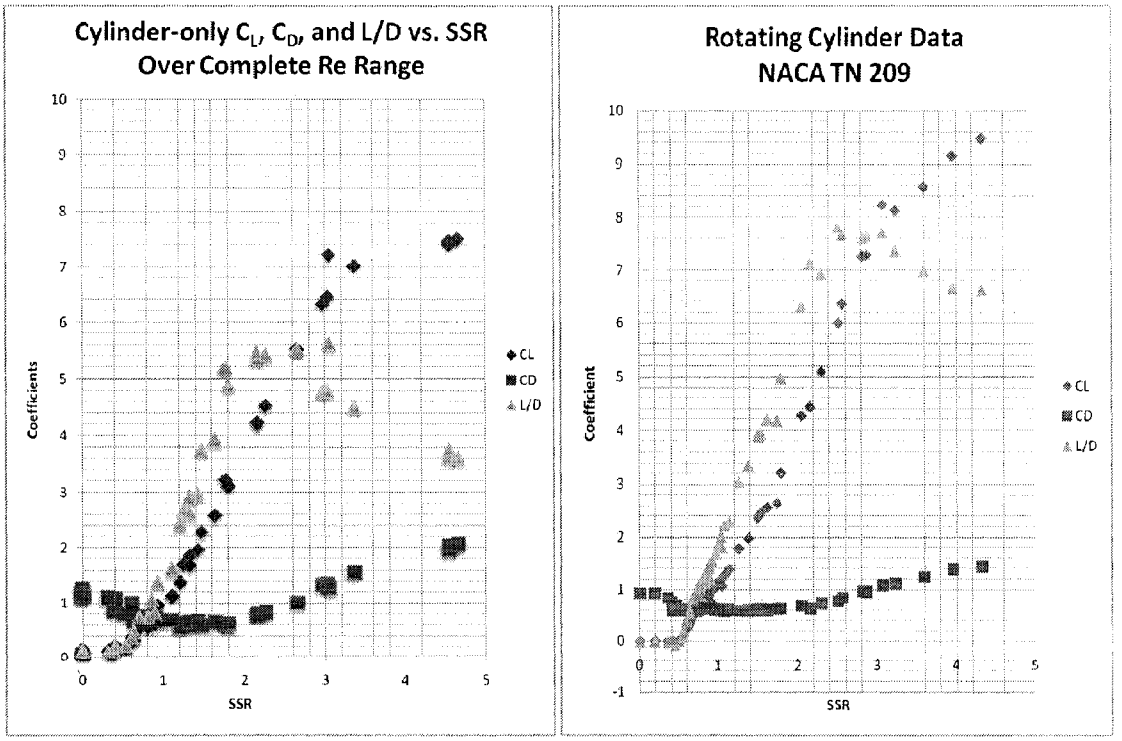

Figure 4-10. Comparison of data to that from NACA TN 209

Overall, the data from the NACA investigation compares well to that obtained in this investigation. The trends in lift, drag, and L/D share the same basic form. The major differences are lower lift and higher drag at low and moderate SSR resulting in a considerably lower L/D peak for the present investigation, as shown in Figure 4-10.

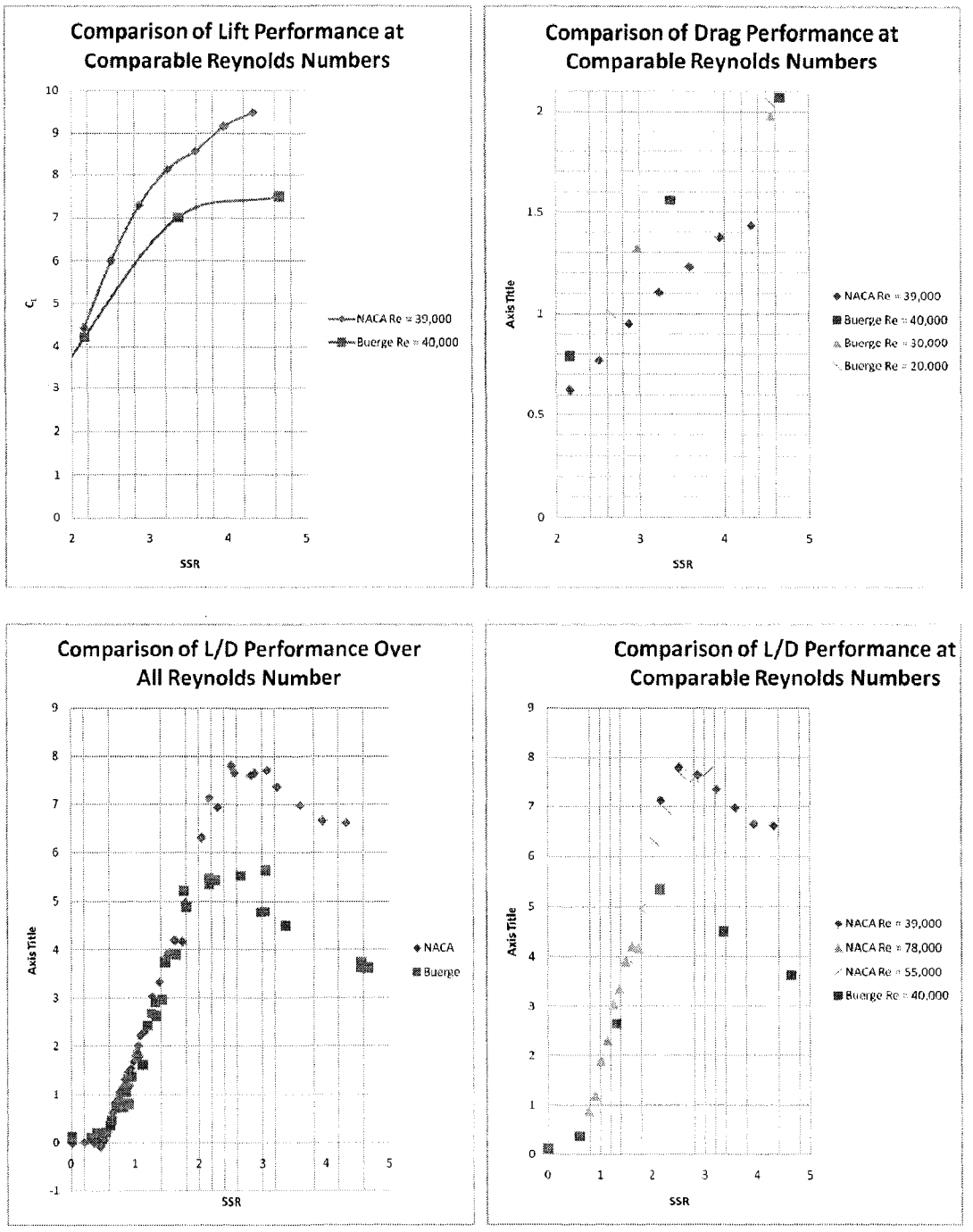

Figure 4-11. Differences in performance compared to that of NACA TN 209.

Figure 4-11 highlights the differences. These differences can be accounted for in three ways. First, the wind tunnel corrections applied to the data resulted in a reduction in lift and drag coefficients on the order of 10% for most tests (see Appendix A for an extensive outline of the wind tunnel data). The percentage reduction in lift due to the wind tunnel corrections increases with increasing drag coefficient; this largely explains the increasing difference in lift coefficients above an SSR of two. Second, the NACA tests were conducted with a cylinder of aspect ratio 13.3 as compared to an aspect ratio of 12 for the present investigation. A lower aspect ratio results in both a lower $C_{L,max}$ and a peak at lower SSR as asserted by Tokumaru (Tokumaru 1993).

Finally, in the tests conducted by Reid (Reid 1924), the rotating cylinder penetrated the test section walls, more accurately simulating 2-D flow. Losses around the gaps between the rotating cylinder and the test section doors probably account for the increase in drag and remaining decrease in lift as compared to the NACA tests.

To make the reader aware of the relative Reynolds numbers for various SSR that are reflected in the tests conducted for this investigation, and those of Reid, the lift performance as a function of SSR for various Reynolds numbers is presented in figure 4-13.

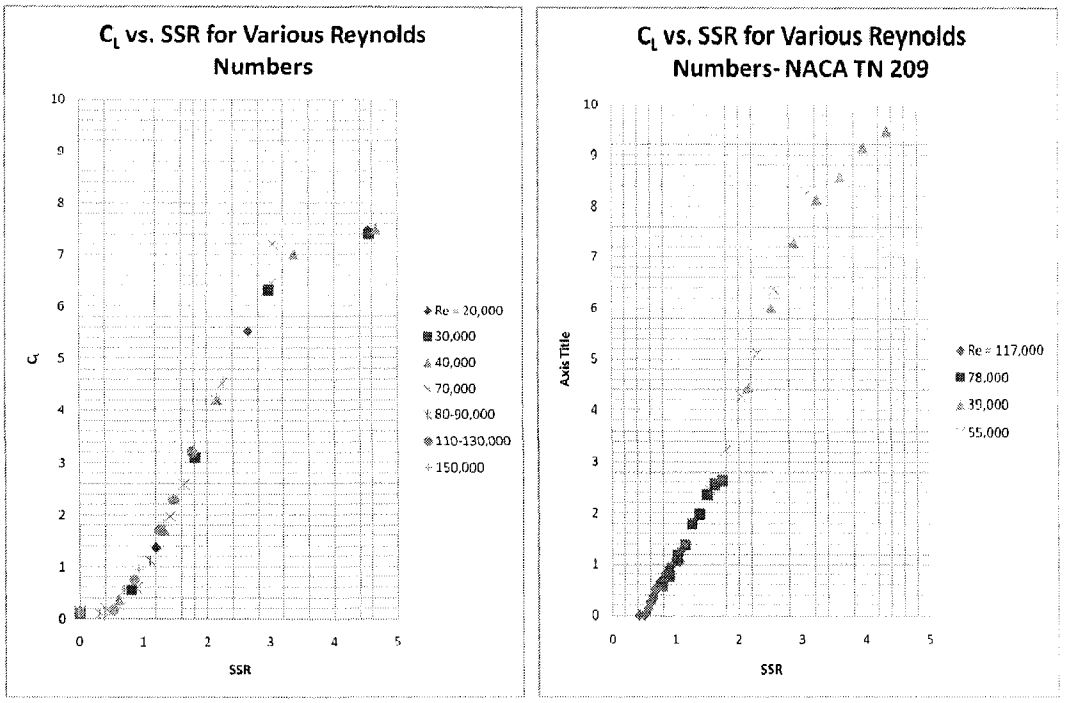

Figure 4-12. Comparison of Reynolds number ranges with data from NACA TN 209.

For completeness, the data published by Hoerner (Hoerner and Borst 1985) is mentioned here. This figure has no legend in the original text, but cross referencing with other sources leads the author to believe that the lines denoted by circles reflect tests run at the David Taylor Model Basin at Reynolds numbers of either 180,000 or 660,000, and the results compare very favorably with the author's data. Finally, the numerical investigation of Ou (Ou 1991) for a rotating cylinder in an incompressible viscous fluid produced results very similar indeed to the experimental results of this investigation. In conclusion, the wind tunnel data obtained for the airfoil-only and cylinder-only compare sufficiently well with the results obtained in the literature to substantiate the methods and means used in the present investigation.

4.3.3 Vortex Flap results

This section outlines the results for the rotating cylinder placed near and underneath the trailing edge of a Clark Y airfoil at $\alpha = 0, 5, 10°$, across a range of SSR, and over a range of Reynolds numbers. A summary of the Vortex Flap data are presented in this section. For the full data set and graphs, see Appendix A.

Geometric considerations

Recall from Section 3 that the cylinder was permanently fixed to the force balance and that in order to change positions, the airfoil had to be moved. The airfoil's vertical and horizontal positions were set with a mechanism independent from that which controlled the α of the airfoil. Finally, the airfoil was supported by a shaft at the half-chord point, and adjustments to the angle of attack produced rotation about this shaft. Thus, to facilitate the maximum number of tests in the minimum amount of time, the vertical and horizontal position of the wing was left unchanged through the range of α at each selected position. This produced a relative change in position of the cylinder with respect to the wing, in the frame of reference of the wing, for each α tested, even though the vertical and horizontal position of the wing shaft was not changed.

For simplicity in recordkeeping, all tests run at a given vertical and horizontal wing shaft position were referred to as a particular 'position' even though each angle of

attack adjustment in fact moved the wing with respect to the cylinder, and produced a unique geometry. Three such 'positions' (1, 2, & 3) were tested, and at each position three α's were tested (0, 5, 10°), producing nine unique geometries. For each geometry, the gap between the cylinder and the bottom of the airfoil was calculated, as well as the distance forward of the trailing edge. These geometries are tabulated in Figure 4-13 and plotted in Figure 4-14.

Position #	*Alpha*	*Cylinder X*	*Cylinder Y*	*Gap*	*Distance forward of trailing edge*
1	0	2.750	-2.250	1.250	1.000
1	5	2.935	-2.002	1.000	0.814
1	10	3.099	-1.738	0.740	0.651
2	0	2.750	-3.250	2.250	1.000
2	5	3.023	-2.998	2.000	0.727
2	10	3.273	-2.723	1.720	0.477
3	0	3.250	-3.250	2.250	0.500
3	5	3.521	-2.954	1.950	0.229
3	10	3.765	-2.636	1.640	-0.015

Figure 4-13. Table of Vortex Flap position information.

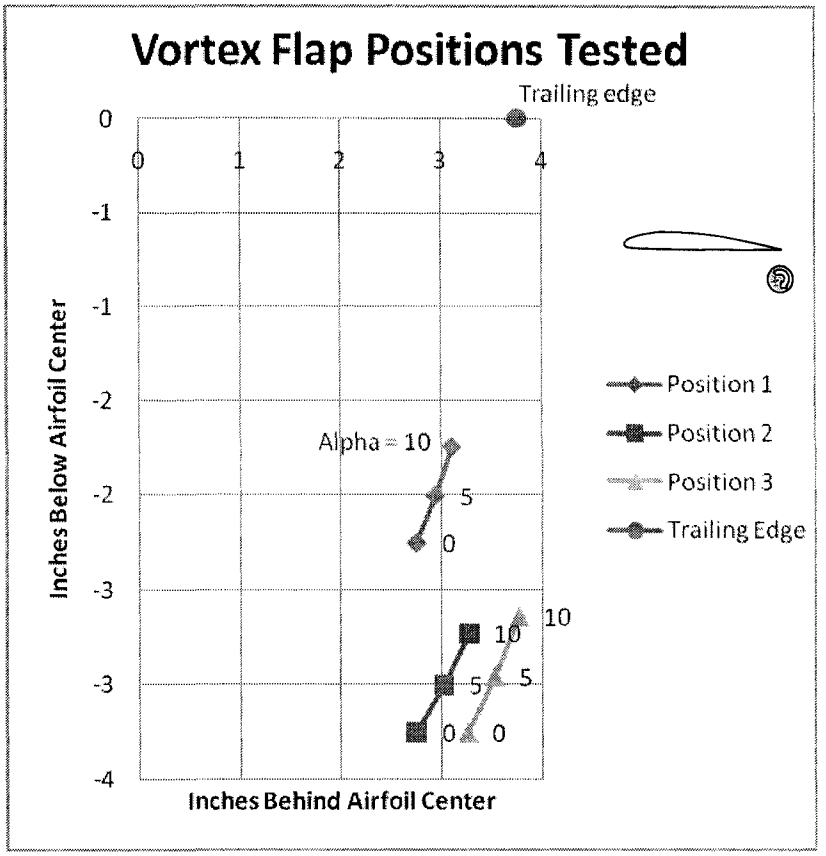

Figure 4-14. Graphical depiction of Vortex Flap geometries tested.

While simplifying the test procedures, this complicates the presentation of the data. No longer can the functional relationship of angle of attack on performance *at a fixed geometry* be determined. This was considered an acceptable sacrifice at the time of testing, given the wide range of positions that were tested (the majority of which are not under consideration here), and the need for efficiency. However, there are two ways to address this shortcoming. For the purposes of this section, the small changes in geometry within each 'position' will be neglected (excepted where noted otherwise) relative to the other parameters under consideration, and the data will be grouped by

'position' as if the geometry were unchanged. In Section 4.6, Response Surface methods developed by the author will be used to address this shortcoming in the data to provide a means of assessing performance across a range of angles of attack at particular geometric configurations and SSR values, as well as some other useful functional relationships. For convenience, all data in this section will be presented as a function of SSR.

Interpreting graph labels

All the information necessary to identify the particular set of data plotted is in the title of each graph, and is set in the following pattern:

1. Coefficient of interest vs. SSR
2. 'Basis' area used to calculate coefficients (airfoil only, or combined airfoil and cylinder area)
3. 'Positions' included (1, 2, 3)
4. 'α' included (0, 5, 10°)
5. Reynolds numbers included

$\Delta C_{L, total}$ refers to the lift *increment* due to the effect of the presence of the cylinder as well as the rotation of the cylinder. $\Delta C_{L, rotation}$ identifies the lift increment due to the rotation of the cylinder *only.* The first is calculated by subtracting the lift produced by

the airfoil alone from the lift produced by the airfoil with the rotating cylinder 'deployed.' The second is calculated by subtracting the lift produced by the airfoil with the *stationary* cylinder deployed from the lift produced by the airfoil with the rotating cylinder deployed.

Basis for calculating coefficients

"Basis" refers to the reference area used to calculate the coefficient of lift and drag. "Basis Total" indicates that the wing area added to the projected area of the cylinder was used as the reference area. This is not a precisely accurate method, as there is substantial overlap between the horizontal projected area of the cylinder, and the wing area, and this is different for each of the geometries tested. However, it is thought better to be consistent in this particular calculation. "Basis Airfoil" indicates that the wing area alone was used as the reference area. The effect is to decrease the calculated coefficients by an amount proportional to the increase in area associated with the cylinder. The effect of basis selection is evident in Figure 4-18.

It is assumed that, for normal cruise flight, the cylinder would not be deployed. Following the customary procedure in dealing with area-increasing high-lift devices, the preferred basis for calculation is the area of the airfoil in normal cruise configuration (high-lift device retracted). Therefore, most of the graphs are "Basis Airfoil." This custom allows easy comparison of different devices in terms of

"increase in (lift, drag) when deployed on a particular aircraft." If, however, it were assumed that the stationary cylinder were to remain deployed for cruise flight, it would change the appropriate basis, and it would be necessary to determine precisely where the cylinder would be located so that the proper chord could be used when calculating the basis wing area, and the data could be transformed (Hoerner and Borst 1985). However, cruise flight with the stationary cylinder deployed is not thought a practical configuration.

Influence of α

For brevity of presentation, all data in Figure 4-15 will reference Position 3. For data on all positions, see Appendix A.

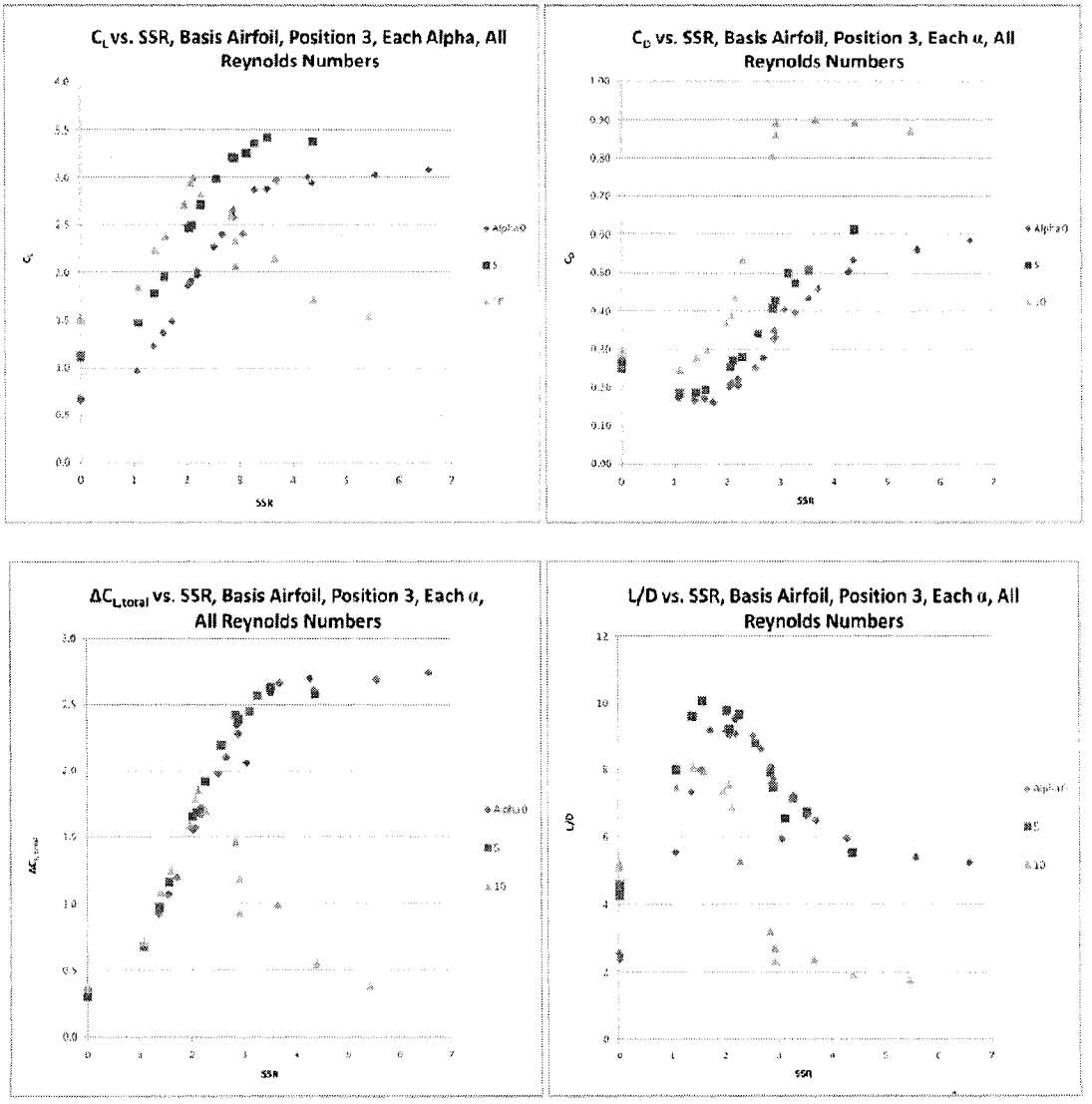

4-15. Summary of data showing the influence of SSR on lift, drag, total lift increment, and L/D.

Influence of Cylinder Position

For brevity of presentation, only the data for $\alpha = 10°$ are shown in Figures 4-16.

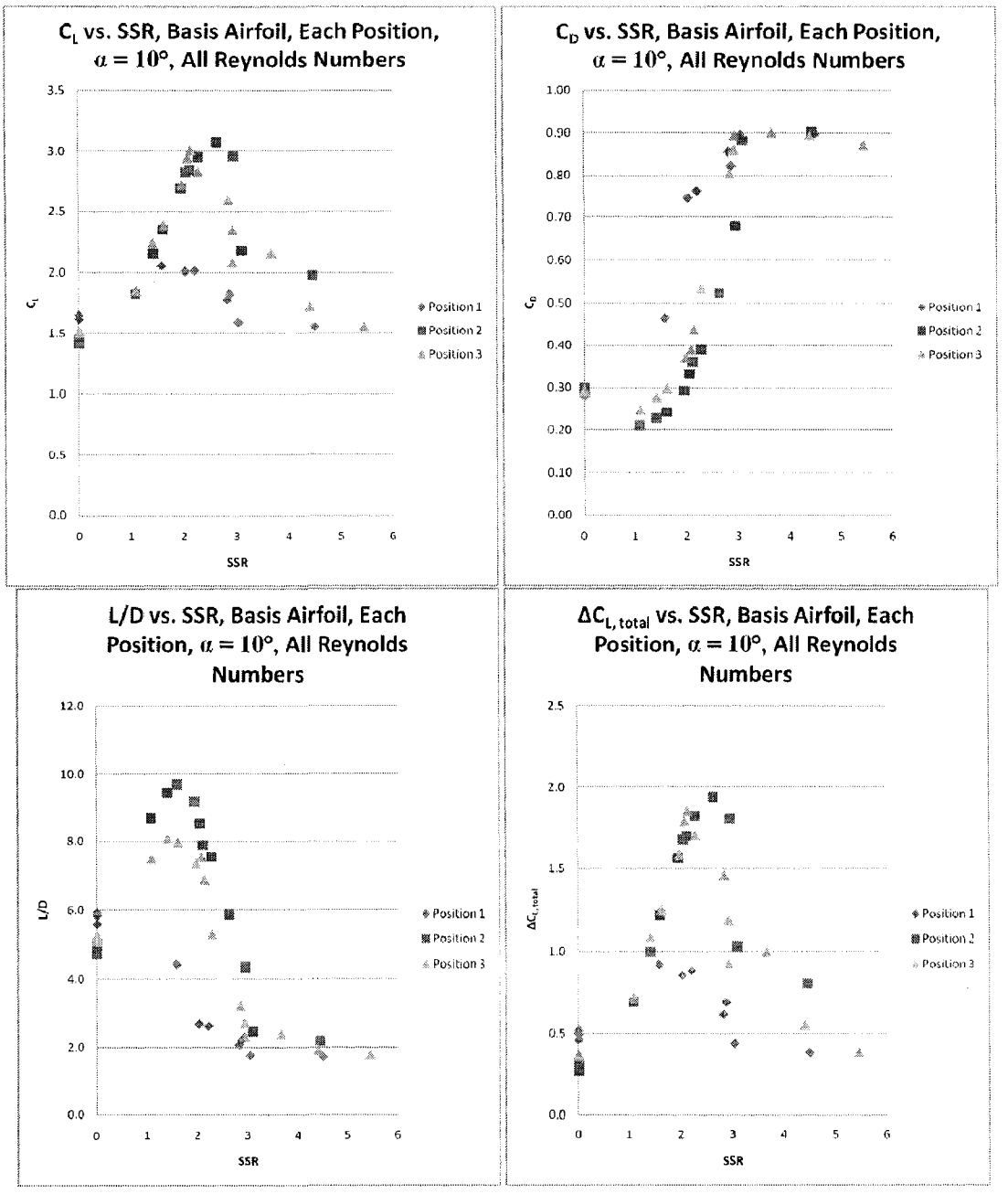

4-16. Summary of data showing effect of cylinder position on Vortex Flap performance.

Influence of Reynolds number

For brevity of presentation, all data in this subsection will reference Position 3, α = 10°, as in Figure 4-17. For data on all positions and α, see Appendix A.

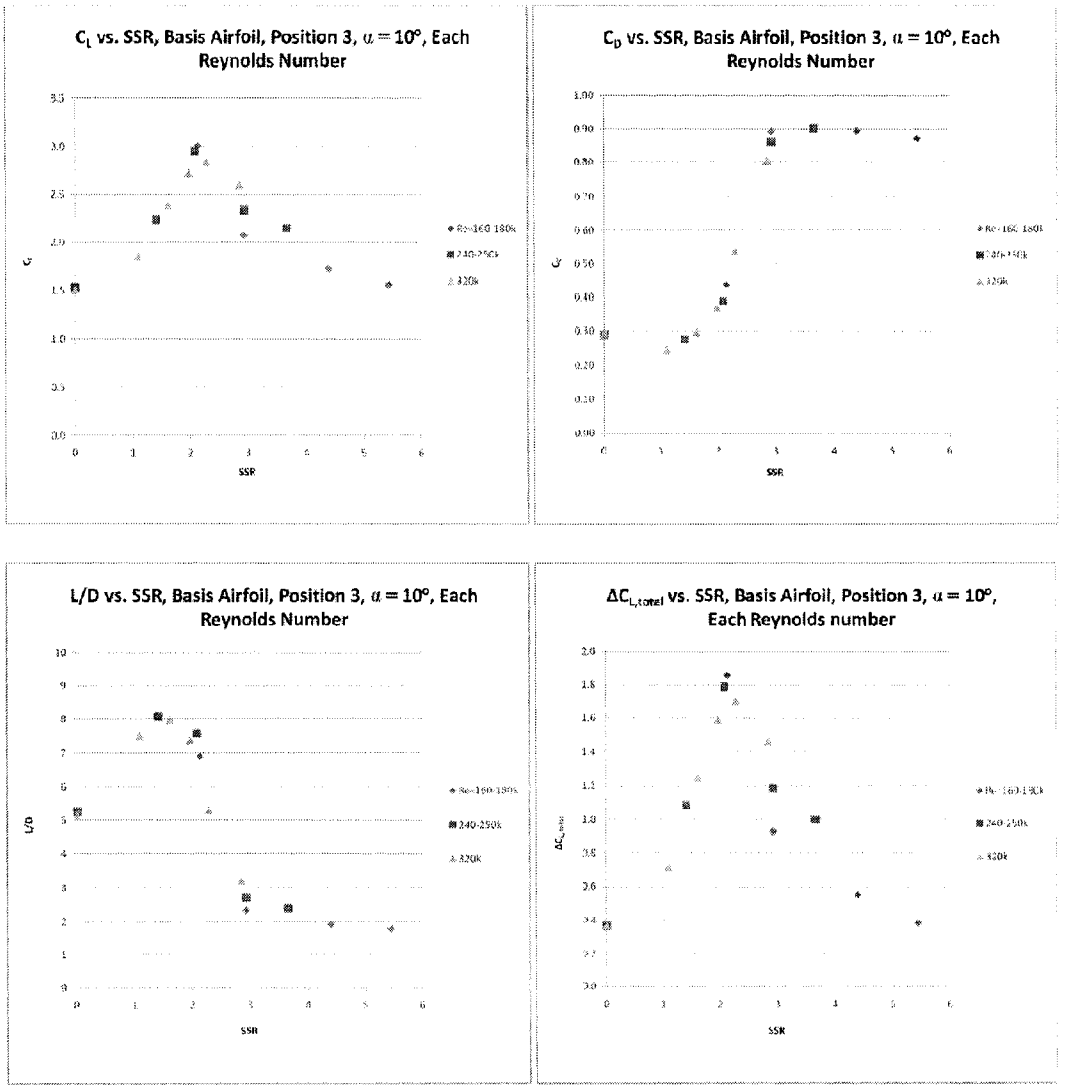

4-17. Summary of data showing the influence of Reynolds number on lift, drag, and lift increment.

It is evident in Figure 4-17 that Reynolds number is not the most significant determinant of performance within the range of values tested.

4.4 Summary of experimental results

Data from position 3 are presented here in terms of 'percentage increase in lift coefficient' as compared to the basis listed in Figure 4-18.

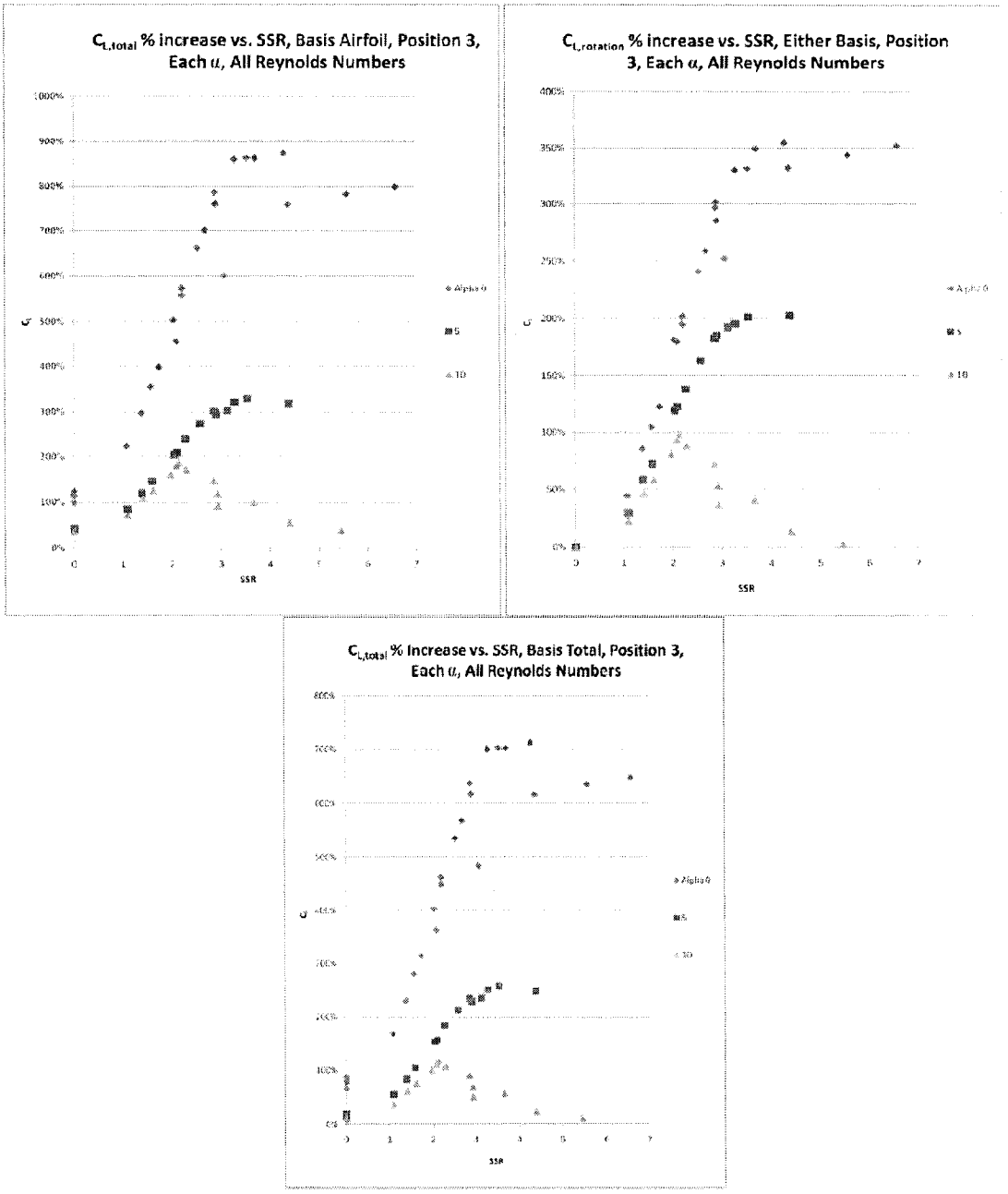

4-18. Summary of lift performance of the Vortex Flap.

Note that the percentage increase of the lift coefficient due to rotation is the same regardless of the basis used for calculation, as in Figure 4-18.

4.5 Application of Response Surface Methods: The Polynomial Curve Net

There are two physical limitations to the test data which hinder the presentation of the data. The first is the change in cylinder position relative to the airfoil when the angle of attack of the airfoil is adjusted (see Section 4.3.3). This makes presenting the effect of angle of attack, for example, at a *fixed* geometry impossible. The second was the inability to precisely control SSR from one test to another. This makes presenting the effect of angle of attack, for example, at a *fixed* or otherwise arbitrary SSR impossible. And of course the combination is impossible as well; the effect of angle of attack at a fixed geometry and SSR cannot be presented strictly from the data available. In this section a derivative of standard Response Surface Methods was used to generate, from the limited discrete data points originally obtained, a more complete set of points from which these relationships, and others, could be observed and presented conveniently.

The method amounts to careful curve-fitting and interpolating. For the data under consideration, there are five dimensions to consider at any one time:

1. Trailing Edge Coordinate (TEC): The distance between the trailing edge of the airfoil and the center of the cylinder shaft in the direction of the chord line of the airfoil

2. Gap: The minimum distance between the cylinder and the chord line of the airfoil
3. α: The geometric angle of attack of the airfoil (0, 5, and 10°)
4. Surface Speed Ratio (SSR): The nondimensional rotation speed of the cylinder (0, 1, 1.5, 2, 2.5, 3)
5. Output parameters considered: C_L, C_D, and $\Delta C_{L,\,Total}$

In order to make the results visually observable, at most three dimensions can be presented at one time in a surface plot. These plots are especially appropriate to observe the effect of the physical position of the cylinder (TEC, Gap) on each output parameter (C_L, C_D, or $\Delta C_{L,\,Total}$), with all other dimensions held constant (SSR, α). In addition, for simple comparison with the data available from other trailing-edge high-lift devices, it is desirable to produce plots which illustrate the effect of only one input parameter at a time on the output parameters. For the full set, see Appendix B.

In the case of the curve plots, "Positions" were defined which, unlike the experimental data, did not change with α. Three "Positions" were defined which closely approximate the three positions of the same number actually tested in the experimental setup, but which do not suffer from the geometric changes with α already described at length. These "Positions" are given in Figure 4-19. These "Positions" generated using RSM are distinguished from the actual geometric positions in the experimental data by

quotation marks in the text and figures. A geometric comparison of the actual positions vs. the RSM "Positions" is shown in Figure 4-20.

"Position"	Trailing Edge Coordinate (TEC)	Gap
1	0.8"	1.0"
2	0.8"	2.0"
3	0.0"	2.0"

Figure 4-19. "Positions" as used in RSM plots.

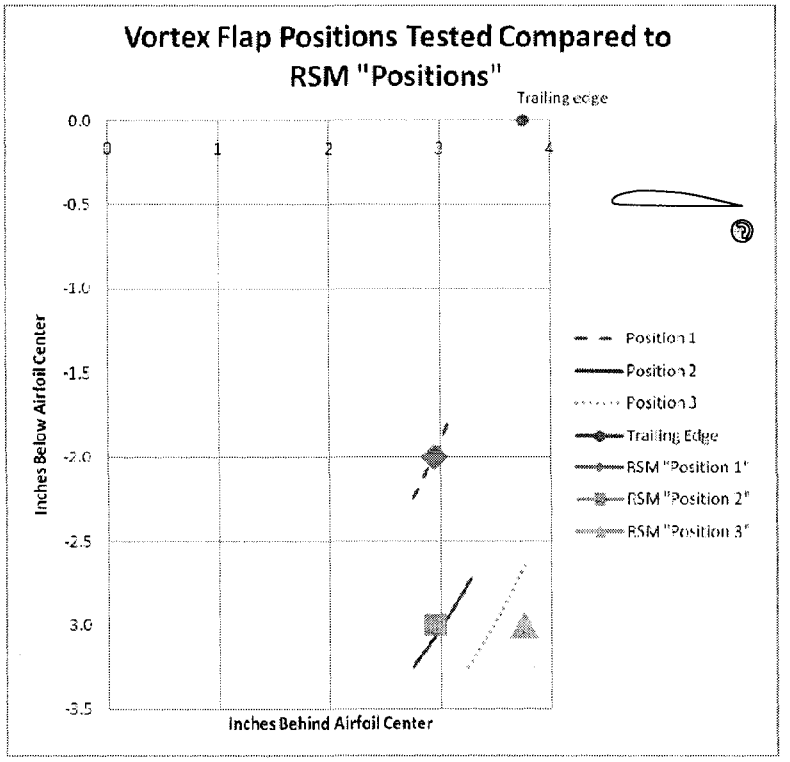

Figure 4-20. RSM "Positions" compared to actual positions tested.

The data available included only the output parameters at factorial α and discrete TEC, Gap, and SSR. In order to produce the above, the output parameters are needed in terms of the same factorial α, and arbitrary (though intentionally selected) TEC, Gap, and SSR (Box and Draper 1987). The standard RSM approach would be to attempt to find the lowest-order multi-dimensional polynomial function in all the input parameters that would describe each experimentally obtained output parameter with reasonable accuracy (as determined using least-squares fit) and which would allow the output parameters to be obtained at the desired arbitrary input parameters. In this case, a single polynomial function for each output parameter and each factorial α in TEC, Gap, and SSR would be sought.

The author's method varies from the standard approach in this: rather than attempting to obtain a single polynomial function which is able to describe the output parameters in terms of the input parameters, curves in two dimensions are fitted to the data (one input parameter, and one output parameter) at every combination of the other input parameters available in the data. The polynomial functions which describe each curve are used to generate the output parameters in terms of the input parameters at arbitrary values. This single step substantially populates the space such that the entire array of plots described above can be produced, with substantially less difficulty than presented by the standard approach, and while maintaining a fidelity to the experimental data which can be readily verified for each data point. For more complex design spaces, more than one level of curve fitting may be required (see Appendix B

for an application of the method which requires three layers of curve fits, forming a multi-dimensional net, from which the method derives its name, "polynomial curve net"), but only one level was necessary for the data presented here.

Specifically, the method was applied as follows for this investigation. Curves were fitted to the data which compared each output parameter to SSR at each available geometric configuration (α, TEC, Gap) using the lowest order polynomial functions which would produce high R^2 (in excess of 0.98) values. These polynomial functions were used to produce the output parameters at SSR 0-3 with an increment of 0.25. From this population of points, all the plots described above were produced. For brevity of preparation and presentation, only SSR = 0.0, 1.0, 1.5, 2.0, 2.5, and 3.0 were plotted, and the points joined with smooth curves or planar surfaces as appropriate.

4.5.1 RSM Surface Plots

Selected RSM surface plots for lift are presented below. For all 99 plots produced, see Appendix B. Commentary will include trends observed in appendicized plots.

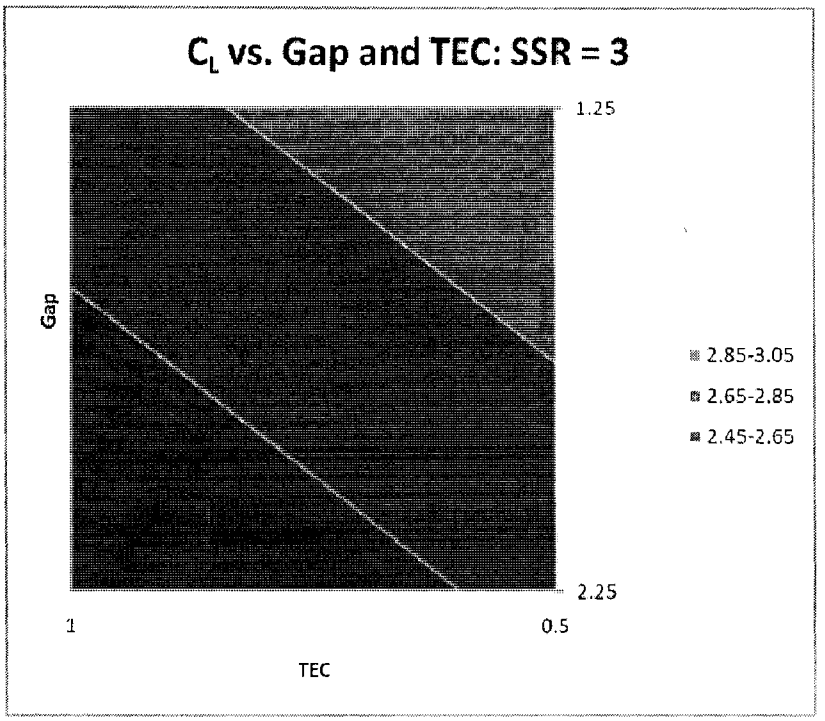

Figure 4-21. Lift surface plot for α = 0°.

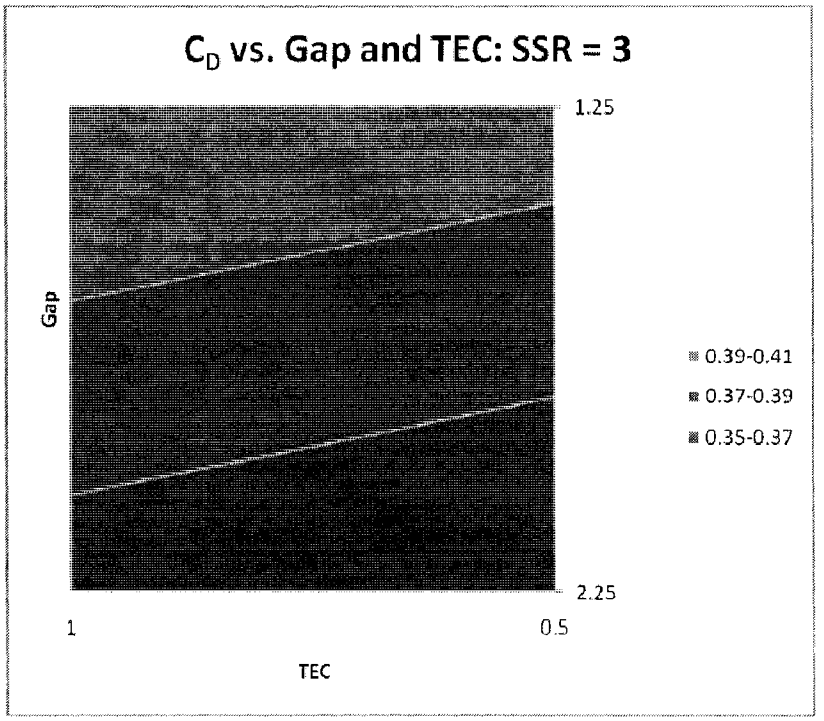

Figure 4-22. Drag surface plot for α = 0°.

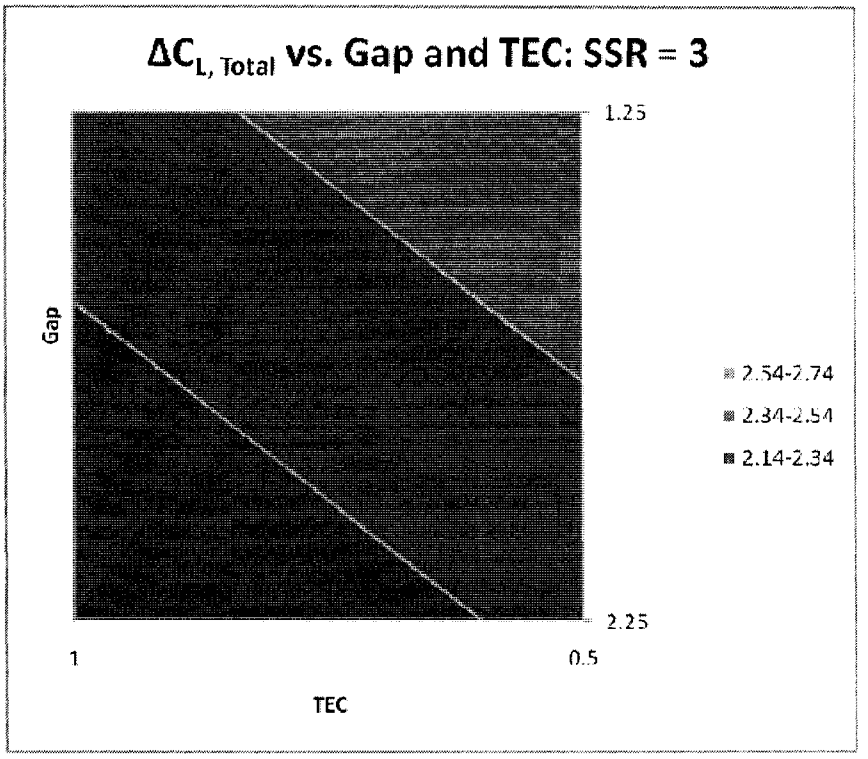

Figure 4-23. Lift increment surface plot for α = 0°.

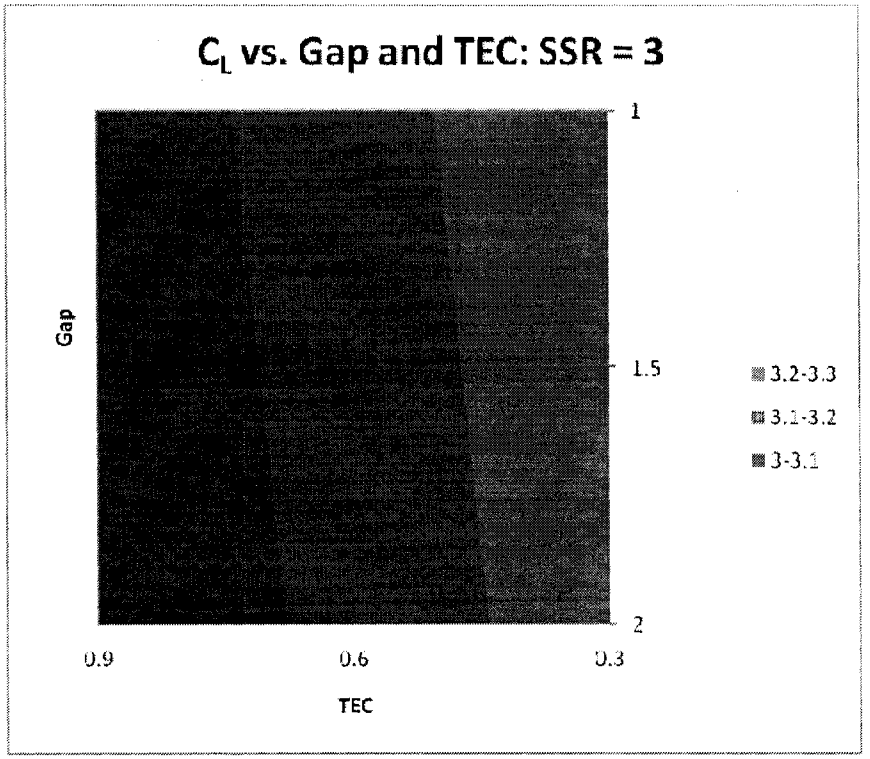

Figure 4-24. Lift surface plot for α = 5°.

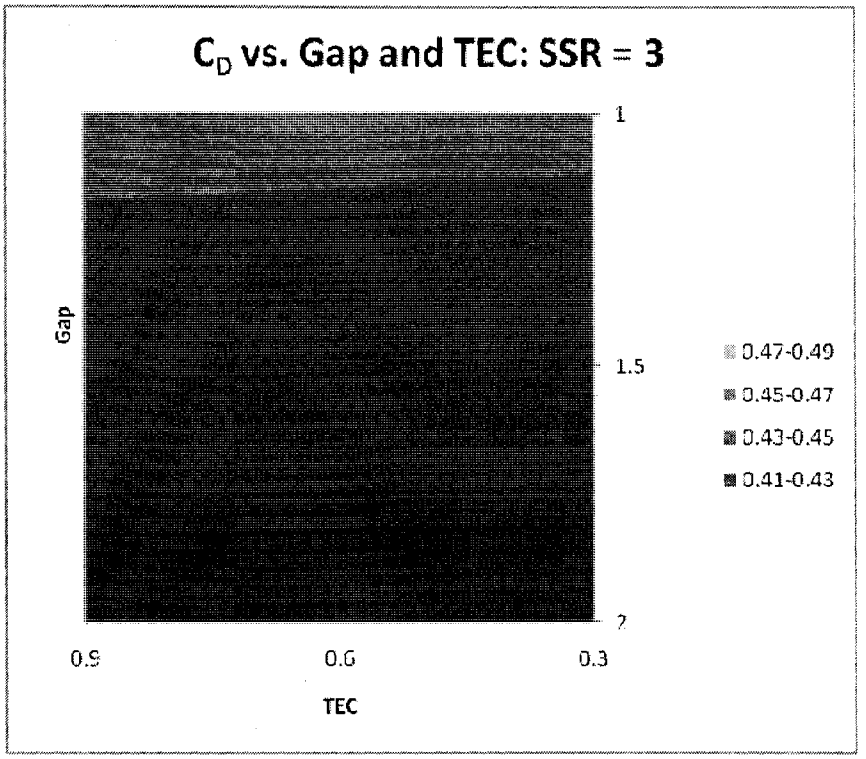

Figure 4-25. Drag surface plot for α = 5°.

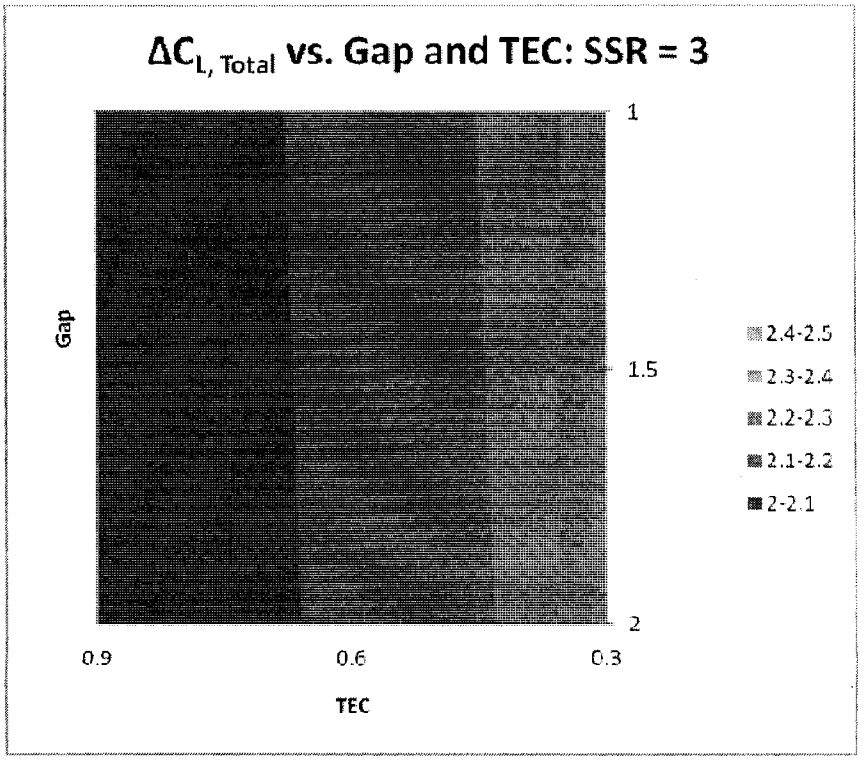

Figure 4-26. Lift surface plot for α = 5°.

4.5.2 RSM Curve Plots

Following are all RSM curve plots for lift. For drag and lift increment plots, see Appendix B.

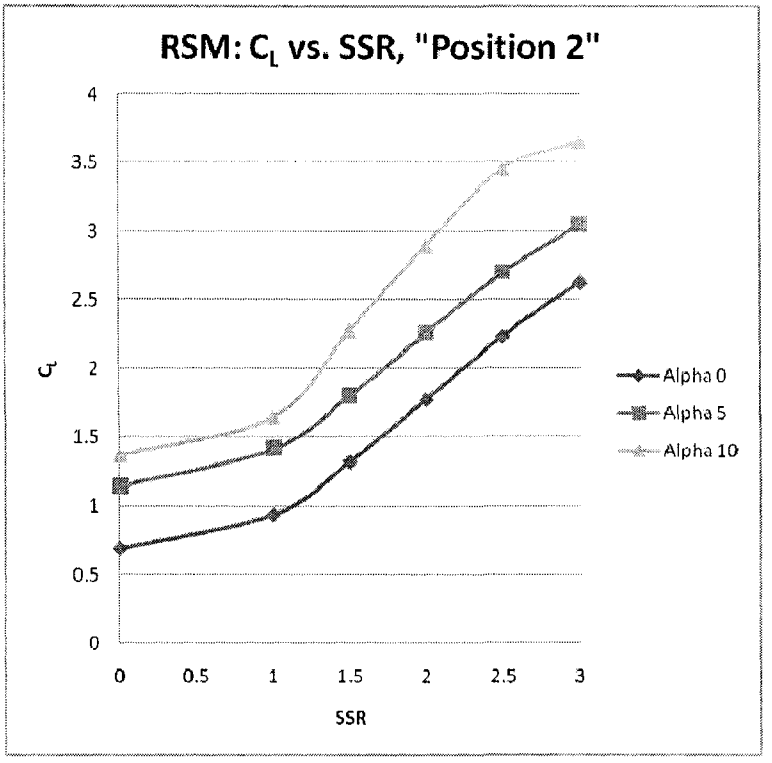

Figure 4-27. Lift vs. SSR curve plot at each α for "Position 2."

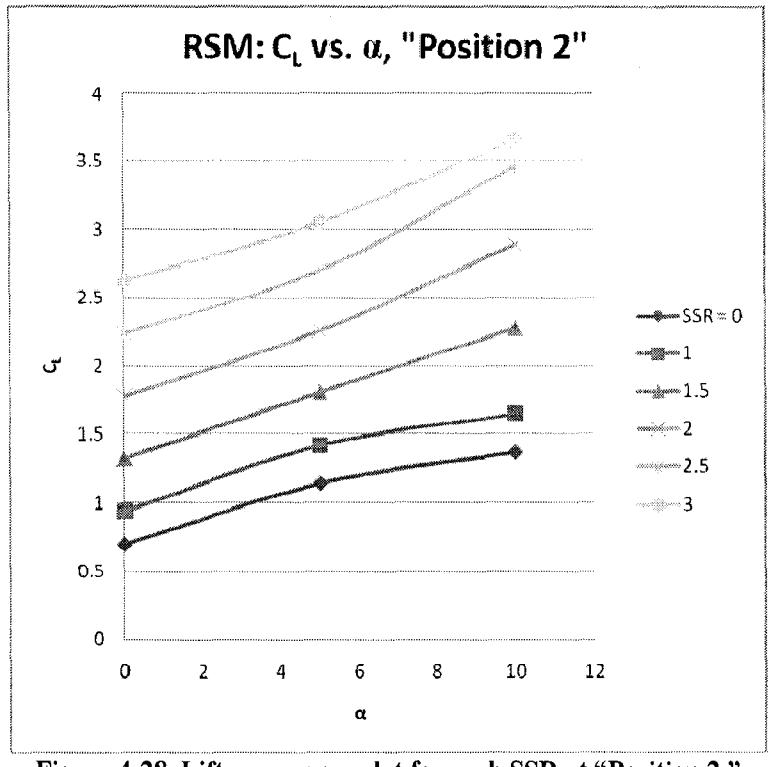

Figure 4-28. Lift vs. α curve plot for each SSR at "Position 2."

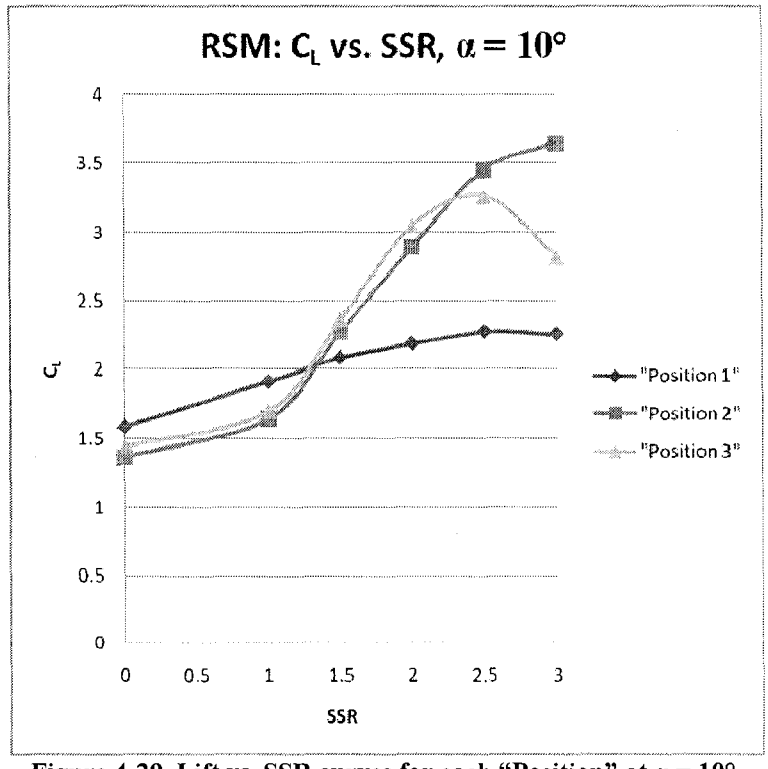

Figure 4-29. Lift vs. SSR curves for each "Position" at α = 10°.

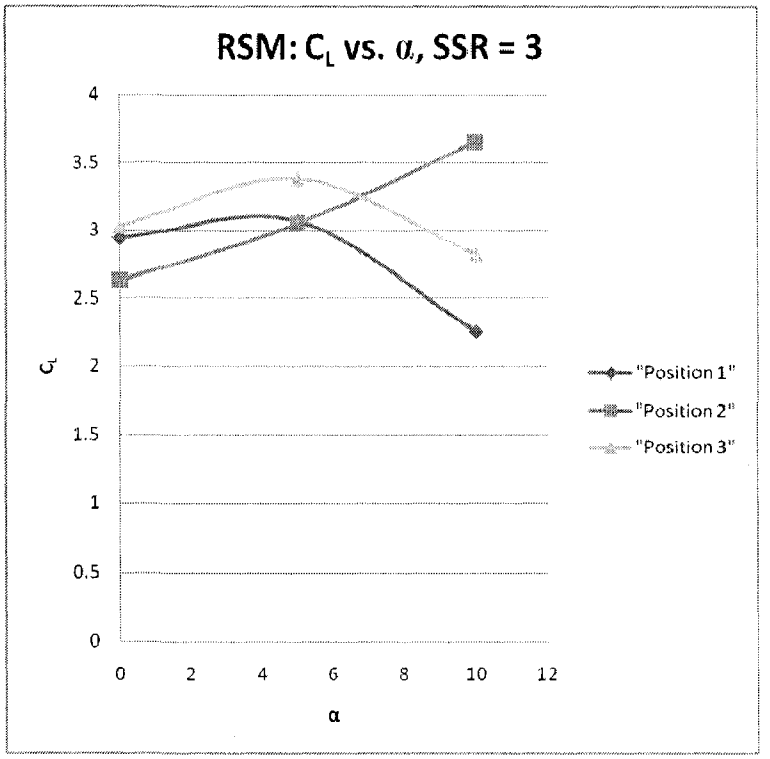

Figure 4-30. Lift vs. α curve plots for each "Position" at SSR=3.

If only one geometry had to be chosen for deployment over the entire range of SSR and α, it appears that "Position 2" is the best of the three selected geometries, and will be used as the representative of the Vortex Flap performance in subsequent analysis and comparison. Note that the data represent only discrete α, SSR, and cylinder position. Thus, even though the so-called "maximum" lift coefficient and increment will be taken at a particular point, or a specific interpolated data point in the case of post-RSM analysis data, the true maximum probably lies between the fairly sparse points. This will not be taken in to account, and represents yet another way in which the results presented are likely more conservative than 'reality.'

4.6 Potential Flow Analysis of the Vortex Flap

To better understand the function of the Vortex Flap, it is useful to attempt a crude potential flow analysis, and see if additional insight into the physical mechanisms of lift can be gained. There already exists in the literature a potential flow model and analysis that is suitable, with only minor modification, for use here.

The phenomenon of autorotating flat plates, rotating airfoils, and rotating airfoil flaps has been the subject of occasional investigation (see Crabtree 1960, Saffman 1977). The Vortex Flap is, in potential flow, no different than the rotating airfoil flap investigated in Germany around World War II and revisited by the Aeronautical Research Council in the late 1950's. It can be crudely modeled as a simple bound vortex. Crabtree developed a satisfactory potential flow treatment of the rotating airfoil flap, and it is this treatment which will be applied to the Vortex Flap for comparison to the experimental results of the present investigation.

To understand Crabtree's model, it is useful to consider prior work by W. G. Bickley, presented to the Royal Society in the late twenties (Bickley 1928). Bickley's original intent was quite different from that of Crabtree. He intended to demonstrate that a classical analysis using so-called "perfect fluid," i.e. incompressible and inviscid, could represent one mechanism responsible for drag as well as lift if the starting vortex was taken in to account, and in doing so, make a contribution to the field of

potential flow analysis comparable to that of Lanchester and Prandtl in adding lift through circulation (Bickley 1928). A summary of his treatment follows.

Taking as a prototypical example the two-dimensional flow past a circular cylinder, he added, to the usual treatment, two free vortices with equal and opposite circulations in the senses shown to simulate the wake of the blunt body (see Figure 4-31) and two additional image vortices at the inverse points inside the cylinder in order to maintain the surface of the cylinder as a streamline.

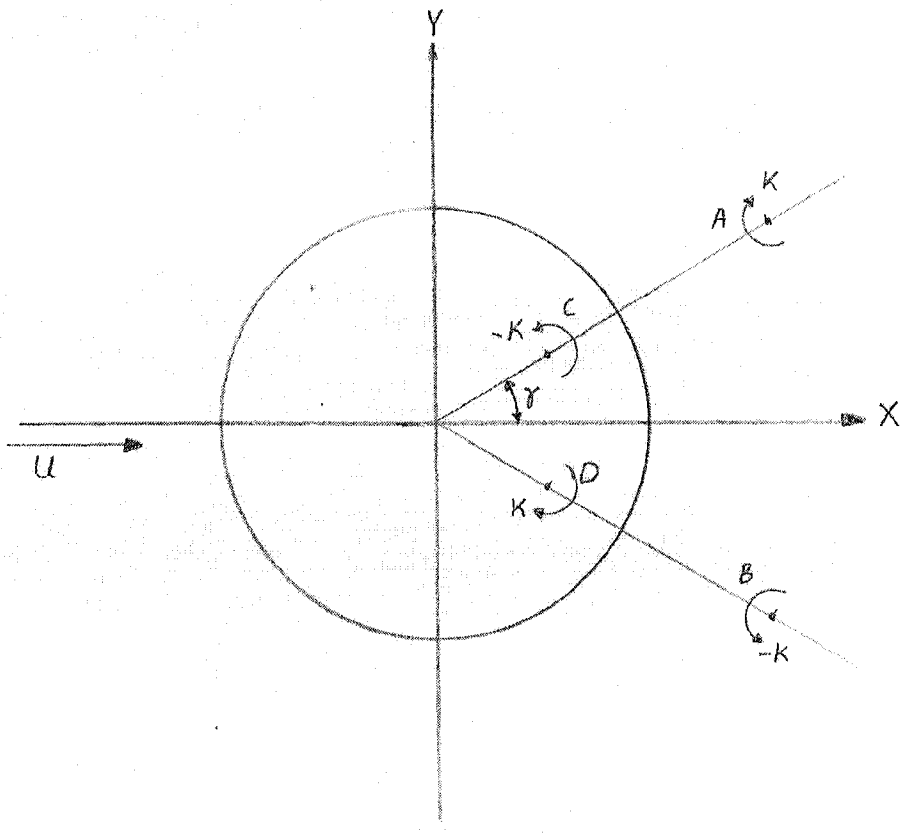

Figure 4-31. Drawing of Bickley's model for a cylinder shedding vorticies in potential flow. Drawing by Brandon Buerge.

Bickley demonstrated that if the free vortices were positioned at stationary points in the flow field (a pair of curves of such points, symmetrical about the x axis, does exist), then there is no drag. If, however, the vortices are positioned outside the curve in γ where they are stationary, such that they will convect downstream, then a non-zero resultant drag is found according to the formula:

$$Drag = \frac{\rho a^2 \kappa^2}{\pi c^3} \cos\gamma \frac{4c^4 \sin^2\gamma - (c^2 - a^2)^2}{c^4 + a^4 - 2a^2 c^2 \cos 2\gamma} \tag{4.18}$$

where a is cylinder radius, c is the distance from the origin to each free vortex, and ρ is the fluid density. Having demonstrated the presence of drag on the cylinder due to the movement of free vortices, Bickley went on to investigate the effect of a single free vortex downstream of a cylinder with circulation (see Figure 4-32). It is particularly important to note the strengths and senses of the vortices present, so that this treatment can be appropriately modified. Vortex at A is strength κ in the negative sense. The image vortex, at the inverse position B, has the same strength κ but in the opposite (positive) sense, as would be expected for an image vortex. Then the vortex placed at the center of the cylinder must be of strength $\Gamma+\kappa$ in the negative sense to produce the net circulation strength around the cylinder Γ (not shown) once the image vortex is added (note well that whatever vortex is added at the center of the cylinder to Γ is the same sense and strength of the free vortex outside of the cylinder).

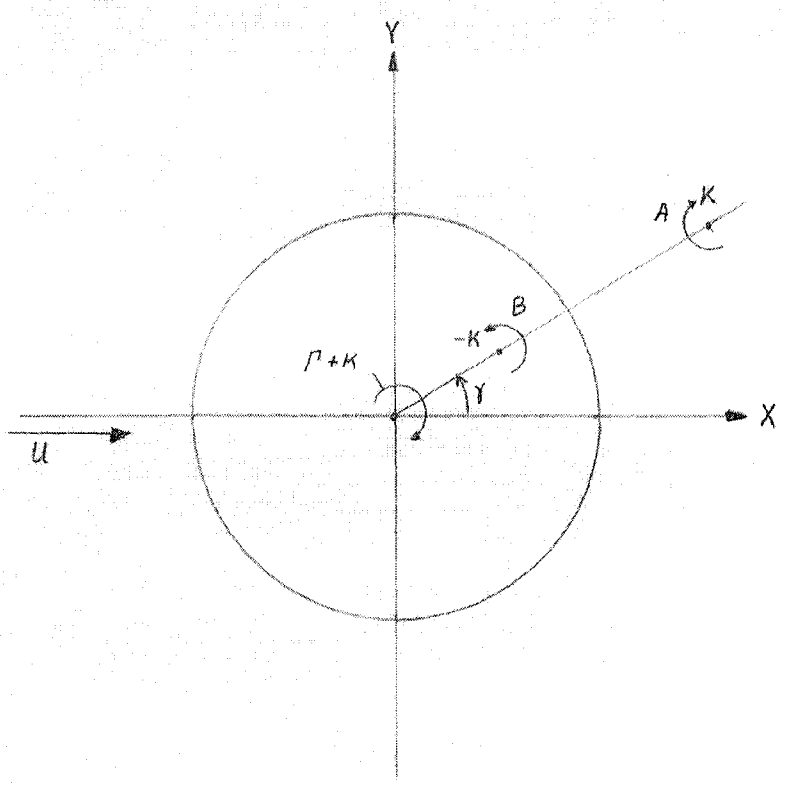

Figure 4-32. Drawing of Bickley's model of a rotating cylinder and the starting vortex in potential flow. Drawing by Brandon Buerge.

From this geometry, the lift and drag as a function of Γ and κ can be calculated:

$$Lift = \rho\left\{(\Gamma + \kappa)U - \kappa u_A\left(1 + \frac{a^2}{c^2}\cos 2\gamma\right) - \kappa v_A \frac{a^2}{c^2}\sin 2\gamma\right\} \qquad (4.19)$$

$$Drag = \rho\kappa\left\{u_A \frac{a^2}{c^2}\sin 2\gamma + v_A\left(1 - \frac{a^2}{c^2}\cos 2\gamma\right)\right\} \qquad (4.20)$$

This is the end of the relevant portion of Bickley's treatment, but he went on to state that if we treat the free vortex as a starting vortex such that the circulation around a line enclosing both the cylinder and the free vortex is zero, then the circulation around the cylinder and the free vortex must be equal and opposite, and the vortex placed at the center of the cylinder will be of strength (Γ+κ) = 0. He finally showed relatively

good correlation of his results, in both lift and drag, with those obtained in practice from Flettner rotors, which asserts the fidelity of his mathematical approach.

The author surmises, though it is not explicitly stated, that Crabtree's theoretical treatment of the rotating airfoil flap is based on Bickley's prior work. Regardless, the results are equivalent if one makes the appropriate modifications to Bickley's model. The modifications are, very simply, to use a fixed rather than a free vortex, and then to include the force on that vortex in the lift of the complete wing-flap system, thus simulating the combined lift of the wing (modeled by the circular cylinder with circulation) and the rotating airfoil flap (modeled by the fixed vortex) (Crabtree 1960). Appropriately for a potential flow model, and as one would expect from Bickley's work, since the vortex no longer moves there is no longer any drag predicted. Crabtree's geometry, the senses of circulation around the vortices, and slight changes in notation are shown in Figure 4-33. The position of the fixed vortex external to the cylinder and the image vortex can be written, in the ζ plane, as $\zeta_1 = \lambda a e^{i\varphi}$ and $\zeta_2 = (a/\lambda)e^{i\varphi}$, respectively. In these equations λ is the distance from the origin to the fixed external vortex (denoted by c in the previous model), and a is the radius of the cylinder.

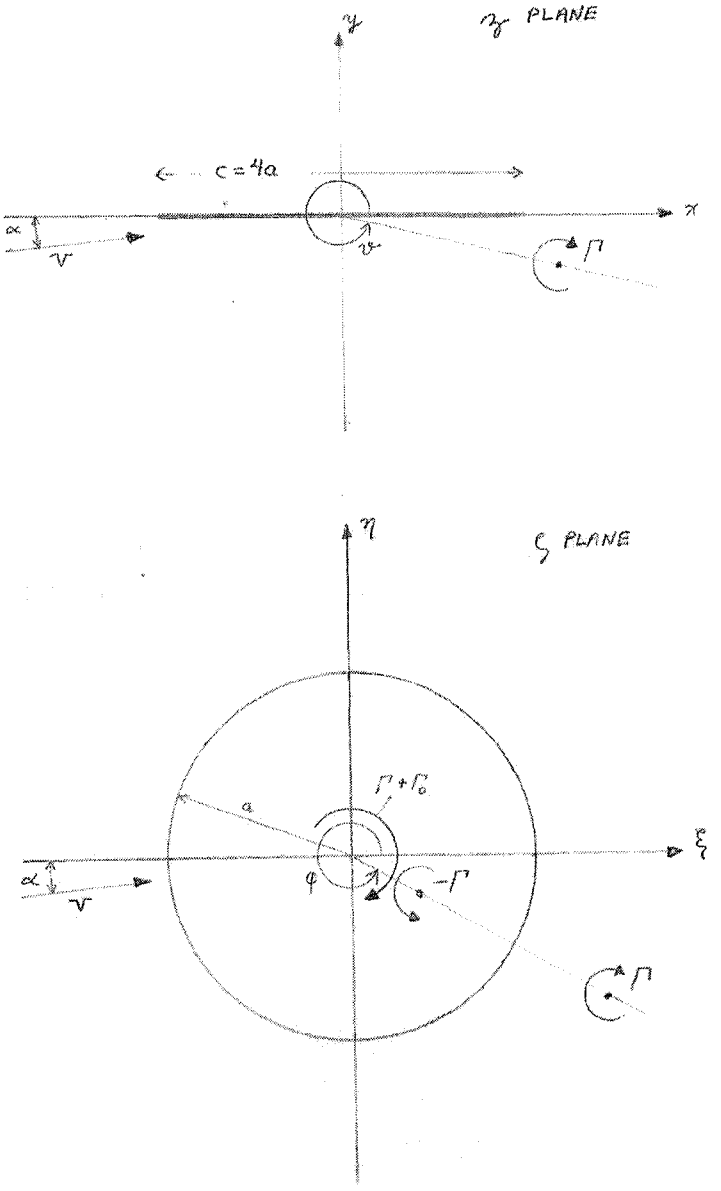

Figure 4-33. Drawing of the potential flow model and conformal mapping used for the rotating airfoil flap by Crabtree. Drawing by Brandon Buerge.

In order to determine appropriate values of circulation around the rotating airfoil flap (denoted here by Γ rather than κ as in the previous model) and the circulation around the primary airfoil (denoted here by Γ_o rather than Γ as in the previous model), the

circulation of the vortex simulating the rotating airfoil flap (or Vortex Flap) is prescribed from the experimental conditions, and then the Kutta condition is applied to determine the appropriate circulation about the primary airfoil. Utilizing Crabtree's treatment, the potential flow analysis of the Vortex Flap follows.

The Vortex Flap can be represented through the Joukowski transformation (Currie 1974) as a flat plate of chord 4a (in the ζ-plane) which is mapped from a circle of diameter 2a (in the z-plane), with a fixed vortex of strength Γ near the trailing edge which represents the Vortex Flap. Using this to find the complex potential of the flow, and then differentiating to find the complex velocity, and finally setting the rear stagnation point to the trailing edge of the flat plate to satisfy the Kutta condition, the total circulation of the airfoil-flap system about the origin can be calculated:

$$\frac{\Gamma+\Gamma_0}{2\pi aV} = 2\sin\alpha + \frac{\lambda-\frac{1}{\lambda}}{\lambda+\frac{1}{\lambda}-2\cos\varphi} * \frac{\Gamma}{2\pi aV} \tag{4.21}$$

The parameter λ describes the location of the external vortex in the circle plane. If the external vortex strength is such that $\Gamma = 0$, the above equation reduces to the typical result from thin airfoil theory:

$$\frac{\Gamma_o}{2\pi aV} = 2\sin\alpha \tag{4.22}$$

or

$$C_L = 2\pi\sin\alpha \tag{4.23}$$

If the additional assumption is made that the velocity at the fixed vortex is equal to the free stream velocity (in fact it would be slightly less for under-the-wing configurations

due to the circulation about the primary airfoil), and use the chord of the primary airfoil for the basis of calculating the lift coefficient, then the total system lift per unit depth can be written:

$$L = C_L \frac{1}{2} \rho V^2 4a \tag{4.24}$$

$$L = \rho V(\Gamma + \Gamma_o) \tag{4.25}$$

$$C_L = \frac{\Gamma + \Gamma_o}{2aV} \tag{4.26}$$

$$C_L = \pi \left\{ 2 \sin \alpha + \frac{\lambda - \frac{1}{\lambda}}{\lambda + \frac{1}{\lambda} - 2 \cos \varphi} * \frac{\Gamma}{2\pi aV} \right\} \tag{4.27}$$

The first term in the bracket represents the lift on the primary airfoil without the Vortex Flap, and the second term represents the lift increase of the system due to the presence of the Vortex Flap. This functional dependence of lift on the strength of circulation about the Vortex Flap supports the conclusion evident in the experimental results that an increase in SSR generally increases the lift.

The relationship between the coordinates in the z-plane (the physical plane) and the ζ-plane can be developed (Crabtree 1960):

$$x = \left(1 + \frac{1}{\lambda^2}\right) * \xi \tag{4.28}$$

$$y = \left(1 - \frac{1}{\lambda^2}\right) * \eta \tag{4.29}$$

$$\lambda^2 = \left(\frac{\xi}{a}\right)^2 + \left(\frac{\eta}{a}\right)^2 \tag{4.30}$$

The purpose of this analysis, aside from confirming general conclusions about the Vortex Flap, is to verify the experimental results. Using these relations, we can model

the geometry and circulation of a particular experimental configuration, and compare them to the actual results.

The matter of prescribing an appropriate circulation to the fixed vortex representing the Vortex Flap can be resolved by a careful inspection of the experimental results. When a cylinder rotates in viscous flow, there develops in the boundary layer a counter-vorticity which reduces the total circulation about the cylinder to less than the theoretically expected value. Appendix D compares the theoretical circulation generated by the rotating cylinder used in the experimental investigation to the actual circulation generated, as determined by the lift measured on the rotating cylinder. A strong functional relationship exists that appears to be insensitive to Reynolds number in the range tested. If, as in the example below, we wish to model the experimental run in which SSR = 2.0, then from Appendix D we can observe that the actual circulation generated for that SSR corresponds to the circulation generated by a cylinder with no losses at SSR = 1.2. Therefore, if we wish to model the results found at an experimental SSR = 2.0, the circulation corresponding to SSR = 1.2 should be applied to the potential flow model.

The most favorable discrete geometry found in the RSM analysis was chosen for comparison: "Position 2," $\alpha = 10°$. Being careful to choose parameters which would avoid flow separation on the primary airfoil (although flow separation on the cylinder

is unavoidable), SSR = 2 was chosen. SSR = 2 in the experimental model corresponds to an 'effective' SSR of 1.2 in the potential flow model.

For "Position 2" in the potential flow model z-plane x = 2.95", y = -2.0", and a = 1.875". To map into the ζ-plane we use (Currie 1974):

$$Z = x + iy \tag{4.31}$$

Which we plug in to the mapping expression:

$$\zeta = \frac{z}{2} \pm \sqrt{\frac{z^2}{2} - a^2} \tag{4.32}$$

And then solve for the components in the ζ-plane:

$$\zeta = \xi + i\eta \tag{4.33}$$

For the selected geometry:

$$\xi = 2.06$$

$$\eta = -1.84$$

From which we can find λ and φ:

$$\lambda = \sqrt{\left(\frac{\xi}{a}\right)^2 + \left(\frac{\eta}{a}\right)^2} \tag{4.34}$$

$$\lambda = 1.47$$

$$\varphi = \tan^{-1}\left(\frac{\eta}{\xi}\right) \tag{4.35}$$

$$\varphi = -41.8°$$

Recalling that for an experimental SSR = 2.0, the theoretical SSR = 1.2, which leads to:

$$\Gamma = 2\pi r\omega = 2\pi r\left(\frac{SSR*V}{r}\right) = 2.4\pi V \tag{4.36}$$

Now (4.27) can be solved to determine the lift coefficient. The results are presented in Figure 4-34.

	RSM Results	Potential Flow Results	% Difference
C_L	2.9	3.21	11%
ΔC_L	1.76	2.12	20%

Figure 4-34. Comparison of RSM and Potential Flow analysis results.

Potential Flow Theory over-predicts the overall performance of the vortex flap by 11%, which is quite acceptable given the simplifying assumptions of inviscid, incompressible flow and free stream velocity at the fixed vortex. Potential Flow Theory appears to correlate well with the experimentally obtained data.

One concern about the fidelity of the potential flow model should be mentioned. It is not completely clear to the author or members of the dissertation committee that the strength of the vortex added to the original circulation at the center to offset the image vortex should be of the same strength and opposite sense as the image vortex (κ and Γ in Bickley and Crabtree's models, respectively). This assumption was originated by Bickley, and Crabtree followed it without elaboration. The author hopes to address

this point more thoroughly in a future paper. For the purpose of the present paper, the assumptions found in the literature will remain.

4.7 Pitching Moment of the Vortex Flap

The equipment used in the present investigation was not capable of measuring the pitching moment of the airfoil or Vortex Flap. It is desirable, however, to provide a reasonable estimate as to the nature and order of the pitching moment that could be expected upon implementation of this type of device. For the purposes of making a first-order estimate of the pitching moment for the Vortex Flap, the experimental data from the theoretically equivalent rotating airfoil flap obtained from the German investigation (Crabtree 1960) will be used as a proxy. The data available from this investigation are incomplete (the full original test results are unobtainable), but sufficient and instructive for the purposes of this section.

The rotating airfoil flap experiments were conducted at Re = 3.2 x 10^5 for three distinct geometries. Both the wing and the rotating airfoil flap employed the NACA 23015 section. The wing chord was 11.81" and the span was 31.5". The rotating airfoil flap chord was 25% of the main airfoil chord, about 2.95". For comparison, the diameter of the rotating cylinder used for the Vortex Flap was 26.7% of the main airfoil chord. It is noteworthy that, though the Vortex Flap was developed and tested without knowledge of the rotating airfoil flap experiments, the basic geometries

developed and tested are very similar, as shown in Figure 4-35. Note that the positions given are the locations of the axis of flap rotation relative to the trailing edge of the main airfoil, that there is virtually no gap for the rotating airfoil flap, and that RSM positions are used for the Vortex Flap.

Position #	**Rotating Airfoil Flap**		**Vortex Flap**	
	x/c	*y/c*	*x/c*	*y/c*
1	-0.13	-0.18	-0.107	-0.267
2	0.05	-0.13	-0.107	-0.4
3	0.13	-0.10	0.0	-0.4
Flap chord	0.25	---	0.267	---

Figure 4-35. Position of flap axis of rotation relative to trailing edge.

The geometry in the German investigation which is most representative of the Vortex Flap investigation is Position 2. When compared to the pitching moment data for other high lift devices, it can be seen that the rotating airfoil flap increases the nose-down pitching moment by a factor of roughly three over what might be expected with a double-slotted flap, and roughly six times over that produced by the NACA 23015 with a plain 0.25c flap.

The base NACA 23015 has a nose-down pitching moment of around 0.01 at maximum lift coefficient. For comparison, the base Clark Y airfoil (as tested) has a pitching moment near maximum lift of 0.064 (reducing pitching moment was one of the

explicit goals of developing the NACA 230- series airfoils, so it should not be surprising that the base pitching moment is so much greater for the Clark Y). Based on this, the Vortex Flap might be expected produce a pitching moment of around 1.5, and perhaps slightly less for a less cambered base airfoil.

4.8 Power Required to Drive the Vortex Flap

The power required to drive the Vortex Flap is driven by two things: surface friction and mechanical friction. An estimate of the surface friction can be made, as below. The mechanical friction is driven by the choice of drive system and bearings. In the present investigation, the dual goals of high Reynolds number and high SSR led to very high RPM requirements (30,000), probably an order of magnitude greater than would be required in full-scale application. Also, robustness was a priority, so the bearings chosen were relatively inefficient. To drive the vortex flap at 30,000 RPM required on the order of 1 kW from the power supplies, and in general turning the cylinder with the tunnel operating took less power than turning the cylinder with the tunnel off, even though normally the load on the bearings increased. It appears that the crossflow slightly reduces the retarding torque on the rotating cylinder, at least in this range of Reynolds numbers.

A first-order estimate of the surface drag on the smooth cylinder can be made in either of two ways. One is to use previously obtained experimental data derived from

rotating cylinders. The other is to use appropriately adjusted experimental flat plate boundary layer results, treating the entire surface of the cylinder like a flat plate with the boundary layer at the appropriate stage of development, in the manner suggested by Hoerner (Hoerner and Borst 1985, Hoerner 1965). A recent investigation into rotating cylinder boundary layers suggests that the analogy is at least approximately suitable, provided the appropriate calculation is undertaken for the Reynolds number (Dierich, Gersten and Schlottmann 1998). Both approaches are demonstrated here, and the differences are revealed in the value predicted for the skin friction coefficient.

$$Power = T\omega = r\omega D_f \tag{4.34}$$

Where, from Munson, Young, and Okiishi:

$$D_f = \frac{1}{2}\rho U^2 lbC_{df} \tag{4.35}$$

$$C_{df} = \frac{0.455}{(\log Re_l)^{2.58}} \tag{4.36}$$

C_{df} in this case is calculated from the boundary layer relations on a flat plate for fully developed turbulent flow, and is equivalent to the method recommended by Hoerner (Hoerner 1965). Re_l for the cylinder will be based on the circumference of the cylinder and the tangential velocity (Hoerner and Borst 1985). For the case of the 2" diameter cylinder used in these investigations at 30,000 RPM:

$$Re_l = 870{,}000$$

$$C_{df} = 0.004589$$

$$Power = r^4\omega^3\rho\pi lC_{df} = 102.181ft \cdot \frac{lb}{s} = 139\ Watts$$

If the experimentally obtained data obtained by the NACA in the 1940's is used (Theodorsen and Regier 1944), the coefficient of skin friction is found to be

$$C_{df} = 0.004194$$

Finally, a recent investigation into rotating cylinder boundary layers (Dierich, Gersten and Schlottmann 1998) suggests that the coefficient of skin friction be

$$C_{df} = 0.003793$$

The drag prediction using flat plate boundary layer data is higher than that taken directly from rotating cylinder investigations by Theodorsen and Dierich, by 8.6% and 17.3% respectively. These demonstrate that the flat plate boundary layer estimates produce conservative results, and so suitable for demonstrating the relatively low power consumption of the Vortex Flap. Further, these calculations suggest that the majority of the power consumed during the present investigation was lost to mechanical friction (normal power consumption during a 30,000 RPM run was on the order of 1,000 watts), which supports the observations of the author during testing.

One empirical point of reference for a hypothetical full-scale application is the NASA YOV-10A. The modified Bronco weighed 11,700 lbs at full gross, and was equipped with Rotating Cylinder flaps (Cook 1975). In this particular installation, the cylinders were one foot in diameter, which is significantly thicker than the local wing thickness, producing a 'bulge' into the airstream. The cylinder occupied roughly 70% of the total 34 foot wingspan (Weiberg 1973). Operating them via hydraulic turbine drive motors at 7,500 rpm required 30 hp, or about 1.3% of the installed 2,200 hp (it should be

noted that, with a thrust-to-weight ratio of 0.45, the YOV-10A aircraft is not unusually powerful for a military aircraft). This RPM produced an SSR of more than 6 at the approach speed of 57 kts, and so is quite a bit faster than would be required by a similarly proportioned Vortex Flap system which tests indicate should operate near SSR = 3-4. In conclusion, it appears that the power required to operate even a fairly aggressive Vortex Flap system will occupy only a vanishingly small proportion of the total power. It was also reported that the cylinders were not a source of maintenance difficulty during the flight test program.

To verify the above estimates used for the experimental cylinder, the same methods applied to the rotating cylinder on the YOV-10A produces a power requirement of 30.5 hp. Assuming that some portion of the actual 30hp usage is due to the mechanical friction of the bearings, which is not captured in the surface friction estimate of 30.5 hp, the methods developed above are conservative but reasonable in order of magnitude.

Compare the relatively low power consumption for smooth rotating cylinders to that estimated by D. A. Kirby (Crabtree 1960) for the rotating external airfoil flap. Of course the rotating external airfoil flap enjoys the benefit of the capacity to autorotate, the benefit at this low SSR is not sufficient to justify the system. For substantial performance improvement, the flaps must be driven to a super-autorotative state. While it is obvious that the power requirement should eventually be higher than for a

smooth cylinder, the estimates suggest that the power requirements are so great with increasing SSR that the entire installed power of the aircraft would be consumed to reduce the approach speed by 17%. For an 11% reduction in approach speed (SSR = 2) the power consumption would be just over 30% the total installed power. It is clear that the power consumption and lower drag give the clear practical advantage to the Vortex Flap over the rotating external airfoil flap.

5 Discussion

In this section, the data will be 'adjusted' for comparison with the peer group devices, and the hypothetical mission analysis will be conducted.

5.1 Scale Effects

Scale effects are those which must be considered when applying data obtained experimentally, normally at low Reynolds and Mach numbers, to the flight or other relevant operating condition, normally at a much higher Reynolds and Mach numbers. The purpose here is to adjust the data obtained from the present wind tunnel investigation for comparison to data obtained from investigations conducted at much higher Reynolds numbers. The results will be 'adjusted' to approximately represent those at a Reynolds number of 1.5×10^6, 3.0×10^6 and 8.3×10^6. These particular points were chosen because they represent key operating conditions for the Mission Analysis section, and the highest Reynolds number available using the Jacobs' method, respectively. The data selected for scale effect 'adjustment' comes from the best of the interpolated but fixed representative "Position" from the RSM analysis. In this case, "Position 2" will be the representative geometry. Note that, though the data are interpolated/extrapolated in various dimensions, it remains close to the cluster of

experimental data points it is to represent, and does not represent a fundamentally new, untested geometry (see Figure 4-20).

5.1.1 Fundamental Considerations

The nondimensional parameters which define the performance of airfoil sections and flaps account for differences in geometrical scale, but do not account for the effects of compressibility and viscosity, as represented by the nondimensional flow parameters Mach number and Reynolds number (Abbot and Doenhoff 1959). The viscous effects are expressed physically by changes in the behavior of the boundary layer, particularly as shifts in the location of transition to turbulent boundary layer flow, and changes in the location of flow separation (Barlow). The Vortex Flap is a low-speed device even at full-scale, so compressibility effects will be ignored. The viscous effects are very significant, however, since the tests were conducted at relatively low Reynolds numbers. In order to make direct comparisons between the Vortex Flap and other devices, the experimental data will have to be adjusted to reflect a scale similar to that which produced the comparison data for the peer group.

A note of caution is in order: adjusting for scale effects is notoriously tricky business, and varies for every individual airfoil section and particular geometry. However, the body of data suggests general trends and some methods have been developed to

approximate full-scale performance from small-scale data. But the results of such an approximation must be treated as suggestive, not conclusive.

Airfoils

It has been long accepted that the general effect of an increase in Reynolds number on airfoil performance is an increase in lift and a decrease in drag. Tests in the NACA Full-scale tunnel for a Clark Y over a wide range of Reynolds numbers produced the results shown in Figure 5-1 (Silverstein 1935). Similar effects can be observed on an NACA 23015 tested over a range of Reynolds numbers (Abbott and Von Doenhoff 1959).

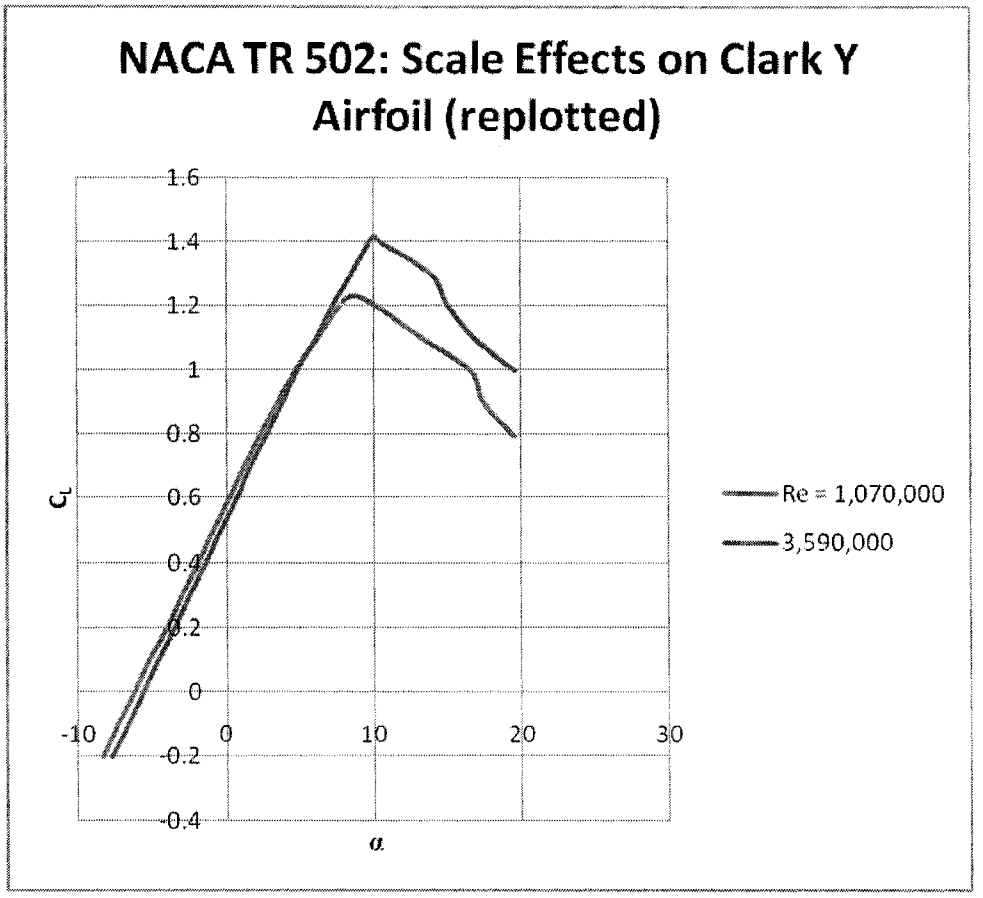

Figure 5-1. Scale Effects on a Clark Y airfoil taken from NACA TR 502.

For Reynolds numbers of less than one million, the presence of considerable laminar flow in the boundary layer adds additional complications. Modern investigations into scale effects in the low-Reynolds number range (below roughly 10^6) for airfoils highlight the so-called laminar separation bubble and its effects on lift and drag (Selig, Donovan, and Fraser 1989). The laminar separation bubble exists in the flow over many airfoils at low Reynolds numbers, and the behavior of this bubble introduces relatively rapid shifts in airfoil characteristics. The general process for the formation of a laminar separation bubble is thus: The boundary layer is laminar near the leading

edge of the airfoil. Due to the low Reynolds number, the laminar nature persists into an area of adverse pressure gradient, causing the flow to separate. At some point farther downstream, the separated boundary layer becomes turbulent, and so energized, reattaches to the surface of the wing, completing the 'bubble' (Jones 1990). The presence of the bubble separates the flow in to at least three distinct regimes: normal, super-critical, and sub-critical.

For an aircraft operating at a moderate Reynolds number, the boundary layer will undergo a transition to turbulent flow before the point of lowest pressure on the upper surface of the airfoil is reached. This transition will allow the boundary layer to persist in remaining attached against the adverse pressure gradient present behind the point of minimum pressure, even over a wide range of angles of attack.

If the Reynolds number is low enough, the boundary layer will not undergo this transition prior to reaching the minimum pressure point, and will deal with an adverse pressure gradient without the additional energy afforded by the transition to turbulent flow. The boundary layer may separate and flow over a recirculating bubble known as the laminar separation bubble. If the Reynolds number has not dropped too far, the separated boundary layer will undergo a transition to turbulent flow while separated and reattach to the upper surface of the wing. If the Reynolds number has dropped too far, the flow will not reattach, and the wing will be stalled. This separation can occur at a very low angle of attack.

If the flow does not separate at all, it can be called normal flow. If the flow separates but reattaches, the flow is said to be super-critical. If the flow separates and fails to reattach, the flow is said to be sub-critical (Simons 2002). These three regions of operation, normal, super-critical, and sub-critical, play an important role in determining the performance of aircraft operating in this regime. Figure 5-2 illustrates these three regions. The general effect of the presence of increasingly laminar flow, growing laminar separation bubbles, and flow separation is to degrade airfoil performance.

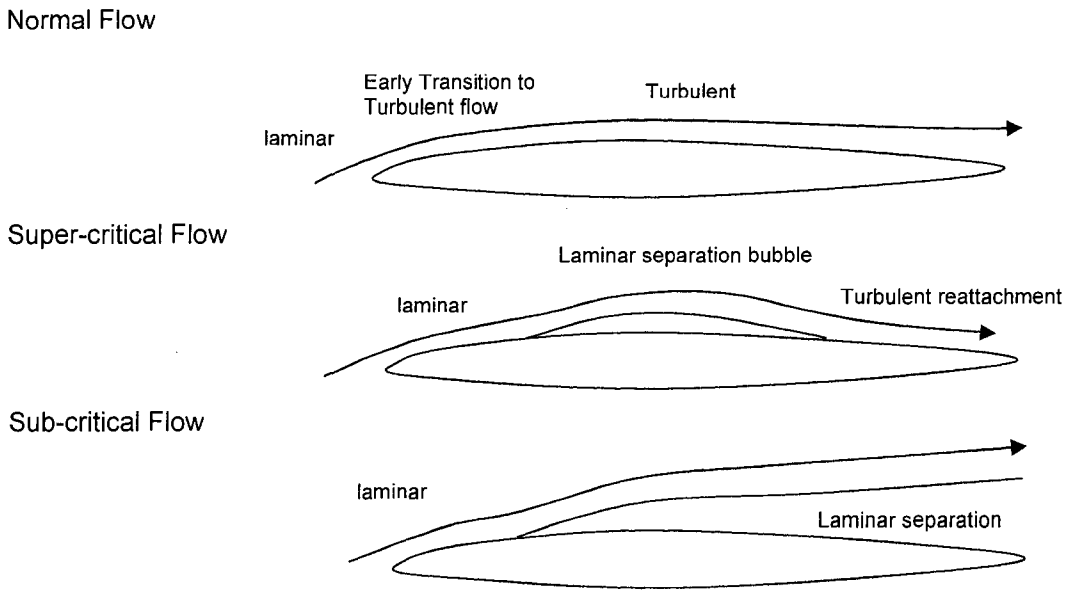

Figure 5-2. Normal, Super-critical, and Sub-critical Flow Over a Wing

The critical Reynolds number for which the laminar separation ceases to reattach for the Clark Y is around 60,000 (Simons 2002). Above this point, the performance is relatively good due to the turbulent reattachment. It is likely that for the present investigation, the critical Reynolds number was lower, probably below the range tested, due to the textured wood surface of the model energizing the boundary layer. It is likely however, that the laminar separation bubble persists over most of the test range, and its presence complicates accurate extrapolation to full scale. There is also frequently observed a lift hysteresis loop in this realm, but as the test setup is unable to detect the presence of such loops, the discussion is herein omitted. Barlow summarizes the general scale effect on the lift curve, the maximum lift coefficient and stall angle by demonstrating that the slope of the lift curve is unchanged, but the angle of attack and magnitude of maximum lift coefficient are both increased with increasing Reynolds number (see Addendum Figure 11).

Cylinders

The boundary layer behavior strongly influences the flow around a circular cylinder (see more in depth discussion, Section 2.1.2). When the boundary layer transitions from laminar to turbulent, the region of flow separation shrinks, and the drag coefficient drops suddenly at around Re = 2.5-3.0 x 10^5 (see Addendum Figure 12) (Munson, Young, and Okishi 1998). The precise effect on rotating cylinders is unknown, and the data obtained in the present investigation for the rotating cylinder only were obtained well below the transition value. No transition was observed at the

lower values, but it is suggestive that some type of transition may occur and significantly reduce the drag of the deployed Vortex Flap. This is yet another complicating factor in accurately extrapolating the data to full scale, but by omitting an adjustment for this particular effect, the results are made more conservative.

Flaps

Of course high lift devices introduce another variable when accounting for scale effects. Barlow suggests that one should expect 'a little more' from a flap at full scale flight conditions (see Addendum Figure 13). Hoerner suggests that while neither the lift increment nor the lift coefficient is constant, the *ratio* of the two is (Hoerner and Borst, 1981). This observation is based on the data from a number of NACA and Aeronautical Research Council investigations (see Addendum Figure 14), and will be used by the author to account for scale effects on the Vortex Flap lift increment.

5.1.2 Scale Effect Corrections Applied to Results

Maximum Lift Coefficient

This will be the combined result of two scale effects:

- Influence on the basic airfoil section lift characteristics
- Influence on lift increment due to the flap

The method developed by Jacobs (Jacobs 1939) and summarized by Barlow (Barlow 1999) has been used in reverse to estimate the maximum lift coefficient of the Clark Y with no flap, using the NACA 2412 as the closest available surrogate for the Clark Y for which the Jacobs method can be applied. This substitution is considered acceptable by the author because the basic NACA 4-digit series profile was derived from Clark Y and similar airfoils, and the NACA 4412 shares similar camber and thickness (Abbott and Doenhoff). Efforts were taken at every step to make estimates conservative rather than liberal in presenting the performance of the 'adjusted' device. The tables used in applying Jacob's method are available in the Addendum as Figures 15 and 16.

Lift Increment

There is a range in which lift increment is roughly constant for some flaps, but Barlow asserts that "we are usually justified in expecting a little more from a flap full scale than is found in a tunnel at low Reynolds numbers..." Hoerner suggests that a roughly constant lift increment is a worst-case scenario, and that assuming a constant lift-increment-to-lift-coefficient ratio can be appropriate. Given the particularly low Reynolds numbers of the original tests, the latter assumption seems appropriate for these estimates.

L/D

Adjusting the drag data is considerably more difficult than adjusting the lift data, particularly with the majority of drag generated by flow separation around the rotating

cylinder. It is safe to conclude that the drag coefficient will decrease substantially with an increase in Reynolds number (see Section 5.1.1 above) but it is impossible to quantify for this device, so it will not be attempted.

Performance Summary

Drawing from the RSM results, the configuration with the best performance ("Position 2") has been chosen, is adjusted for scale effects, and later will be used for comparison to the peer group of trailing-edge high-lift devices. The adjustment procedure follows: First the method developed by Jacobs will be used to adjust the maximum lift coefficient of the unflapped Clark Y airfoil at the higher Reynolds numbers. Then the lift increment ratio ($\Delta C_{L,\,Total}/C_{L,\,max,\,no\text{-}flap}$) at the lower Reynolds numbers will be used to estimate the maximum lift coefficient of the flapped airfoil at full scale, following the suggestion of Hoerner. These calculations are summarized in Figure 5-3. Note that the $C_{L,\,max}$ figure represents the highest figure found at the discrete angles of attack tested, with an increment of 2.5°, and therefore probably do not represent the actual absolute maximum, which may lie between tested points.

Reynolds Number	$C_{L, max}$ no flap	Jacobs	$\frac{\Delta C_{L, Total}}{C_{L, max, no-flap}}$	$C_{L, max}$ with VF	$\Delta C_{L, max}$	C_D	L/D @ $C_{L, max}$
2.5 x 10^5 (results)	1.19 @ α = 10°	---	3.06	**3.65* @ α = 10°**	2.46	.55	6.64
1.5 x 10^6 (adjusted)	1.32	0.13	---	**4.04**	2.72	?	7.35
3.0 x 10^6 (adjusted)	1.48	0.29	---	**4.53**	3.05	?	8.24
8.3 x 10^6 (adjusted)	1.64	0.45	---	**5.02**	3.38	?	9.13

*RSM "Position 2", α = 10°.

Figure 5-3. Summary of application of scale effect adjustments to Vortex Flap data.

Note that the L/D is calculated at the maximum lift coefficient, and is *not* the L/D max. The L/D for the Clark Y airfoil alone under the same conditions is only around 15.4 vs. and L/D_{max} of just under 19. The L/D_{max} for the Clark Y with the Vortex Flap at "Position 2" is just under 10 as compared to 6.64 as listed in the table.

5.1.3 Geometric and Configuration Effects

There are a number of geometric considerations which suggest that the results presented above could be improved upon. These configurations are summarized here:

* Non-optimal airfoil selection.
* No other high-lift devices
* Non-optimal Vortex Flap geometry selection

The Clark Y was chosen for its ubiquitous use in both the modeling and full-scale aviation community, not because it is the highest performance airfoil. With a better-performing base airfoil, it is likely that the Vortex Flap would be even more effective. Better yet, it is possible that with the aid of CFD, an airfoil could be optimized for use with the Vortex Flap.

It is also likely that the vortex flap could be used in conjunction with a variety of high-lift devices. These include vortex generators, drooped leading edges, slats, and perhaps other trailing-edge high-lift devices. Finally, it is clear that, unless the author was very 'lucky,' the optimal geometry was not tested directly. Due to the discrete selection of α, and the limited selection of rotating cylinder positions, the maximum performance was almost certainly not found. There remains a great deal of testing necessary to optimize the Vortex Flap. For those reasons, the present performance projections are probably conservative.

5.2 Comparison with Other Trailing-Edge High-Lift Devices

A summary of the performance of the various high-lift devices as compared to the vortex flap is given in this section. These data are taken from an eclectic mix of sources, but primarily from tests conducted by the NACA, which has produced the most complete and monolithic index of comparable data for the peer group. Note that the external airfoil flap is similar to the single-slotted flap, provides no performance advantage, and is deleted. The Venetian-blind flap is deleted for the same reason.

The information is presented in three groups. The first is the base airfoils in Figure 5-4, the next is the 'passive' devices in Figure 5-5, and finally the mechanically assisted flaps and high-lift systems are presented in Figure 5-6. Note that a great deal of data manipulation, estimation, and adjustment was required to develop a single set of 'comparable' data. Every effort was made to give relative advantage to the comparable devices over the Vortex Flap when estimating performance. Note that in many cases, the desired 'comparable' configuration was unavailable. For example, the rotating cylinder flap data are only available with a double-flap and a very large slat.

None	Clark Y	0.06		1.18	--	0.033	--	1
		0.30		1.21	--	0.028	--	1
	Clark Y	0.61	AR = 6	1.25	--	0.125	-0.080	11
		1.10		1.23	--	0.042	-0.062	2
		3.50		1.42	--	0.041	-0.064	2
	Clark Y (Buerge)‡	0.08		1.07	--	0.097	--	--
		0.25		1.19	--	0.093	--	--
	NACA 0012	3.00		1.02	--	0.016	0.000	3
		9.00		1.55	--	0.012	0.000	3
	NACA 23012	3.00		1.24	--	0.021	-0.020	3
		8.80		1.72	--	0.018	-0.020	3
	NACA 23015	2.60		1.19	--	0.027	-0.010	3
		8.90		1.72	--	0.020	-0.010	3
	NASA Supercritical 9.3% Blunt based	2.83		1.72	--	0.035	-0.450	9
	Joukowsky	0.05		0.88	--	--	--	8

Figure 5-4. Summary of base airfoil data (see references below).

Plain Flap	Clark Y (AR = 6)	0.61	0.20	60	2.00	0.74	0.40	-0.27	4,11
	NACA 23012 (AR = 6)	3.50	0.20	75	2.40	0.88	--	-0.23	4,11
	NACA 23015	3.50	0.25	60	2.00	0.92	0.40	-0.23	4,12
Split Flap	NACA 23012	3.50	0.30	60	2.60	1.06	0.24		4
		6.00			2.81	1.33			4
	NACA 23015	3.00	0.20	60	2.79	1.26			4
		6.00			2.90	1.20			4
Zap Flap	Clark Y (AR = 6) hinge @ 0.9c	0.60	0.40	45	2.45	1.17	0.62	0.48c	4, 10
Single Slotted Flaps (Fowler)	Clark Y (AR = 6)	0.60	0.40	40	3.10	1.89	0.74	-0.95	4,13
	NACA 23012	3.50	0.30	40	3.29	2.05	0.19	-0.68	4,14
Double Slotted Flaps	NACA 23012	3.50	0.40	30/70	3.47	2.23	0.27	-0.62	4
Vortex Flap	Clark Y (Buerge)	0.25	0.27		3.65	2.46	0.69	-1.50	--
		3			4.53***	3.05**			
		8.3			5.02***	3.38**			

Figure 5-5. Summary of performance of passive trailing-edge high-lift devices (see references below).

Rotating Cylinder Flaps (in conjunction with single-slotted double-flaps and 0.22c slats and endplates)	not listed	2.0-2.9	0.46 AR = 6	60/18 SSR = 8	3.60	--	1.50 SSR = 6.6	--	6
Trailing Edge Cylinder Flaps	**NACA 23015 α = 15°**	**0.10**	**0.08**	**SSR = 6**	**2.35**	**1.53****	**--**	**--**	**7**
Moving Surface Boundary Layer Control									
Trailing Edge Cylinder	**Joukowsky**	**0.05**		**SSR = 4**	**1.68**	**0.80**	**--**	**--**	**8**
Leading Edge Cylinder		0.05		SSR = 4	2.10	1.22	--	--	
Both Cylinders		0.05		SSR = 4/4	2.60	1.72	--	--	
Single Slotted Flap"	NASA Supercritical 9.3% Blunt based	2.83	0.29	20	3.01	1.29	0.03	-0.40	9
Double Slotted Flap and Slat"		2.83	0.44	28.5/50.2	4.70	2.98	0.09	-0.55	
Triple Slotted Flap and Slat"		2.83	0.49	20/44.7/64.7	5.55	3.83	0.14	-0.65	
Rotating Airfoil Flap	**NACA 23015**	**0.14**	**0.25**	**SSR = 4**	**3.04***	**2.22****	**1.35**	**-1.45**	**5**
		3.00			**4.41*****	**3.22**			
Vortex Flap*	**Clark Y (Buerge)**	**0.25**	**0.27**	**SSR = 3**	**3.65**	**2.46**	**0.69**	**-1.5†**	**--**
		3			**4.53*****	**3.05****			
		8.3			**5.02*****	**3.38****			

* Adjusted by author to account for wind tunnel wall effects. Uncorrected data for rotating airfoil flap: CL, Max = 3.8
** Estimated by author using Jacobs' method
*** Estimated by author using Hoerner's guidelines
† First-order estimate by author from Crabtree
‡ Not the absolute maximum

1 Selig, Donovan, and Fraser (1989) Soartech 8
2 Silverstein (1935) NACA TR 502
3 Abbott and Doenhoff (1959)
4 Cahill (1949) NACA TR 938
5 Crabtree (1960) ARC TR CP 408
6 Deckert (1966) NASA SP-116
7 Hoerner and Borst (1981)
8 Modi, Mokhtarian, and Yokomizo (1990)
9 Omar (1973) NASA CR-2215
10 Platt (1935) NACA TR 541
11 Wenzinger (1935) NACA TR 554
12 Ames (1940) NACA TN 763
13 Platt (1935) NACA TR 534
14 Lowry (1941) NACA TN 808

Figure 5-6. Summary of power-assisted flaps and some high-lift systems (peer group in bold).

A first-order estimate of the performance of the Vortex Flap as a part of a complete high-lift system as compared to other high-lift devices and systems is given in Figure 5-7.

Plain and split flaps	0.9	1
Fowler	1.3c'/c	2
Double Slotted Flaps	1.6c'/c	3
Triple Slotted Flaps	1.9c'/c	4
Rotating Cylinder Flap	2	5
Rotating Airfoil Flap	3.2	4
Moving Surface Boundary Layer Control (leading and trailing edge cylinders)	2.7	5
Vortex Flap	3.1	4
Typical Modern High-Lift System (Triple-Slotted Flaps and Slats)	3.8	5
Vortex Flap plus Slat and Plain Flap (hypothetical configuration)	5	6

Adapted from:
Loftin (1985) NASA SP-468
Raymer (1999)
Filiponne (2006)
Modi et al (1990)

Figure 5-7. Summary of estimated performance of the Vortex Flap and other high-lift devices and systems.

Lift

The superiority of the Vortex Flap as a single element is apparent, provided the assumptions made in adjusting the data prove correct. In particular, the Vortex Flap provides a lift increment alone which it would otherwise require fully three secondary elements to produce, as in the double-slotted flap with slats arrangement. The lifting potential of a Vortex Flap in combination with other devices is interesting indeed.

Drag

The drag of the Vortex Flap (though it has not been adjusted for scale effects and would almost certainly be lower) is not unreasonable during high-lift operations. In particular, at around one-half the drag of the rotating cylinder flap and the rotating external airfoil flap, it seems to have a clear advantage in this area over devices of similar function. However, the drag penalties are large indeed when compared with traditional high-lift systems, an order of magnitude greater than the similarly-performing double-slotted flap and slat system. Reducing the drag during high-lift operations is an area requiring additional study for the device to be practical.

One other disadvantage of the Vortex Flap is the lack of an obvious cruise configuration. Most flaps retract readily into the wing (or are integral to the wing, as in the case of rotating cylinder flaps and others). Even the rotating airfoil flap must only

be stopped at the appropriate angle in order to provide a low-drag cruise configuration. Unless the Vortex Flap is of sufficiently small diameter to be retracted into the wing, more radical measures would have to be taken to retract the cylinders into the fuselage, or pivot them so that they lay streamwise during cruise flight. There is also the possibility that a future configuration of the Vortex Flap (See Section 6.3) will have sufficiently low drag that it can remain extended.

Complexity

The complexity is on the order of similar high-lift systems like the rotating cylinder flap. In fact, if the Vortex Flap were implemented as a part of a larger high-lift system, the final complexity would be nearly identical to that of the rotating cylinder flap tested by NASA. These are both considerably more complicated than the traditional 'passive' systems normally employed. It is to the Vortex Flap's advantage, however, that the performance improvement is relatively more, and the drag is relatively less, than for the rotating cylinder flap system, even when deployed without the aid of additional elements.

5.3 Discussion of Physical Phenomena of the Vortex Flap

It is clear from the data that for the Vortex Flap, the whole is greater than the sum of the parts. If you add the lift of the wing-only and cylinder-only configurations the sum will be less than the lift of the comparable combined configuration. This is outlined in terms of C_L for $\alpha = 5°$ and Position 2 in Figure 5-8.

SSR	Wing-only	Cylinder-only	Added	Vortex Flap	Bonus Lift
0	0.6	0	0.6	1.2	0.6
1	0.6	0.3	0.9	1.4	0.5
2	0.6	1.0	1.6	2.2	0.6
3	0.6	1.7	2.3	3.2	0.9
4	0.6	2.0	2.6	3.4	0.8

Figure 5-8. "Bonus" lift of the Vortex Flap.

This "Bonus Lift" highlights the beneficial interactions which take place between the rotating cylinder and the wing. As outlined in detail for the peer group devices in Section 2, the physical means of lift production for the Vortex Flap are threefold: slat effects, Magnus effects, and dam effects. As mentioned before the "Circulation" and "Dumping" slat effects most likely account for the significant benefit of the presence of the stationary cylinder. That the rotation of the cylinder enhances the slat effects and generates lift directly through the Magnus effect is also evident. To study the role of the Magnus effect more closely would require an experimental rig capable of measuring the lift and drag forces on the cylinder and primary airfoil separately. The 'dam' effect is the suggestion that the presence of the cylinder in the flow field beneath the wing, coupled with the cylinder's considerable drag, serves to physically

restrain the flow below the wing relative to the flow above the wing, thus enhancing lift. This is clearly a viscous effect, was not mentioned in A. M. O. Smith's "Aerodynamics of High-Lift Airfoil Systems," or any of the other literature. The function might be similar to that of a Gurney flap, which is a simple wall perpendicular to the surface of the wing which extends down into the flow from the trailing edge (Liebeck 1978). It might also be similar to the function a fence placed on the lower surface of a stationary circular cylinder, which can achieve appreciable lift coefficients (Horner and Borst 1985). The "Bonus Lift" is a product of the slat and dam effects.

There are several qualitative ways to describe the effect and function of the Vortex Flap, two of which follow:

- Potential flow description: The presence of the Vortex Flap is analogous to the presence of a vortex underneath the trailing edge (see Section 4.6). This places the primary airfoil in the 'upwash' of the vortex, increasing the effective angle of attack, which accounts for the increase in circulation around the primary airfoil necessary to satisfy the Kutta condition. This influence can be observed directly as the rotation of the cylinder can cause the separation of flow from the upper surface of the airfoil at relatively low angles of attack. This is in addition to the lift force on the rotating cylinder itself, which is well established in potential flow theory (Currie 1974).

- Bernoullian description: The rotation of the cylinder itself clearly induces a region of accelerated (and thus low-pressure) flow above the cylinder, and decelerated (and thus relatively high-pressure) flow above the cylinder. This is the function of the Magnus effect, and accounts for the lift force on the cylinder itself, which is assumed to exist. What requires more explanation is the "Bonus Lift" which is not immediately evident in this point of view. In fact, it could be argued that the high-velocity region above the cylinder (but below the wing) could "suck" the wing down and have a counterproductive effect. However, this assertion would argue the same for slotted flaps, as the low-pressure area of the flap is below the trailing edge of the wing. It must be recalled that the influence of the circulation around the secondary element does not stop at the lower surface of the primary element, but rather permeates the flow field, and the larger effect of this circulation is to place the primary airfoil in the upwash of the cylinder, which amounts to a higher effective angle of attack. This higher effective angle of attack produces higher lift on the primary airfoil in the normal manner. In addition to this, the dam effect serves to lower velocities below the primary airfoil, which enhances lift further, in this view.

5.4 Mission Analysis: Ship-borne Observation VTUAV

The author hopes that the potential utility of the Vortex Flap in enabling STOL utility missions is self-evident. However, the existence of at least one mission currently filled by a rotary-wing aircraft which could conceivably be filled by a fixed-wing aircraft should be highlighted to demonstrate the power of the Vortex Flap. The US Navy currently employs a heavily modified Schwiezer 300 helicopter as an eyes-in-the-sky VTUAV which operates off of its destroyers (Northrup-Grumman 2008). The basic mission is to lift off, climb to 10,000 feet, cruise out 110 NM as quickly as possible, loiter for 5 hours, return and land with reserves while carrying a 200 lb. payload.

If the stall speed of a fixed wing aircraft could be lowered sufficiently below the speed of the ship, then that aircraft could operate from the ship in a manner similar to that of a helicopter, with a vertical rise and steep climb-out. The author submits that the power of the Vortex Flap, particularly when employed as a part of a high-lift system, is sufficient to lower the stall speed of a number of light single-engine aircraft to below 30 knots, which is within the speed range of the Destroyer, allowing vertical operations with the fixed wing aircraft. While a clean sheet of paper design would be best, for the sake of demonstration, an existing aircraft will be used as a starting point. The Helio Courier, while not perfect, is a suitable starting point for this demonstration.

The Helio Courier was the brainchild of Otto Koppen and Lynn Bolinger, intended to be an 'everyman's safety-plane' to fulfill the plane-in-every-garage vision still anticipated in the late 1940's. These men took it as self-evident that very safe and very low-speed operation, as well as the capacity to operate from unusually short fields, was the primary consideration in designing a fundamentally safe airplane. Through the judicious application of basic high-lift devices, and the installation of a truly enormous propeller, the pair was able to build a prototype example capable of operating off a tennis court (Rowe 2006).

The eventual result of their work was the Helio Courier which became known, rather than an everyman's safety-plane, as a very expensive, very capable short-field machine with a respectable cruise speed. The Helio Courier, in all its various forms, made use of full-span automatic Handley-Page slats, and large span single-slotted Fowler flaps. The installation of a geared engine (unusual in light planes where direct-drive is the standard) allowed an unusually large propeller for the horsepower, dramatically increasing thrust at low-speeds. For example, at full gross weight the Helio Courier H-395 is able to take-off and land on a 500' strip with 50' obstacles located at each end. While credit in the popular aviation media for the incredible low-speed performance is normally given to the slats, the author's own analysis indicates that it is due also to two other factors rarely considered. The first is simply that the airspeed indicator errors are large (>50%) at low speeds, giving pilots the impression that the aircraft performs more impressively than it does. The actual minimum control

speed is probably around 37 knots under full power rather than the often-reported 22 knots (US Air Force 2001). The second is that the unusually large propeller (8' diameter 3-bladed propeller vs. 6' 8" 3-bladed propeller installed on the Cessna C-185, a similar utility aircraft (Taylor 1979) allows the aircraft to generate tremendous thrust at low speeds. In combination with the slats that allow the aircraft to reach unusually high angles of attack, the large propeller ends up generating a very considerable vertical component thrust which significantly reduces the weight that must be supported by the wings at low speeds. According to the author's calculations, in level flight this reduction can be well over 20%. This serves to reduce the minimum control speed to below the range of more conventional aircraft.

Eventually an entire line of aircraft was developed, including twin engine and turbine powered variants. Helios saw service in the CIA's Air America operations during the Vietnam War, and served very well as jungle delivery planes. Many of the civilian aircraft ultimately found their way into service under similar conditions for the Jungle Aircraft And Radio Service (JAARS), an evangelistic and humanitarian organization. JAARS currently operates the largest fleet of Helios. With over 500 of all variants built before the end of production in 1984, the Helio Courier was a modest business success (Rowe).

5.4.1 Modification of the Helio Courier

The base aircraft selected is a military version of the Helio Courier Model 395, known as the U-10B. This particular model was chosen for its combination of performance parameters, and the availability of performance information in the form of a flight manual (US Air Force 1966). The basic description follows.

The Helio Courier H-395/U-10B is a high-wing monoplane with a cantilever wing, all-flying stabilator, and fixed conventional landing gear. Capable of seating five, the aircraft is primarily aluminum with fabric-covered ailerons and a steel safety cage around the cabin. Provisions for STOL include full-span Handley-Page automatic leading edge slats, 64% span single slotted Fowler flaps, and spoilers called 'interceptors' to aid lateral control at low speeds. The plane is powered by a geared Lycoming GO-480-G1D6 good for 295 hp for takeoff and 280 maximum continuous power driving a 3-bladed constant speed Hartzell propeller of 8' diameter. The U-10B has provisions for up to 879# useable fuel, and a gross weight of 3,600# as compared to 3,000# for the civilian version. This is probably due to the smaller margins of safety accepted for military operations rather than structural modifications.

Performance and Specifications (True Calibrated Airspeed)

Length	31 ft.	Top Speed	148 knots
Span	39 ft.	Minimum Speed	35 knots*
Height	8 ft. 10 in.	(power on)	
Wing Area	231 sq. ft.	Minimum Speed	47.4 knots*
Wing Chord	6 ft.	Initial Climb Rate	935 fpm*
Aspect Ratio	6.6	Empty weight	2,000 lbs.*
Power (5 min.)	295 hp	Gross weight	3,600 lbs.
Power (continuous)	230 hp	Best climb speed	75 knots

* Estimated from flight manual and author's calculations.
Data collected from Rowe 2006 and U-10B Flight Manual.

Figure 5-9. Performance and Specifications of the U-10B Aircraft

First-order estimation methods suggested in design textbooks by Raymer (Raymer 1999) and Roskam (Roskam 2001) and data from Jane's All-The-World's Aircraft (Taylor 1961) were used to adapt the Helio Courier for this mission. The assumptions made for this analysis follow:

- Takeoff speed must be 31 knots or less for 'vertical' operation. This is below the top speed of modern US Navy Destroyers (ref).
- Power-on stall speed must be less than 31 knots/1.2 = 25.8 knots. This drives the wing sizing and lift coefficient requirements.
- If it can take off, it can climb (this was later verified analytically).
- The weight build-up for the modified Helio aircraft follows:
    - Original U-10B empty weight: 2,000 lbs.
    - "UAV Conversion" obtained by comparison with the Schweizer 330 conversion to the Fire Scout: 688 lbs.

- Building the aircraft out of composites instead of aluminum would save, using Raymer and Roskam's estimates: 726 lbs.
- Vortex flap weighs 10% of gross weight: 360 lbs.
- Larger wing weighs an additional 5% of gross weight over the weight of the normally sized wing: 180 lbs.
- Total zero fuel weight: 2,500 lbs.

- The Vortex Flaps pivot during climb and cruise to align with the wind. The details of this configuration are not specified.
- The drag of the Vortex Flaps in the cruise/climb configuration will be estimated by comparison with the drag of pontoon floats installed on the same aircraft. The performance data are available, and the drag of the floats can be calculated.
- The drag of the tailwheel is neglected.
- Running the Vortex Flap at an SSR = 2 will reduce the profile drag of the cylinder by 1/3, based on experimental observation. This aids during initial climb.
- The mission specification that the service ceiling be 20,000 ft is neglected, though this could ultimately be met with a turbocharged engine or other similar accommodation.
- Raymer's methods were used to calculate the maximum coefficient of lift that could be expected from the high-lift devices that were used.

- Of the options available to make an estimate of the maximum Vortex Flap lift increment, the most conservative (constant lift increment) was used.
- It was assumed that the basic function of the Vortex Flap would not be hindered by the presence of a single-slotted Fowler flap deflected 20°, and also that the presence of the Vortex Flap would not change the lift increment provided by the slat or Fowler flap. This would need verification in wind tunnel testing.

Based on these assumptions and methods, an analysis following Roskam's Class I and some Class II methods was conducted which produced the following performance and specifications in Figure 5-10.

Performance and Specifications (True Calibrated Airspeed)

Length	31 ft.	Top Speed	97 knots
Span	47 ft.	Stall Speed	25.8 knots
Height	8 ft. 10 in.	(power on)	
Wing Area	284 sq. ft.	Stall Speed	29 knots
Wing Chord	6 ft.	Initial Climb Rate	660 fpm
Aspect Ratio	8	Empty weight*	2,500 lbs.
Power (5 min.)	295 hp	Gross weight	3,600 lbs.
Power (continuous)	230 hp	Best climb speed	64 knots

* Includes the weight of the UAV conversion, 688 lbs.

Figure 5-10. Performance and Specifications of the new aircraft

With this performance, a mission analysis was conducted to determine how much fuel would be required, and how much payload could be carried on that mission.

5.4.2 Analysis of Original and Modified Helio Courier for Mission

The mission analysis results for the original U-10B Helio Courier and the modified Helio follow in Figure 5-10. Note that the U-10B does not meet the requirement for vertical takeoff and landing, but the ground roll with a 31 knot headwind was calculated and is included below. Note also that 688 lbs. will be deducted from the payload for the U-10B to account for the UAV conversion.

Phase	Weight at end (modified/original)	Time (minutes) (modified/original)	Fuel burned (lbs.) (modified/original)
Start, warmup	3600/3600	10/10	18/18
Takeoff	3,596.5/3,598.25	1/0.5	3.5/1.75
Climb to 10k	3,550/3571	24.5/15	47/27
Cruise to 110 NM	3,479/3,514	51.3/41.5	70/57
Loiter 5 hrs	3,197/3,289	300/300	282/225
Return 110 NM	3,098/3,220	72.5/50.4	99.4/69
Descent	3,086/3,208	15/15	12/12
Maneuver/Land	3,071/3,193	5/5	15/15
20 minute reserve	3,054/3,178	20/20	15/15
Shutdown	3,052/3,178	5/5	2.5/2.5
Totals		**484/442**	**566/443**

Figure 5-11. Mission Analysis for U-10B and the modified Helio.

The takeoff ground run of the U-10B aircraft under these conditions is approximately 200 feet. The landing ground run is approximately 40 feet. Assuming the aircraft are fueled to 3,618 lbs. before startup, which permits liftoff at 3,600 lbs, the remaining payload of each aircraft is:

U-10B: 3,618 - 442.5 - 688-2,000 = 488 lbs.

Modified Helio: 3,618 - 566.3-2,500 = 552 lbs.

Note well that if the U-10B were assumed to be made of composite instead of aluminum, the payload would be increased to 1214 lbs. The major difference in payload can be readily attributed to the vertical takeoff and landing requirement, which necessitates additional high-lift devices and a wing stretch which together at 15% of the aircraft gross weight to the empty weight. Also, this is a loiter mission, and it is apparent that payload can be exchanged for additional time on station, provided fuel tanks are sufficiently large, as shown in Figure 5-11.

Payload (lbs)	Fuel (lbs)	Loiter time (hrs)
552	566	5
400	718	8
200 (minimum specified)	918	12

Figure 5-12. Payload vs. loiter time for modified Helio aircraft.

It should be further noted that what is required for vertical liftoff is 31 knots over-the-deck, by any combination of boat speed and wind which will produce that combined velocity. At lighter weights, less is required for vertical takeoff, though not so much as to make payload reduction an efficient means of reducing wind requirements, as shown in Figure 5-12.

Gross Takeoff Weight (lbs)	Required Wind-over-deck for VTOL (kts)
3,600	31
3,300	28.8
3,000	26.4

Figure 5-13. Relationship between gross takeoff weight and wind-over-deck required for VTOL.

The purpose of this exercise is to demonstrate the hypothetical potential of the Vortex Flap, not to assert that a vehicle so modified is a better fit than the present helicopter serving in this particular mission. Nonetheless, this exercise does demonstrate that this type of mission is at least hypothetically possible with the application of the Vortex Flap.

6 Conclusion

The Vortex Flap is herein demonstrated to be a novel, powerful, and potentially useful concept. It is a significant step in the evolution toward useful high-lift devices which make use of rotating cylinders, and may figure directly or indirectly in a practical future application. Following are a summary of the author's contributions to the state of the art through this investigation, followed by an outline of the relevance and significance of those contributions. Finally, avenues of future research and application are explored, and particular ideas set forth for investigation.

6.1 Review of Contributions

The author presents this paper as evidence of significant contributions to the state of the art. These contributions are summarized below.

- The vortex flap is the first application of a rotating circular cylinder in combination with an airfoil which does not function as a boundary layer control device. This is clear from the literature review outlined in Sections 2 and 5.
- This investigation is the first to explore the rotating cylinder as a distinct element which is able to take full advantage of the 'slat' effects outlined in

Section 2. This 'separate cylinder' paradigm represents a fundamental shift in the direction of research in this area.

- The Vortex Flap is the first rotating flap design which addresses the vibration and power consumption issues associated with the only other rotating flap design to date, which employs a rotating airfoil. The rotating airfoil generates lift in a periodic fashion related to its rotation, and the shedding of large periodic vortices requires far greater torque than turning a smooth cylinder.
- An extensive and specialized experimental investigation, requiring design and fabrication of unique test equipment, which demonstrates the effectiveness and potential usefulness of the Vortex Flap.
- As demonstrated by the literature review (See Section 2, Section 5, and the Addendum), the Vortex Flap is the most effective single-circular-cylinder-and-airfoil configuration known for the generation of lift. There is none other, to the author's knowledge.
- This dissertation required the development of a simplified form of Response Surface Methods which did not require the development of a single polynomial in order to generate meaningful response surfaces (see Section 4 and Appendix B).
- It was demonstrated, in a hypothetical manner, that the Vortex Flap has sufficient lifting capacity to enable missions not previously possible for fixed wing aircraft (See Section 5).

- Since this investigation represents a shift in the direction of research in this area, it suggests a compelling program for future research based on the results of this investigation including lower-drag configurations, and true VTOL applications (see Section 6.3).

6.2 Significance of Findings

The findings of the present investigation are significant for at least three reasons. The first is simply that this fills a hole left by the research done to date into the use of rotating cylinders as high-lift devices. Almost every conceivable use of a rotating cylinder as an integral part of an airfoil has been explored, and these configurations do show promise. However, this investigation is the first to break in to the use of a rotating cylinder as a separate element in a multi-element airfoil. This significant step opens the way to many logical variations on this theme that were not present in the literature to date. The influence on the direction of future research in this section of the field could be significant.

The second reason is that the results were sufficiently good for the Vortex Flap that there are conceivable applications in some iteration of the present form. These include those similar to that outlined in the Mission Analysis section, but also others which do not demand VTOL. For example, the Vortex Flap could prove useful in the kind of traditional STOL utility missions for which the Helio Courier was originally designed.

Alternatively, the Vortex Flap could alleviate a problem which has limited the development of the single-engine turboprop market: the 61-knot rule. These high-performance aircraft approximate the high-speed performance of twin-engine turboprop aircraft, but must comply with a 61 knot maximum stall speed, which drives the wing sizing in the design, and makes it larger than necessary, compromising high-speed performance. The use of a very powerful high-lift device like the Vortex Flap could allow the use of a smaller wing, potentially improving high-speed performance, and getting around this regulatory hurdle.

Finally, these results are significant because they suggest specific (not just general) avenues for meaningful future research which may lead to significant advances in the development of high-lift devices. Further, applications may exist in other fields. Research into efficient marine propulsion highlights central role vortexes play in thrust and control (Baird 1977, Bandyopadhay 1997, Drucker 1998). This investigation could form the basis for new uses of rotating cylinders in the propulsion and control of marine vehicles.

6.3 Future Work

The future work that the author desires to complete can be separated into four categories. The first is to complete the analysis of the results from the present

investigation, as well as re-examining some results to infer the effects of vortex shedding. The second amounts to a completion of the present investigation. The third involves branching out into fundamentally new configurations for rotating cylinders as high-lift devices. The fourth involves finding solutions to the fundamental problems of application, identifying suitable aircraft configurations, and ultimately flight testing the device.

Reexamine the Data

A great deal of insight was gained in the process of writing this paper. The author would like to revisit the complete data set more carefully. In particular the author would like to:

- Verify that the suppression of vortex shedding for SSR > 2 results in a reduction of lift and drag fluctuation.
- Observe the particular fluctuating force characteristics of the rotating cylinder in this range of Re and SSR to contribute to the catalog of available experimental data.
- Observe the influence of the presence of the airfoil, in its various positions, on the fluctuating forces.

Refining the Vortex Flap

The questions left unanswered by the present investigation need to be answered:

- What are the pitching moment characteristics of the Vortex Flap?
- What is the effect of the Vortex Flap chord ratio on performance?
- What is the optimal Vortex Flap position? What influences this position?
- How does the Vortex Flap perform at full-scale Reynolds numbers?

Next, there are some simple refinements that should be attempted:

- That a simple fairing should be placed on the cylinder was so obvious that a preliminary investigation of the rotating cylinder with such a fairing was conducted. While the test rig was not capable of testing the fairing, cylinder, and the primary airfoil, tests of the cylinder and fairing indicate that the L/D performance could be increased by perhaps a factor of two. This configuration would, make the Vortex Flap more similar to that investigated by NASA on the Bronco, but still distinct as a slotted rotating cylinder flap. A photograph of this investigation is presented in Figure 6-1.
- Other drag reduction devices and schemes should be investigated for the cylinder. In particular, a number of devices have been conceived by the author which could be called, borrowing architectural language, "scuppers" and "gulleys" intended to preserve the lifting power while reducing the degree of flow separation. These devices are sketched in Figure 6-2. The scupper would

cover the portion of the cylinder between the stagnation points to reduce the degree of flow separation around the cylinder at higher SSR. The gulley would allow a channel for 'return' air underneath the cylinder, while providing a fairing which would be intended to reduce turbulence and flow separation. These are both intended to be small treatments which might mitigate the need for a large fairing.

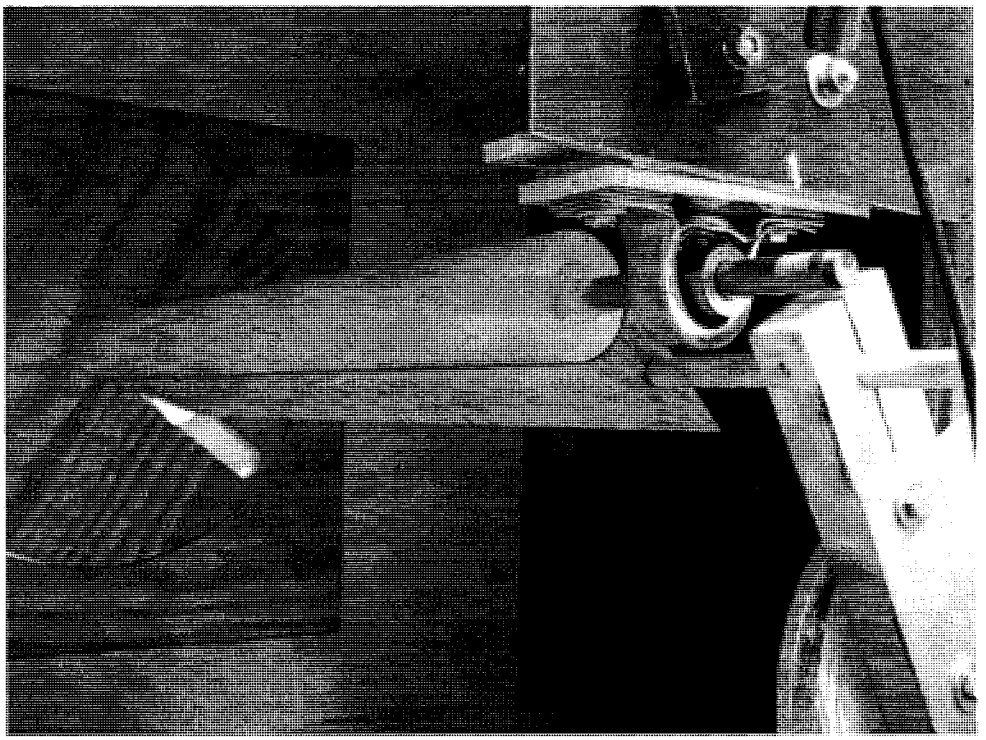

Figure 6-1. Rotating cylinder with fairing.

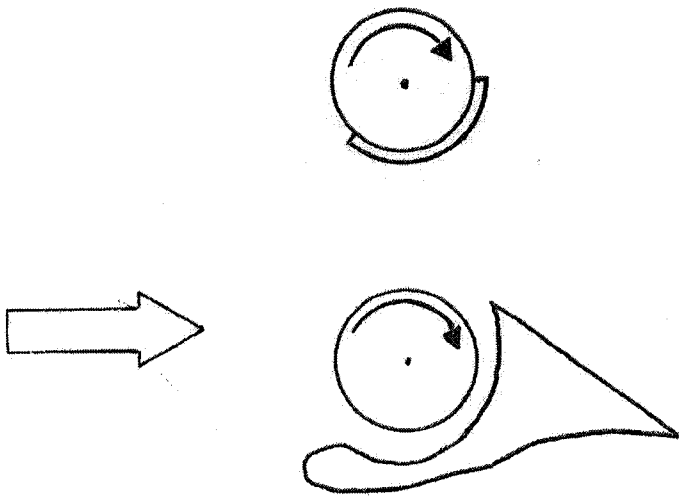

Figure 6-2. Concept sketches of "scuppers" (top) and "gulleys." (bottom).

Finally, there are some practical concerns that could be investigated readily. These include:

- Finding a suitable drive scheme to minimize weight. In particular the author is interested in finding a method of autorotation which could drive the device. For example, since it is likely that the Vortex Flap will be used under low-speed high-power conditions, and the useful SSR range is between two and four, then perhaps the portion of the Vortex Flap submerged in the slipstream could be shaped using a cross-section that would autorotate, while leaving the balance of the Vortex Flap smooth to minimize drag. The slipstream-

submerged portion would then 'drive' the rest of the flap. For example, while the local SSR of the slipstream-submerged portion would be operating at a local SSR of 0.6-0.8 (Skews 1991, Crabtree 1960), the portion of the Vortex Flap in the free stream, operating in a flow that might be going less than half as fast as that in the slipstream at sufficiently low speed, might be operating at a local SSR of around 2. This would be one very light drive system. There is a large body of experimental data to consider when designing such a device, and there are many possible cross sections to consider (Iverson 1979, Skews 1991, Smith 1971) to maximize SSR and minimize drag and vibration.

- A suitable cruise configuration needs to be found. In particular, if there is a reasonably low-drag configuration for which the Vortex Flap could be left deployed, this would be ideal. If a reasonably small diameter cylinder proves to be useful, perhaps driving it to SSR = 1.5 during cruise would provide sufficient L/D for certain types of missions. Excepting this, a means to retract the Vortex Flap needs to be found. Again, if a smaller diameter is found suitable, retraction into the wing itself becomes an option.
- It would be interesting to expand the range of the investigation originally conducted by Thom in the 1930's regarding cylinders with coaxial disks, which at low Reynolds numbers provided very low dray and even thrust (Zdravkovich 2003).

Fundamentally New Configurations

The present investigation included a significant number of over-the-wing investigations. The author would like to revisit the promising configurations among these. Of particular interest is capitalizing on the recirculating flow to create the same very-high-lift and very-low-drag vortex claimed by Kasper and demonstrated numerically by Saffman. Some initial success was achieved to this end in the present investigation. Recirculating flow above the wing can be seen in the tufts in Figure 6-3.

Figure 6-3. Picture of recirculating tufts on Clark Y during over-the-wing testing.

In addition, the author would like to thoroughly investigate the group of configurations called "Vortex Slats" wherein a rotating cylinder is placed in, or near, a slotted leading edge. There are at least three basic configurations of interest at the present time, sketched in Figure 6-4.

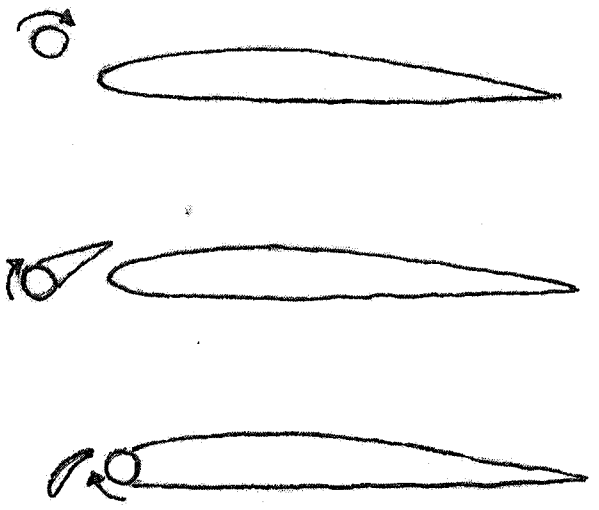

Figure 6-4. Vortex slat configurations.

Finally, the author is interested in investigating the effect of a mechanically bound vortex in and around airfoils in a more general manner. For example, rotating cylinders (or autorotating bodies) should be tested in streamwise and swept configurations near unswept and swept airfoils. It is possible that some configuration which would prove useful for micro-UAVs or as control effectors might be found.

Considering Applications

With the Vortex Flap in some iteration of its present form, the author can conceive of potential full-scale applications. In particular, if the Vortex Flap were used as part of a deflected-slipstream aircraft, perhaps a poor-man's tilt-rotor could be developed. For example, while the tilt-rotor is efficient in hover and high-speed forward flight, the cost is tremendous mechanical complexity. At the other end of the complexity spectrum, fixed wing aircraft can be made to hover (with sufficient thrust) by simply pointing the nose straight up (as in tail-sitting aircraft). The presence of a Vortex Flap in the slipstream of a propeller driven aircraft, for example, deflects the slipstream downward, and also generates considerable drag. Perhaps there exists a configuration exists wherein the Vortex Flap generates sufficient lift and drag that the result could be an aircraft that can 'hover' with the nose at, say, a 45° angle above the horizon, rather than 90° as in tail-sitting aircraft. Perhaps this attitude is manageable for takeoff and landing operations where the tail-sitting attitude proved impractical. Such a configuration of forces is sketched in Figure 6-5.

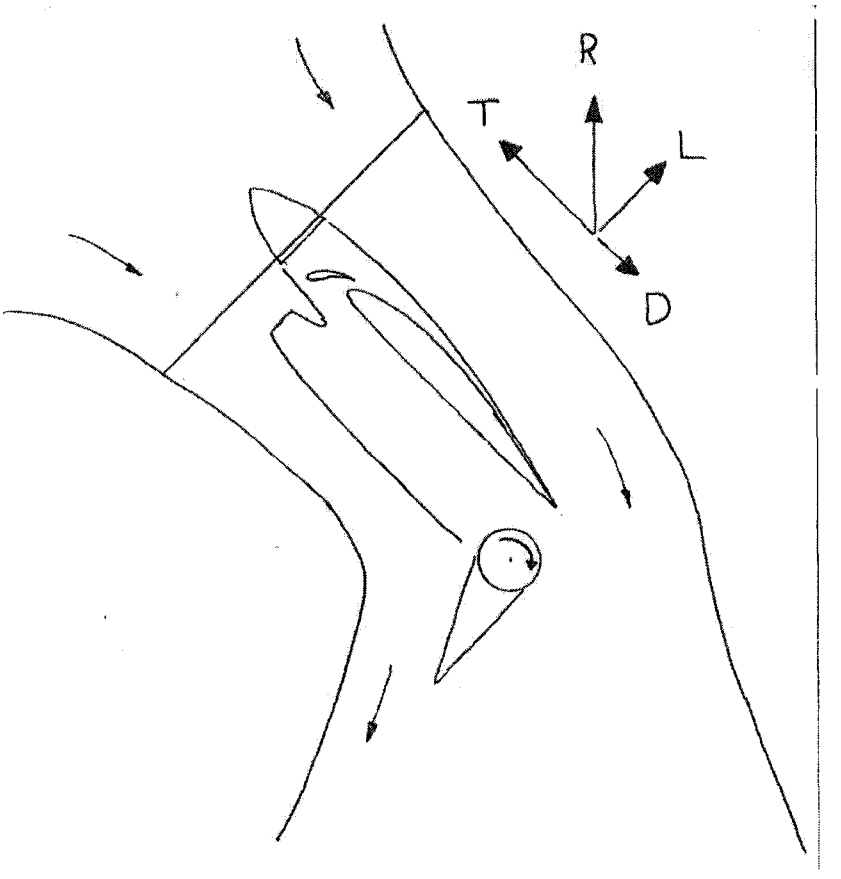

Figure 6-5. Drawing of wing and nacelle of "poor man's tilt-rotor" showing force vectors.

One potential single-propeller aircraft configuration potentially suitable for application of the Vortex Flap is suggested in a preliminary concept sketch in Figure 6-6. This type of aircraft would be using the Vortex Flap to deflect the slipstream and increase low-speed lift.

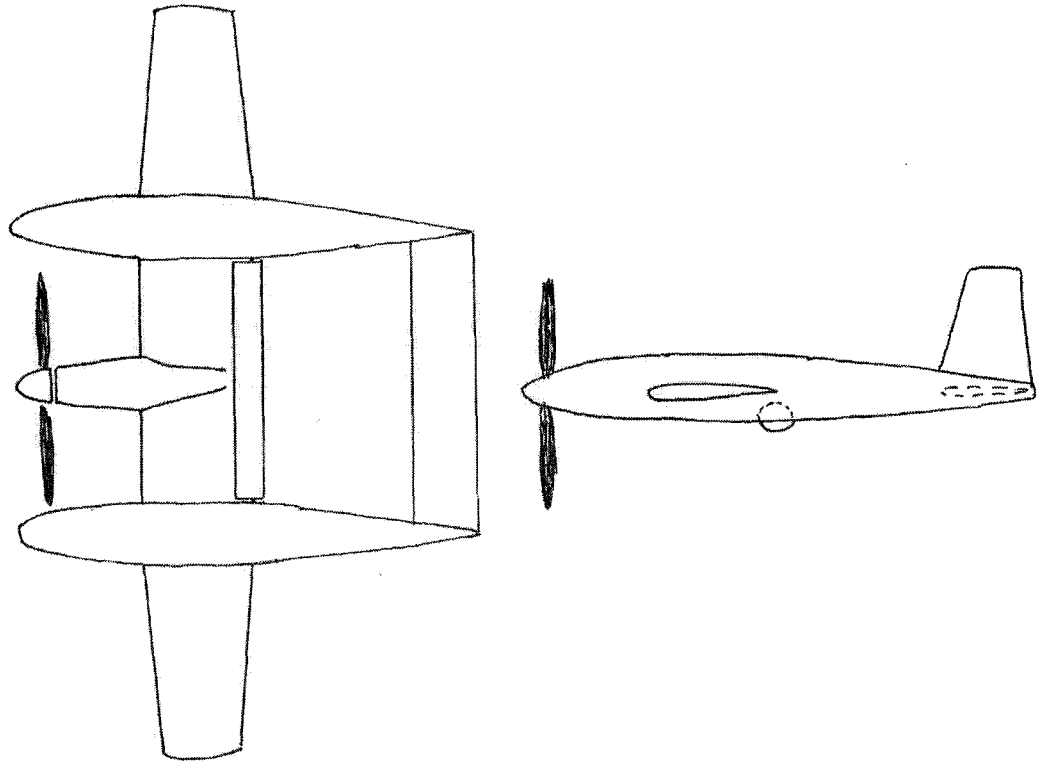

Figure 6-6. Concept sketch of single-engine aircraft configuration for Vortex Flap. Bottom view (left) and side view (right).

It is the author's opinion that a rich vein of potential research and possible future applications lies in wait beyond the present Vortex Flap investigation.

Appendix A- Wind Tunnel Data Summary

Following is roughly 10% of the total data that were obtained during this investigation. The following configurations are excluded: flat plate, cylinder with flat plate, cylinder above Clark Y airfoil, and cylinder with fairing.

Data for Clark Y Airfoil Tests

Geometry			Results			
Test #	Config	alpha	Re	Cl	Cd	L/D
1540	Clark Y Only	0	80,000	0.31	0.022	14.0
1541	Clark Y Only	0	120,000	0.33	0.026	12.6
1542	Clark Y Only	0	160,000	0.33	0.031	10.8
1543	Clark Y Only	0	240,000	0.30	0.028	10.8
1544	Clark Y Only	0	310,000	0.29	0.028	10.4
1545	Clark Y Only	2.5	80,000	0.57	0.055	10.4
1546	Clark Y Only	2.5	120,000	0.61	0.042	14.5
1547	Clark Y Only	2.5	160,000	0.61	0.043	14.2
1548	Clark Y Only	2.5	250,000	0.61	0.039	15.7
1549	Clark Y Only	2.5	320,000	0.60	0.035	17.3
1550	Clark Y Only	5	80,000	0.76	0.050	15.2
1551	Clark Y Only	5	120,000	0.78	0.046	16.8
1552	Clark Y Only	5	160,000	0.78	0.041	19.0
1553	Clark Y Only	5	240,000	0.78	0.044	17.6
1554	Clark Y Only	5	320,000	0.77	0.043	17.7
1555	Clark Y Only	7.5	80,000	0.93	0.070	13.2
1556	Clark Y Only	7.5	120,000	0.99	0.072	13.7
1557	Clark Y Only	7.5	160,000	0.96	0.062	15.5
1558	Clark Y Only	7.5	240,000	0.97	0.059	16.6
1559	Clark Y Only	7.5	320,000	0.96	0.053	18.0
1560	Clark Y Only	10	80,000	1.07	0.097	11.1
1561	Clark Y Only	10	120,000	1.12	0.086	13.0
1562	Clark Y Only	10	160,000	1.10	0.078	14.2
1563	Clark Y Only	10	240,000	1.11	0.072	15.5
1564	Clark Y Only	10	320,000	1.09	0.070	15.5
1565	Clark Y Only	12.5	80,000	0.94	0.187	5.0
1566	Clark Y Only	12.5	120,000	1.01	0.190	5.3

1567	Clark Y Only	12.5	160,000	1.02	0.183	5.5
1568	Clark Y Only	12.5	250,000	1.19	0.093	12.7
1569	Clark Y Only	12.5	320,000	1.16	0.099	11.7
1570	Clark Y Only	15	80,000	0.84	0.235	3.6
1571	Clark Y Only	15	120,000	0.92	0.259	3.6
1572	Clark Y Only	15	160,000	0.89	0.258	3.4
1573	Clark Y Only	15	240,000	1.07	0.221	4.8
1574	Clark Y Only	15	320,000	1.05	0.204	5.1
1575	Clark Y Only	17.5	80,000	0.80	0.293	2.7
1576	Clark Y Only	17.5	120,000	0.85	0.301	2.8
1577	Clark Y Only	17.5	180,000	0.94	0.300	3.1
1578	Clark Y Only	17.5	240,000	1.09	0.268	4.1
1579	Clark Y Only	17.5	320,000	1.10	0.255	4.3
1580	Clark Y Only	20	80,000	0.82	0.333	2.4
1581	Clark Y Only	20	110,000	0.87	0.343	2.5
1582	Clark Y Only	20	180,000	0.90	0.355	2.5
1583	Clark Y Only	20	240,000	1.07	0.313	3.4
1584	Clark Y Only	20	320,000	1.17	0.310	3.8
1585	Clark Y Only	22.5	80,000	0.87	0.391	2.2
1586	Clark Y Only	22.5	120,000	0.89	0.403	2.2
1587	Clark Y Only	22.5	160,000	0.93	0.417	2.2
1588	Clark Y Only	22.5	250,000	1.07	0.413	2.6
1589	Clark Y Only	22.5	310,000	1.14	0.382	3.0
1590	Clark Y Only	25	80,000	0.92	0.472	1.9
1591	Clark Y Only	25	120,000	0.94	0.472	2.0
1592	Clark Y Only	25	160,000	0.96	0.477	2.0
1593	Clark Y Only	25	240,000	0.98	0.480	2.0
1594	Clark Y Only	25	310,000	1.06	0.468	2.3
1595	Clark Y Only	27.5	80,000	1.07	0.550	1.9
1596	Clark Y Only	27.5	120,000	1.01	0.535	1.9
1597	Clark Y Only	27.5	160,000	1.02	0.551	1.8
1598	Clark Y Only	27.5	240,000	1.03	0.550	1.9
1599	Clark Y Only	27.5	310,000	1.03	0.540	1.9
1600	Clark Y Only	30	80,000	1.14	0.663	1.7
1601	Clark Y Only	30	120,000	1.15	0.670	1.7
1602	Clark Y Only	30	160,000	1.14	0.665	1.7
1603	Clark Y Only	30	240,000	1.14	0.667	1.7
1604	Clark Y Only	30	310,000	1.12	0.658	1.7

Figure 6-7. Clark Y airfoil-only data in tabular form.

Data for Rotating Cylinder Tests

Geometry			Results			
CRN	Configuration	SSR	Reynolds	Cl	Cd	L/D
1958	Cylinder Only	0.00	20,000	0.11716	1.10709	0.10583
1977	Cylinder Only	1.20	20,000	1.37279	0.56473	2.43088
1984	Cylinder Only	2.65	20,000	5.51892	1.00083	5.51433
1991	Cylinder Only	4.54	20,000	7.46017	2.04609	3.64607
1996	Cylinder Only	6.84	20,000	7.51507	2.29260	3.27796
2001	Cylinder Only	9.65	20,000	8.05550	2.58550	3.11564
1959	Cylinder Only	0.00	30,000	0.10365	1.16282	0.08913
1978	Cylinder Only	0.81	30,000	0.55390	0.74727	0.74124
1985	Cylinder Only	1.81	30,000	3.10048	0.63398	4.89051
1992	Cylinder Only	2.97	30,000	6.32141	1.32266	4.77933
1999	Cylinder Only	4.55	30,000	7.40145	1.97559	3.74645
2004	Cylinder Only	6.53	30,000	7.66764	2.27222	3.37451
1960	Cylinder Only	0.00	40,000	0.12487	1.16893	0.10683
1979	Cylinder Only	0.61	40,000	0.36420	0.99011	0.36784
1986	Cylinder Only	1.33	40,000	1.69772	0.64241	2.64272
1993	Cylinder Only	2.16	40,000	4.21611	0.78933	5.34140
2000	Cylinder Only	3.36	40,000	7.01020	1.55758	4.50071
1971	Cylinder Only	4.66	40,000	7.49799	2.06771	3.62623
1961	Cylinder Only	0.00	70,000	0.13241	1.22887	0.10775
1973	Cylinder Only	3.04	70,000	7.20566	1.27964	5.63100
1980	Cylinder Only	0.40	70,000	0.21741	1.07040	0.20311
1987	Cylinder Only	0.89	70,000	0.59946	0.73490	0.81569
1994	Cylinder Only	1.42	70,000	1.98008	0.66572	2.97433
1997	Cylinder Only	2.15	70,000	4.22395	0.77261	5.46712
1972	Cylinder Only	3.03	70,000	6.44987	1.34532	4.79432
1962	Cylinder Only	0.00	80,000	0.14236	1.25167	0.11373
1981	Cylinder Only	0.31	80,000	0.09746	1.09525	0.08898
1988	Cylinder Only	0.69	80,000	0.55237	0.75133	0.73519
1989	Cylinder Only	1.11	80,000	1.12205	0.68790	1.63111
1998	Cylinder Only	1.64	90,000	2.58098	0.65840	3.92007
2002	Cylinder Only	2.26	90,000	4.52945	0.83426	5.42931
1963	Cylinder Only	0.00	110,000	0.14687	1.19136	0.12328
1966	Cylinder Only	0.53	110,000	0.17254	0.80511	0.21430
1967	Cylinder Only	0.86	110,000	0.75416	0.71718	1.05156
1969	Cylinder Only	1.25	110,000	1.70872	0.63568	2.68802
1975	Cylinder Only	1.77	110,000	3.20355	0.61544	5.20533
1974	Cylinder Only	1.47	130,000	2.28179	0.60863	3.74903
1964	Cylinder Only	0.00	150,000	0.14695	1.13164	0.12986
1965	Cylinder Only	0.39	150,000	0.07590	0.85242	0.08904
1968	Cylinder Only	0.63	150,000	0.30912	0.66247	0.46661

1970	Cylinder Only	0.93	150,000	0.94742	0.68472	1.38367
1976	Cylinder Only	1.32	150,000	1.84845	0.63489	2.91144

Figure 6-8. Cylinder-only data in tabular form.

Data for Vortex Flap Tests

Geometry								Performance							
									Basis All Elements			Basis Primary Element			
Test #	Config	Shaft X	Shaft Y	alpha	Gap	T.E.C.	SSR	Re	Cl		Cd	Cl		Cd	L/D
1780	Clark Y & Cyl	2.75	2.25	0	1.25	1	0.0	80,000	-0.71	0.71	0.22	-0.85	0.85	0.26	3.3
1781	Clark Y & Cyl	2.75	2.25	0	1.25	1	0.0	120,000	-0.76	0.76	0.22	-0.92	0.92	0.27	3.4
1782	Clark Y & Cyl	2.75	2.25	0	1.25	1	0.0	170,000	-0.72	0.72	0.24	-0.87	0.87	0.28	3.1
1783	Clark Y & Cyl	2.75	2.25	0	1.25	1	0.0	250,000	-0.72	0.72	0.24	-0.87	0.87	0.29	3.0
1784	Clark Y & Cyl	2.75	2.25	0	1.25	1	0.0	330,000	-0.73	0.73	0.23	-0.88	0.88	0.28	3.1
1785	Clark Y & Cyl	2.75	2.25	0	1.25	1	0.8	250,000	-0.83	0.83	0.15	-1.00	1.00	0.18	5.4
1786	Clark Y & Cyl	2.75	2.25	0	1.25	1	0.7	320,000	-0.73	0.73	0.15	-0.88	0.88	0.18	5.0
1788	Clark Y & Cyl	2.75	2.25	0	1.25	1	2.6	80,000	-2.14	2.14	0.46	-2.57	2.57	0.55	4.7
1789	Clark Y & Cyl	2.75	2.25	0	1.25	1	1.7	120,000	-1.48	1.48	0.19	-1.78	1.78	0.23	7.8
1790	Clark Y & Cyl	2.75	2.25	0	1.25	1	1.3	170,000	-1.12	1.12	0.16	-1.34	1.34	0.19	6.9
1791	Clark Y & Cyl	2.75	2.25	0	1.25	1	1.1	320,000	-0.93	0.93	0.15	-1.11	1.11	0.18	6.3
1792	Clark Y & Cyl	2.75	2.25	0	1.25	1	4.2	80,000	-2.16	2.16	0.56	-2.60	2.60	0.68	3.8
1793	Clark Y & Cyl	2.75	2.25	0	1.25	1	2.8	120,000	-2.23	2.23	0.42	-2.68	2.68	0.50	5.4
1794	Clark Y & Cyl	2.75	2.25	0	1.25	1	2.1	170,000	-1.74	1.74	0.22	-2.08	2.08	0.26	8.0
1795	Clark Y & Cyl	2.75	2.25	0	1.25	1	1.4	250,000	-1.17	1.17	0.15	-1.40	1.40	0.19	7.5
1797	Clark Y & Cyl	2.75	2.25	0	1.25	1	1.6	320,000	-1.26	1.26	0.16	-1.51	1.51	0.19	8.0
1798	Clark Y & Cyl	2.75	2.25	0	1.25	1	6.2	80,000	-2.20	2.20	0.59	-2.64	2.64	0.71	3.7
1799	Clark Y & Cyl	2.75	2.25	0	1.25	1	2.0	250,000	-1.72	1.72	0.20	-2.06	2.06	0.24	8.5
1800	Clark Y & Cyl	2.75	2.25	0	1.25	1	4.2	120,000	-2.24	2.24	0.56	-2.69	2.69	0.67	4.0
1801	Clark Y & Cyl	2.75	2.25	0	1.25	1	3.1	170,000	-2.33	2.33	0.45	-2.80	2.80	0.54	5.1
1802	Clark Y & Cyl	2.75	2.25	0	1.25	1	2.2	330,000	-1.75	1.75	0.20	-2.10	2.10	0.24	8.8
1804	Clark Y & Cyl	2.75	2.25	0	1.25	1	8.6	80,000	-2.34	2.34	0.57	-2.81	2.81	0.69	4.1
1805	Clark Y & Cyl	2.75	2.25	0	1.25	1	2.2	330,000	-1.79	1.79	0.20	-2.14	2.14	0.24	8.8
1806	Clark Y & Cyl	2.75	2.25	0	1.25	1	2.9	250,000	-2.36	2.36	0.37	-2.83	2.83	0.44	6.4
1807	Clark Y & Cyl	2.75	2.25	0	1.25	1	6.0	120,000	-2.27	2.27	0.57	-2.73	2.73	0.68	4.0
1808	Clark Y & Cyl	2.75	2.25	0	1.25	1	4.3	170,000	-2.28	2.28	0.55	-2.74	2.74	0.66	4.2
1809	Clark Y & Cyl	2.75	2.25	0	1.25	1	2.2	420,000	-1.58	1.58	0.18	-1.89	1.89	0.21	8.9
1810	Clark Y & Cyl	2.75	2.25	0	1.25	1	2.9	320,000	-2.12	2.12	0.29	-2.54	2.54	0.35	7.3
1811	Clark Y & Cyl	2.75	2.25	0	1.25	1	3.7	250,000	-2.39	2.39	0.50	-2.87	2.87	0.60	4.8
1812	Clark Y & Cyl	2.75	2.25	-5	1	0.814	0.0	170,000	-1.09	1.09	0.23	-1.30	1.30	0.27	4.8
1813	Clark Y & Cyl	2.75	2.25	-5	1	0.814	0.0	250,000	-1.10	1.10	0.23	-1.32	1.32	0.27	4.8
1814	Clark Y & Cyl	2.75	2.25	-5	1	0.814	0.0	320,000	-1.11	1.11	0.22	-1.33	1.33	0.27	5.0
1815	Clark Y & Cyl	2.75	2.25	-5	1	0.814	4.3	170,000	-1.89	1.89	0.58	-2.27	2.27	0.70	3.3

1816	Clark Y & Cyl	[redacted]	[redacted]	-5	1	0.814	1.4	250,000	-1.64	1.64	0.17	-1.96	1.96	0.20	9.9
1817	Clark Y & Cyl	[redacted]	[redacted]	-5	1	0.814	1.1	320,000	-1.37	1.37	0.15	-1.64	1.64	0.17	9.4
1819	Clark Y & Cyl	[redacted]	[redacted]	-5	1	0.814	2.1	170,000	-2.18	2.18	0.41	-2.61	2.61	0.49	5.3
1821	Clark Y & Cyl	[redacted]	[redacted]	-5	1	0.814	1.6	320,000	-1.77	1.77	0.19	-2.12	2.12	0.23	9.4
1822	Clark Y & Cyl	[redacted]	[redacted]	-5	1	0.814	3.1	160,000	-1.97	1.97	0.57	-2.36	2.36	0.69	3.4
1823	Clark Y & Cyl	[redacted]	[redacted]	-5	1	0.814	2.0	250,000	-2.08	2.08	0.41	-2.50	2.50	0.49	5.1
1824	Clark Y & Cyl	[redacted]	[redacted]	-5	1	0.814	2.2	320,000	-2.31	2.31	0.30	-2.77	2.77	0.36	7.8
1826	Clark Y & Cyl	[redacted]	[redacted]	-5	1	0.814	2.9	250,000	-1.91	1.91	0.57	-2.29	2.29	0.68	3.3
1827	Clark Y & Cyl	[redacted]	[redacted]	-5	1	0.814	2.9	320,000	-2.56	2.56	0.39	-3.07	3.07	0.46	6.6
1828	Clark Y & Cyl	[redacted]	[redacted]	-5	1	0.814	2.2	410,000	-2.11	2.11	0.24	-2.53	2.53	0.28	8.9
1829	Clark Y & Cyl	[redacted]	[redacted]	[redacted]	0.74	0.651	0.0	160,000	-1.35	1.35	0.24	-1.62	1.62	0.29	5.6
1830	Clark Y & Cyl	[redacted]	[redacted]	[redacted]	0.74	0.651	0.0	250,000	-1.38	1.38	0.24	-1.66	1.66	0.28	5.8
1831	Clark Y & Cyl	[redacted]	[redacted]	[redacted]	0.74	0.651	0.0	320,000	-1.38	1.38	0.23	-1.65	1.65	0.28	5.9
1833	Clark Y & Cyl	[redacted]	[redacted]	[redacted]	0.74	0.651	1.6	320,000	-1.71	1.71	0.39	-2.05	2.05	0.46	4.4
1834	Clark Y & Cyl	[redacted]	[redacted]	[redacted]	0.74	0.651	3.0	170,000	-1.33	1.33	0.75	-1.59	1.59	0.90	1.8
1835	Clark Y & Cyl	[redacted]	[redacted]	[redacted]	0.74	0.651	2.0	250,000	-1.68	1.68	0.62	-2.01	2.01	0.75	2.7
1836	Clark Y & Cyl	[redacted]	[redacted]	[redacted]	0.74	0.651	2.8	250,000	-1.48	1.48	0.71	-1.77	1.77	0.86	2.1
1837	Clark Y & Cyl	[redacted]	[redacted]	[redacted]	0.74	0.651	4.5	160,000	-1.30	1.30	0.75	-1.56	1.56	0.90	1.7
1838	Clark Y & Cyl	[redacted]	[redacted]	[redacted]	0.74	0.651	2.2	320,000	-1.68	1.68	0.64	-2.02	2.02	0.76	2.6
1841	Clark Y & Cyl	[redacted]	[redacted]	[redacted]	0.74	0.651	2.9	320,000	-1.52	1.52	0.69	-1.83	1.83	0.82	2.2
1842	Clark Y & Cyl	[redacted]	[redacted]	0	2.25	1	0.0	160,000	-0.53	0.53	0.24	-0.63	0.63	0.29	2.2
1843	Clark Y & Cyl	[redacted]	[redacted]	0	2.25	1	0.0	250,000	-0.51	0.51	0.25	-0.62	0.62	0.30	2.1
1844	Clark Y & Cyl	[redacted]	[redacted]	0	2.25	1	0.0	320,000	-0.51	0.51	0.25	-0.61	0.61	0.30	2.0
1845	Clark Y & Cyl	[redacted]	[redacted]	0	2.25	1	1.1	320,000	-0.73	0.73	0.15	-0.88	0.88	0.17	5.0
1847	Clark Y & Cyl	[redacted]	[redacted]	0	2.25	1	2.1	170,000	-1.44	1.44	0.18	-1.73	1.73	0.22	7.9
1848	Clark Y & Cyl	[redacted]	[redacted]	0	2.25	1	1.4	250,000	-0.93	0.93	0.15	-1.12	1.12	0.18	6.3
1849	Clark Y & Cyl	[redacted]	[redacted]	0	2.25	1	2.0	250,000	-1.39	1.39	0.17	-1.66	1.66	0.21	8.1
1850	Clark Y & Cyl	[redacted]	[redacted]	0	2.25	1	1.6	320,000	-1.02	1.02	0.15	-1.22	1.22	0.18	6.8
1852	Clark Y & Cyl	[redacted]	[redacted]	0	2.25	1	3.1	160,000	-2.13	2.13	0.34	-2.55	2.55	0.40	6.3
1853	Clark Y & Cyl	[redacted]	[redacted]	0	2.25	1	2.3	320,000	-1.51	1.51	0.18	-1.81	1.81	0.22	8.3
1854	Clark Y & Cyl	[redacted]	[redacted]	0	2.25	1	2.9	250,000	-1.99	1.99	0.28	-2.39	2.39	0.34	7.0
1856	Clark Y & Cyl	[redacted]	[redacted]	0	2.25	1	4.4	160,000	-2.27	2.27	0.44	-2.72	2.72	0.53	5.1
1857	Clark Y & Cyl	[redacted]	[redacted]	-5	2	0.727	0.0	160,000	-0.93	0.93	0.23	-1.12	1.12	0.28	4.0
1858	Clark Y & Cyl	[redacted]	[redacted]	-5	2	0.727	0.0	250,000	-0.93	0.93	0.24	-1.12	1.12	0.28	3.9
1859	Clark Y & Cyl	[redacted]	[redacted]	-5	2	0.727	0.0	320,000	-0.97	0.97	0.22	-1.16	1.16	0.26	4.5
1861	Clark Y & Cyl	[redacted]	[redacted]	-5	2	0.727	1.4	250,000	-1.44	1.44	0.15	-1.73	1.73	0.19	9.3
1862	Clark Y & Cyl	[redacted]	[redacted]	-5	2	0.727	1.1	320,000	-1.21	1.21	0.15	-1.45	1.45	0.18	8.2
1863	Clark Y & Cyl	[redacted]	[redacted]	-5	2	0.727	2.1	170,000	-1.99	1.99	0.21	-2.39	2.39	0.26	9.3
1864	Clark Y & Cyl	[redacted]	[redacted]	-5	2	0.727	2.1	250,000	-1.98	1.98	0.21	-2.38	2.38	0.25	9.5
1865	Clark Y & Cyl	[redacted]	[redacted]	-5	2	0.727	1.6	320,000	-1.57	1.57	0.16	-1.89	1.89	0.19	9.9
1867	Clark Y & Cyl	[redacted]	[redacted]	-5	2	0.727	3.2	160,000	-2.60	2.60	0.42	-3.12	3.12	0.50	6.2
1868	Clark Y & Cyl	[redacted]	[redacted]	-5	2	0.727	2.3	320,000	-2.12	2.12	0.22	-2.55	2.55	0.27	9.5
1870	Clark Y & Cyl	[redacted]	[redacted]	-5	2	0.727	3.0	250,000	-2.55	2.55	0.36	-3.05	3.05	0.43	7.1
1871	Clark Y & Cyl	[redacted]	[redacted]	-5	2	0.727	4.4	170,000	-2.69	2.69	0.51	-3.23	3.23	0.61	5.3
1872	Clark Y & Cyl	[redacted]	[redacted]	-5	2	0.727	2.9	320,000	-2.49	2.49	0.33	-2.99	2.99	0.39	7.6

1873	Clark Y & Cyl		-5	2	0.727	3.7	250,000	-2.73	2.73	0.45	-3.27	3.27	0.55	6.0
1874	Clark Y & Cyl		-5	2	0.727	5.6	170,000	-2.70	2.70	0.54	-3.24	3.24	0.65	5.0
1875	Clark Y & Cyl			1.72	0.477	0.0	160,000	-1.18	1.18	0.25	-1.42	1.42	0.30	4.7
1876	Clark Y & Cyl			1.72	0.477	0.0	250,000	-1.21	1.21	0.24	-1.46	1.46	0.29	5.0
1877	Clark Y & Cyl			1.72	0.477	0.0	320,000	-1.21	1.21	0.24	-1.45	1.45	0.29	5.0
1878	Clark Y & Cyl			1.72	0.477	1.1	320,000	-1.52	1.52	0.17	-1.82	1.82	0.21	8.7
1880	Clark Y & Cyl			1.72	0.477	2.1	160,000	-2.37	2.37	0.30	-2.85	2.85	0.36	7.9
1881	Clark Y & Cyl			1.72	0.477	1.4	240,000	-1.79	1.79	0.19	-2.15	2.15	0.23	9.4
1883	Clark Y & Cyl			1.72	0.477	2.1	250,000	-2.36	2.36	0.28	-2.83	2.83	0.33	8.5
1884	Clark Y & Cyl			1.72	0.477	1.6	320,000	-1.95	1.95	0.20	-2.35	2.35	0.24	9.7
1885	Clark Y & Cyl			1.72	0.477	3.1	170,000	-1.81	1.81	0.74	-2.18	2.18	0.88	2.5
1886	Clark Y & Cyl			1.72	0.477	1.9	320,000	-2.25	2.25	0.24	-2.70	2.70	0.29	9.2
1887	Clark Y & Cyl			1.72	0.477	2.3	320,000	-2.46	2.46	0.33	-2.95	2.95	0.39	7.6
1889	Clark Y & Cyl			1.72	0.477	3.0	250,000	-2.47	2.47	0.57	-2.96	2.96	0.68	4.4
1890	Clark Y & Cyl			1.72	0.477	4.4	160,000	-1.65	1.65	0.75	-1.98	1.98	0.90	2.2
1891	Clark Y & Cyl			1.72	0.477	2.6	320,000	-2.56	2.56	0.44	-3.07	3.07	0.52	5.9
1892	Clark Y & Cyl		0	2.25	0.5	0.0	170,000	-0.57	0.57	0.22	-0.68	0.68	0.27	2.5
1893	Clark Y & Cyl		0	2.25	0.5	0.0	250,000	-0.55	0.55	0.23	-0.66	0.66	0.28	2.4
1894	Clark Y & Cyl		0	2.25	0.5	0.0	330,000	-0.56	0.56	0.23	-0.67	0.67	0.27	2.5
1896	Clark Y & Cyl		0	2.25	0.5	2.1	160,000	-1.59	1.59	0.18	-1.91	1.91	0.21	9.0
1897	Clark Y & Cyl		0	2.25	0.5	1.4	250,000	-1.02	1.02	0.14	-1.23	1.23	0.17	7.4
1898	Clark Y & Cyl		0	2.25	0.5	1.1	320,000	-0.80	0.80	0.14	-0.97	0.97	0.17	5.6
1899	Clark Y & Cyl		0	2.25	0.5	2.0	250,000	-1.55	1.55	0.17	-1.86	1.86	0.20	9.2
1900	Clark Y & Cyl		0	2.25	0.5	1.6	320,000	-1.14	1.14	0.14	-1.37	1.37	0.17	8.0
1902	Clark Y & Cyl		0	2.25	0.5	3.1	170,000	-2.00	2.00	0.34	-2.41	2.41	0.40	5.9
1903	Clark Y & Cyl		0	2.25	0.5	2.2	330,000	-1.68	1.68	0.18	-2.02	2.02	0.22	9.1
1904	Clark Y & Cyl		0	2.25	0.5	1.7	420,000	-1.24	1.24	0.14	-1.49	1.49	0.16	9.2
1905	Clark Y & Cyl		0	2.25	0.5	2.9	250,000	-2.22	2.22	0.29	-2.66	2.66	0.35	7.6
1907	Clark Y & Cyl		0	2.25	0.5	4.4	170,000	-2.46	2.46	0.44	-2.95	2.95	0.53	5.5
1908	Clark Y & Cyl		0	2.25	0.5	5.6	160,000	-2.53	2.53	0.47	-3.03	3.03	0.56	5.4
1909	Clark Y & Cyl		0	2.25	0.5	3.7	250,000	-2.48	2.48	0.38	-2.97	2.97	0.46	6.5
1910	Clark Y & Cyl		0	2.25	0.5	2.9	320,000	-2.21	2.21	0.27	-2.65	2.65	0.33	8.1
1911	Clark Y & Cyl		0	2.25	0.5	2.2	420,000	-1.64	1.64	0.17	-1.97	1.97	0.21	9.5
1912	Clark Y & Cyl		0	2.25	0.5	2.5	410,000	-1.90	1.90	0.21	-2.28	2.28	0.25	9.0
1913	Clark Y & Cyl		0	2.25	0.5	3.3	320,000	-2.40	2.40	0.33	-2.87	2.87	0.40	7.3
1914	Clark Y & Cyl		0	2.25	0.5	4.3	250,000	-2.51	2.51	0.42	-3.01	3.01	0.50	6.0
1915	Clark Y & Cyl		0	2.25	0.5	6.6	160,000	-2.57	2.57	0.49	-3.09	3.09	0.59	5.3
1916	Clark Y & Cyl		0	2.25	0.5	2.7	420,000	-2.00	2.00	0.23	-2.40	2.40	0.28	8.6
1917	Clark Y & Cyl		0	2.25	0.5	2.9	390,000	-2.15	2.15	0.28	-2.58	2.58	0.33	7.7
1918	Clark Y & Cyl		0	2.25	0.5	3.5	320,000	-2.40	2.40	0.36	-2.88	2.88	0.43	6.6
1919	Clark Y & Cyl		-5	1.95	0.229	0.0	160,000	-0.93	0.93	0.22	-1.12	1.12	0.26	4.3
1920	Clark Y & Cyl		-5	1.95	0.229	0.0	250,000	-0.94	0.94	0.22	-1.12	1.12	0.26	4.3
1921	Clark Y & Cyl		-5	1.95	0.229	0.0	320,000	-0.95	0.95	0.21	-1.14	1.14	0.25	4.6
1923	Clark Y & Cyl		-5	1.95	0.229	1.4	250,000	-1.48	1.48	0.15	-1.78	1.78	0.19	9.6
1924	Clark Y & Cyl		-5	1.95	0.229	1.1	320,000	-1.23	1.23	0.15	-1.48	1.48	0.18	8.0

1925	Clark Y & Cyl	[redacted]	-5	1.95	0.229	2.1	170,000	-2.08	2.08	0.23	-2.49	2.49	0.27	9.2
1926	Clark Y & Cyl		-5	1.95	0.229	2.0	250,000	-2.06	2.06	0.21	-2.47	2.47	0.25	9.8
1927	Clark Y & Cyl		-5	1.95	0.229	1.6	320,000	-1.63	1.63	0.16	-1.96	1.96	0.19	10.1
1929	Clark Y & Cyl		-5	1.95	0.229	3.1	160,000	-2.72	2.72	0.42	-3.26	3.26	0.50	6.5
1930	Clark Y & Cyl		-5	1.95	0.229	2.3	320,000	-2.26	2.26	0.23	-2.72	2.72	0.28	9.7
1931	Clark Y & Cyl		-5	1.95	0.229	2.9	250,000	-2.67	2.67	0.36	-3.20	3.20	0.43	7.5
1933	Clark Y & Cyl		-5	1.95	0.229	4.4	170,000	-2.82	2.82	0.51	-3.38	3.38	0.61	5.5
1934	Clark Y & Cyl		-5	1.95	0.229	2.6	320,000	-2.49	2.49	0.28	-2.99	2.99	0.34	8.8
1935	Clark Y & Cyl		-5	1.95	0.229	2.9	320,000	-2.68	2.68	0.34	-3.22	3.22	0.41	7.9
1936	Clark Y & Cyl		-5	1.95	0.229	3.3	320,000	-2.80	2.80	0.39	-3.36	3.36	0.47	7.1
1937	Clark Y & Cyl		-5	1.95	0.229	3.5	320,000	-2.86	2.86	0.42	-3.43	3.43	0.51	6.8
1938	Clark Y & Cyl			1.64	-0.015	0.0	160,000	-1.26	1.26	0.24	-1.52	1.52	0.29	5.2
1939	Clark Y & Cyl			1.64	-0.015	0.0	240,000	-1.27	1.27	0.24	-1.52	1.52	0.29	5.2
1940	Clark Y & Cyl			1.64	-0.015	0.0	320,000	-1.25	1.25	0.25	-1.51	1.51	0.30	5.1
1942	Clark Y & Cyl			1.64	-0.015	2.1	160,000	-2.51	2.51	0.36	-3.01	3.01	0.44	6.9
1943	Clark Y & Cyl			1.64	-0.015	1.4	240,000	-1.87	1.87	0.23	-2.24	2.24	0.28	8.1
1944	Clark Y & Cyl			1.64	-0.015	1.1	320,000	-1.54	1.54	0.21	-1.85	1.85	0.25	7.5
1946	Clark Y & Cyl			1.64	-0.015	2.1	250,000	-2.45	2.45	0.32	-2.94	2.94	0.39	7.6
1947	Clark Y & Cyl			1.64	-0.015	1.6	320,000	-1.99	1.99	0.25	-2.38	2.38	0.30	8.0
1948	Clark Y & Cyl			1.64	-0.015	2.9	180,000	-1.73	1.73	0.74	-2.08	2.08	0.89	2.3
1949	Clark Y & Cyl			1.64	-0.015	2.0	320,000	-2.27	2.27	0.31	-2.72	2.72	0.37	7.4
1951	Clark Y & Cyl			1.64	-0.015	2.3	320,000	-2.36	2.36	0.45	-2.83	2.83	0.54	5.3
1952	Clark Y & Cyl			1.64	-0.015	4.4	160,000	-1.44	1.44	0.75	-1.72	1.72	0.90	1.9
1953	Clark Y & Cyl			1.64	-0.015	2.9	250,000	-1.95	1.95	0.72	-2.34	2.34	0.86	2.7
1955	Clark Y & Cyl			1.64	-0.015	2.8	320,000	-2.16	2.16	0.67	-2.59	2.59	0.81	3.2
1956	Clark Y & Cyl			1.64	-0.015	5.4	170,000	-1.30	1.30	0.73	-1.55	1.55	0.87	1.8
1957	Clark Y & Cyl			1.64	-0.015	3.7	250,000	-1.79	1.79	0.75	-2.15	2.15	0.90	2.4

Figure 6-9. Vortex Flap data in tabular form.

Influence of α on Vortex Flap Performance

Figures 1 through 15 show the influence of α on Vortex Flap performance.

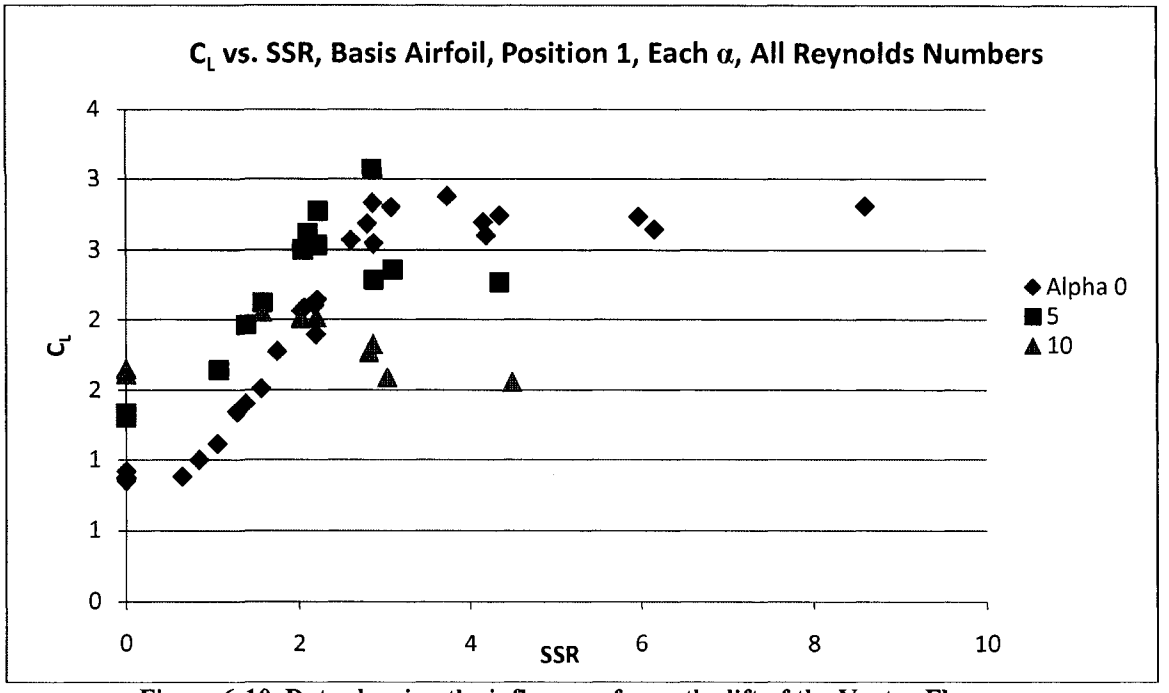

Figure 6-10. Data showing the influence of α on the lift of the Vortex Flap.

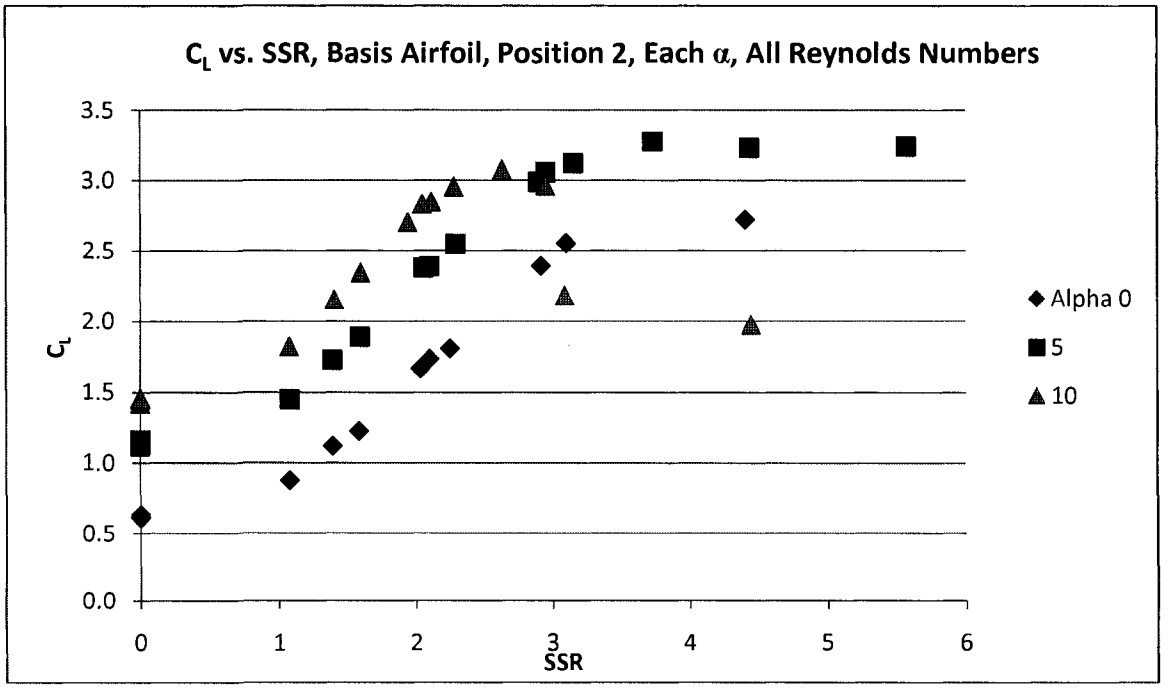

Figure 6-11. Data showing the influence of α on the lift of the Vortex Flap.

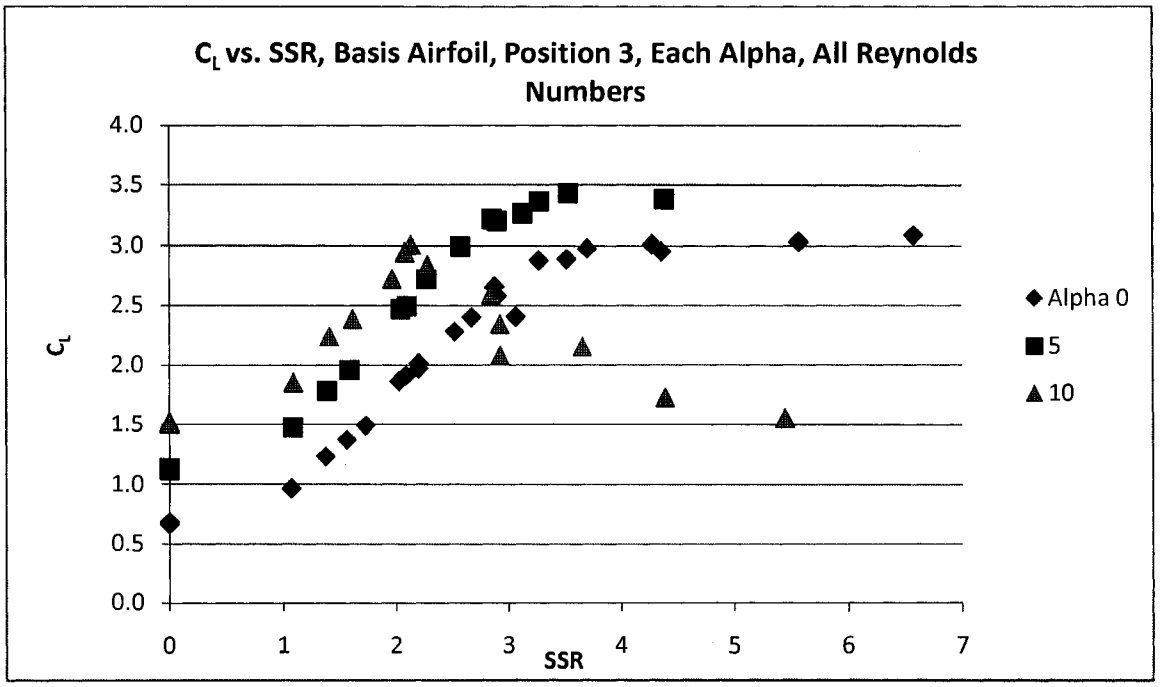

Figure 6-12. Data showing the influence of α on the lift of the Vortex Flap.

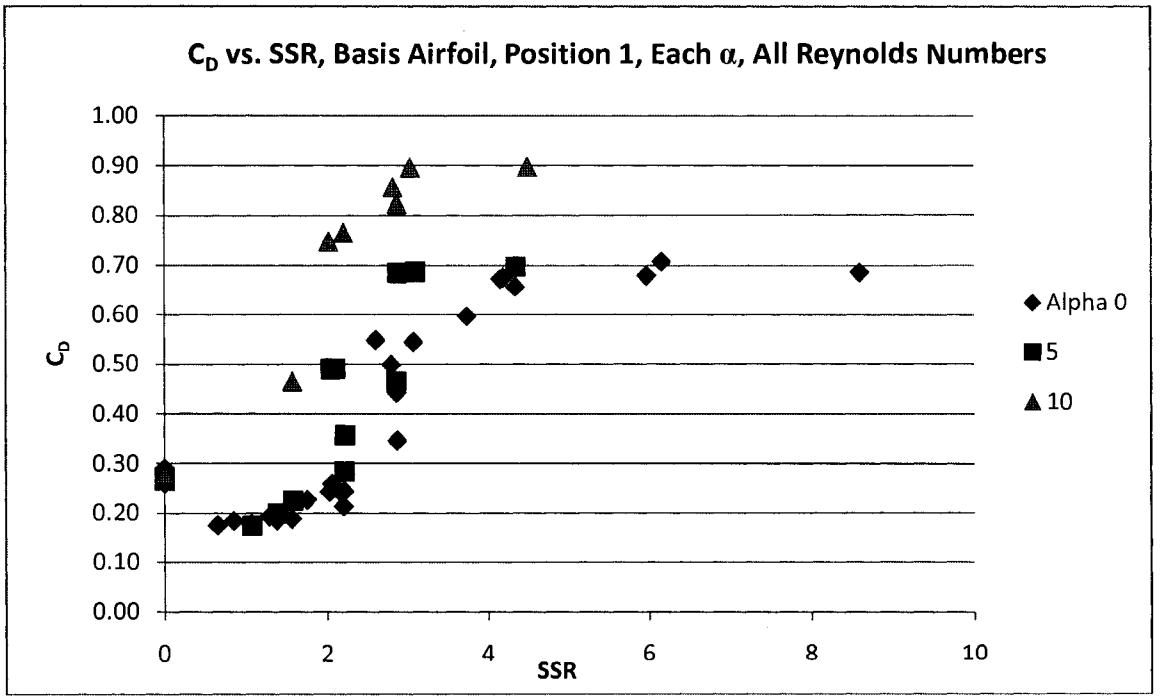

Figure 6-13. Data showing the influence of α on the drag of the Vortex Flap.

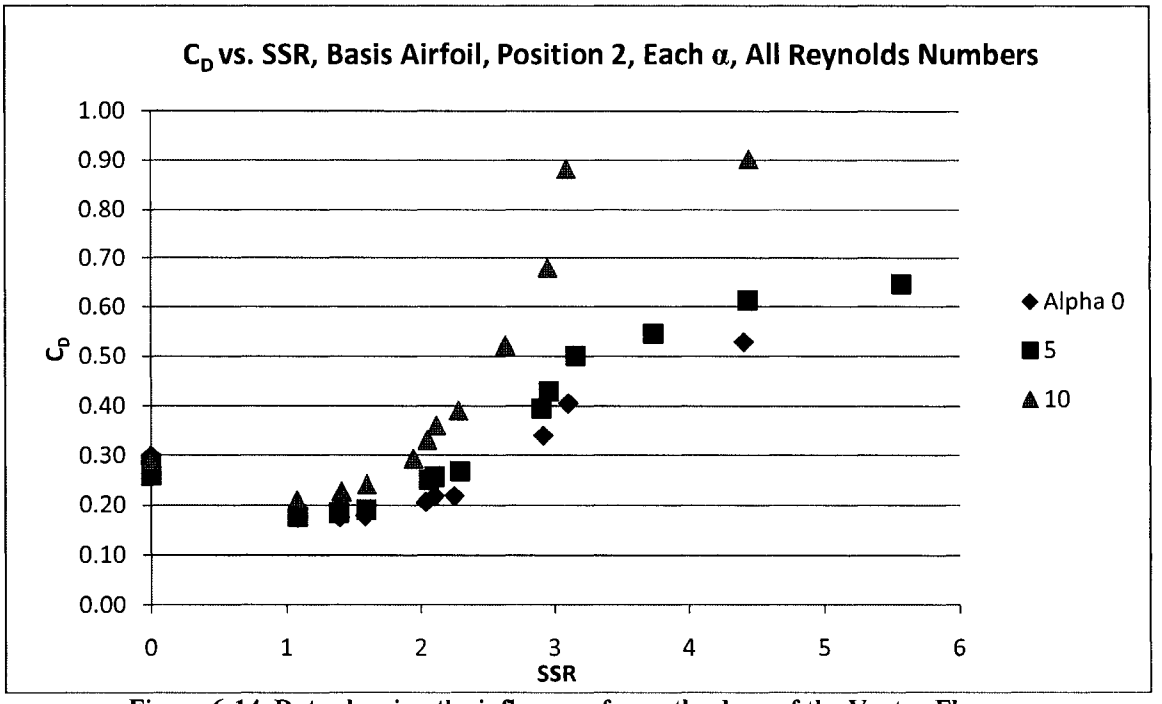

Figure 6-14. Data showing the influence of α on the drag of the Vortex Flap.

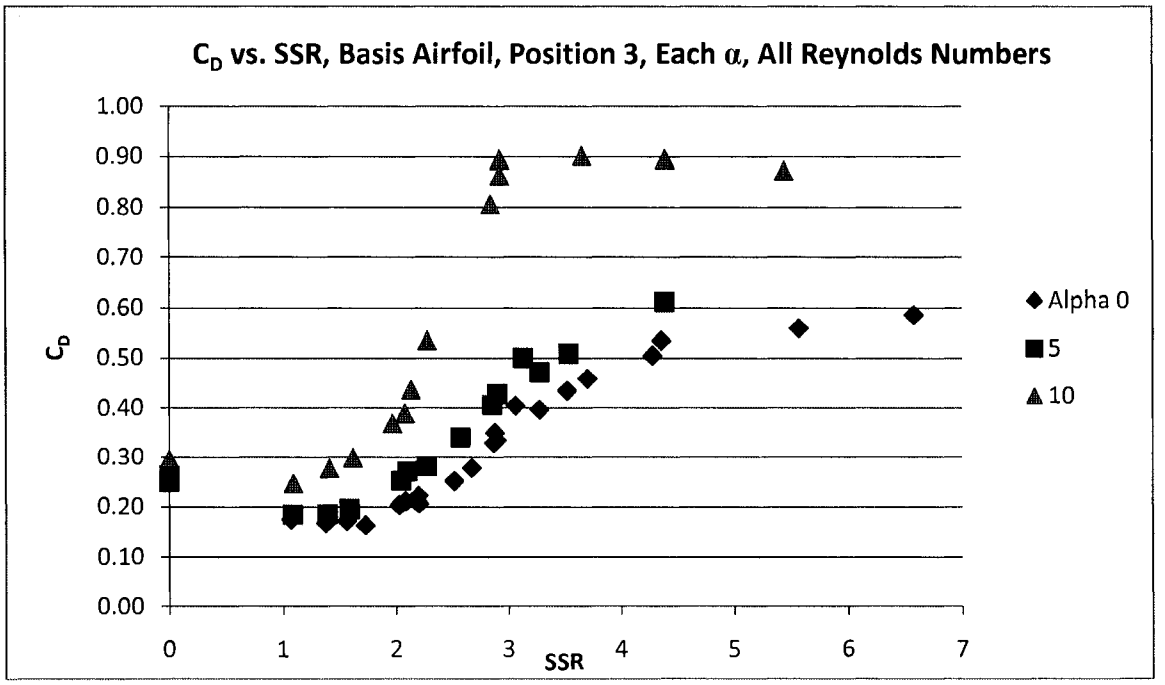

Figure 6-15. Data showing the influence of α on the drag of the Vortex Flap.

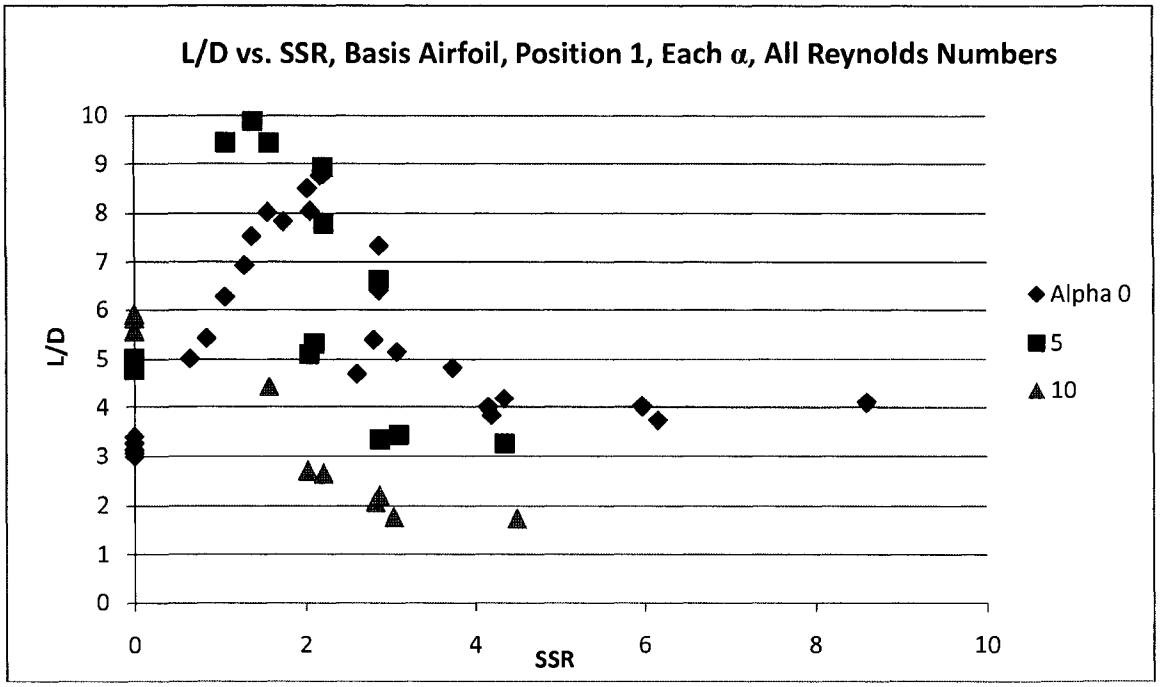

Figure 6-16. Data showing the influence of α on the L/D of the Vortex Flap.

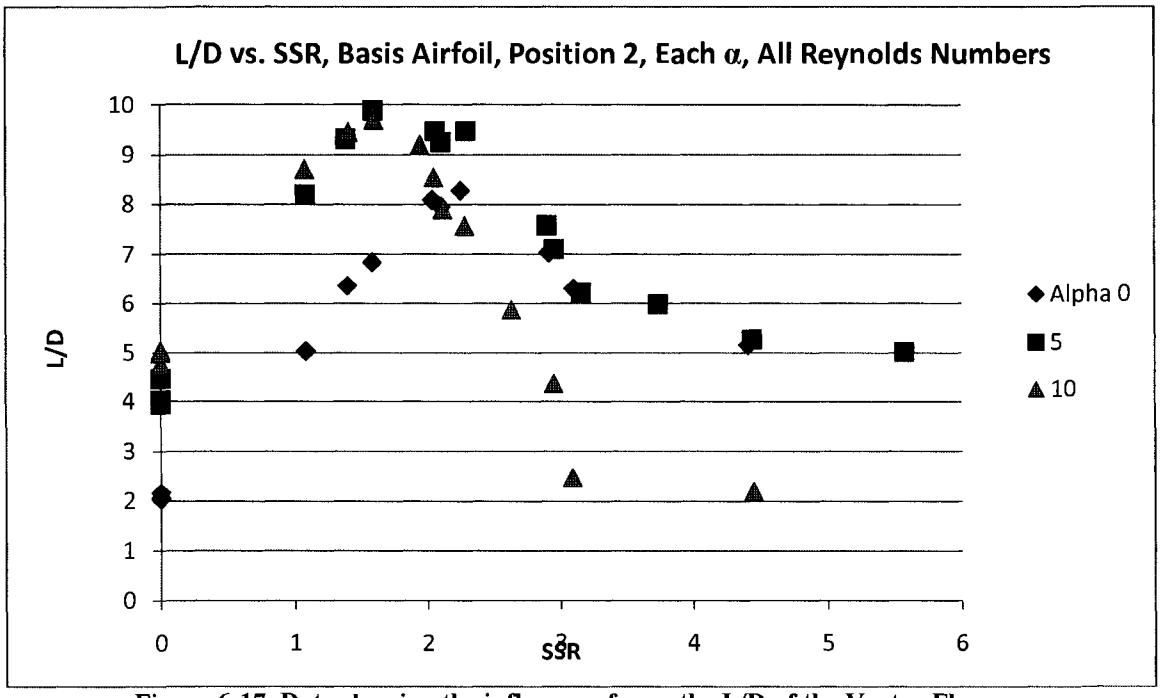

Figure 6-17. Data showing the influence of α on the L/D of the Vortex Flap.

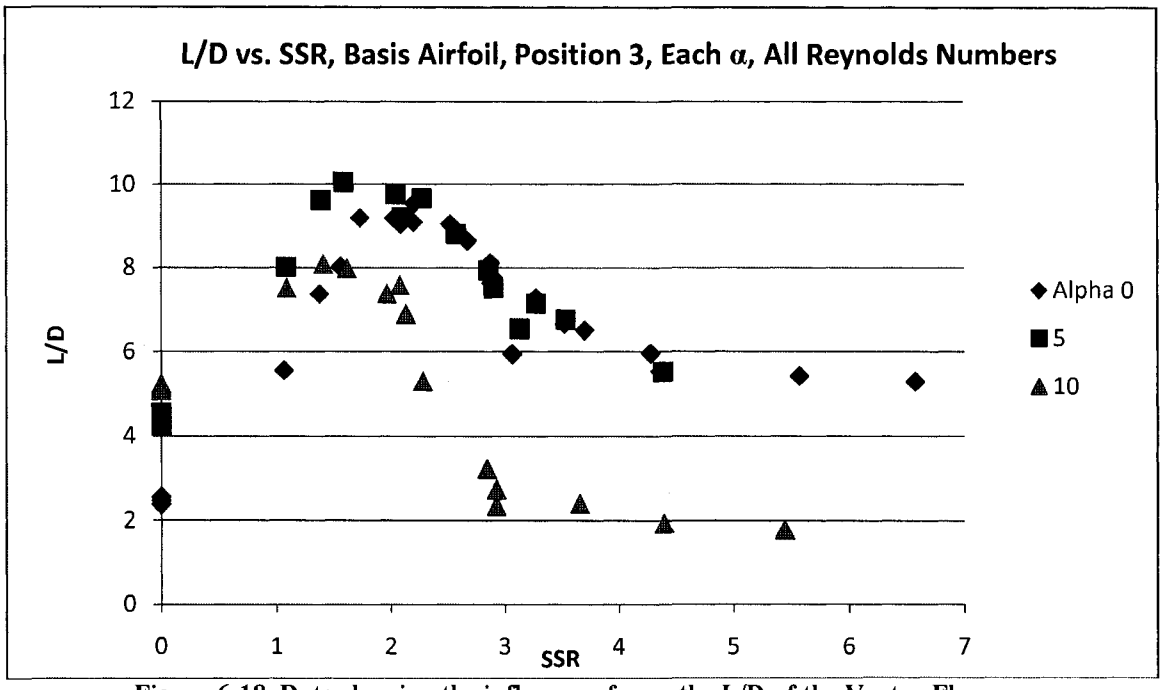

Figure 6-18. Data showing the influence of α on the L/D of the Vortex Flap.

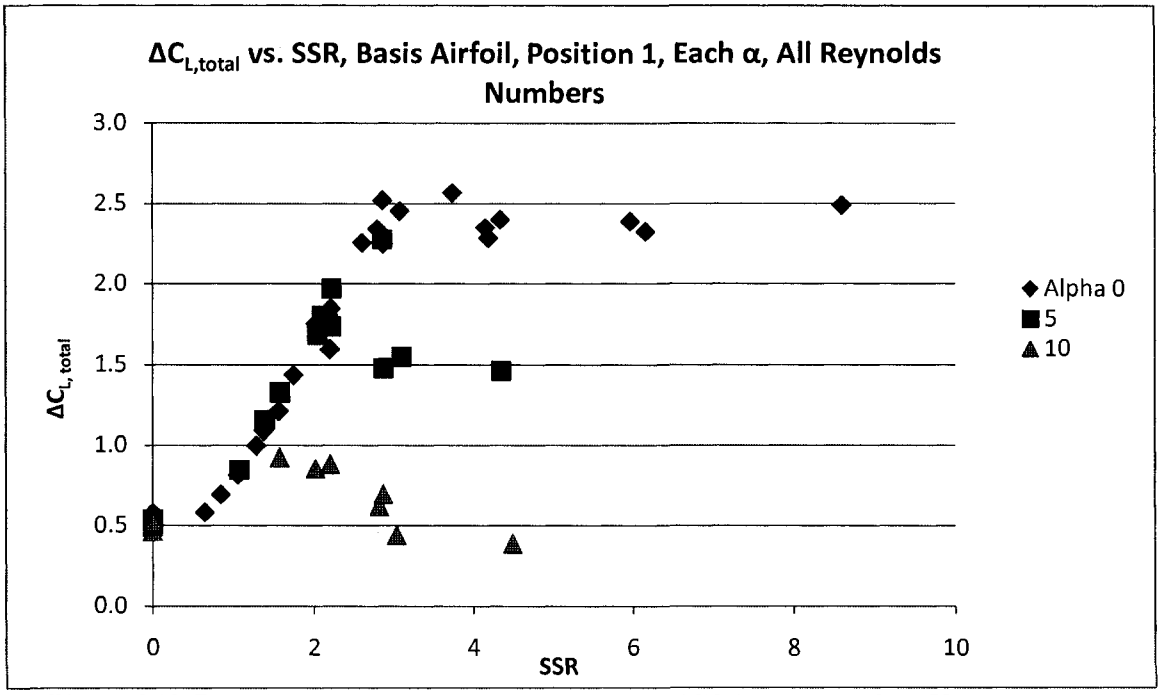

Figure 6-19. Data showing the influence of α on the total lift increment of the Vortex Flap.

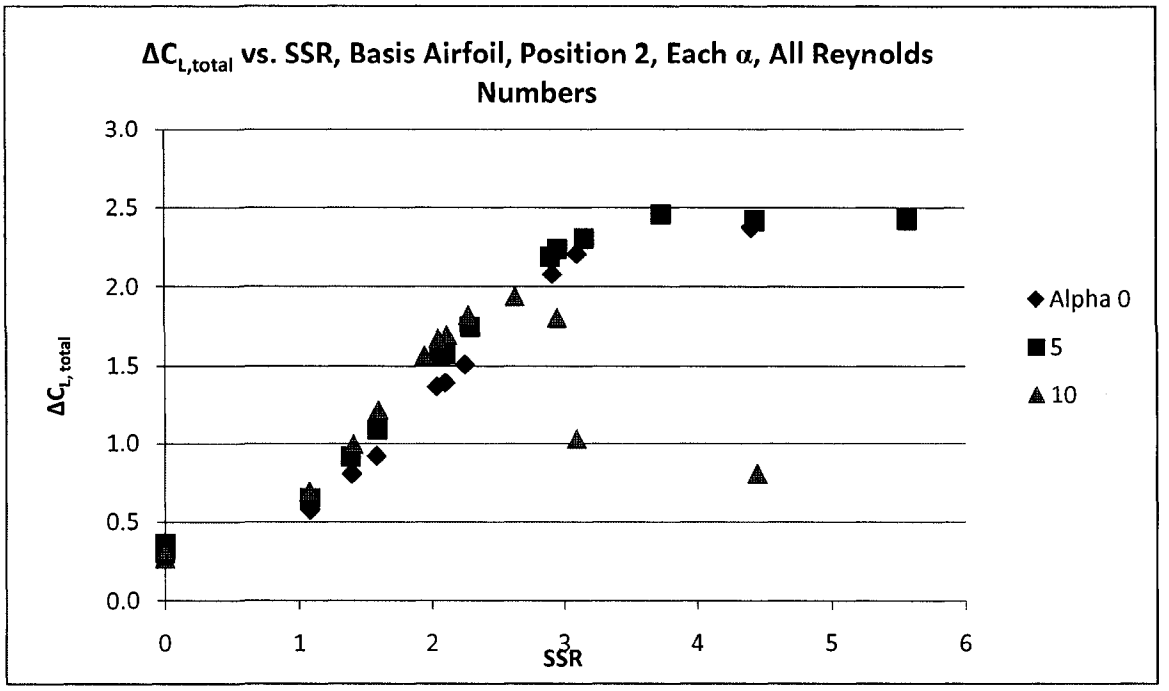

Figure 6-20. Data showing the influence of α on the total lift increment of the Vortex Flap.

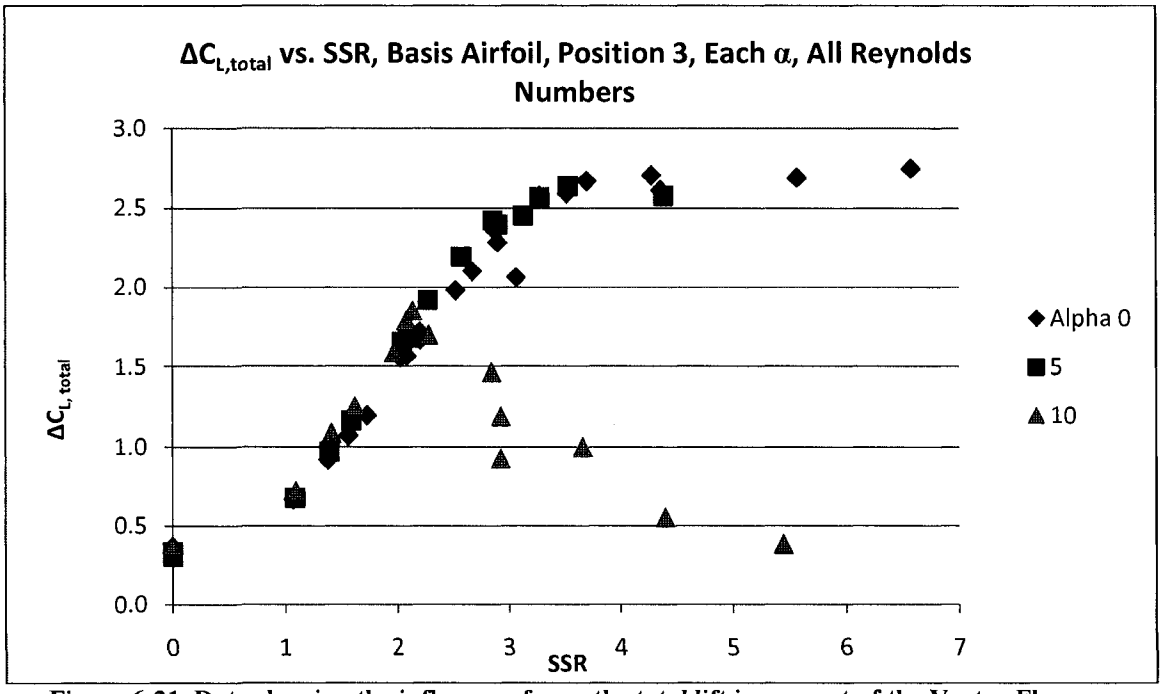

Figure 6-21. Data showing the influence of α on the total lift increment of the Vortex Flap.

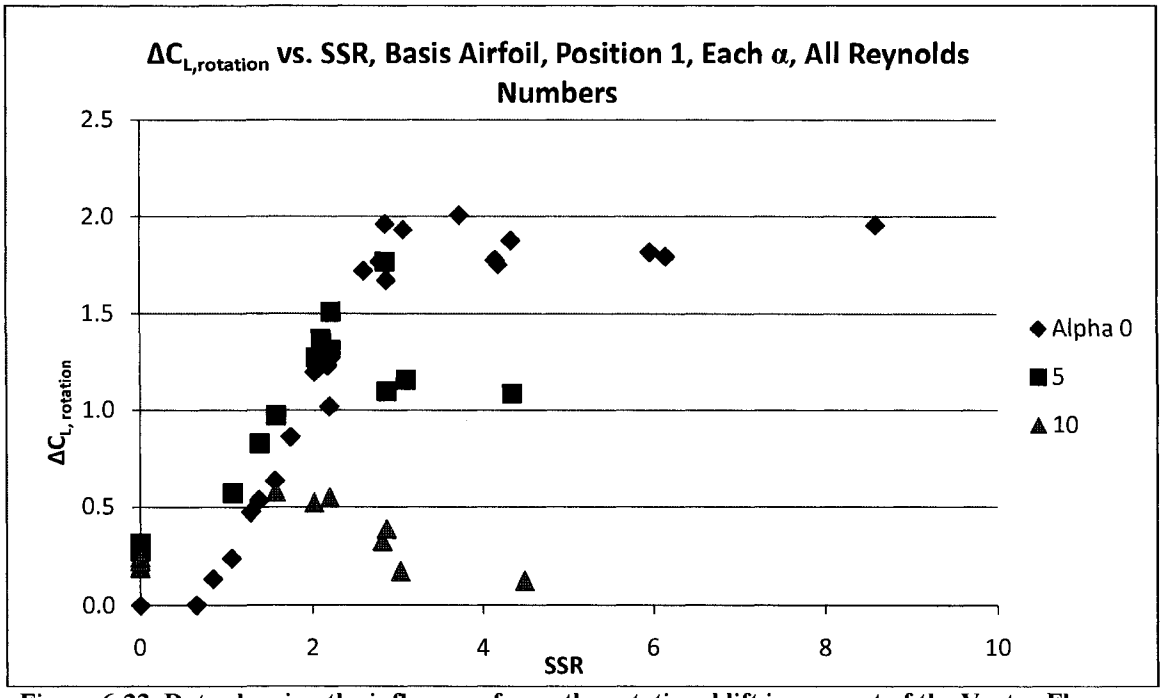

Figure 6-22. Data showing the influence of α on the rotational lift increment of the Vortex Flap.

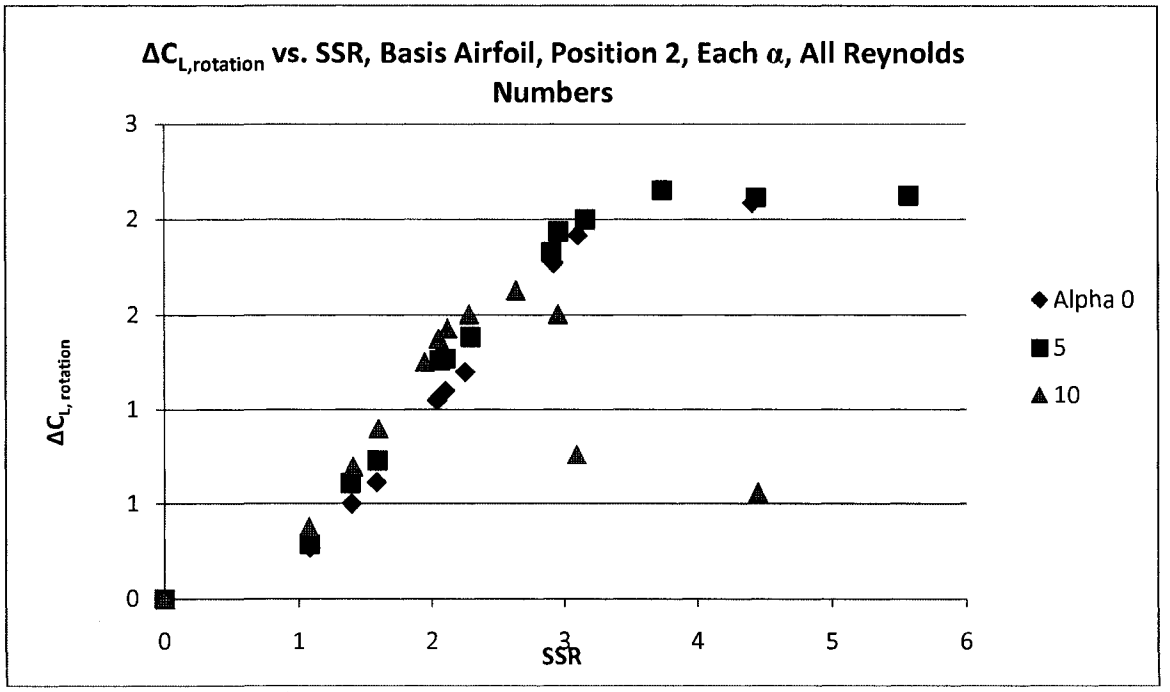

Figure 6-23. Data showing the influence of α on the rotational lift increment of the Vortex Flap.

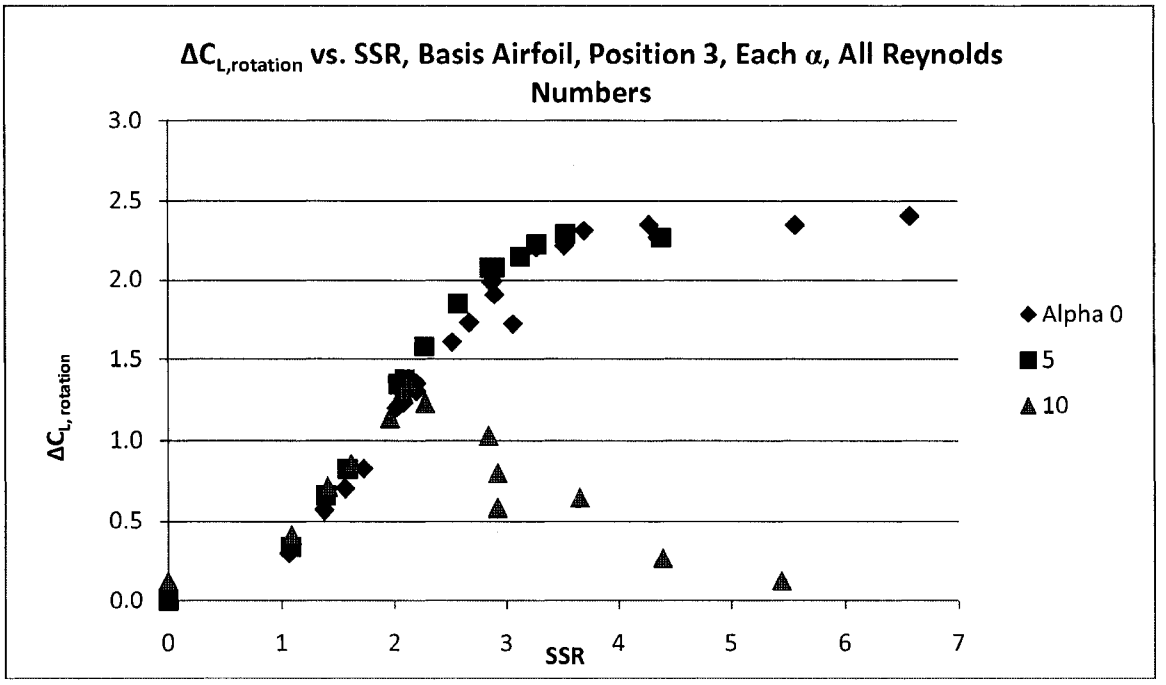

Figure 6-24. Data showing the influence of α on the rotational lift increment of the Vortex Flap.

Influence of Cylinder Position on Vortex Flap performance

Figures 6-16 through 6-27 show the complete summary of data showing the influence of cylinder position on Vortex Flap performance.

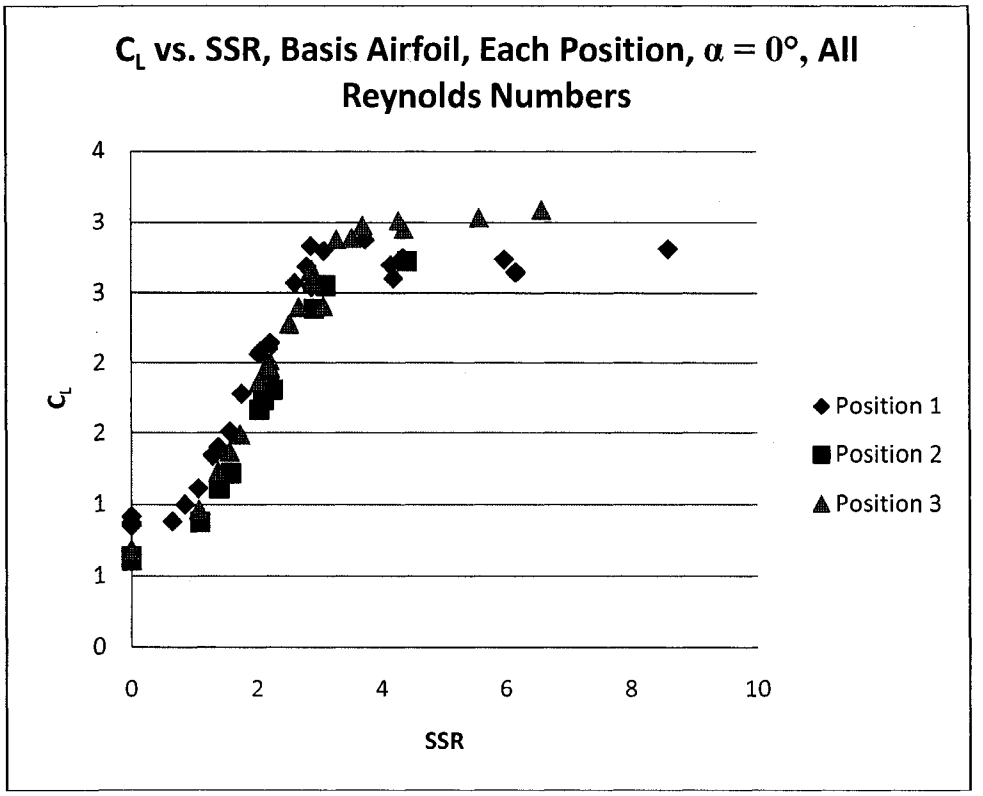

Figure 6-25. Data showing effect of cylinder position on the lift of the Vortex Flap.

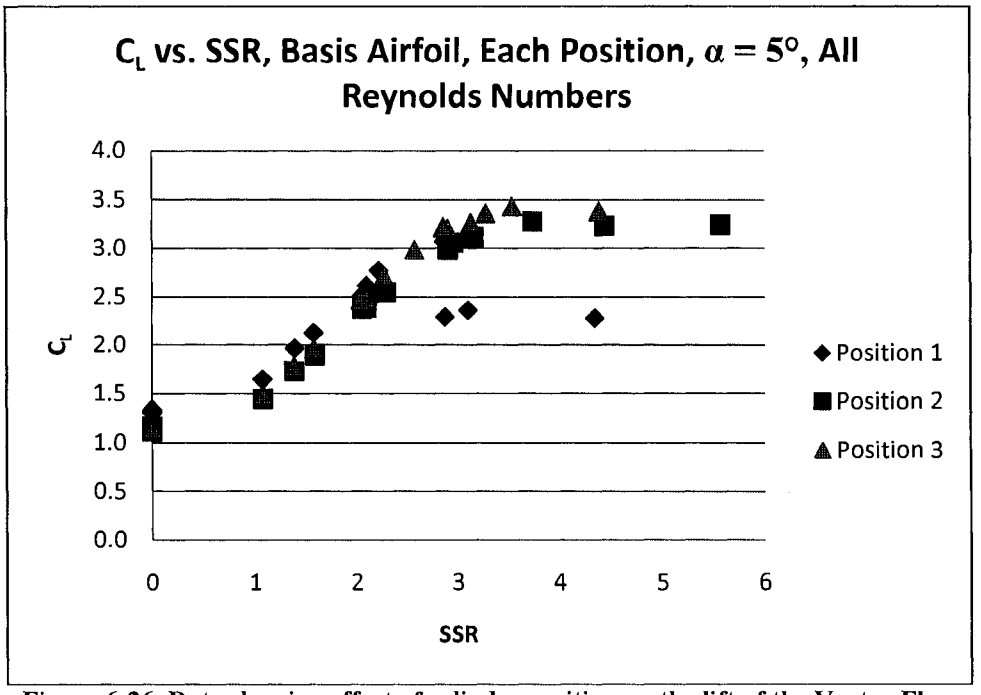

Figure 6-26. Data showing effect of cylinder position on the lift of the Vortex Flap.

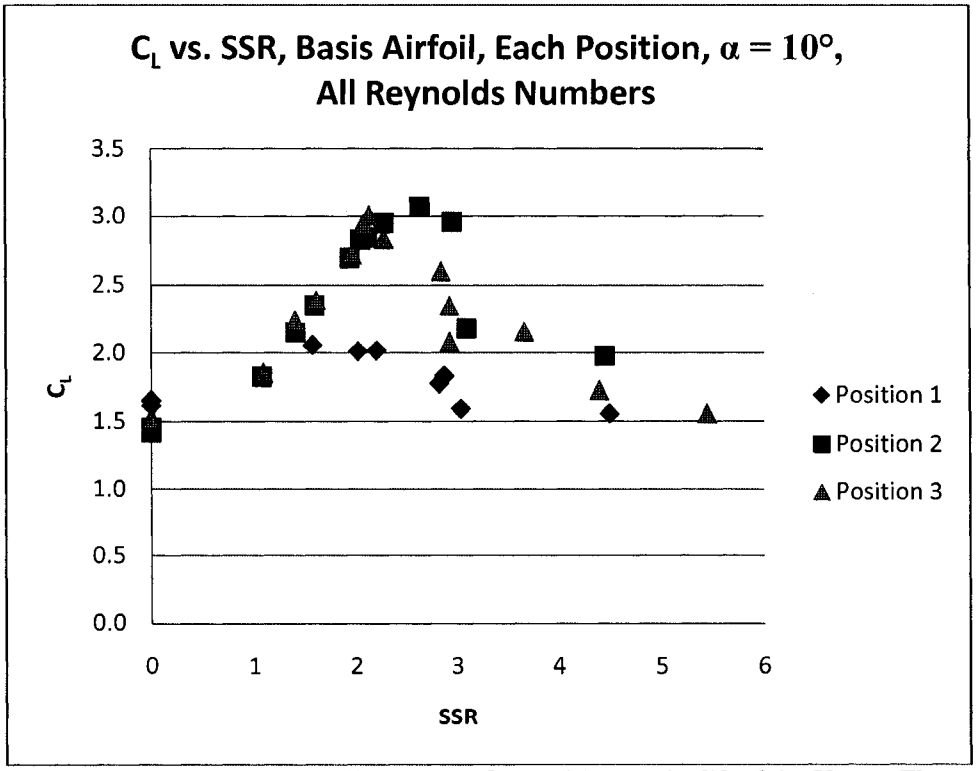

Figure 6-27. Data showing effect of cylinder position on the lift of the Vortex Flap.

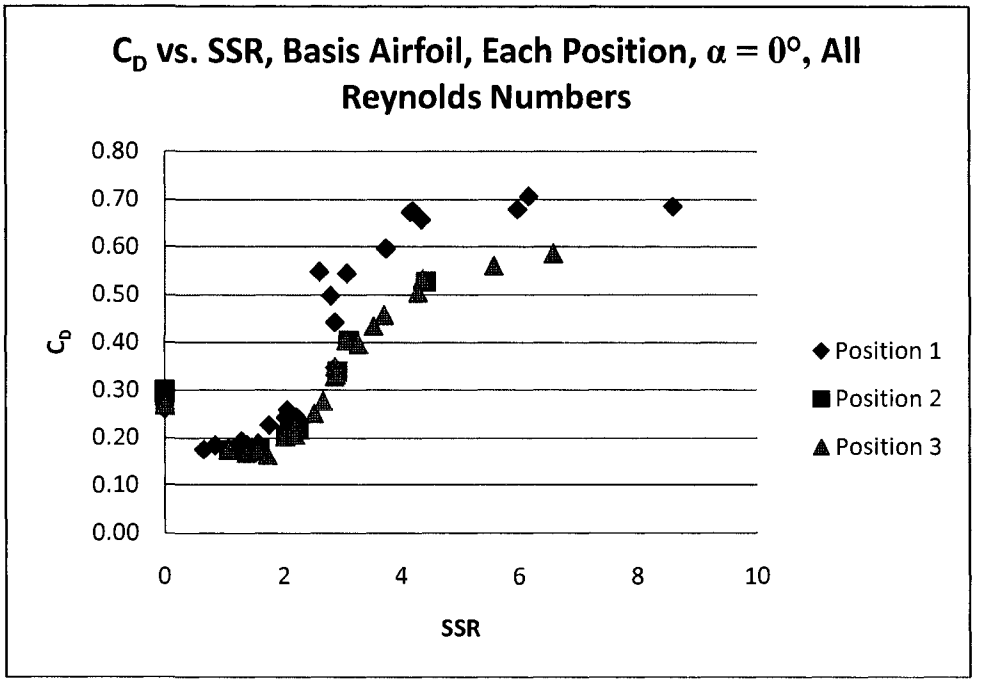

Figure 6-28. Data showing effect of cylinder position on the drag of the Vortex Flap.

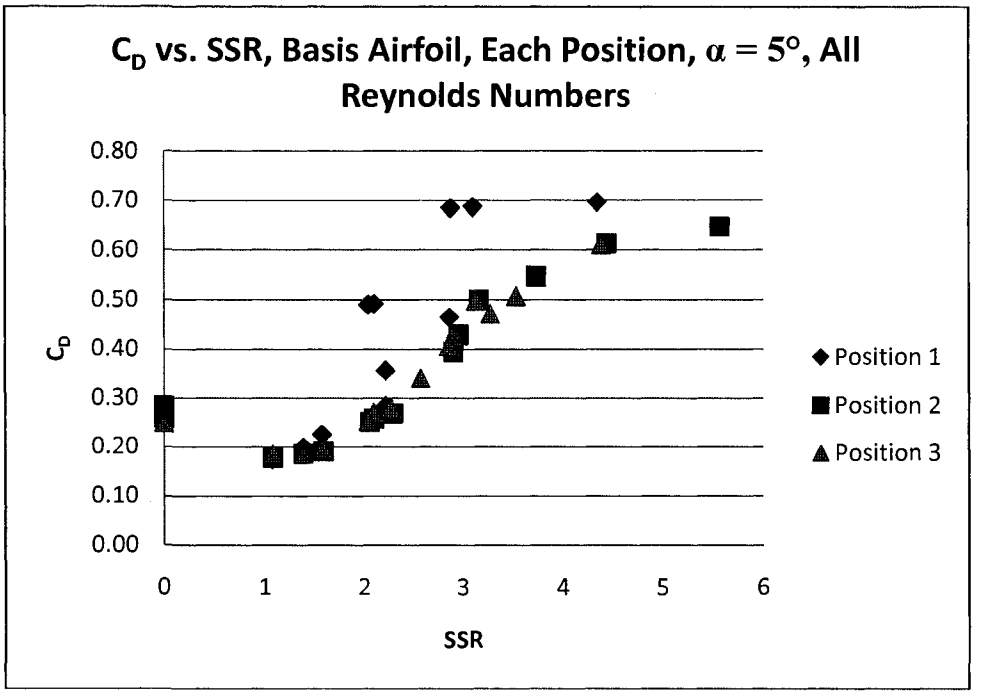

Figure 6-29. Data showing effect of cylinder position on the drag of the Vortex Flap.

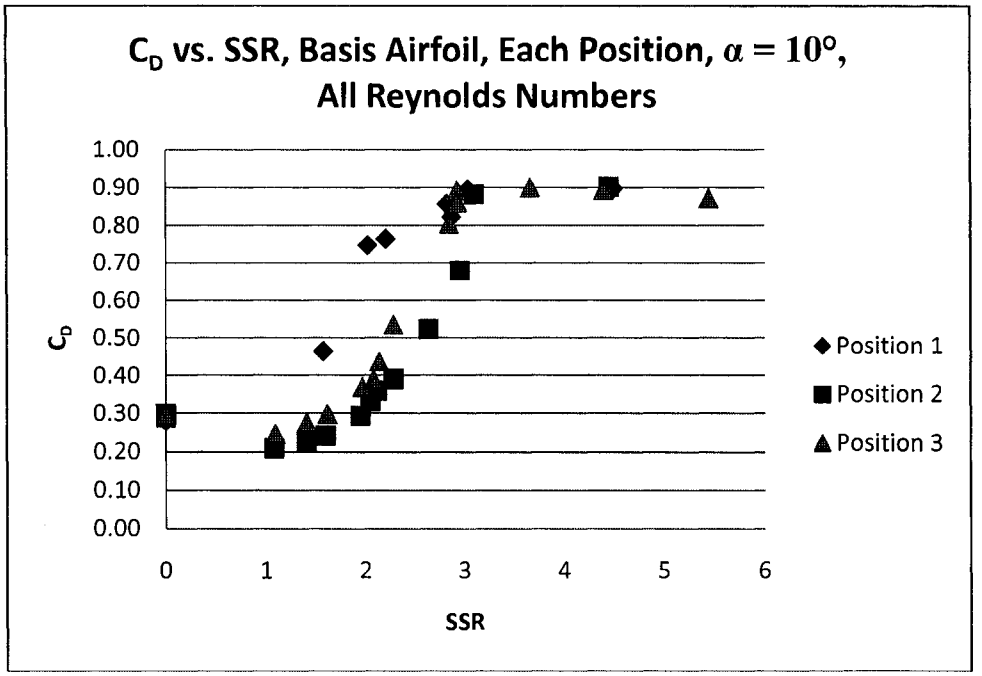

Figure 6-30. Data showing effect of cylinder position on the drag of the Vortex Flap.

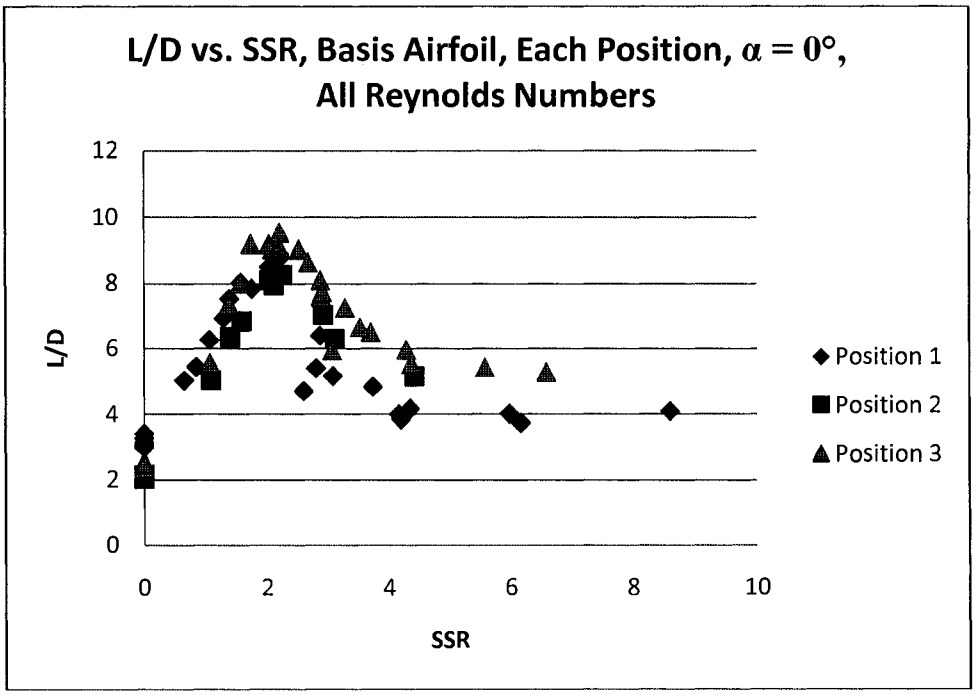

Figure 6-31. Data showing effect of cylinder position on the L/D of the Vortex Flap.

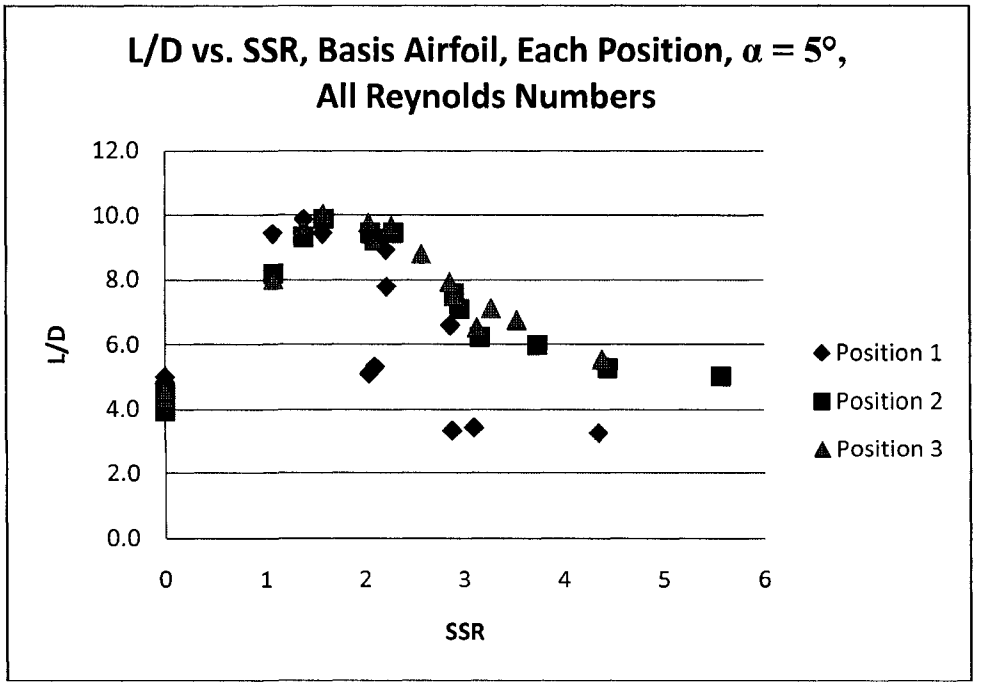

Figure 6-32. Data showing effect of cylinder position on the L/D of the Vortex Flap.

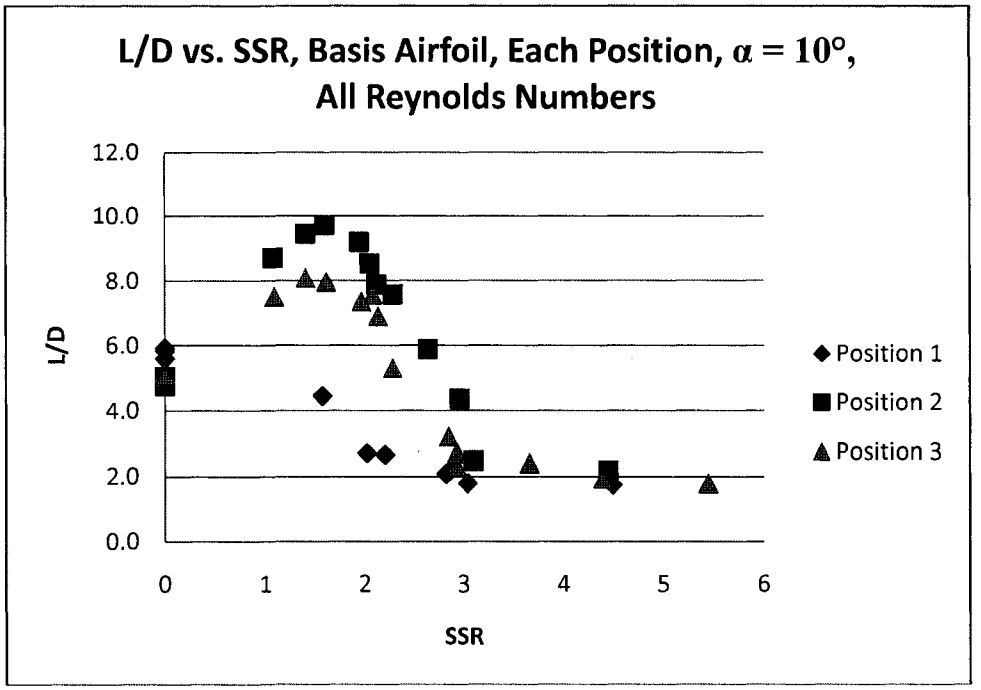

Figure 6-33. Data showing effect of cylinder position on the L/D of the Vortex Flap.

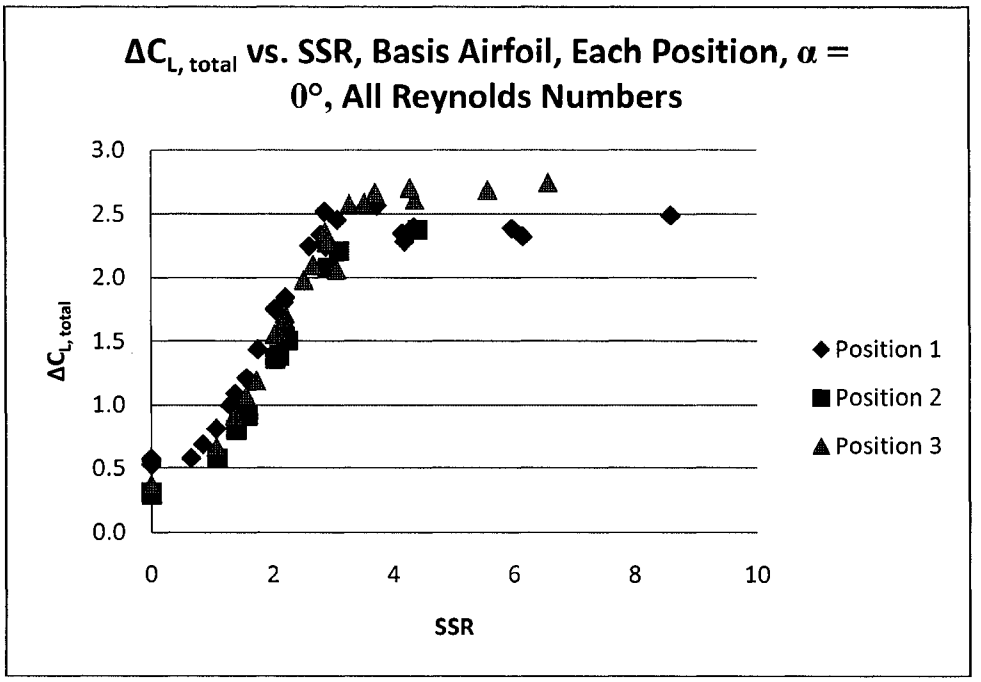

Figure 6-34. Data showing effect of cylinder position on the total lift increment of the Vortex Flap.

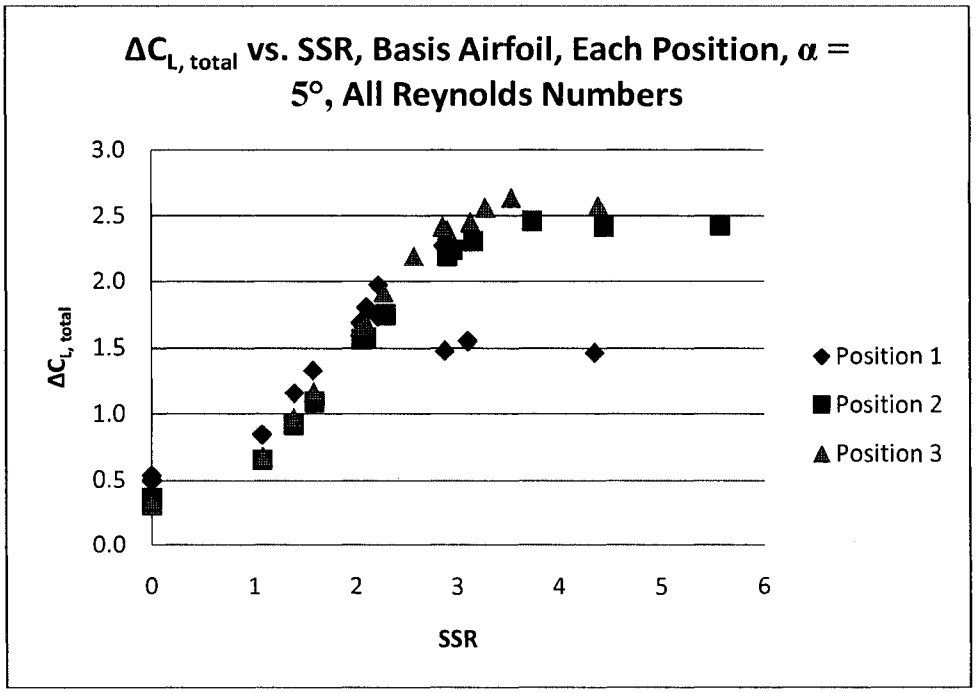

Figure 6-35. Data showing effect of cylinder position on the total lift increment of the Vortex Flap.

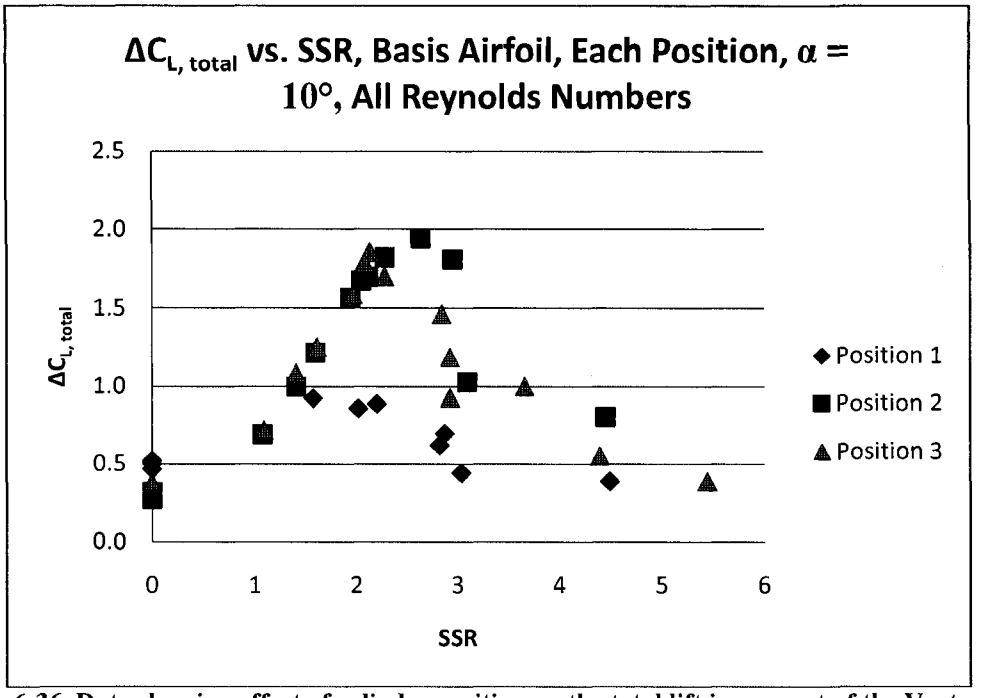

Figure 6-36. Data showing effect of cylinder position on the total lift increment of the Vortex Flap.

Influence of Reynolds Number on Vortex Flap Performance

Figures 6-28 through 6-39 summarize data showing the influence of Reynolds number on the performance and behavior of the Vortex Flap.

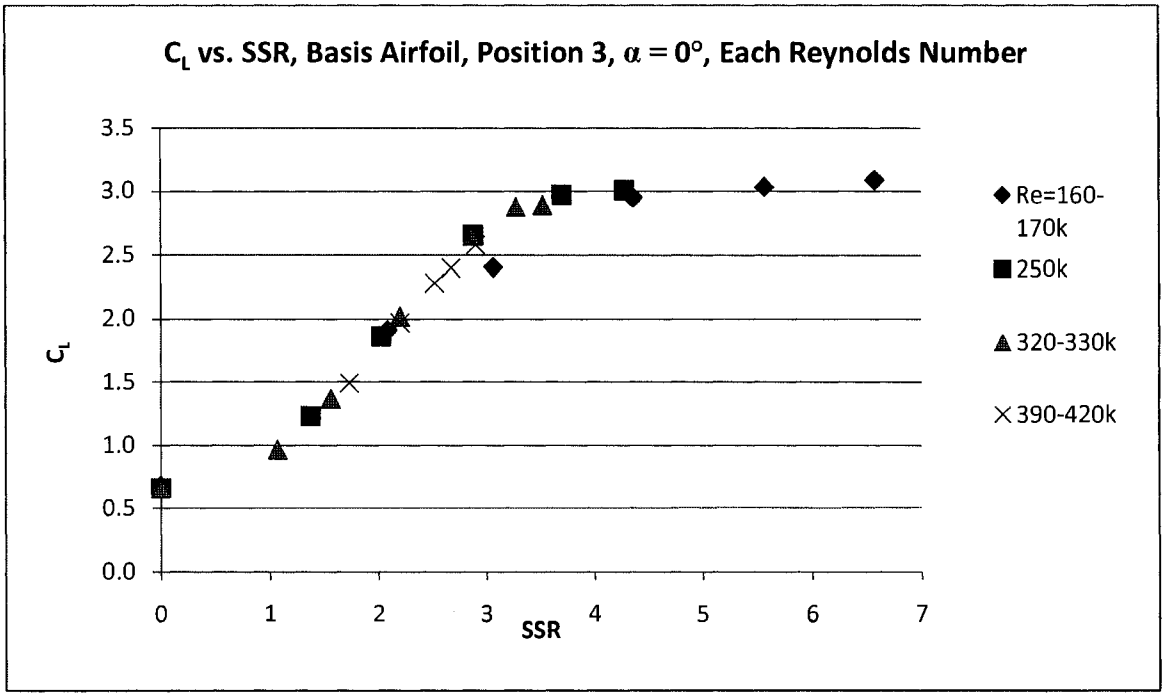

Figure 6-37. Data showing the influence of Reynolds number on the lift of the vortex flap.

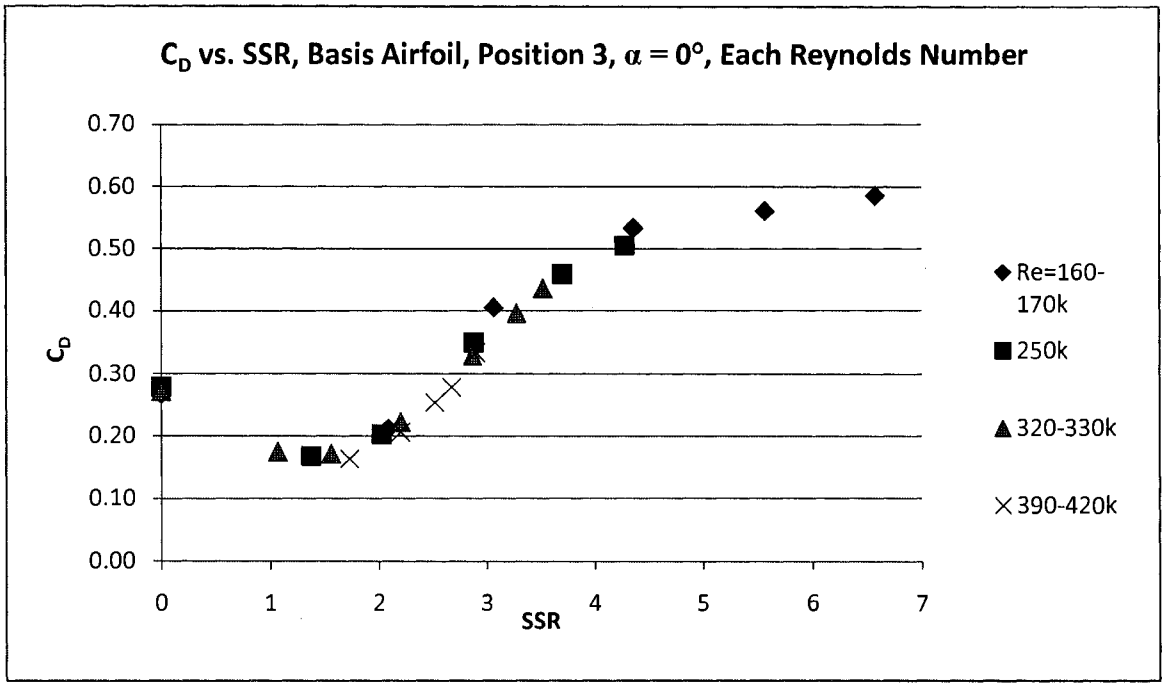

Figure 6-38. Data showing the influence of Reynolds number on the drag of the vortex flap.

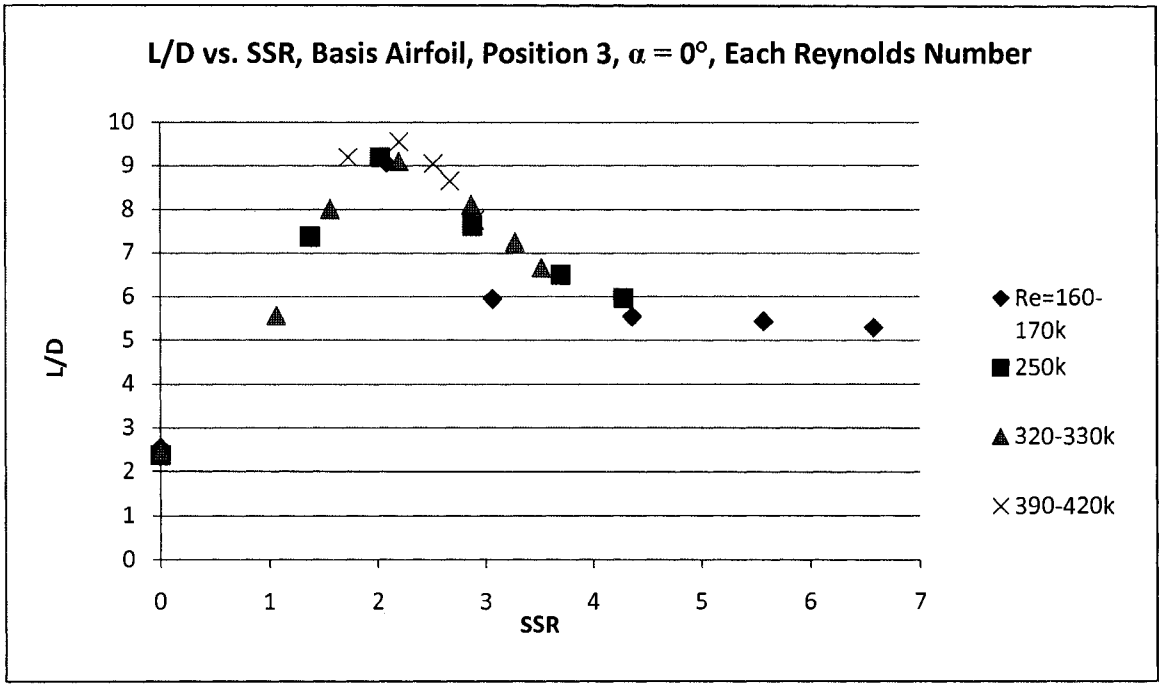

Figure 6-39. Data showing the influence of Reynolds number on the L/D of the vortex flap.

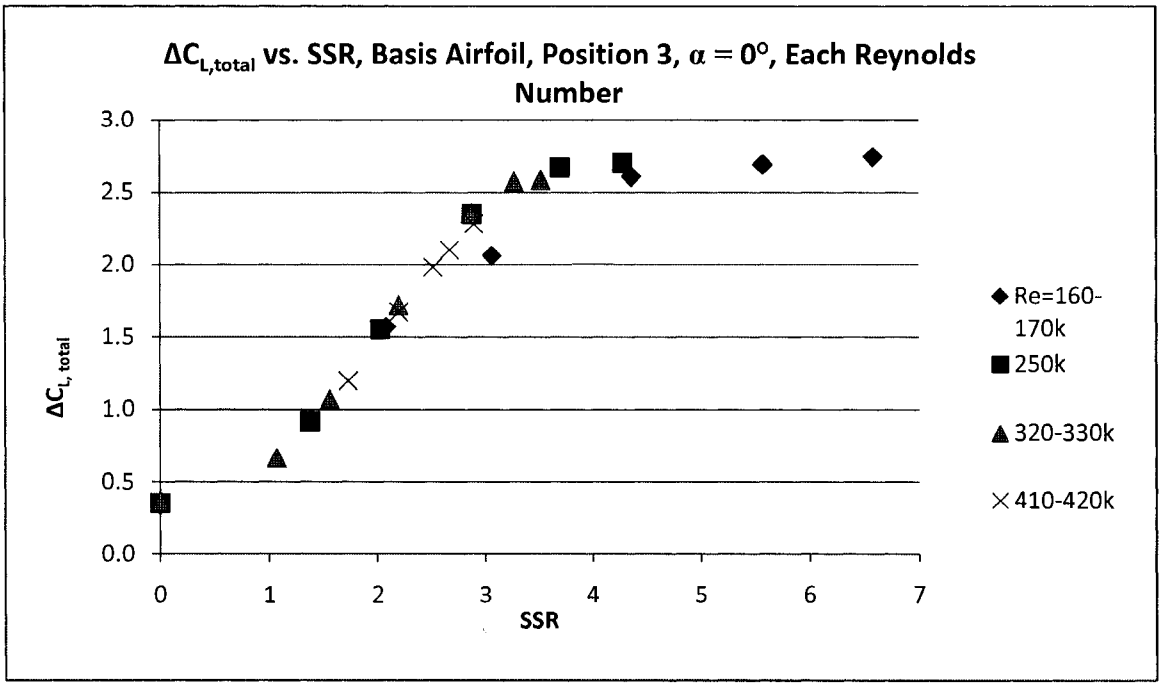

Figure 6-40. Data showing the influence of Reynolds number on the total lift increment of the vortex flap.

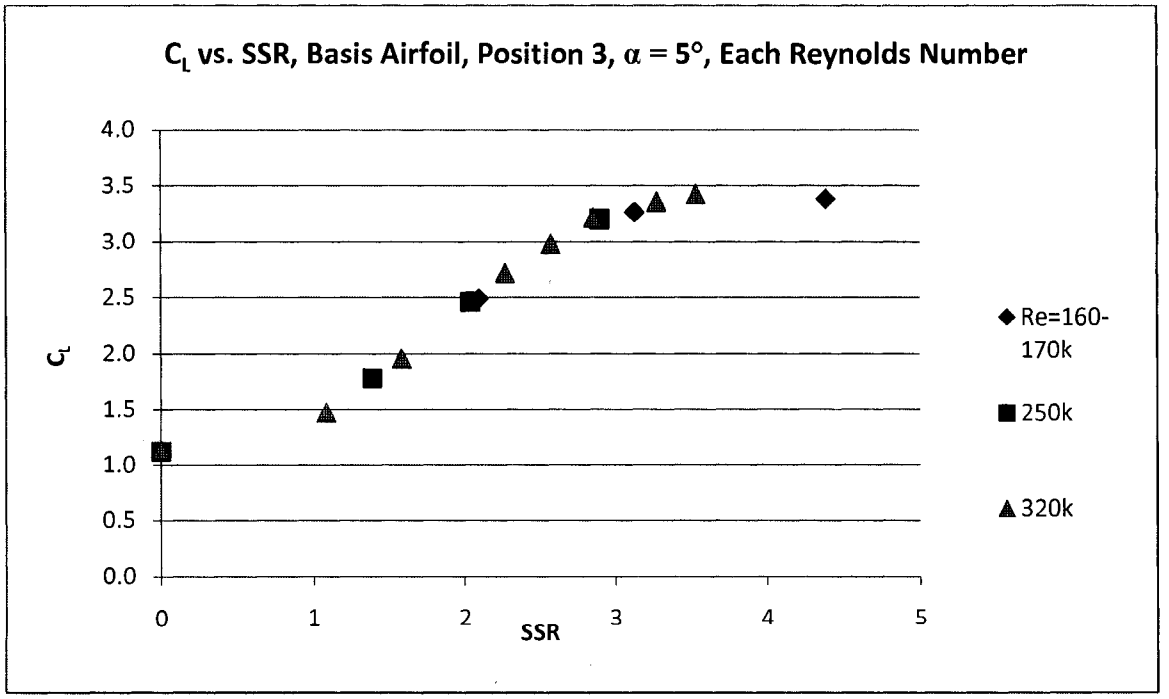

Figure 6-41. Data showing the influence of Reynolds number on the lift of the vortex flap.

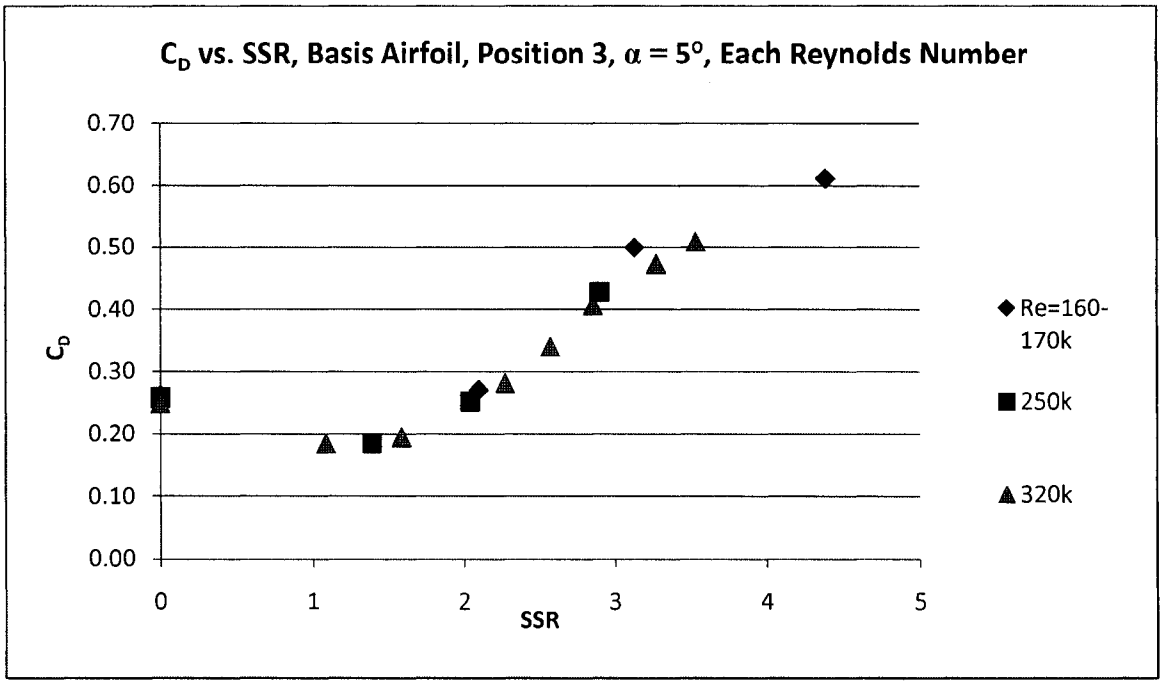

Figure 6-42. Data showing the influence of Reynolds number on the drag of the vortex flap.

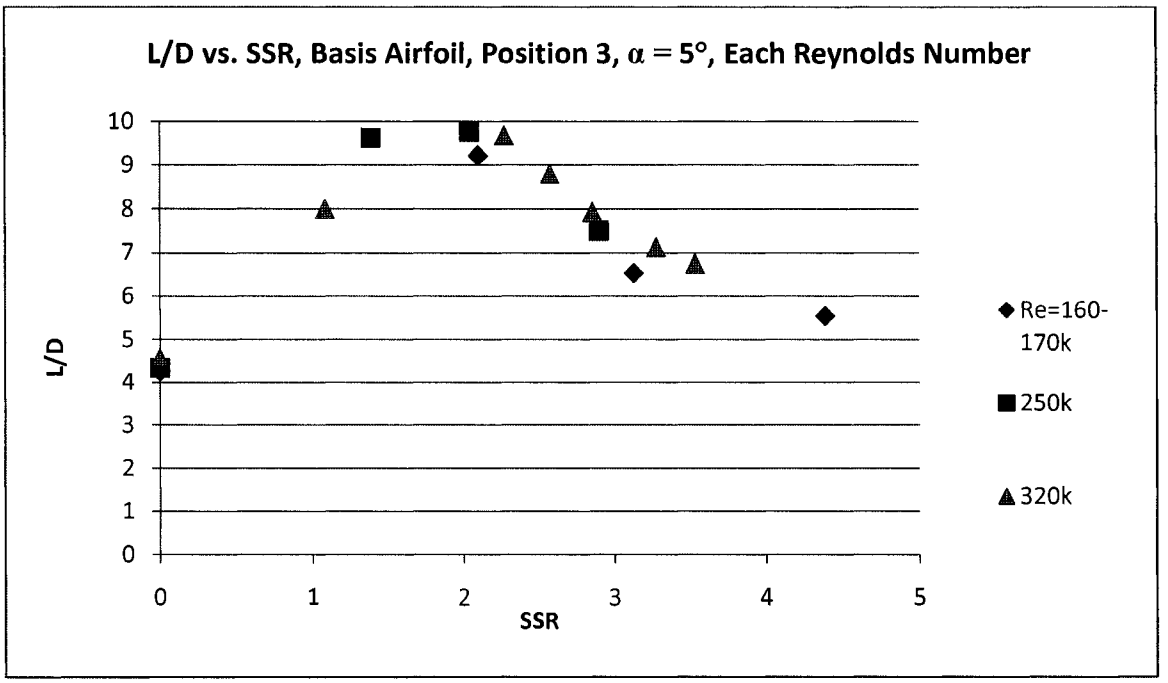

Figure 6-43. Data showing the influence of Reynolds number on the L/D of the vortex flap.

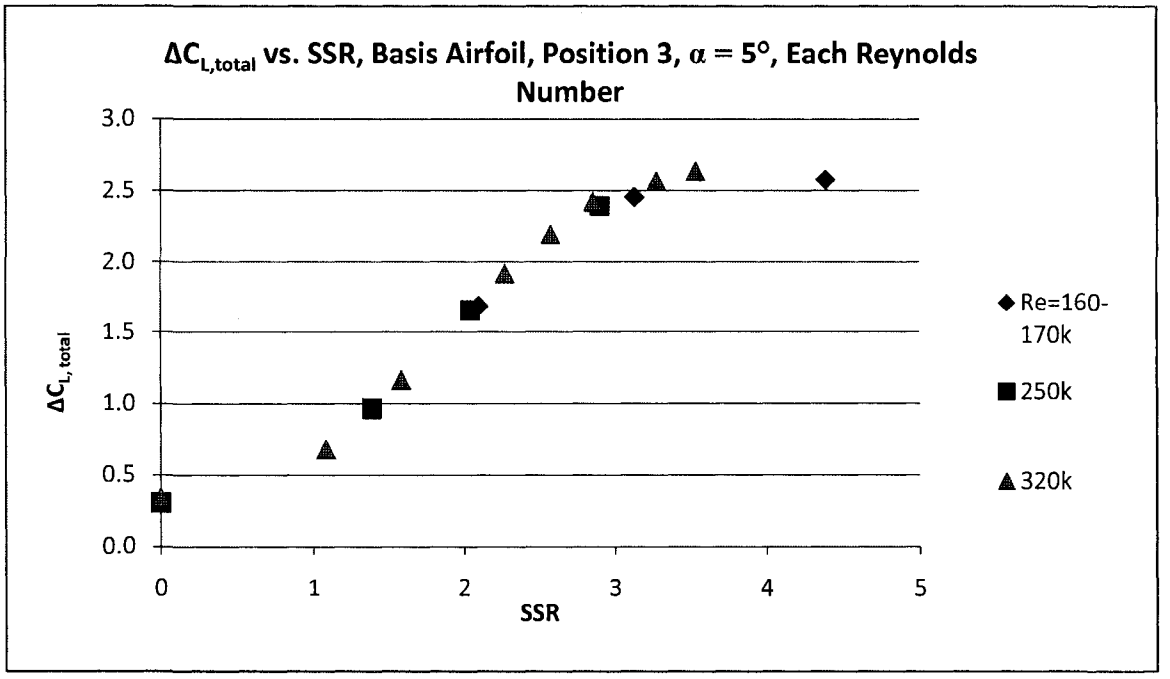

Figure 6-44. Data showing the influence of Reynolds number on the total lift increment of the vortex flap.

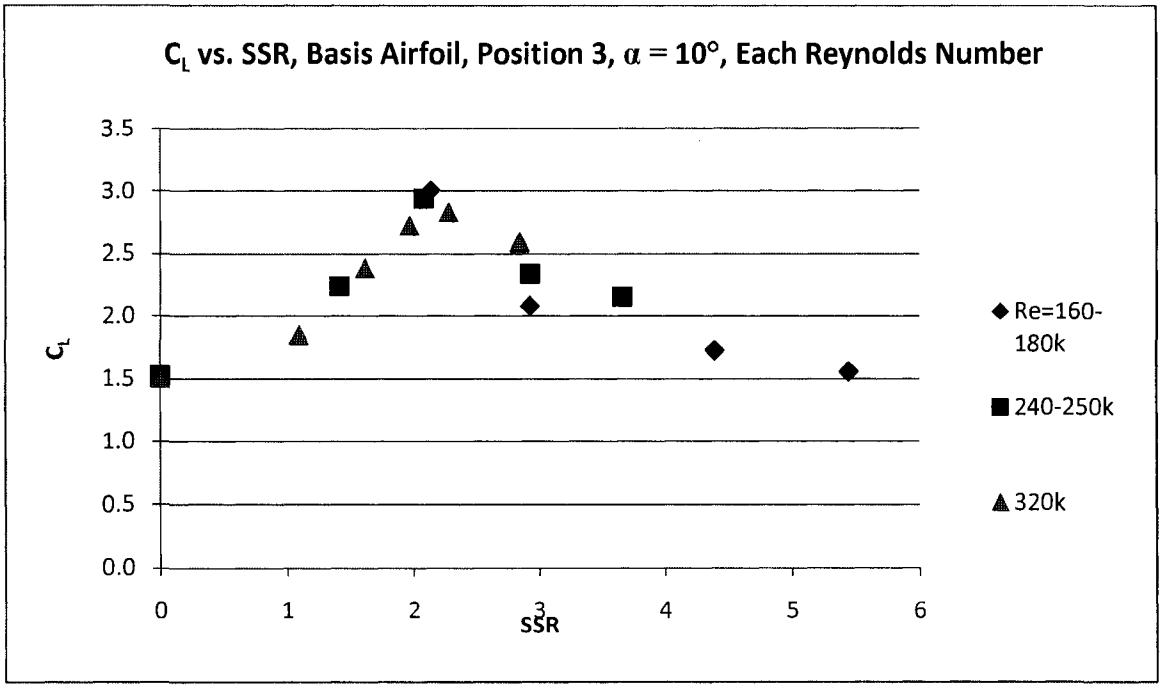

Figure 6-45. Data showing the influence of Reynolds number on the lift of the vortex flap.

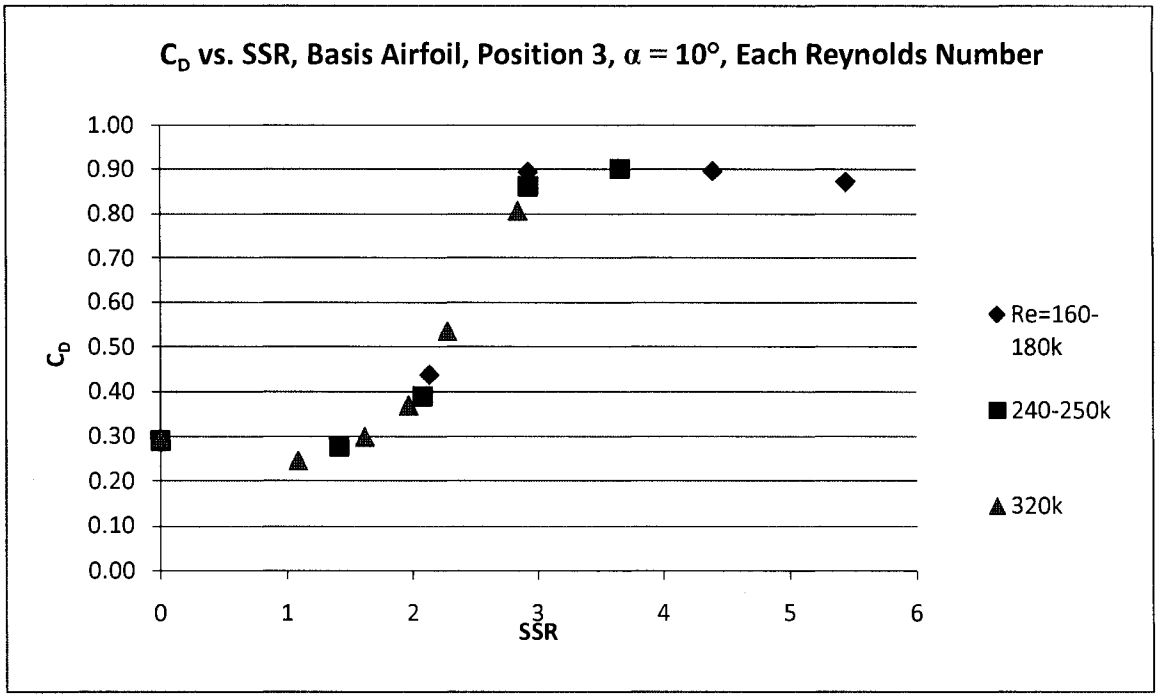

Figure 6-46. Data showing the influence of Reynolds number on the drag of the vortex flap.

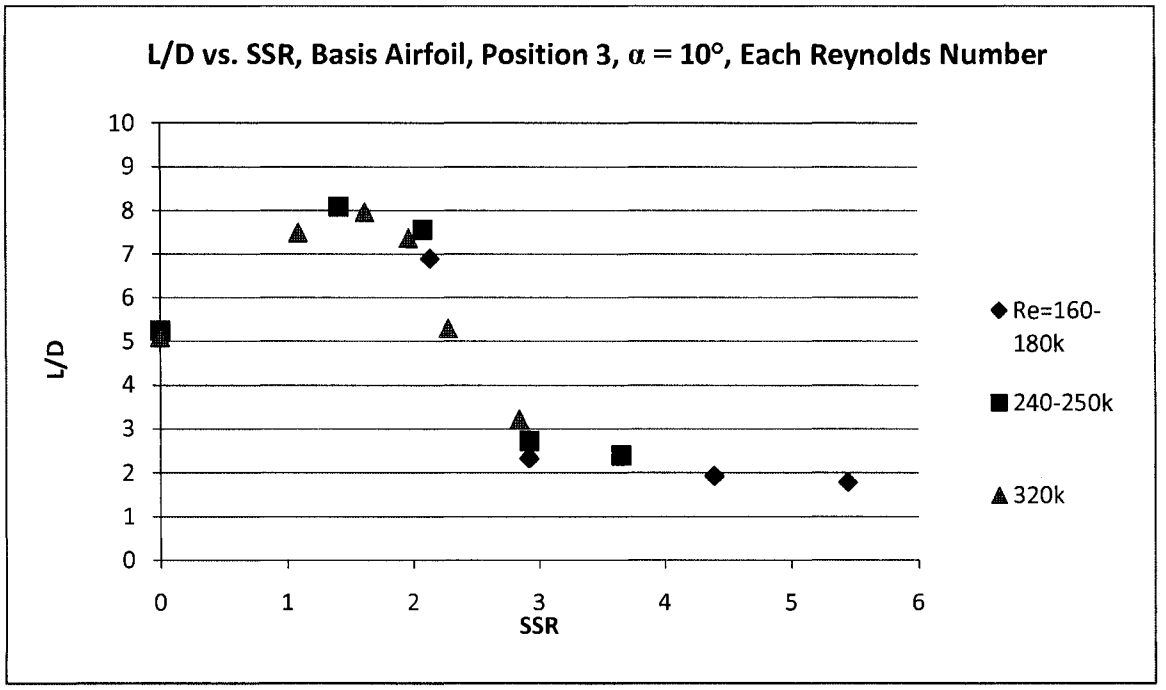

Figure 6-47. Data showing the influence of Reynolds number on the L/D of the vortex flap.

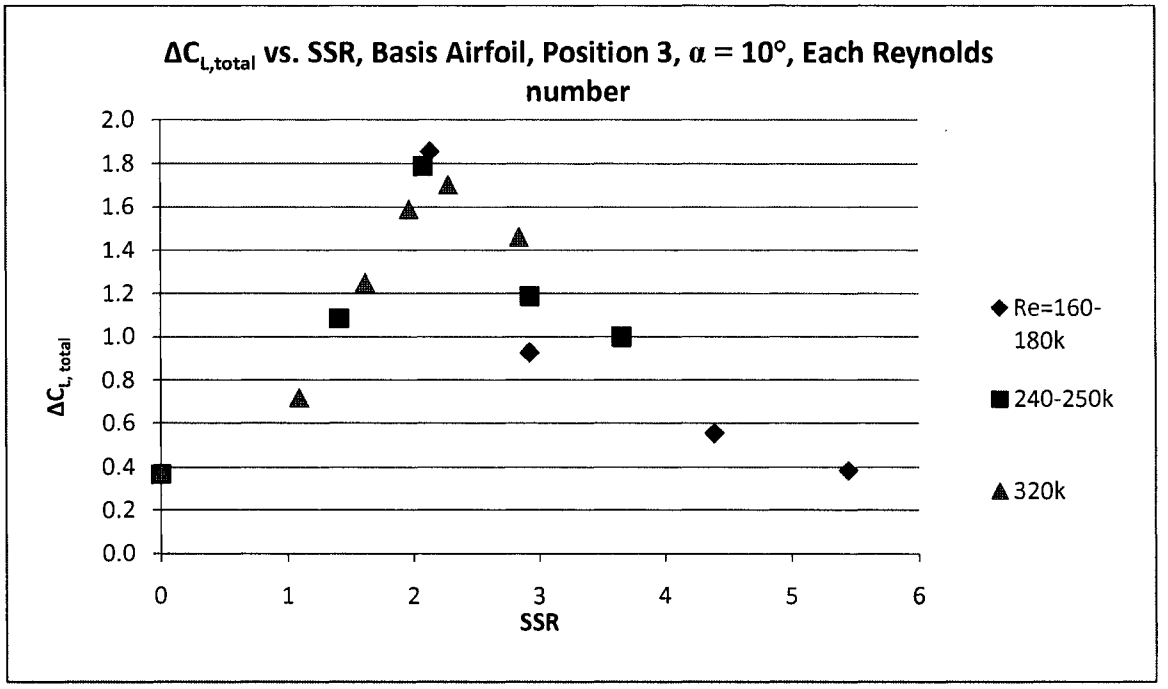

Figure 6-48. Data showing the influence of Reynolds number on the total lift increment of the vortex flap.

Appendix B- Response Surface Method Results

Surface plots for $\alpha = 0°$

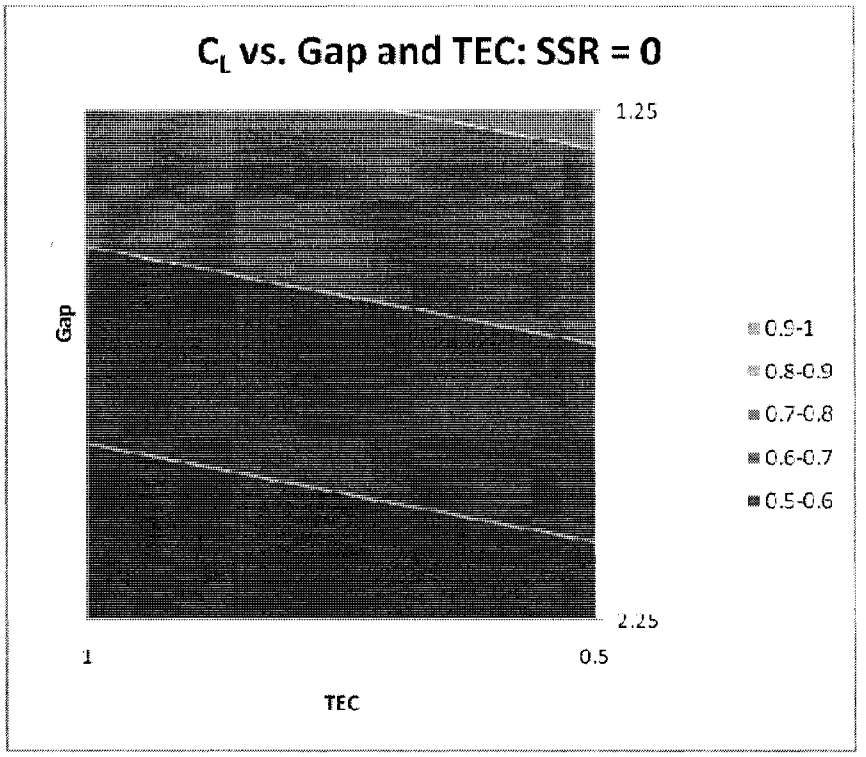

Figure 6-49. Lift surface plot, SSR = 0.

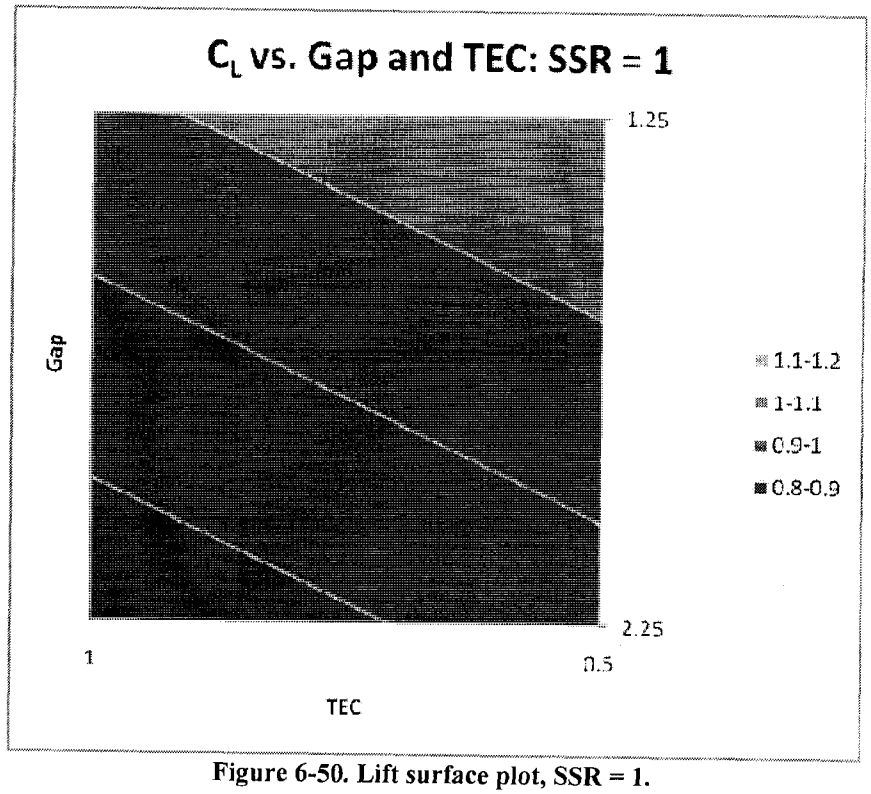

Figure 6-50. Lift surface plot, SSR = 1.

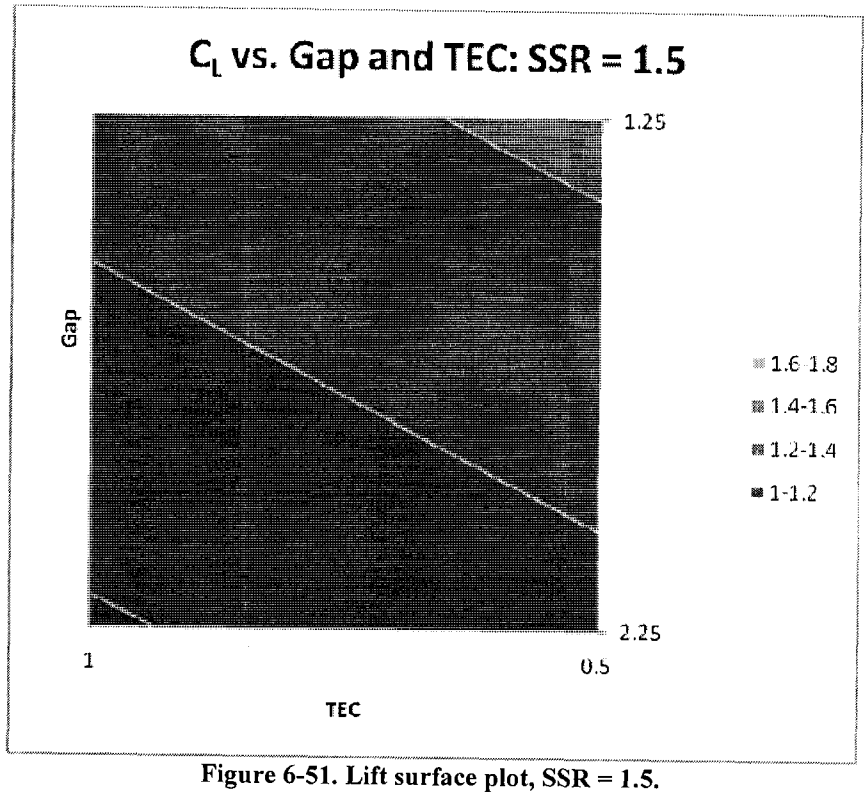

Figure 6-51. Lift surface plot, SSR = 1.5.

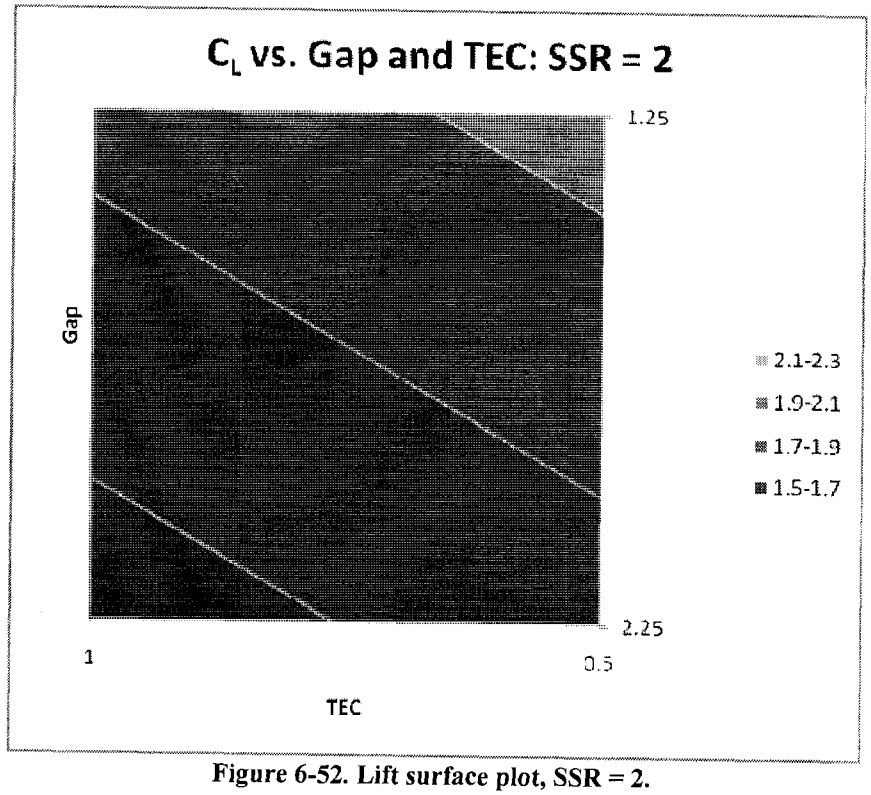

Figure 6-52. Lift surface plot, SSR = 2.

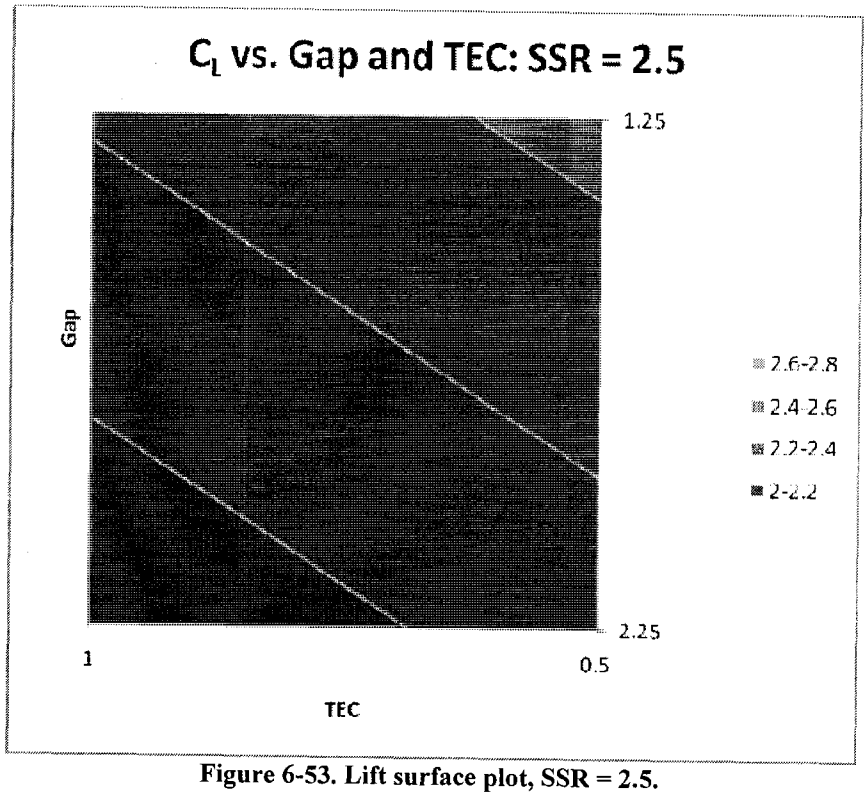

Figure 6-53. Lift surface plot, SSR = 2.5.

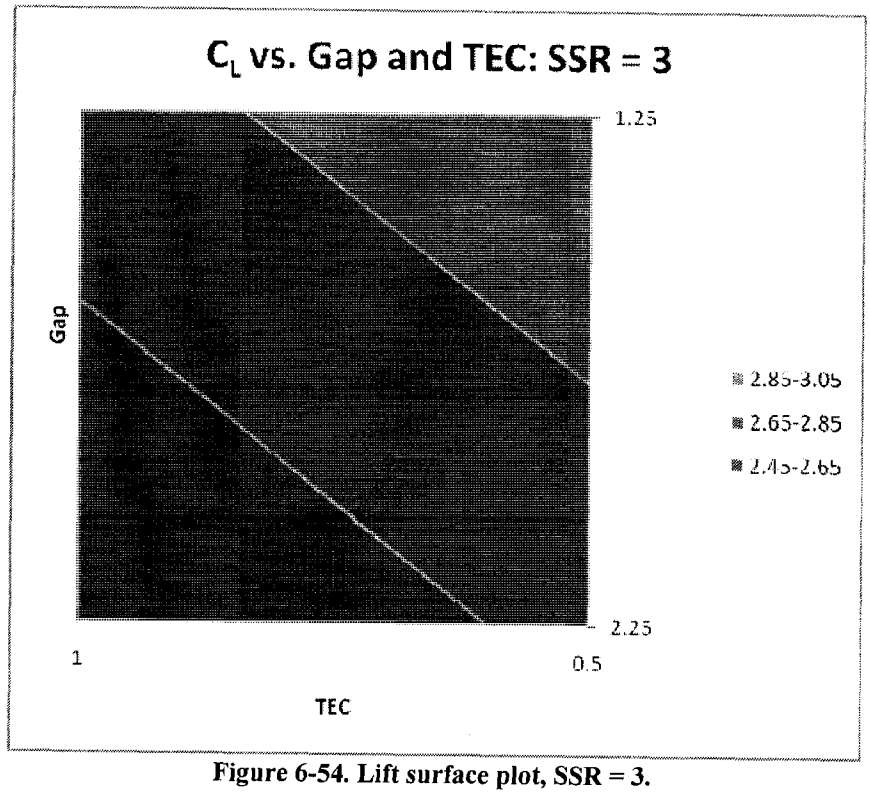

Figure 6-54. Lift surface plot, SSR = 3.

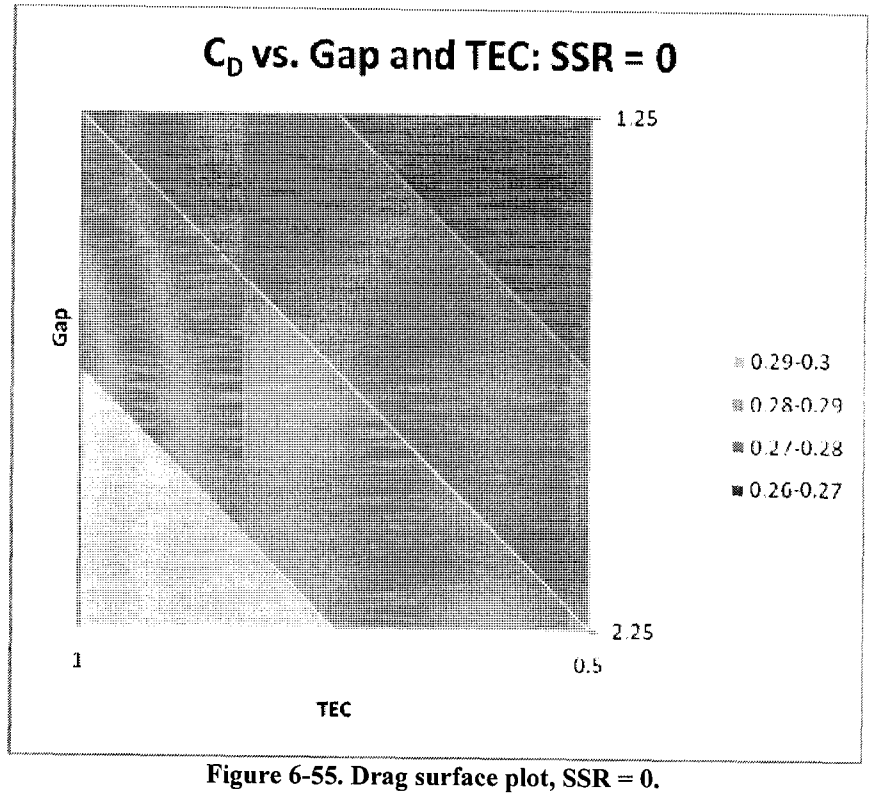

Figure 6-55. Drag surface plot, SSR = 0.

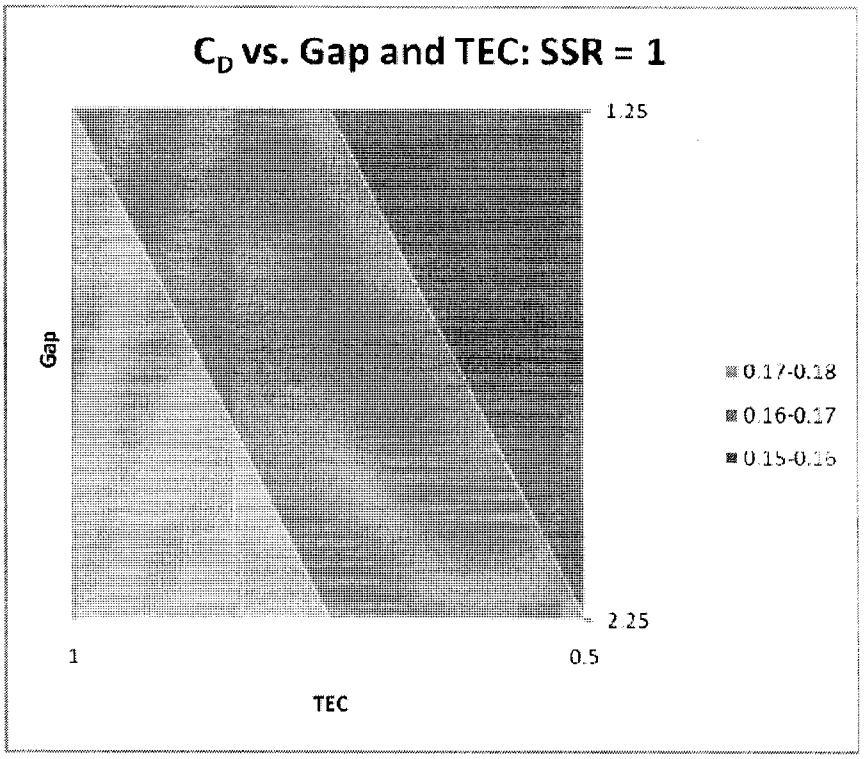

Figure 6-56. Drag surface plot, SSR = 1.

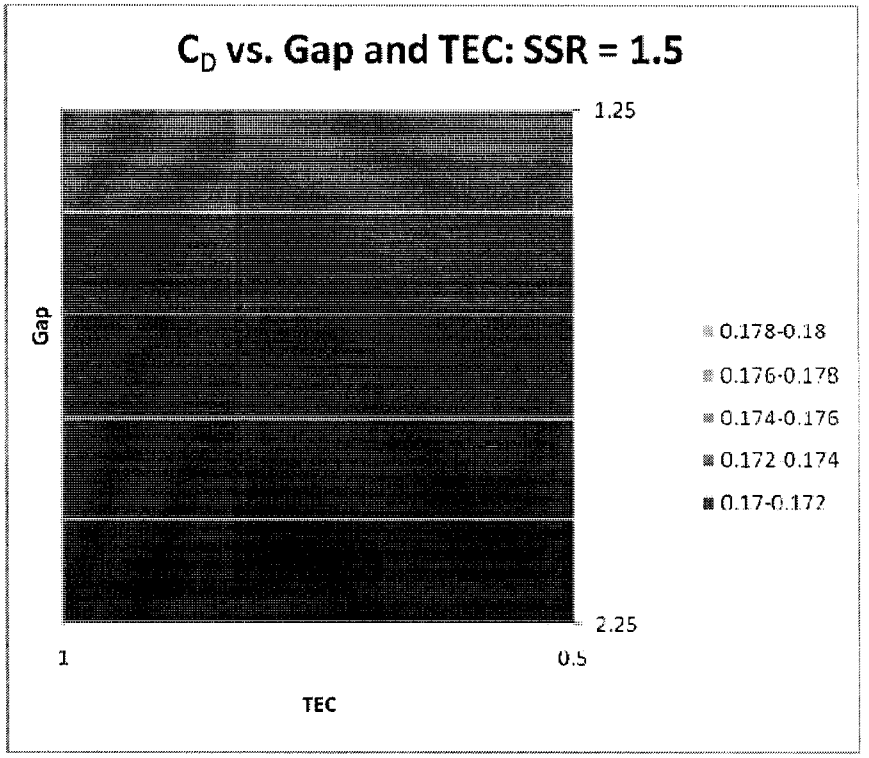

Figure 6-57. Drag surface plot, SSR = 1.5.

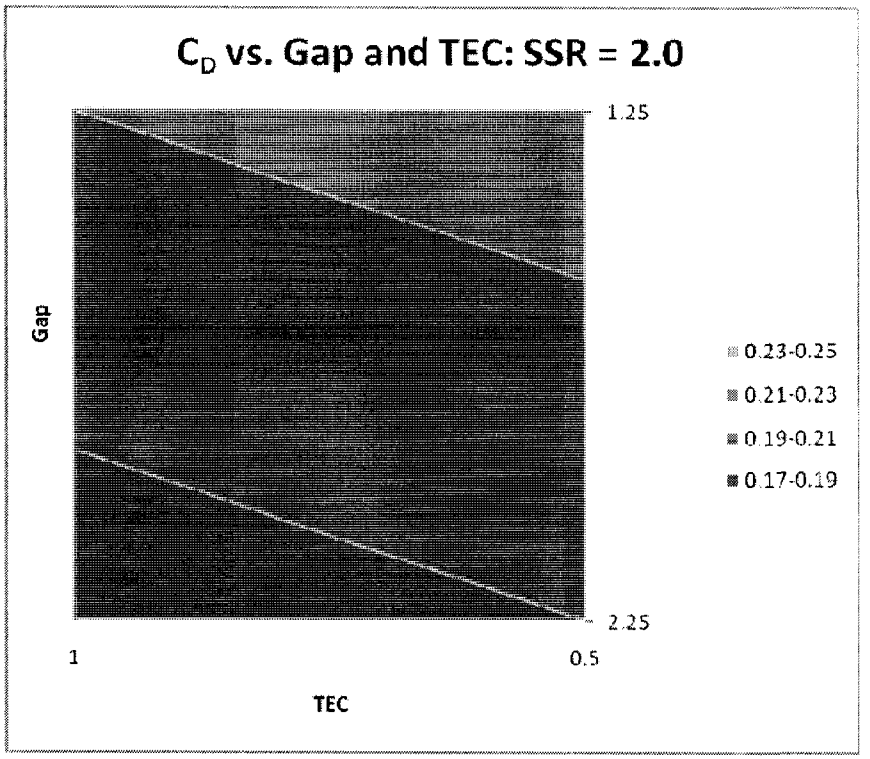

Figure 6-58. Drag surface plot, SSR = 2.0.

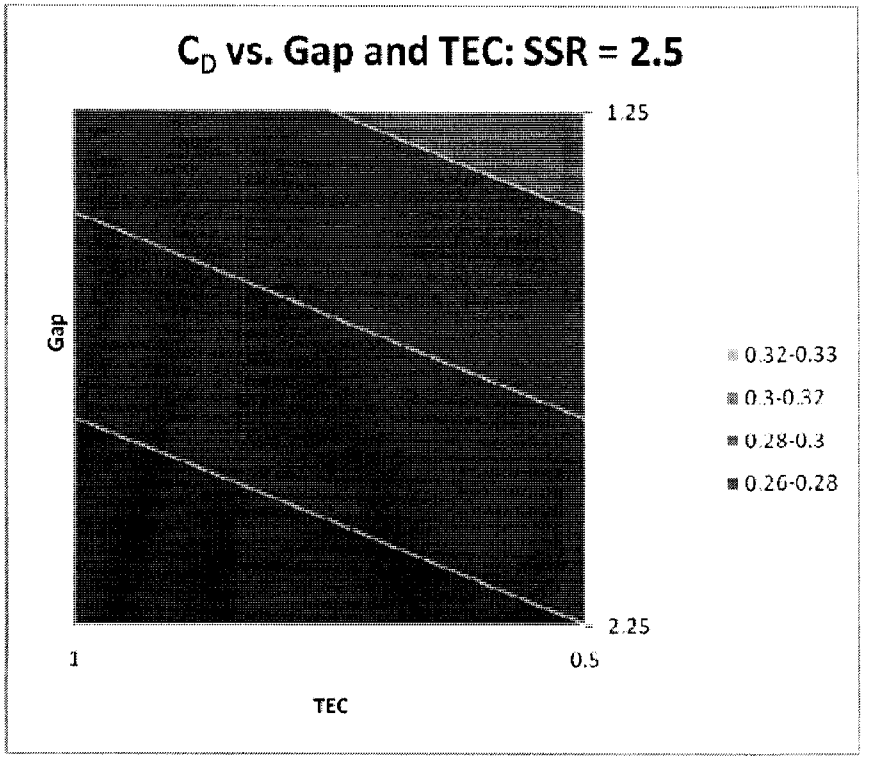

Figure 6-59. Drag surface plot, SSR = 2.5.

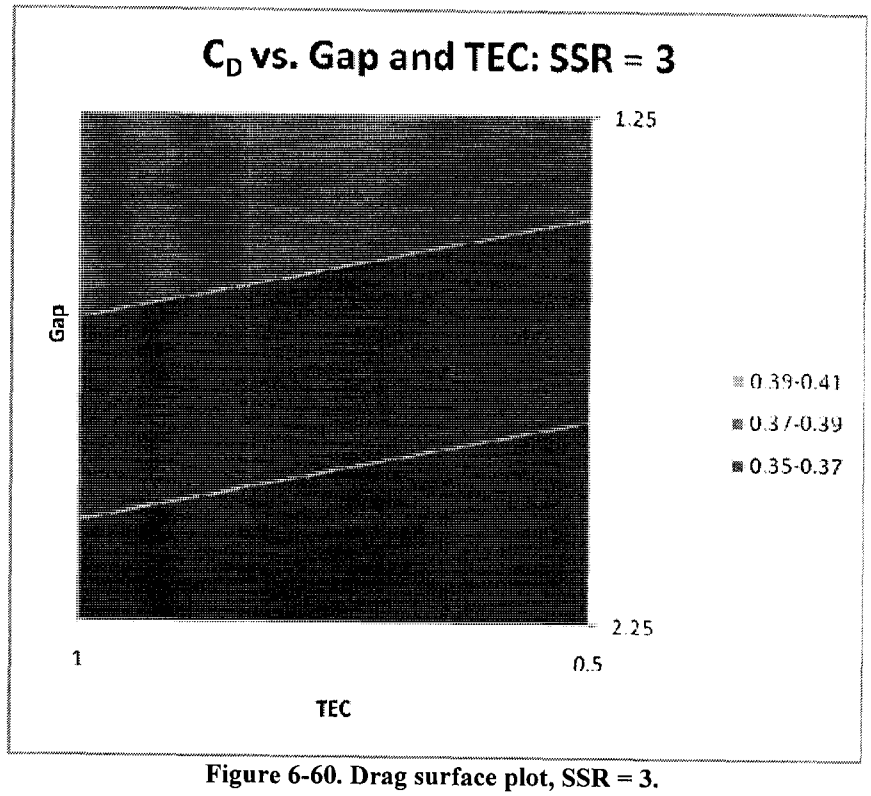

Figure 6-60. Drag surface plot, SSR = 3.

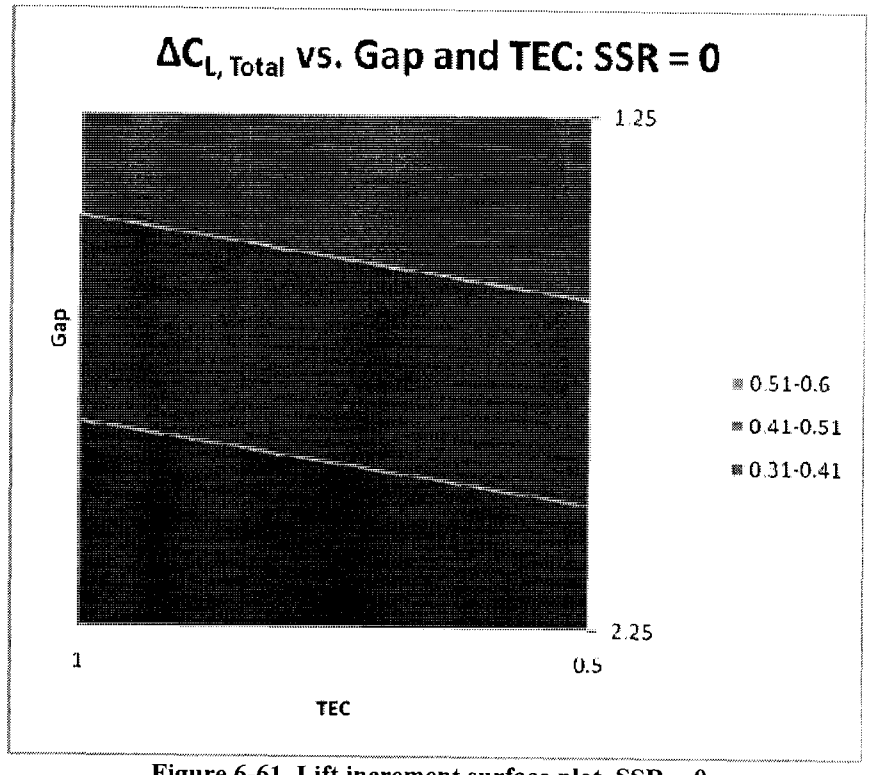

Figure 6-61. Lift increment surface plot, SSR = 0.

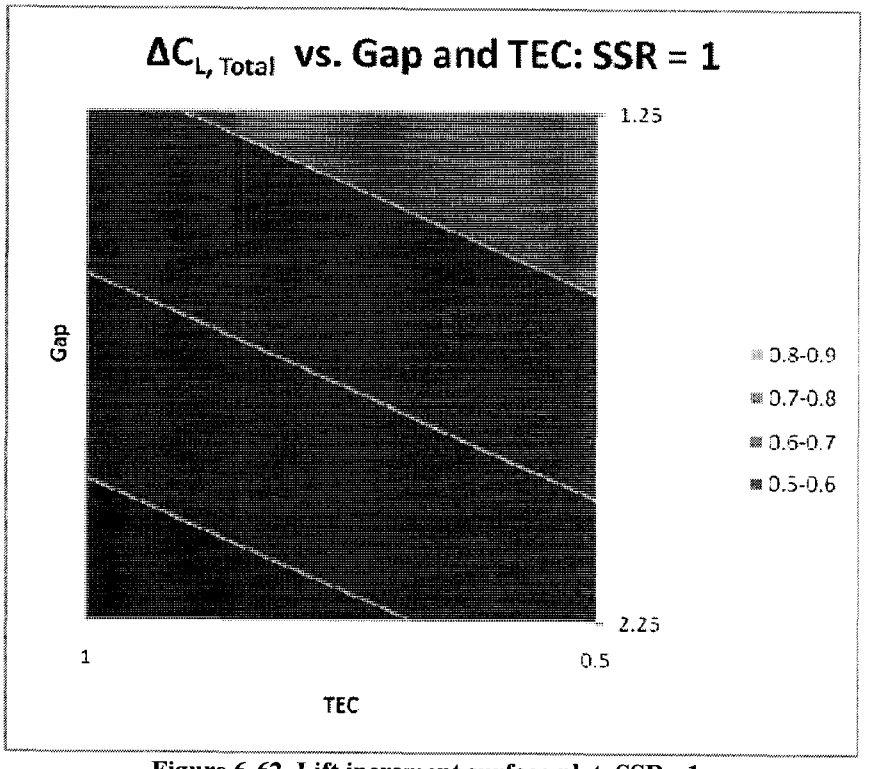

Figure 6-62. Lift increment surface plot, SSR =1.

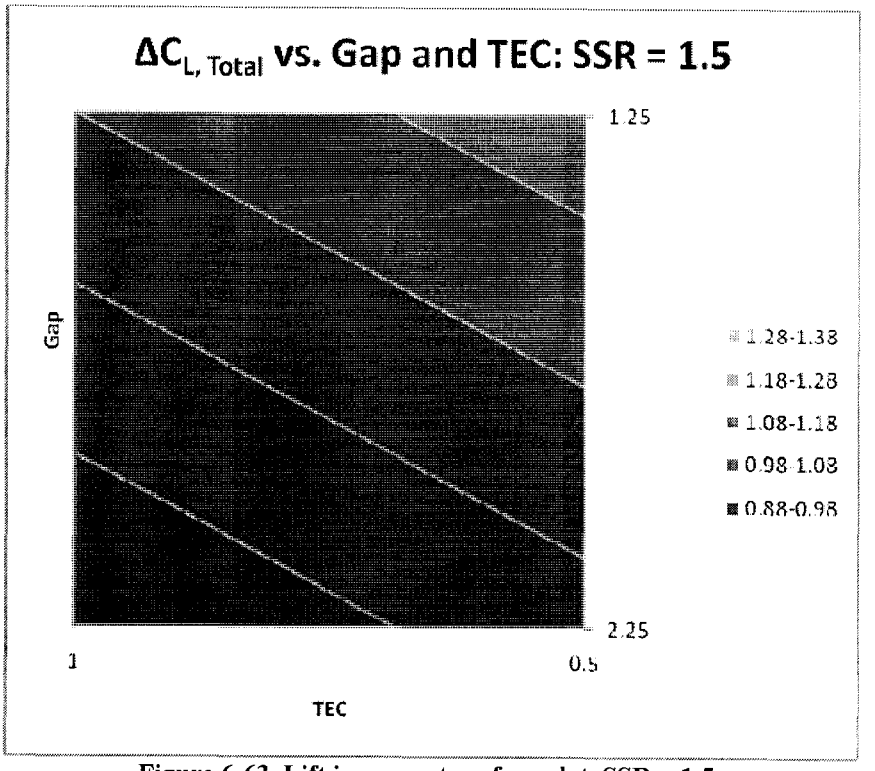

Figure 6-63. Lift increment surface plot, SSR = 1.5.

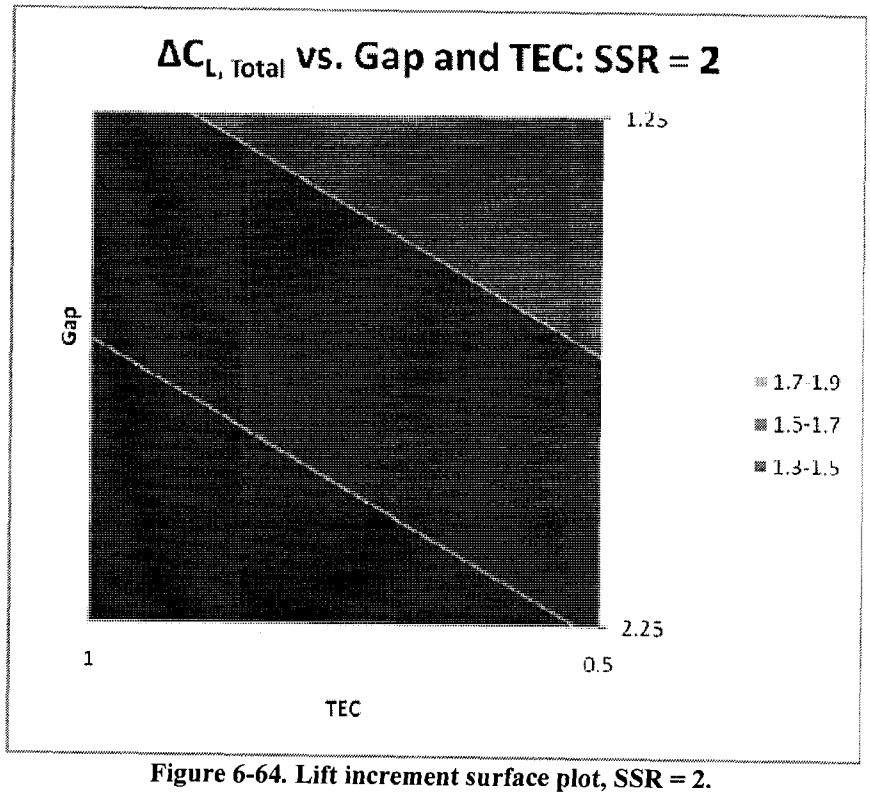

Figure 6-64. Lift increment surface plot, SSR = 2.

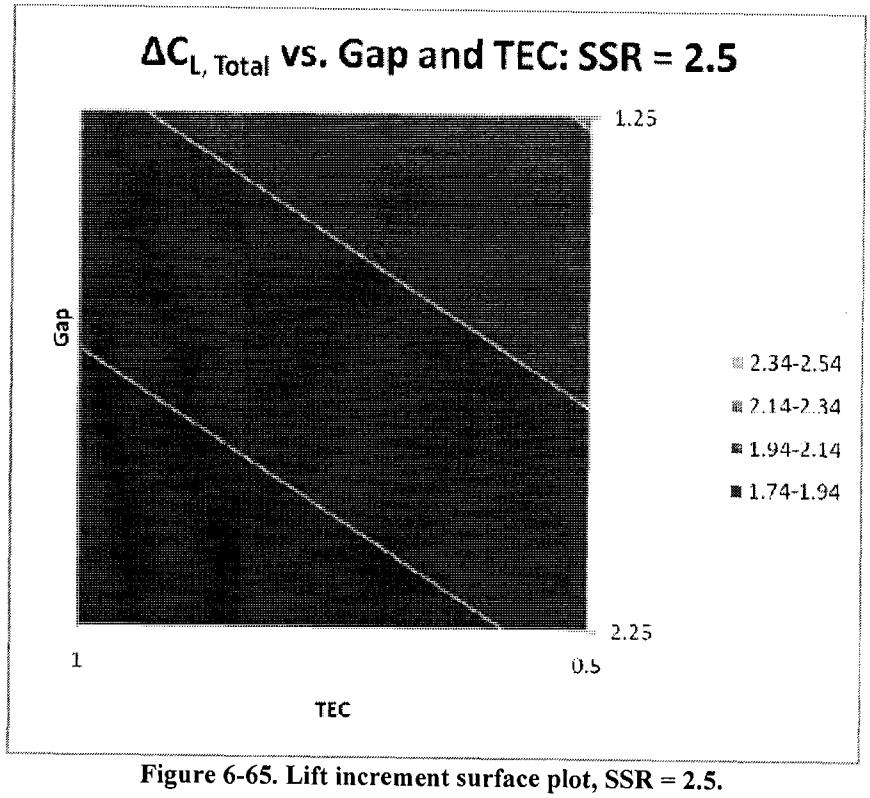

Figure 6-65. Lift increment surface plot, SSR = 2.5.

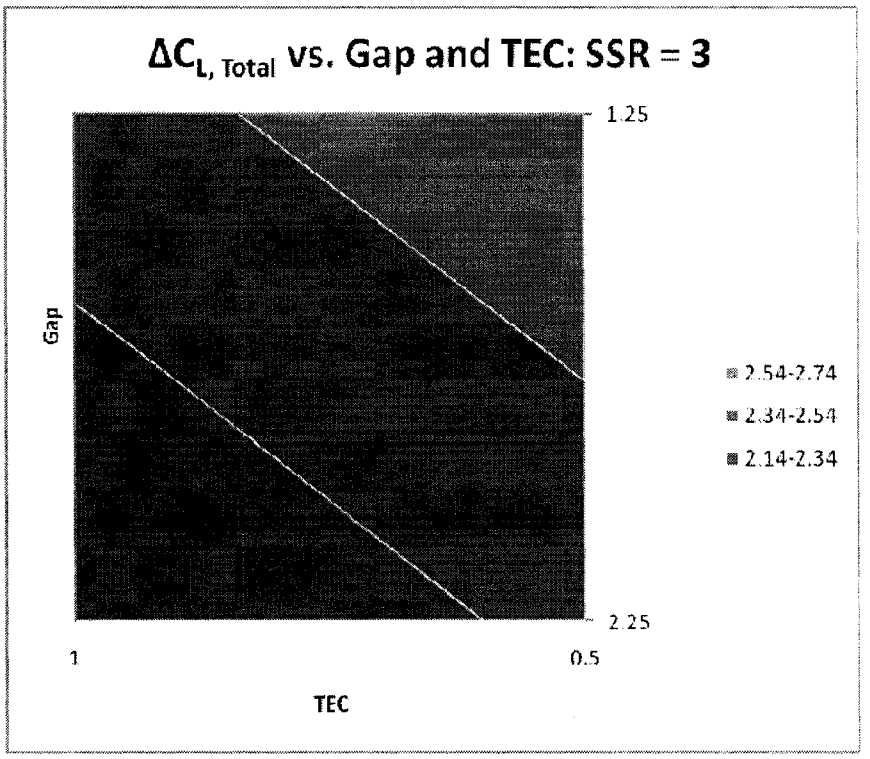

Figure 6-66. Lift increment surface plot, SSR = 3.

Surface Plots for $\alpha = 5°$

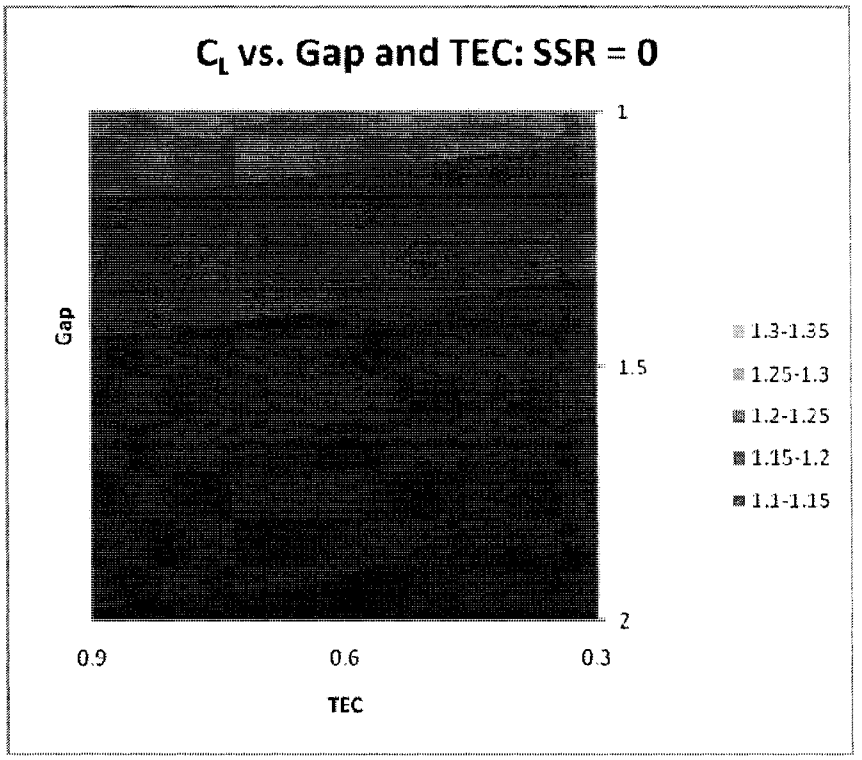

Figure 6-67. Lift surface plot, SSR = 0.

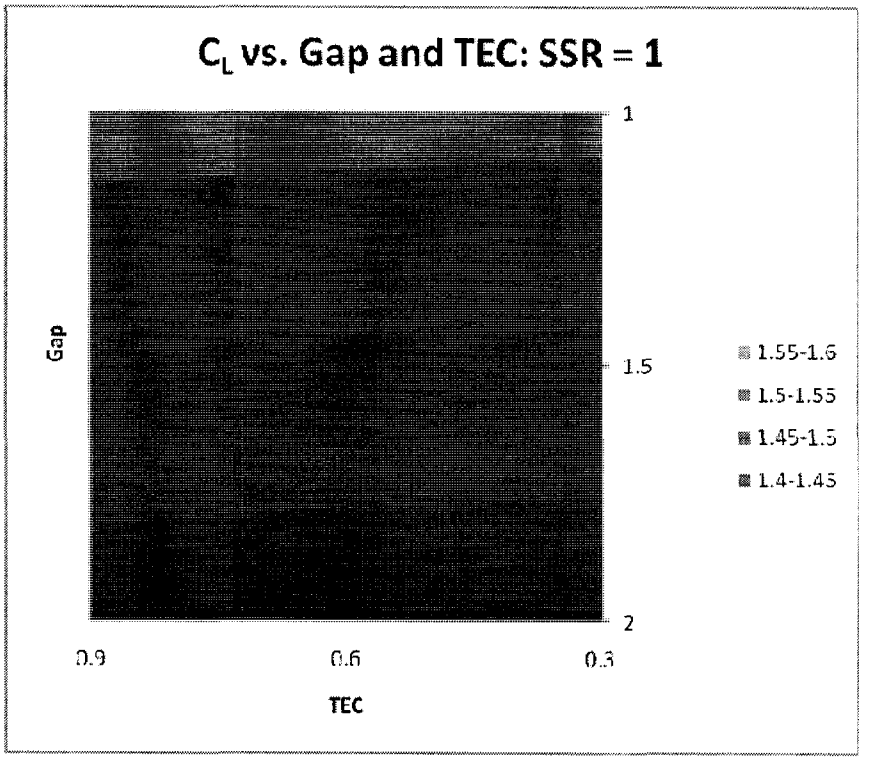

Figure 6-68. Lift surface plot, SSR = 1.

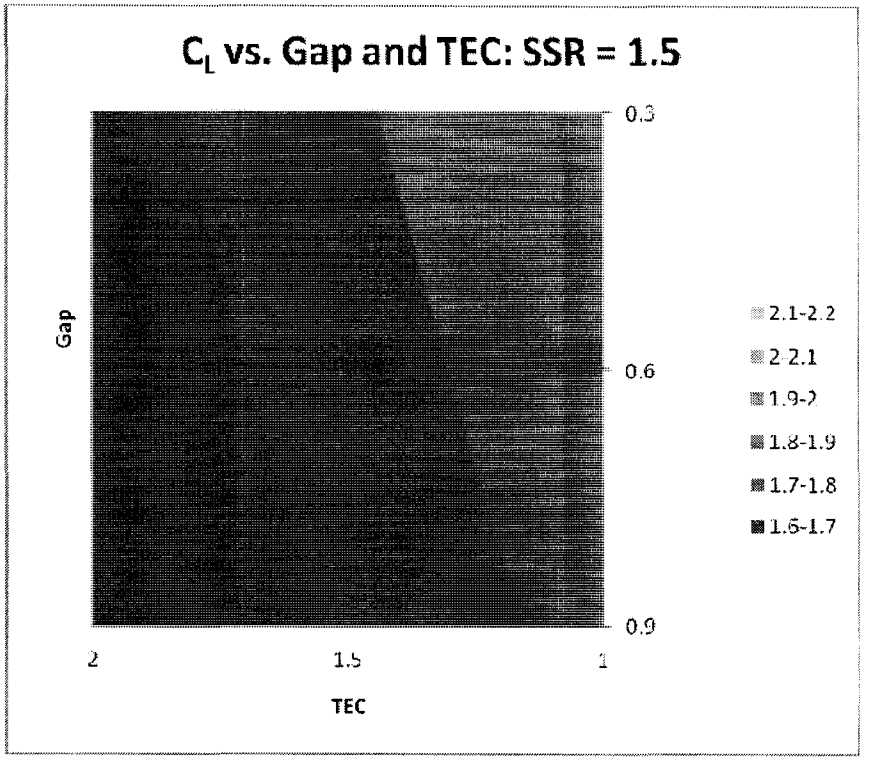

Figure 6-69. Lift surface plot, SSR = 1.5.

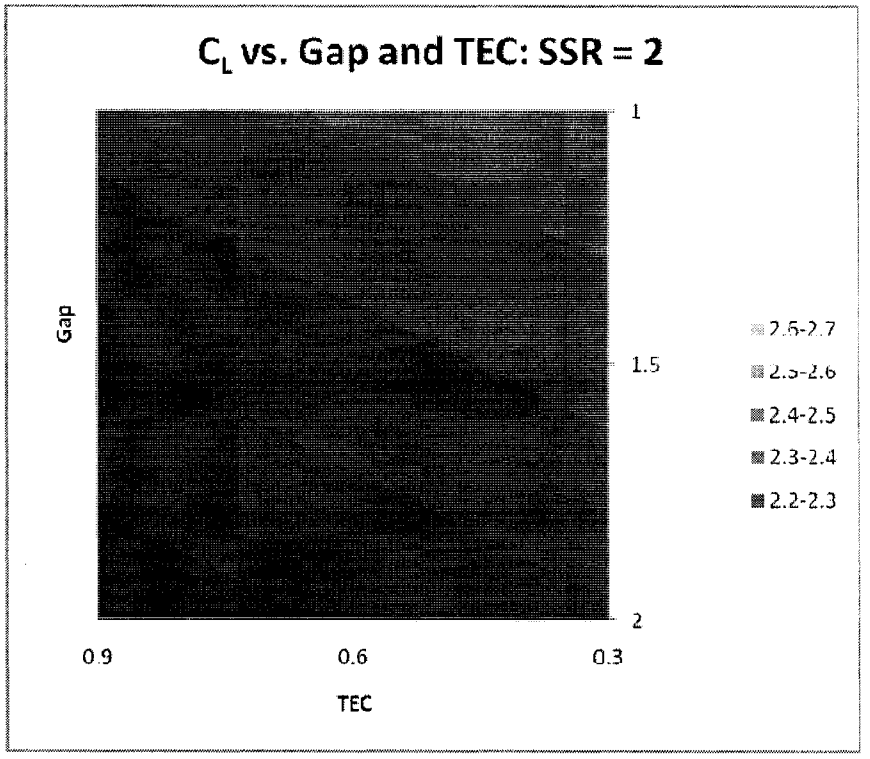

Figure 6-70. Lift surface plot, SSR = 2.

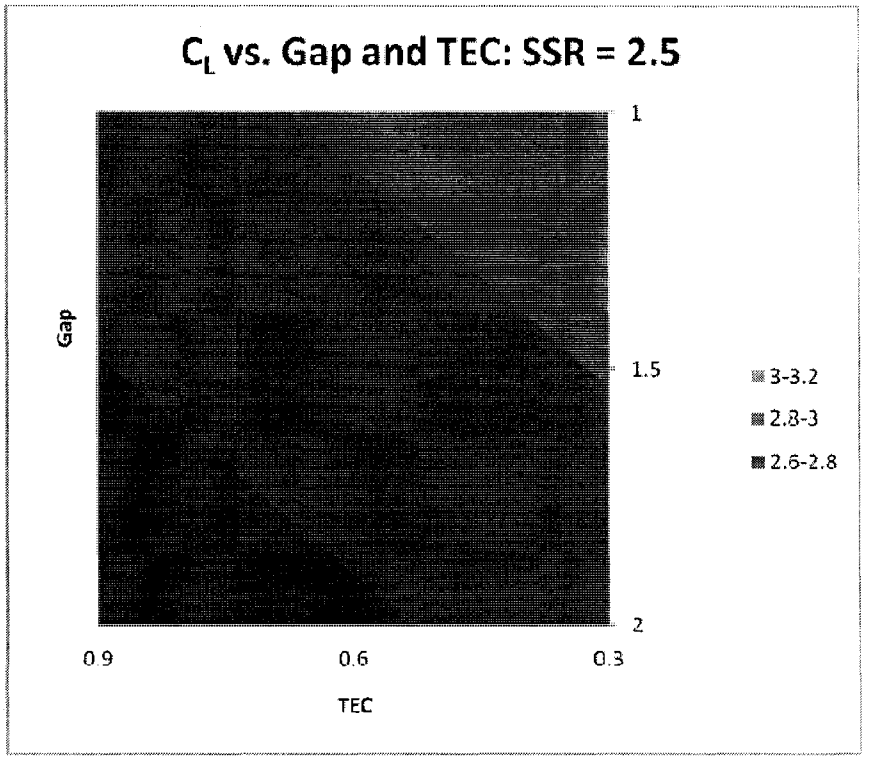

Figure 6-71. Lift surface plot, SSR = 2.5.

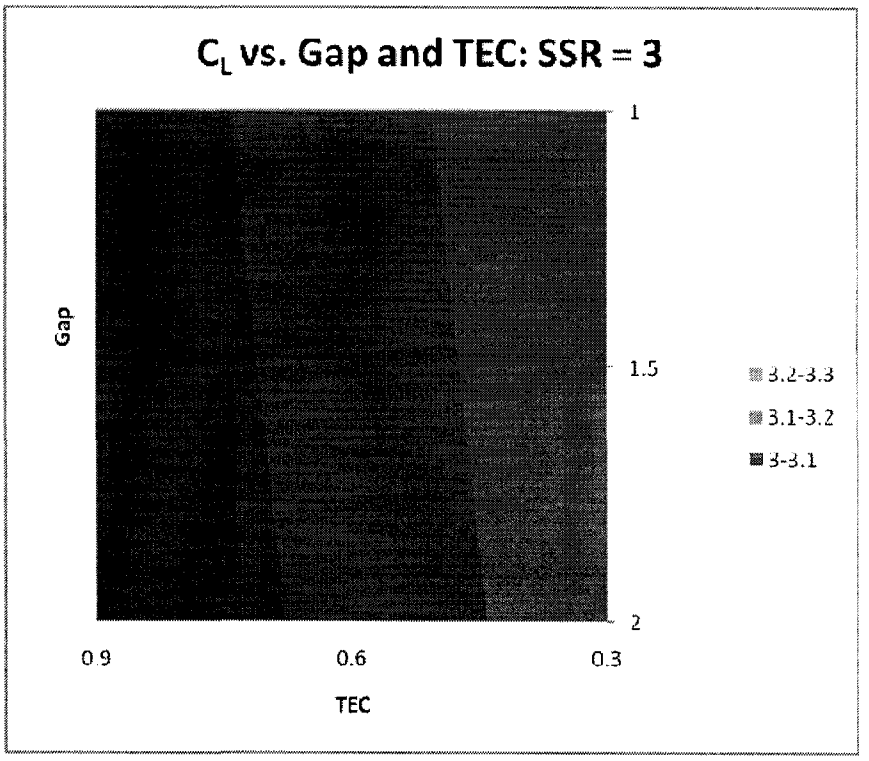

Figure 6-72. Lift surface plot, SSR = 3.

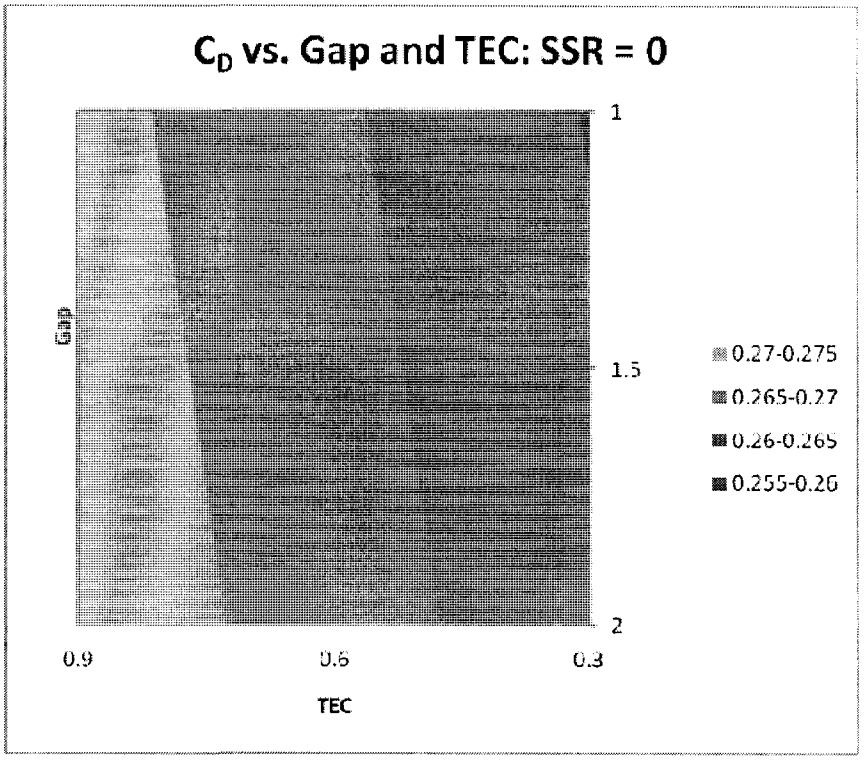

Figure 6-73. Drag surface plot, SSR = 0.

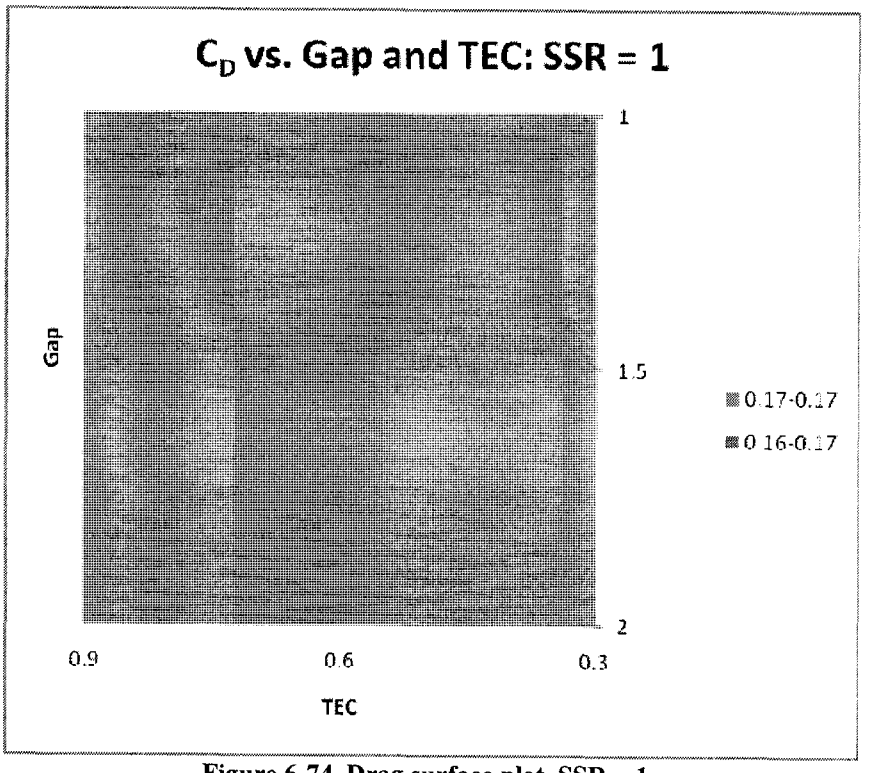

Figure 6-74. Drag surface plot, SSR = 1.

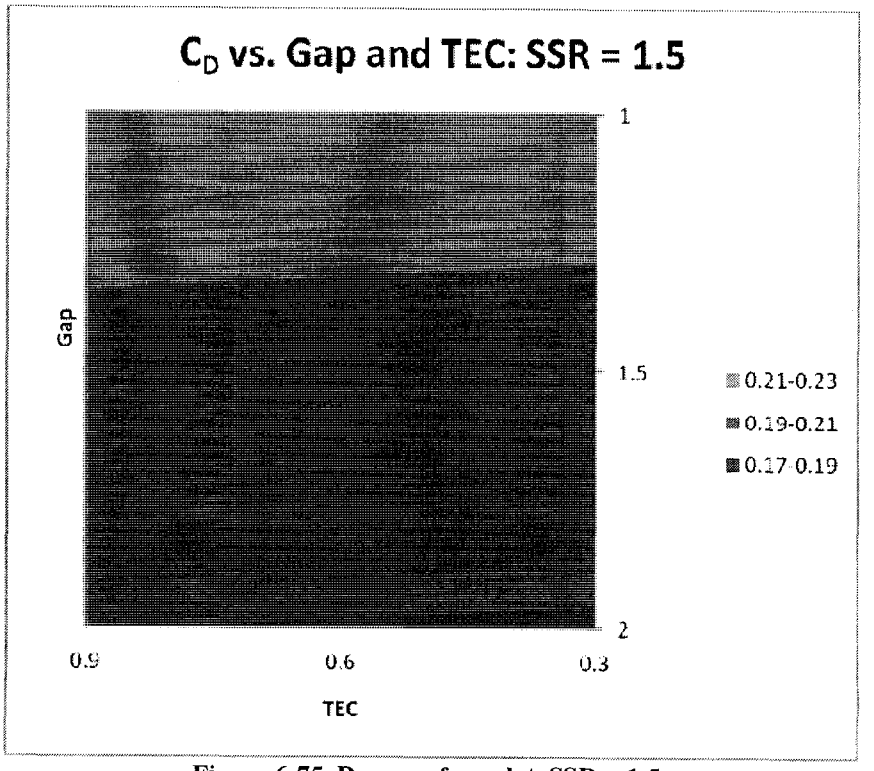

Figure 6-75. Drag surface plot, SSR = 1.5.

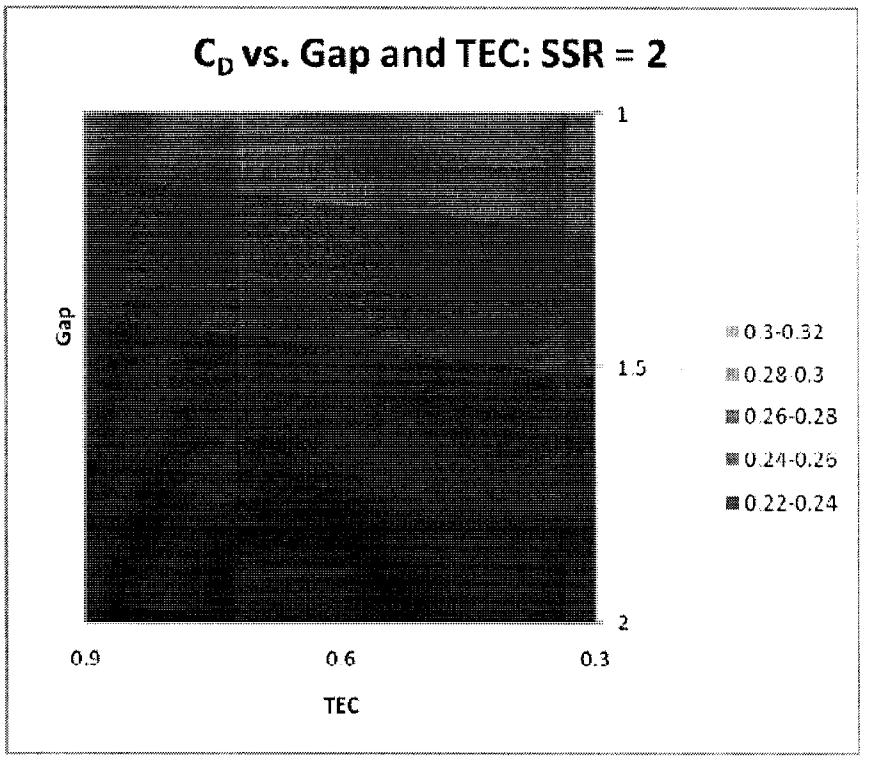

Figure 6-76. Drag surface plot, SSR = 2.

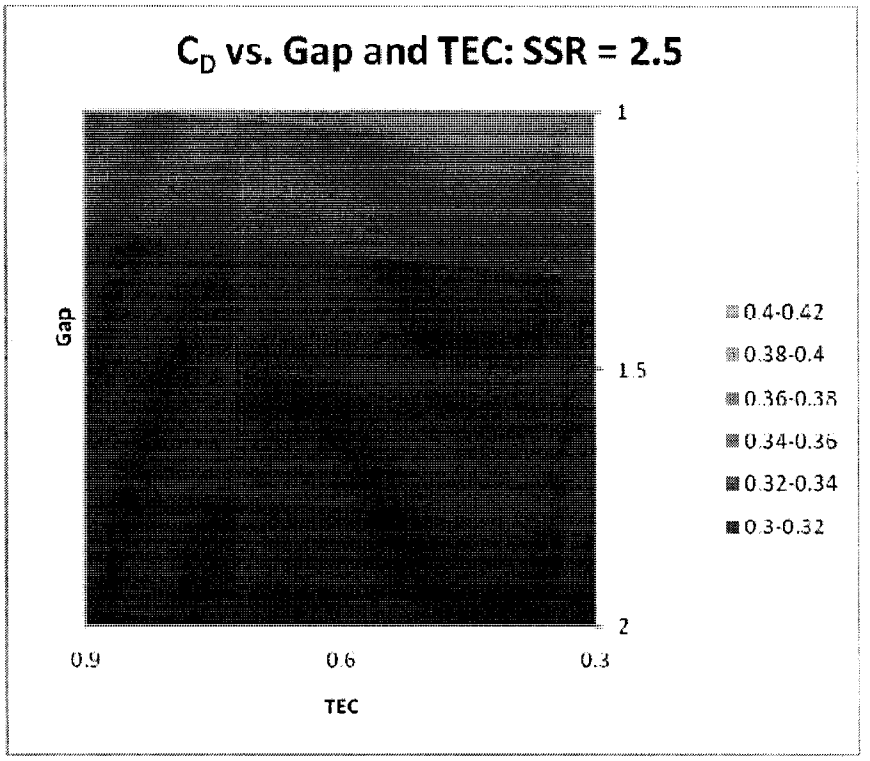

Figure 6-77. Drag surface plot SSR = 2.5.

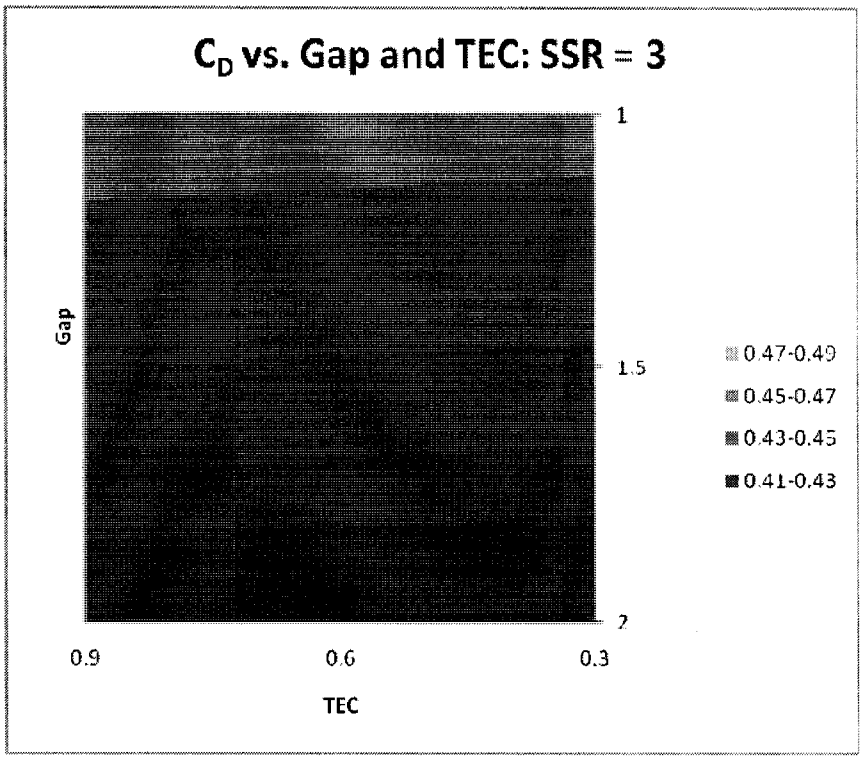

Figure 6-78. Drag surface plot, SSR = 3.

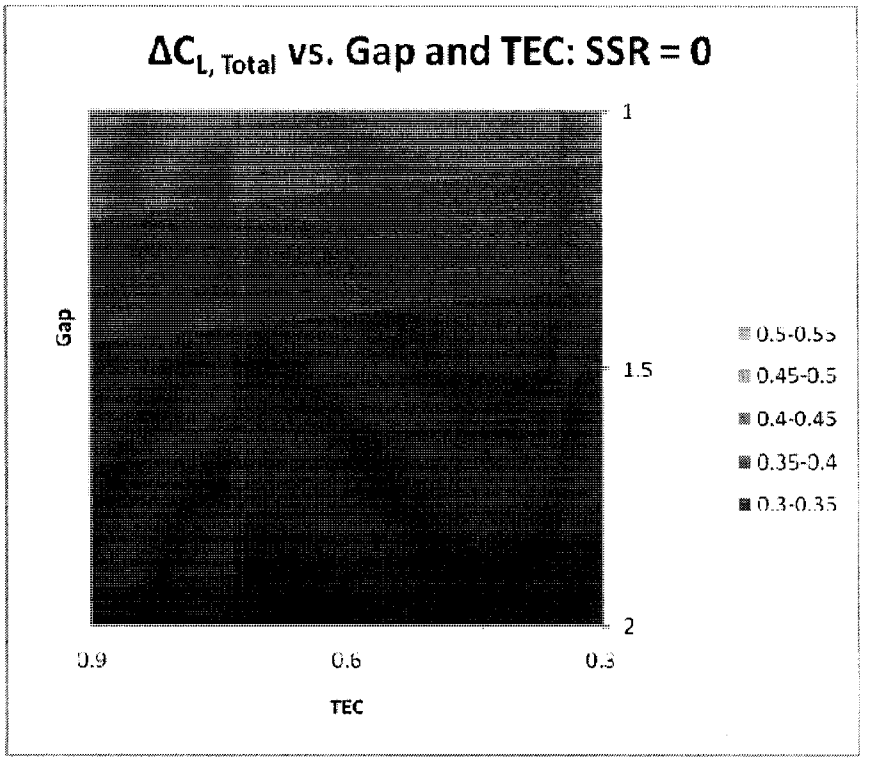

Figure 6-79. Lift increment surface plot, SSR = 0.

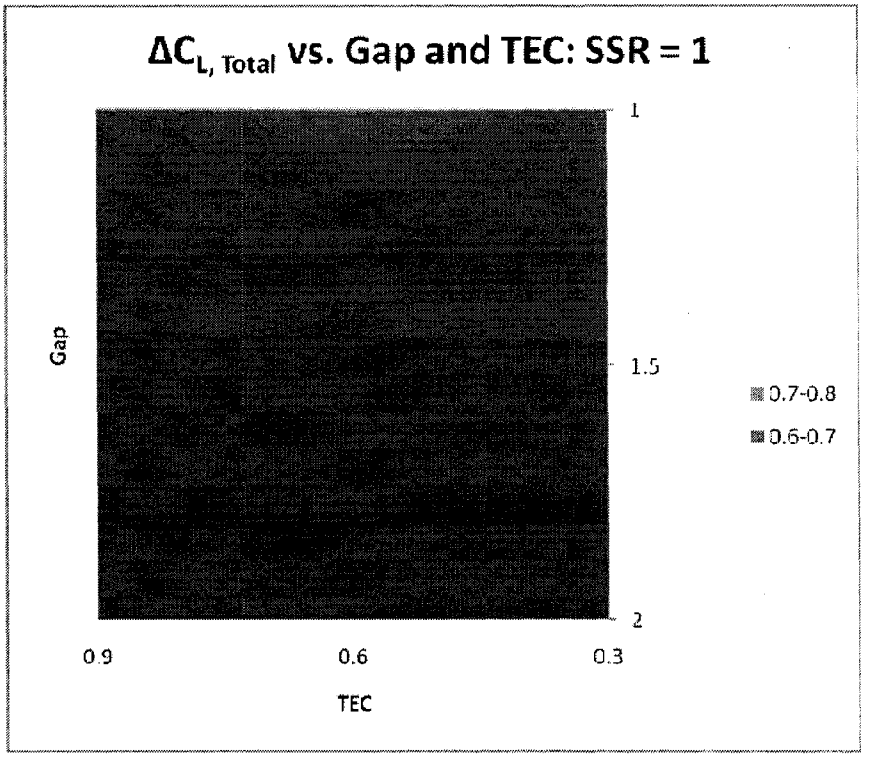

Figure 6-80. Lift increment surface plot, SSR = 1.

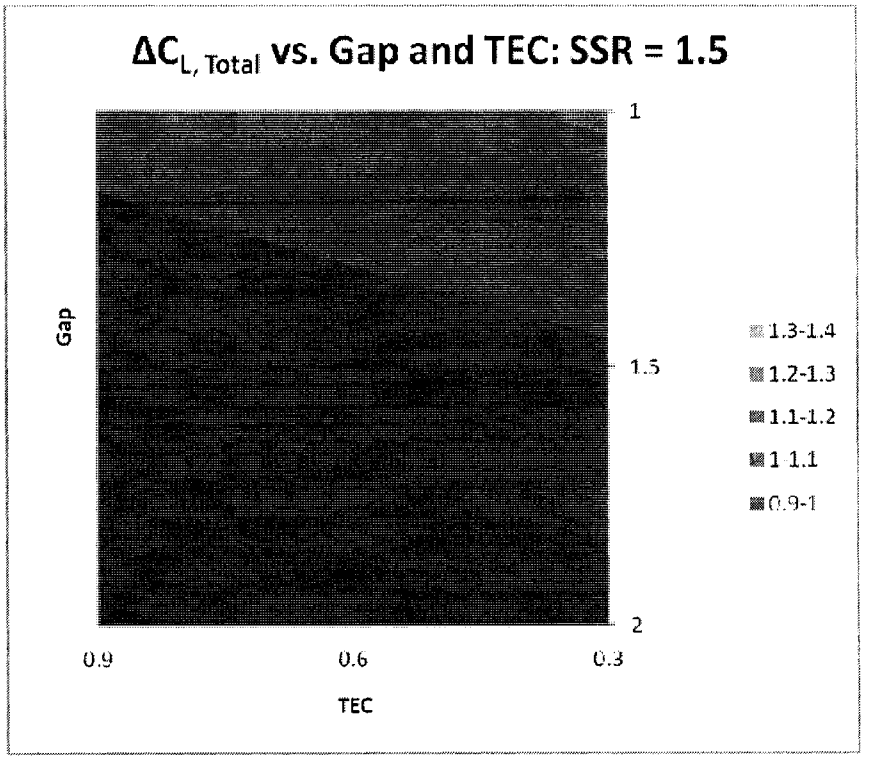

Figure 6-81. Lift increment surface plot, SSR = 1.5.

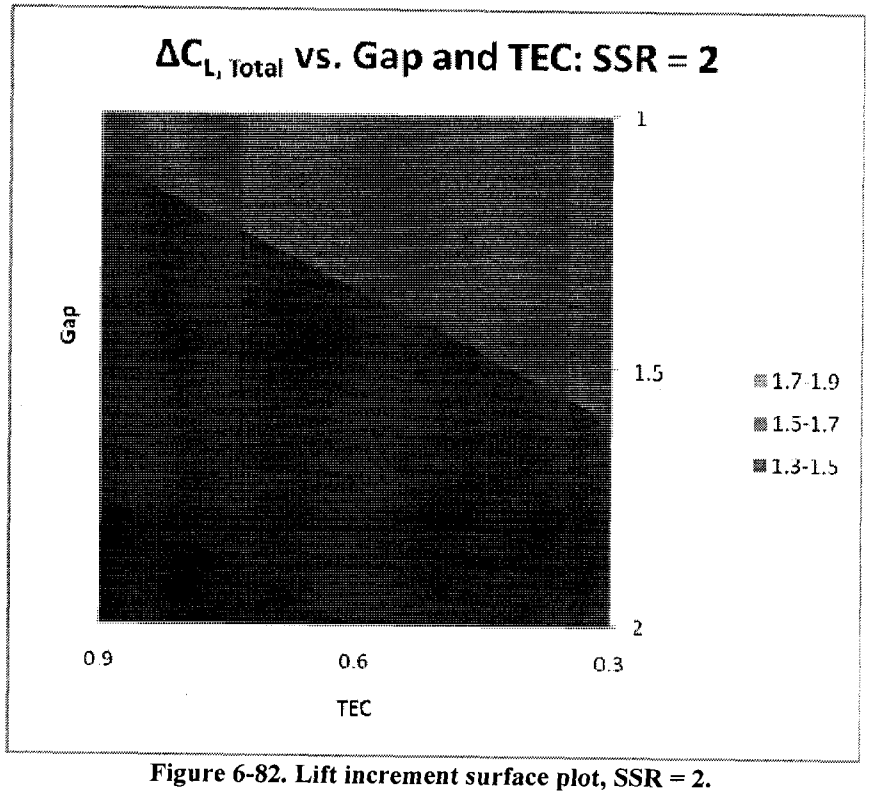

Figure 6-82. Lift increment surface plot, SSR = 2.

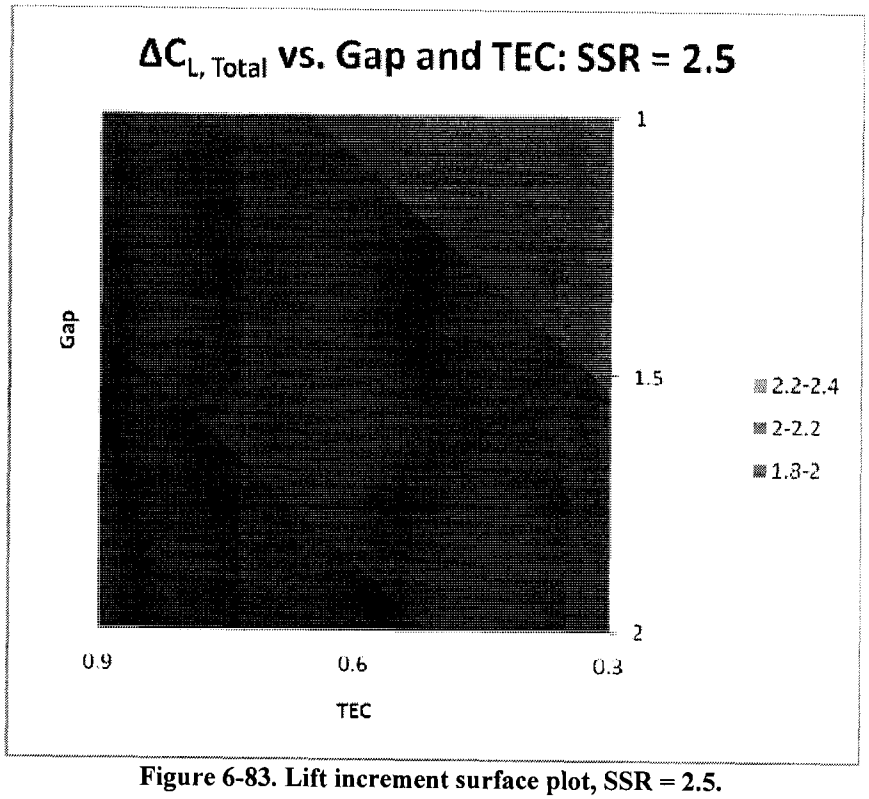

Figure 6-83. Lift increment surface plot, SSR = 2.5.

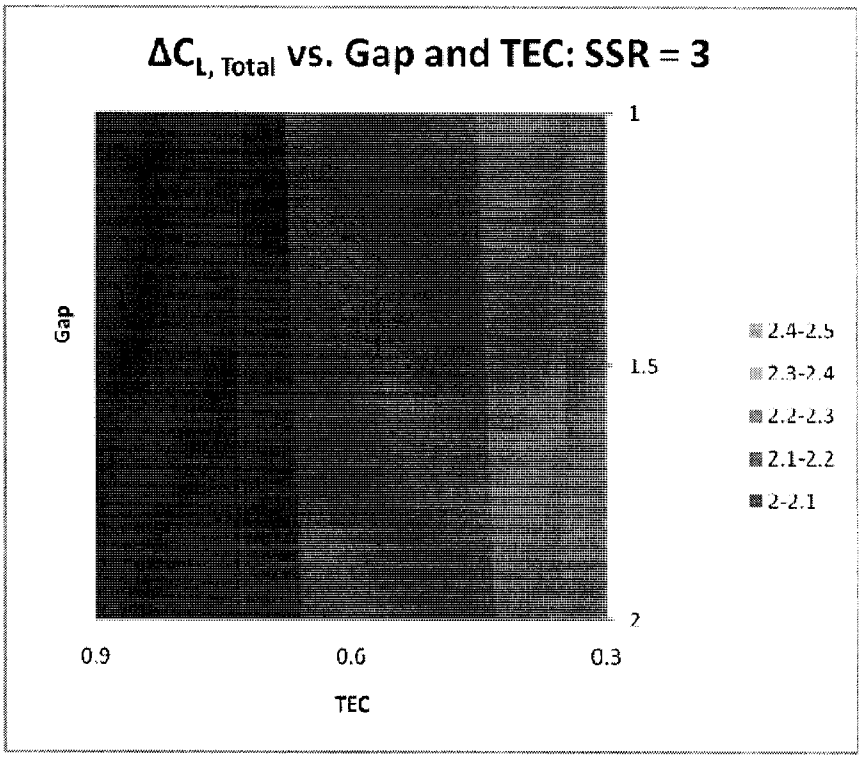

Figure 6-84. Lift increment surface plot, SSR = 3.

Surface Plots for $\alpha = 10°$

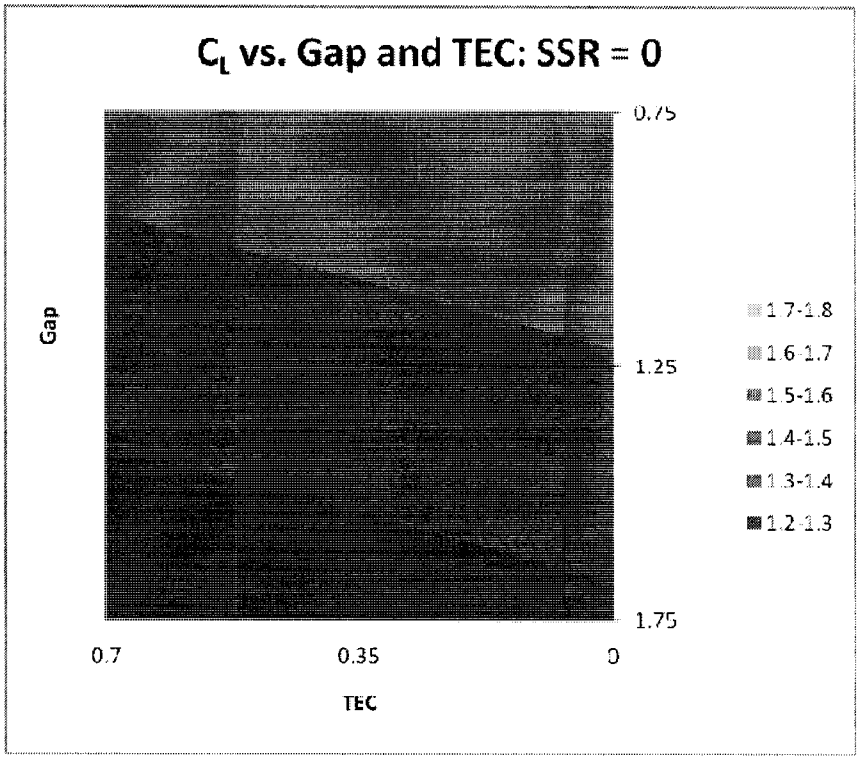

Figure 6-85. Lift surface plot, SR = 0.

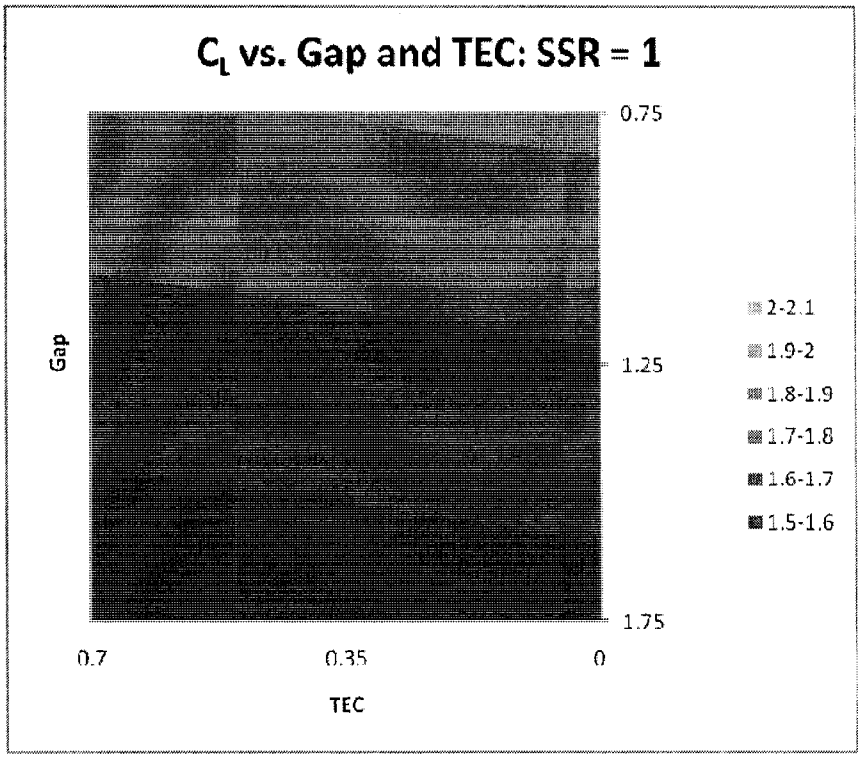

Figure 6-86. Lift surface plot, SSR = 1.

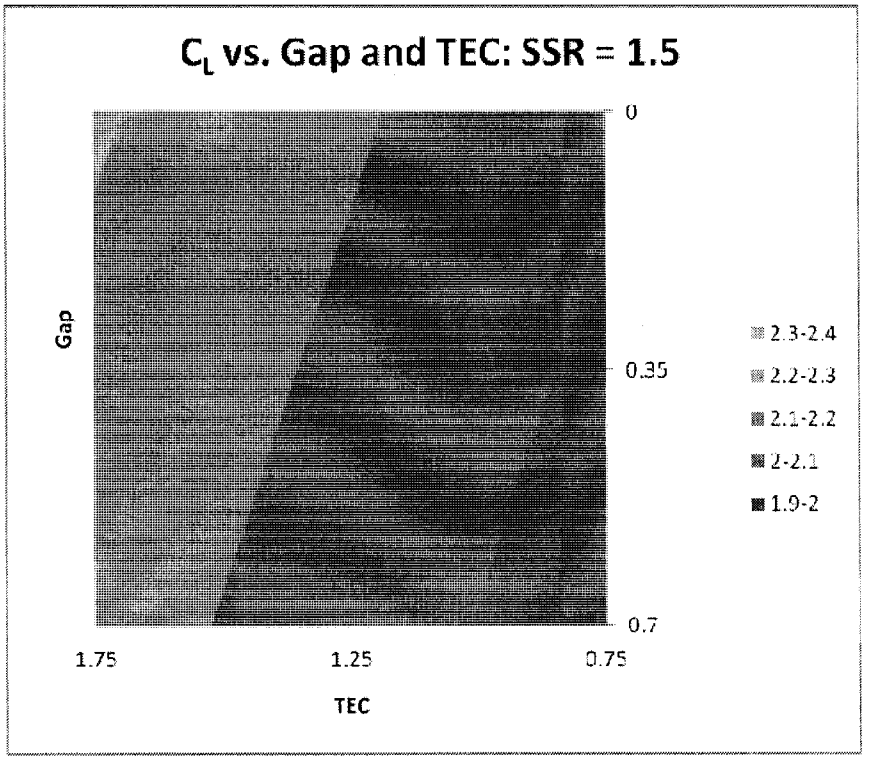

Figure 6-87. Lift surface plot, SSR = 1.5.

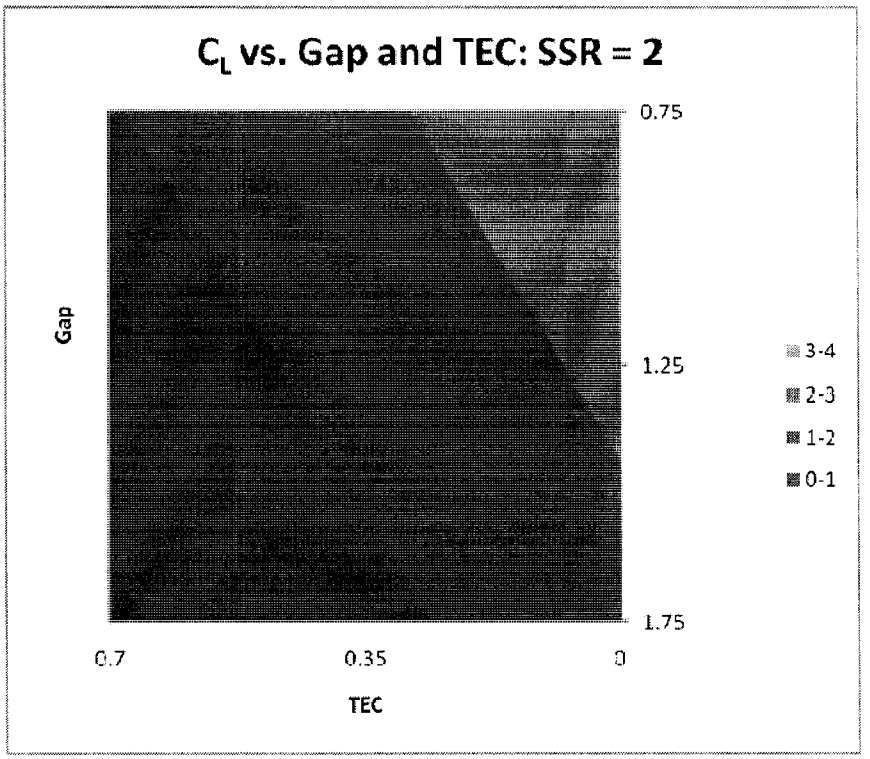

Figure 6-88. Lift surface plot, SSR = 2.

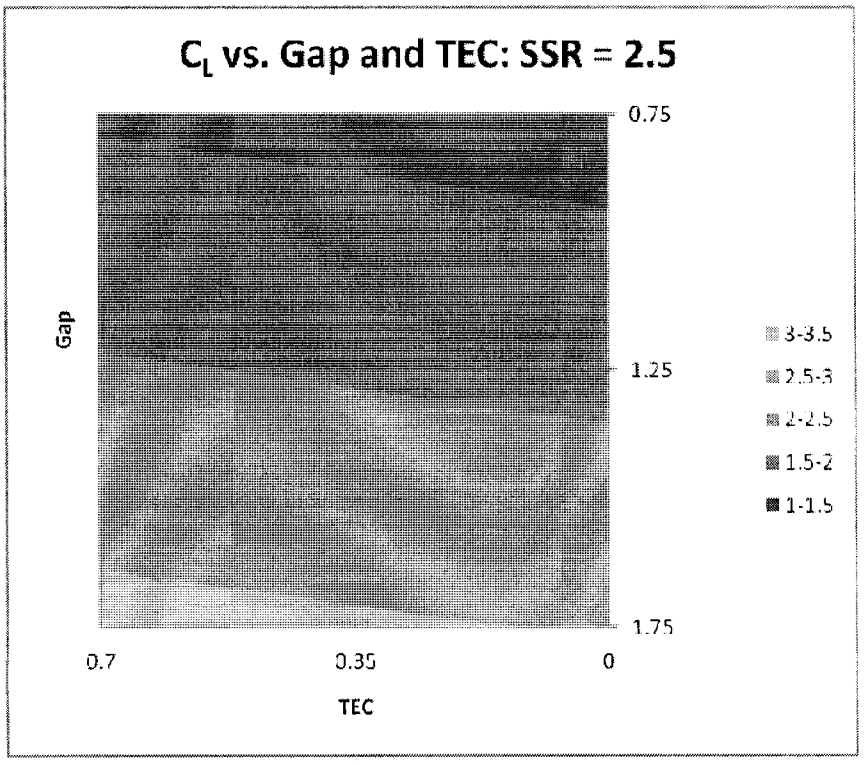

Figure 6-89. Lift surface plot, SSR = 2.5.

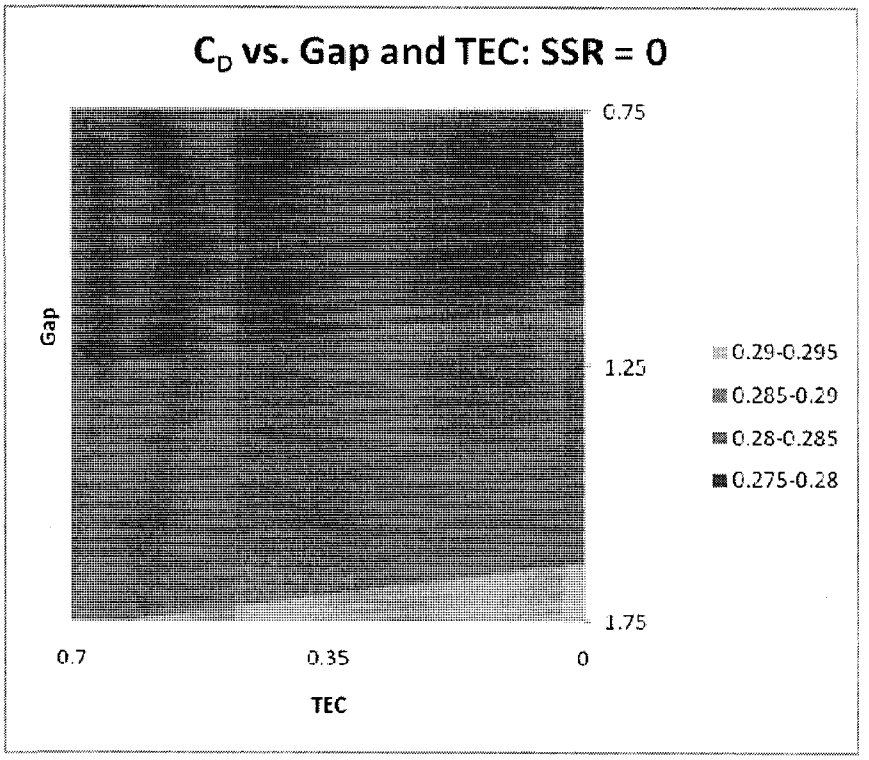

Figure 6-90. Drag surface plot, SSR = 0.

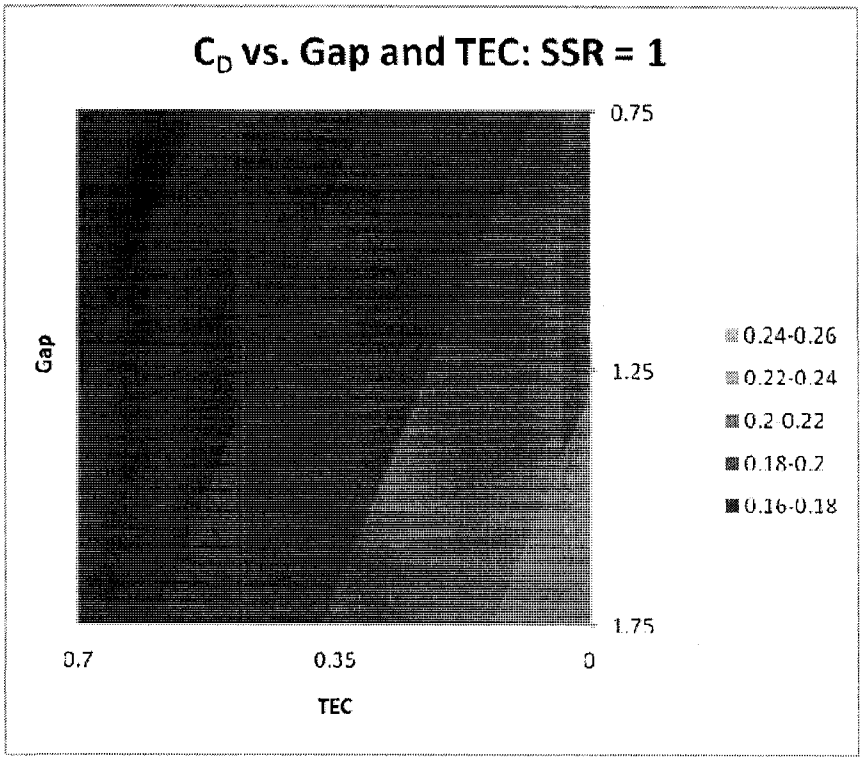

Figure 6-91. Drag surface plot, SSR = 1.

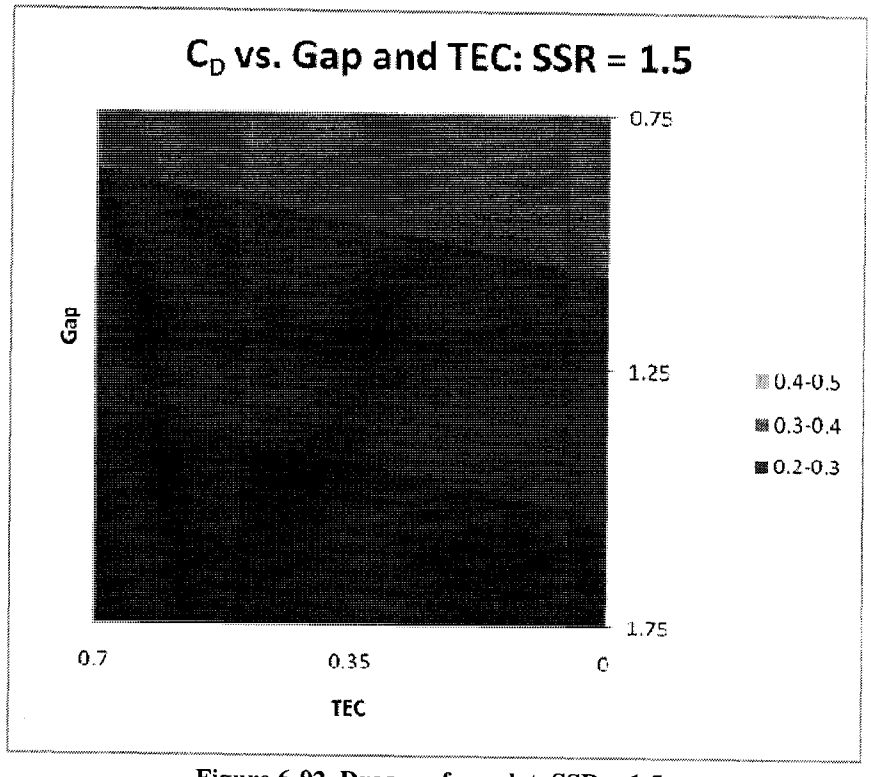

Figure 6-92. Drag surface plot, SSR = 1.5.

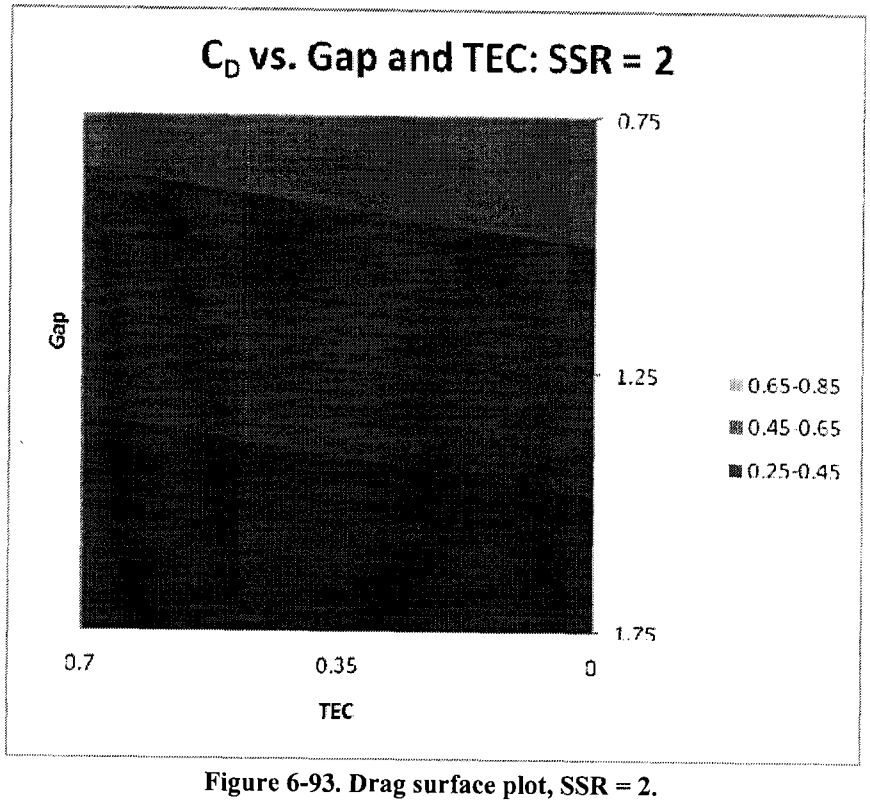

Figure 6-93. Drag surface plot, SSR = 2.

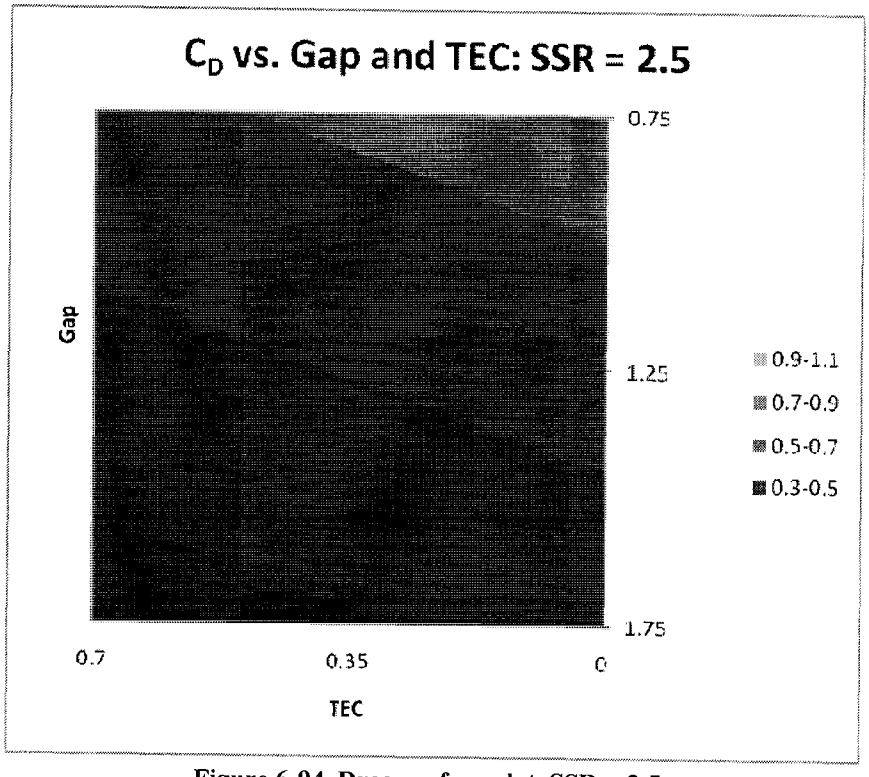

Figure 6-94. Drag surface plot, SSR = 2.5.

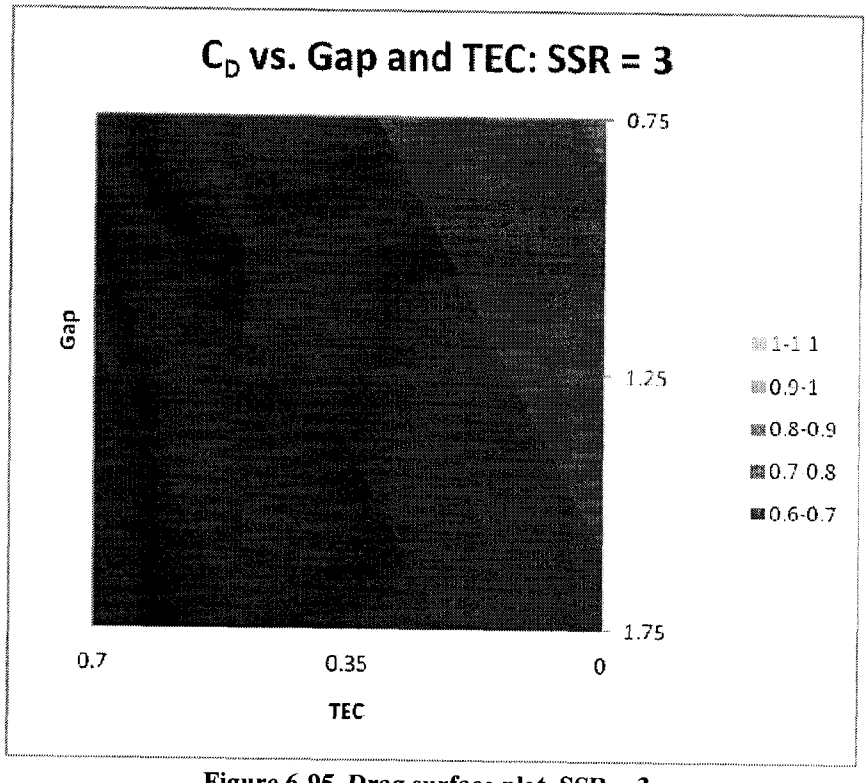

Figure 6-95. Drag surface plot, SSR = 3.

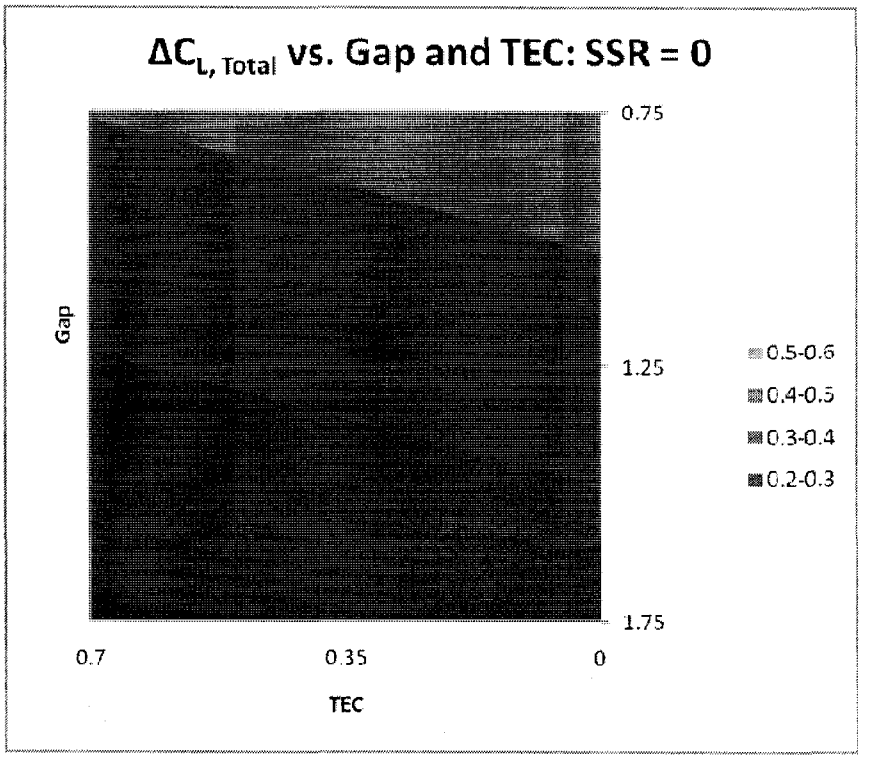

Figure 6-96. Lift increment surface plot, SSR = 0.

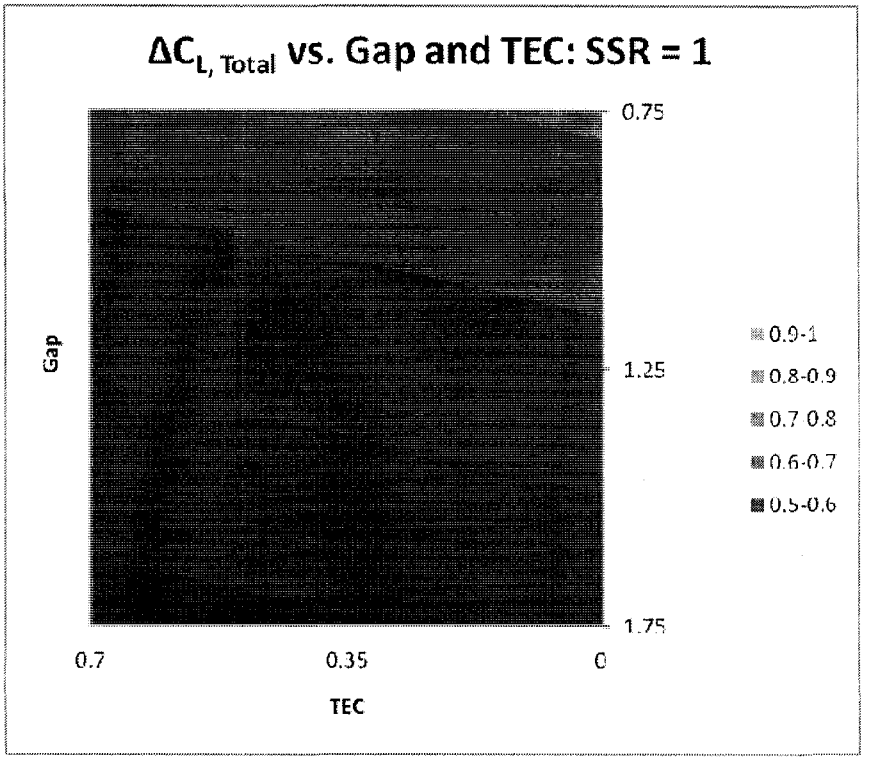

Figure 6-97. Lift increment surface plot, SSR = 1.

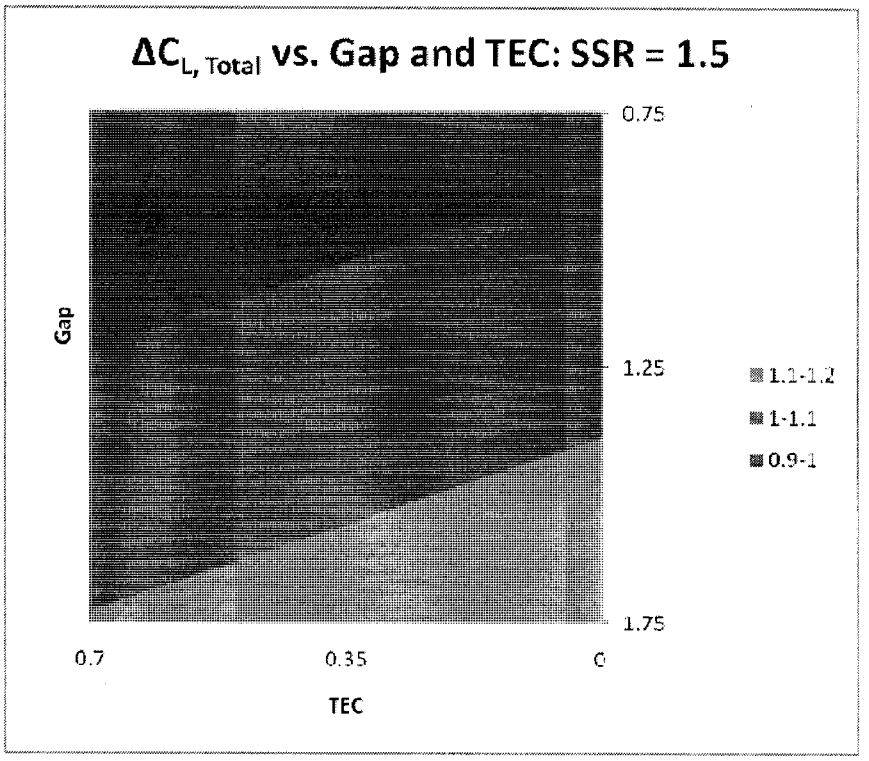

Figure 6-98. Lift increment surface plot, SSR = 1.5.

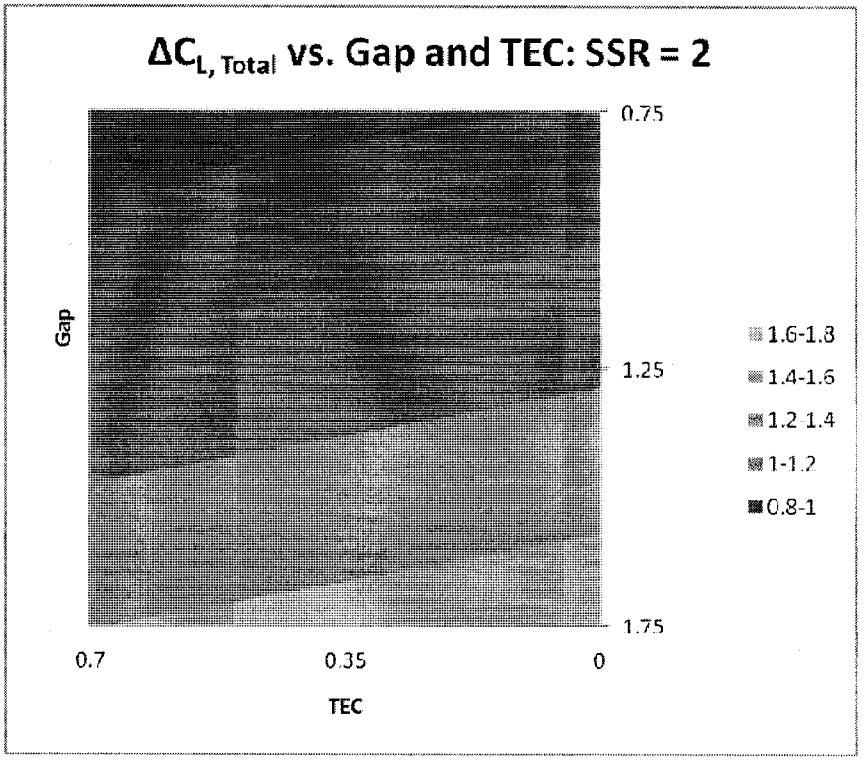

Figure 6-99. Lift increment surface plot, SSR = 2.

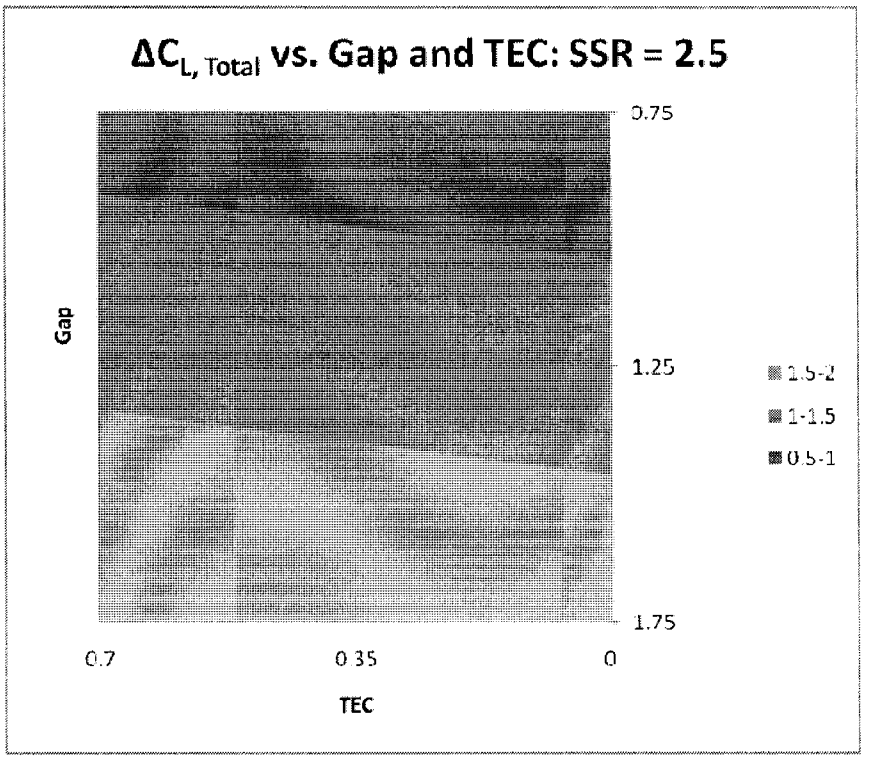

Figure 6-100. Lift increment surface plot, SSR = 2.5.

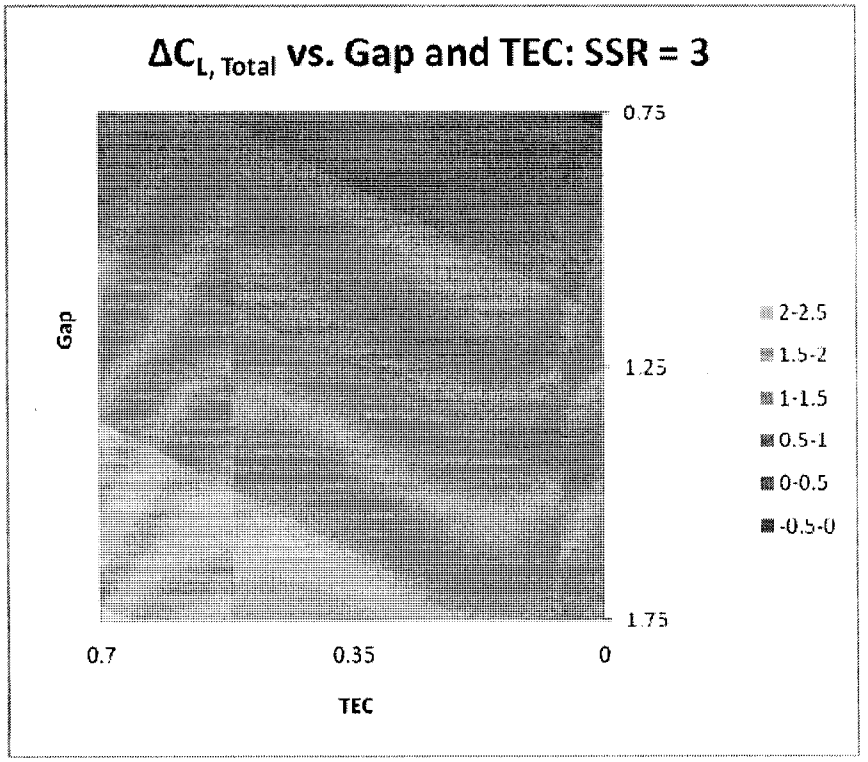

Figure 6-101. Lift increment surface plot, SSR = 3.

Curve Plots Illustrating the Effect of SSR at Various α

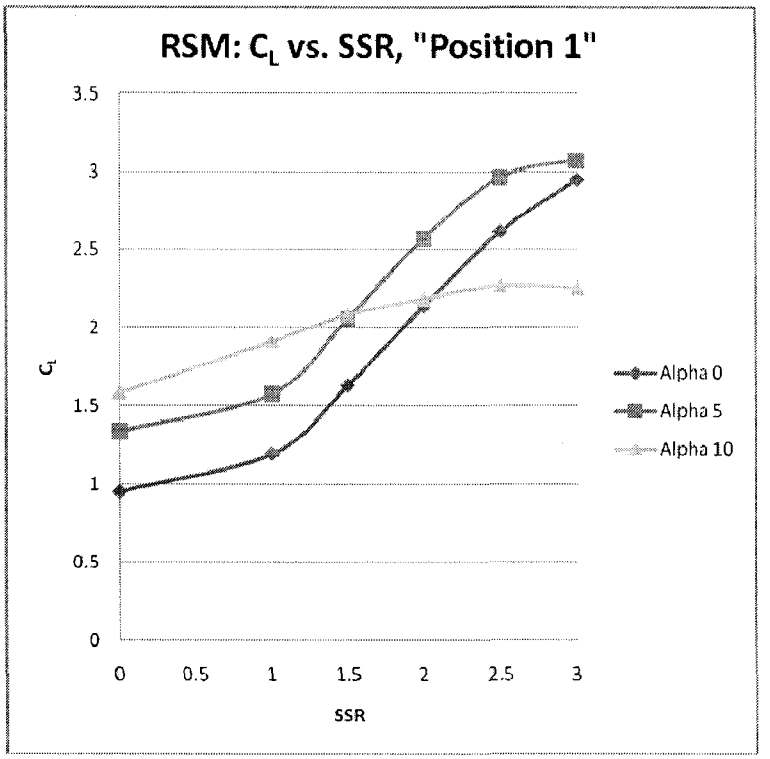

Figure 6-102. Lift curve plot, "Position 1."

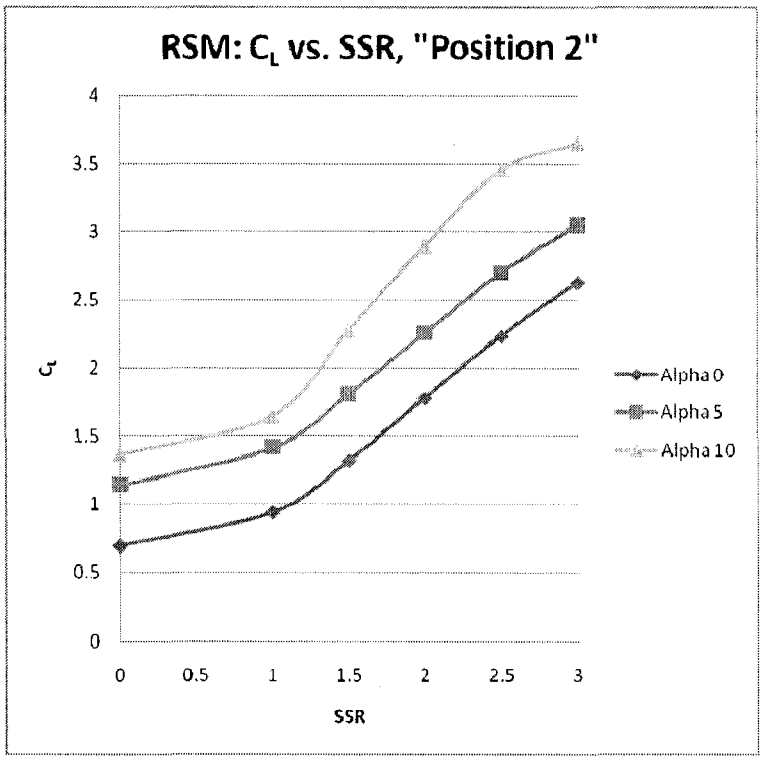

Figure 6-103. Lift curve plot, "Position 2."

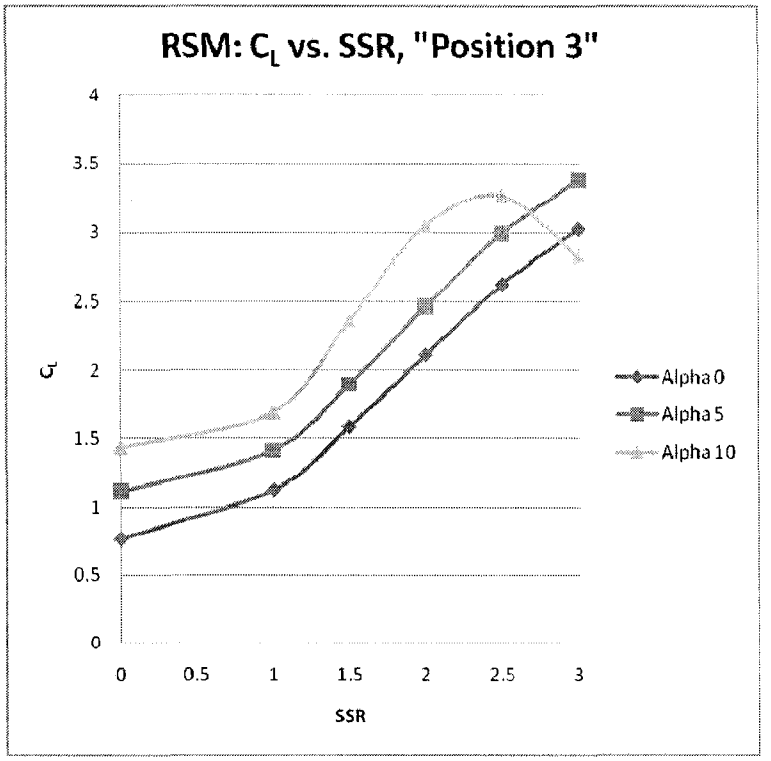

Figure 6-104. Lift curve plot, "Position 3."

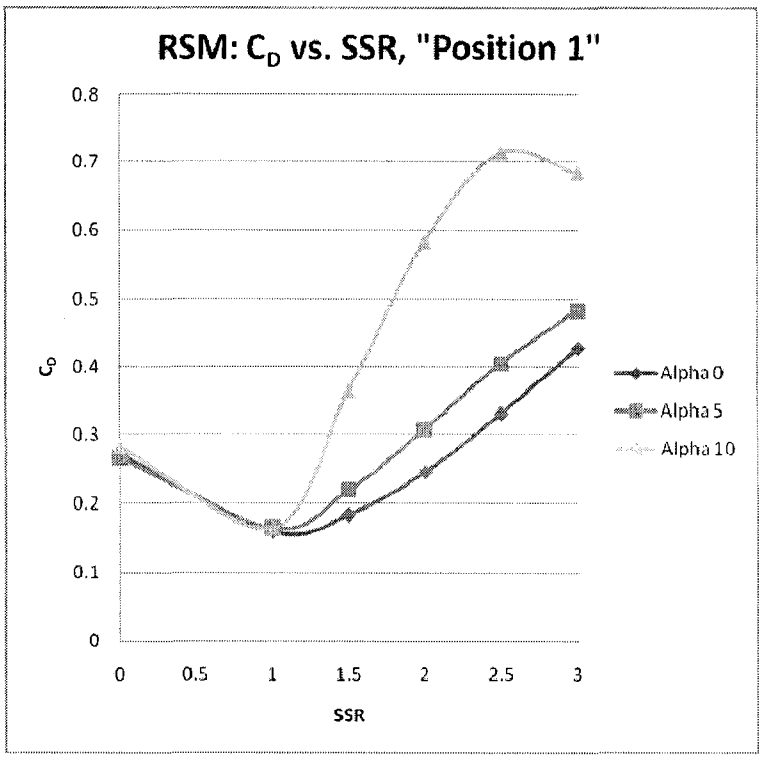

Figure 6-105. Drag curve plot, "Position 1."

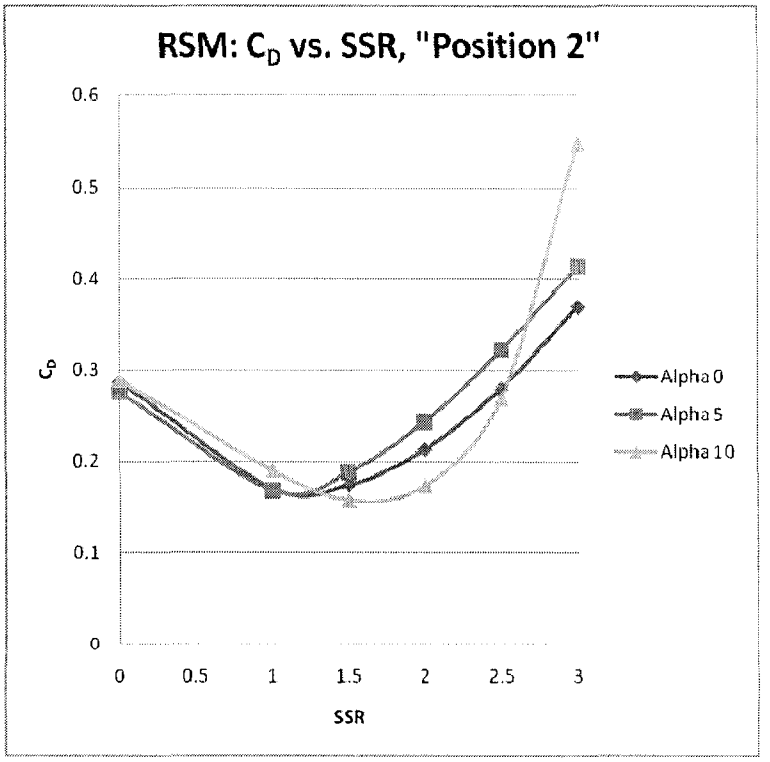

Figure 6-106. Drag curve plot, "Position 2."

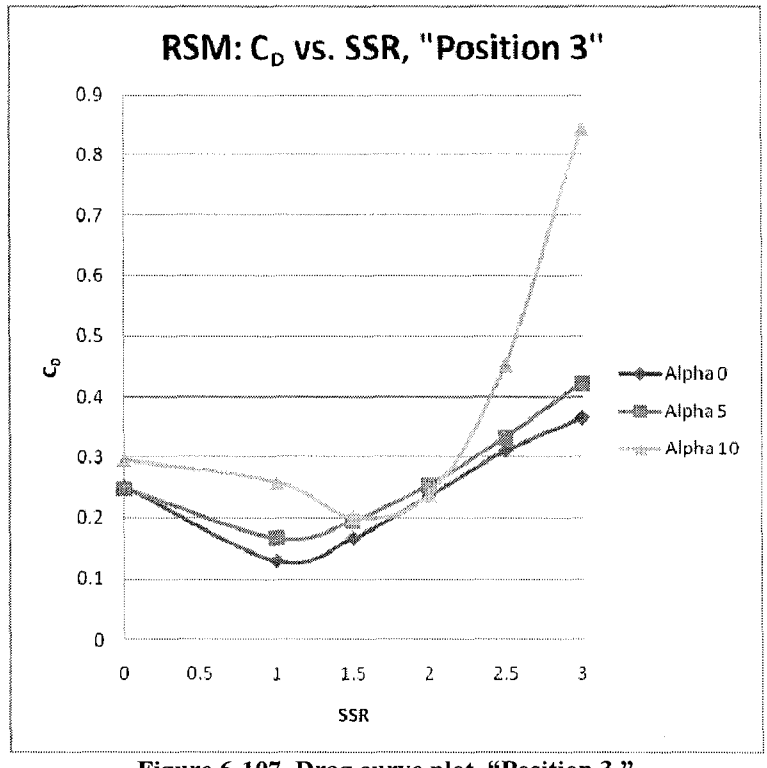

Figure 6-107. Drag curve plot, "Position 3."

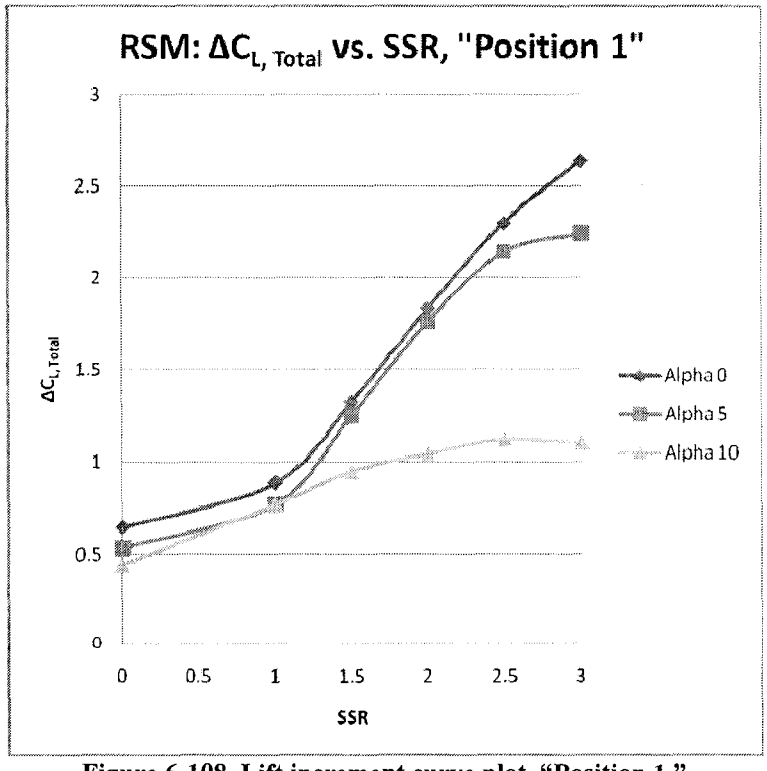

Figure 6-108. Lift increment curve plot, "Position 1."

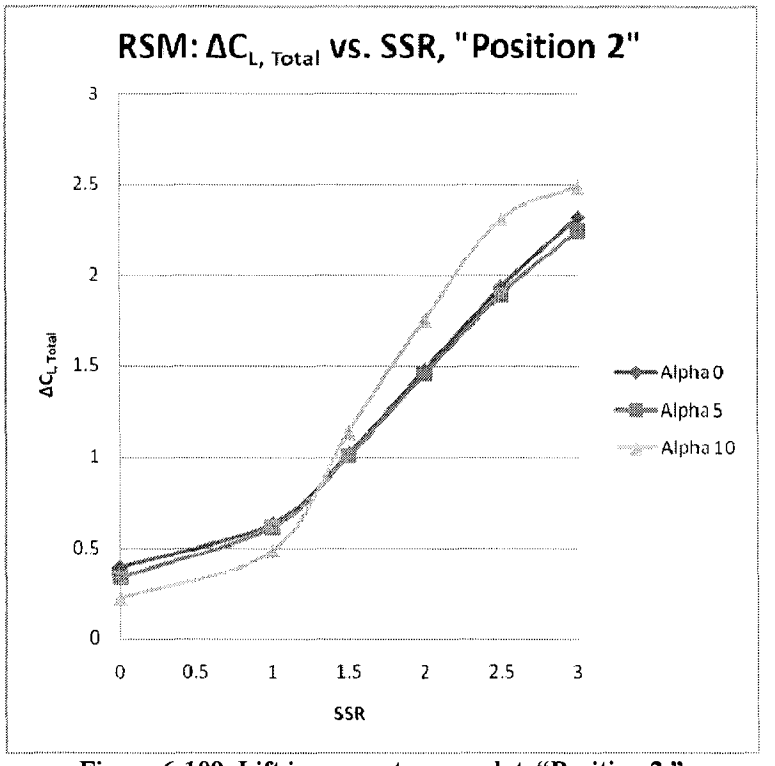

Figure 6-109. Lift increment curve plot, "Position 2."

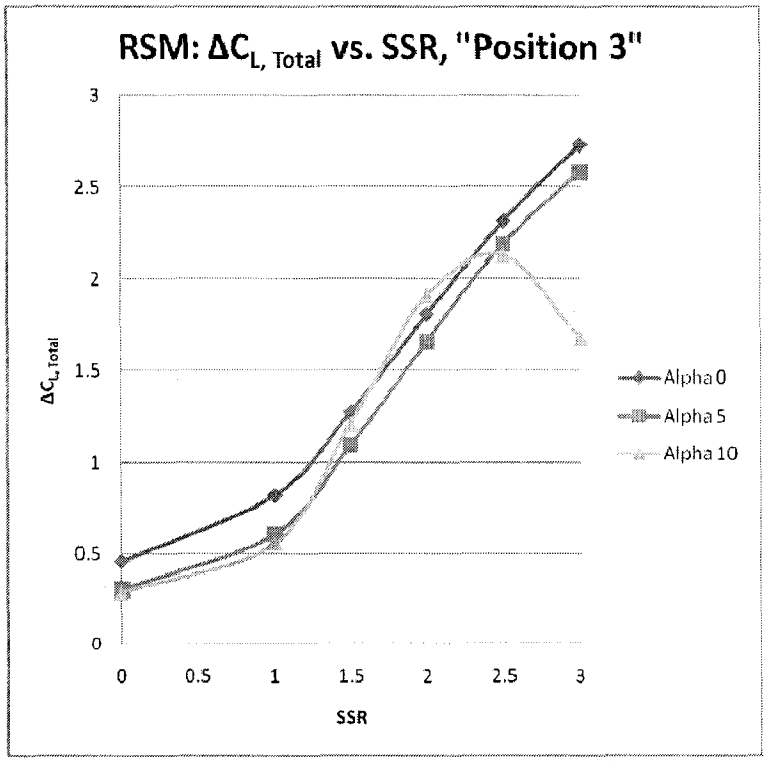

Figure 6-110. Lift increment curve plot, "Position 3."

Curve Plots Illustrating the Effect of α at Various SSR

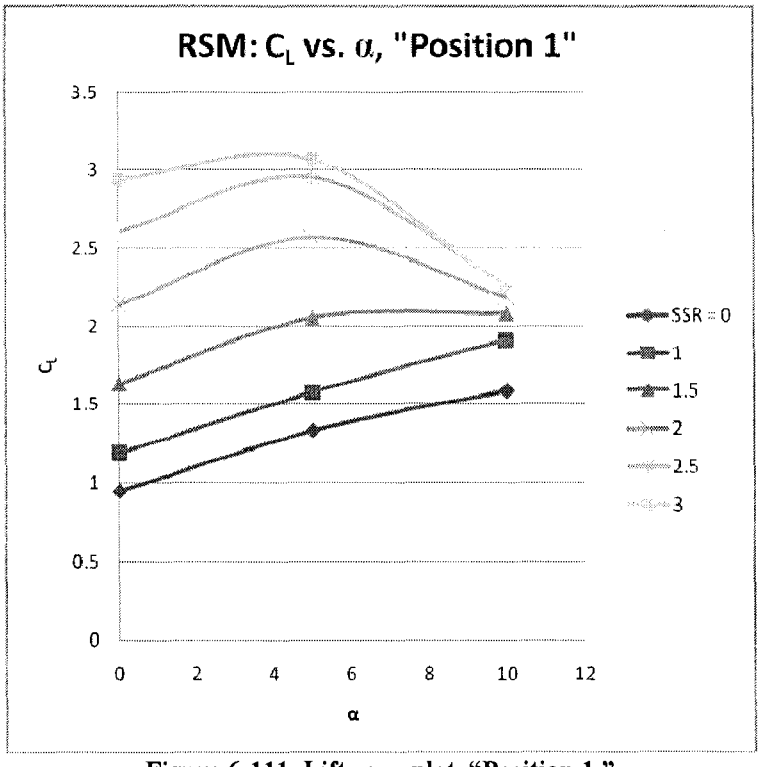

Figure 6-111. Lift vs. α plot, "Position 1."

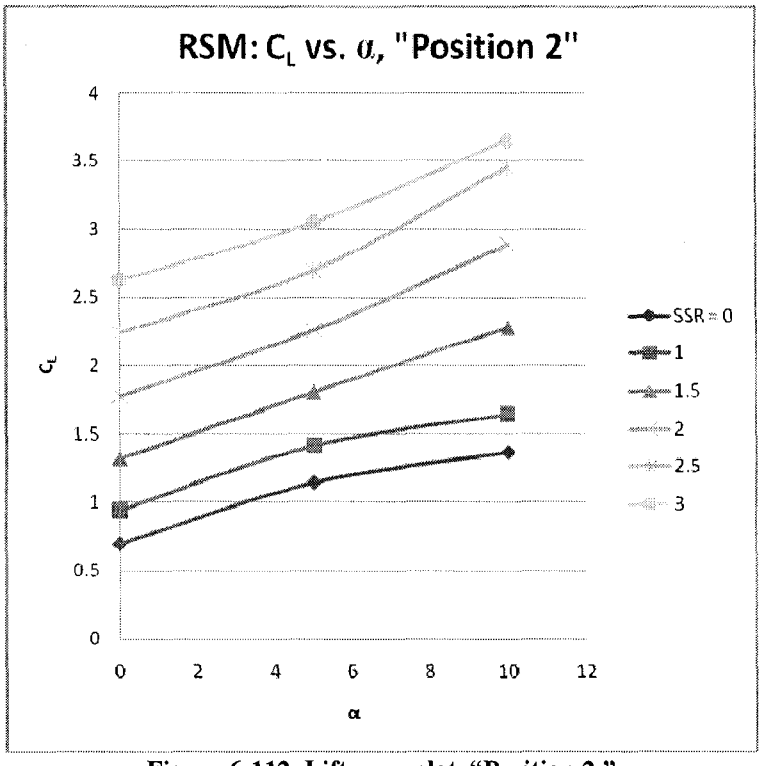

Figure 6-112. Lift vs. α plot, "Position 2."

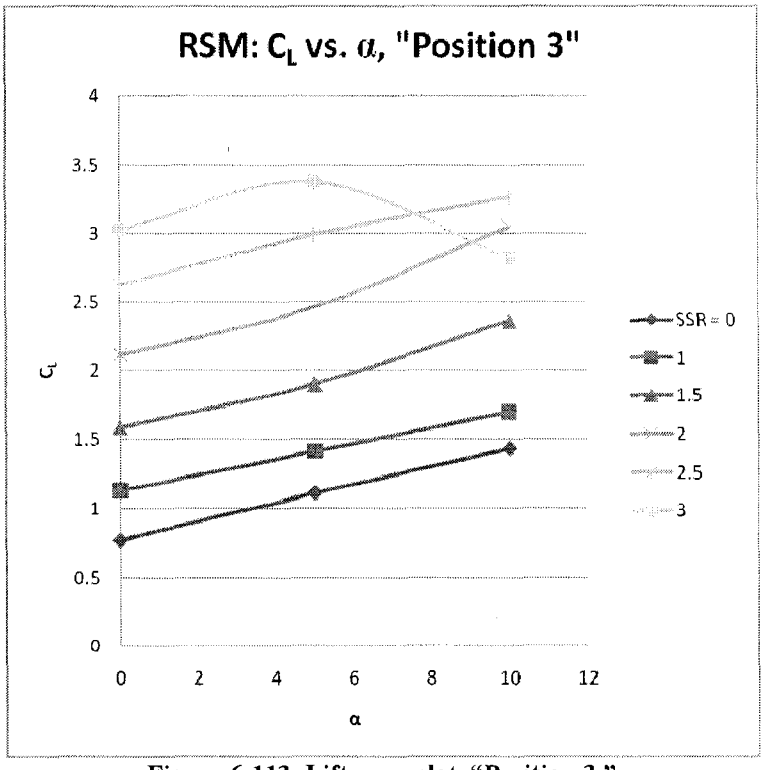

Figure 6-113. Lift vs. α plot, "Position 3."

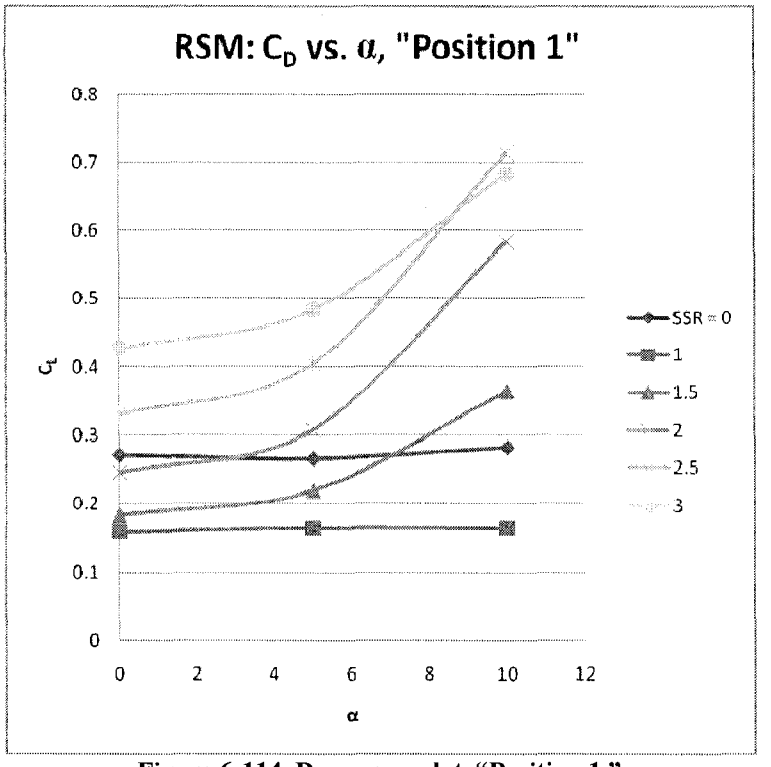

Figure 6-114. Drag vs. α plot, "Position 1."

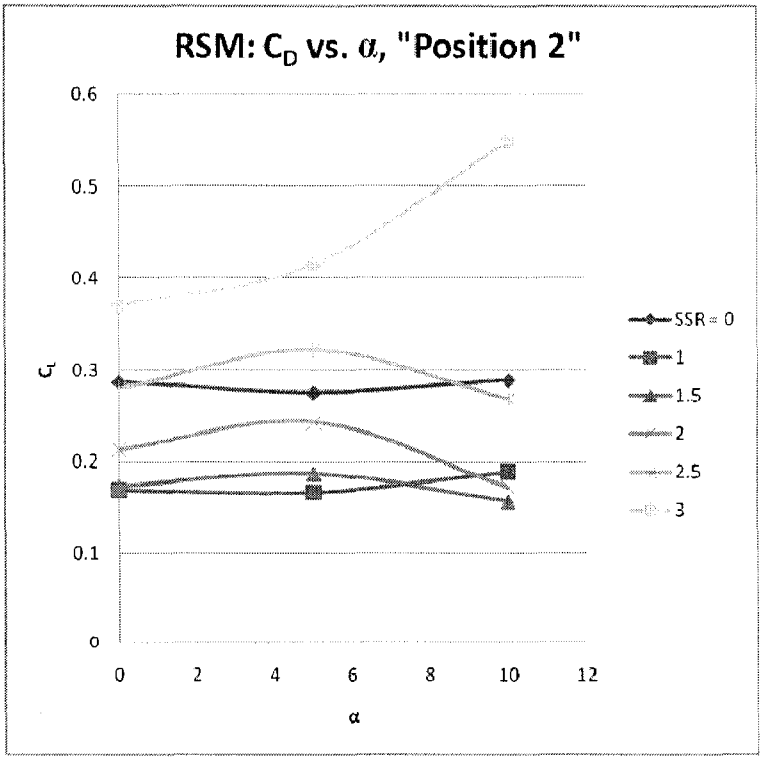

Figure 6-115. Drag vs. α plot, "Position 2."

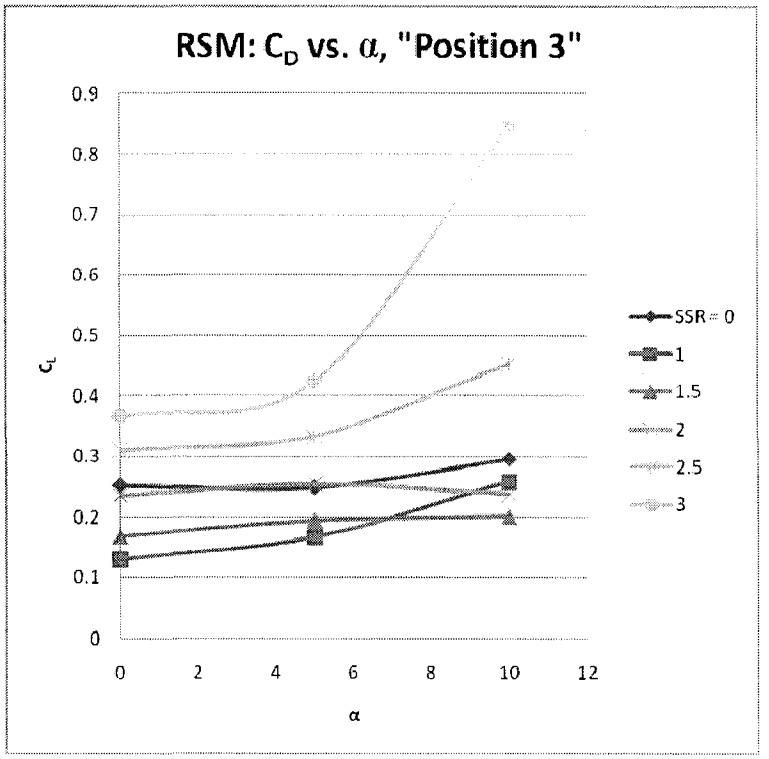

Figure 6-116. Drag vs. α plot, "Position 3."

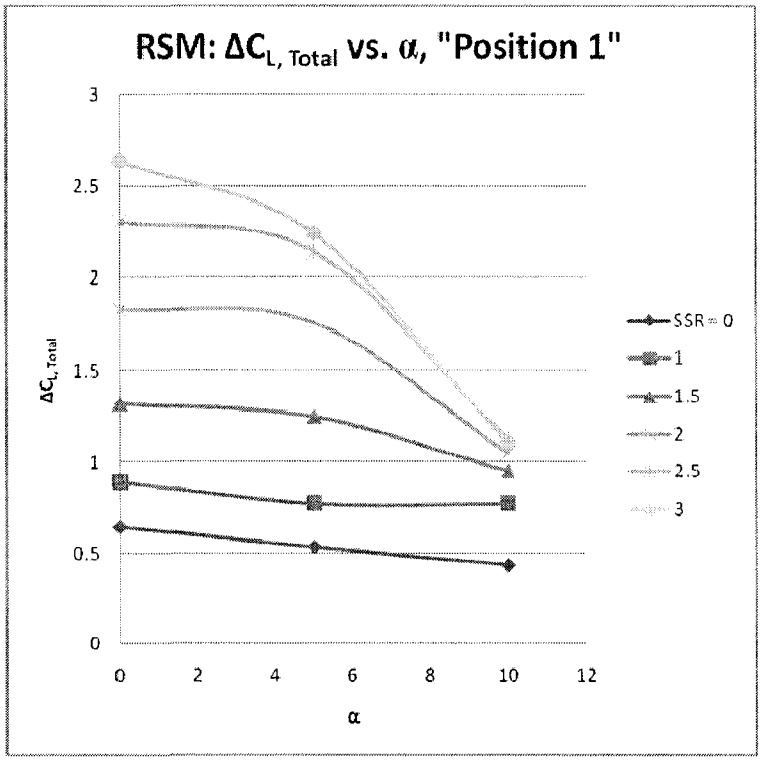

Figure 6-117. Lift increment vs. α plot, "Position 1."

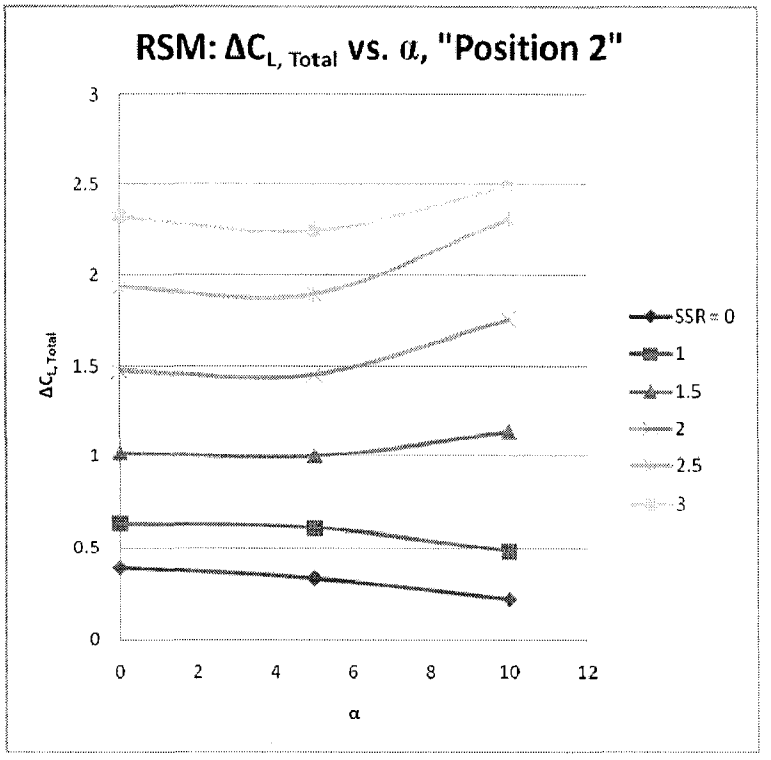

Figure 6-118. Lift increment vs. α plot, "Position 2."

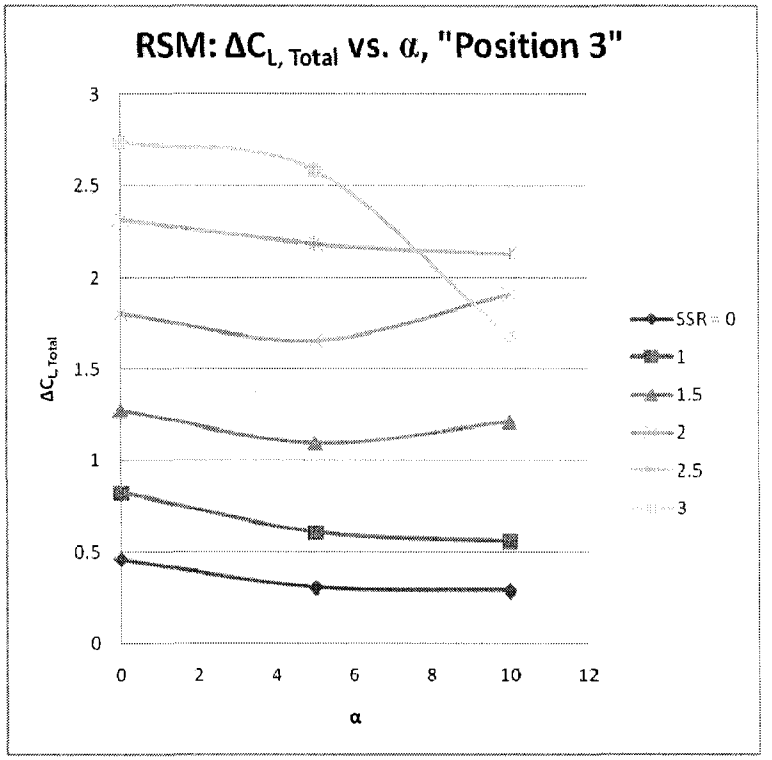

Figure 6-119. Lift increment vs. α plot, "Position 3."

Curve Plots Illustrating the Effect of SSR at Each "Position"

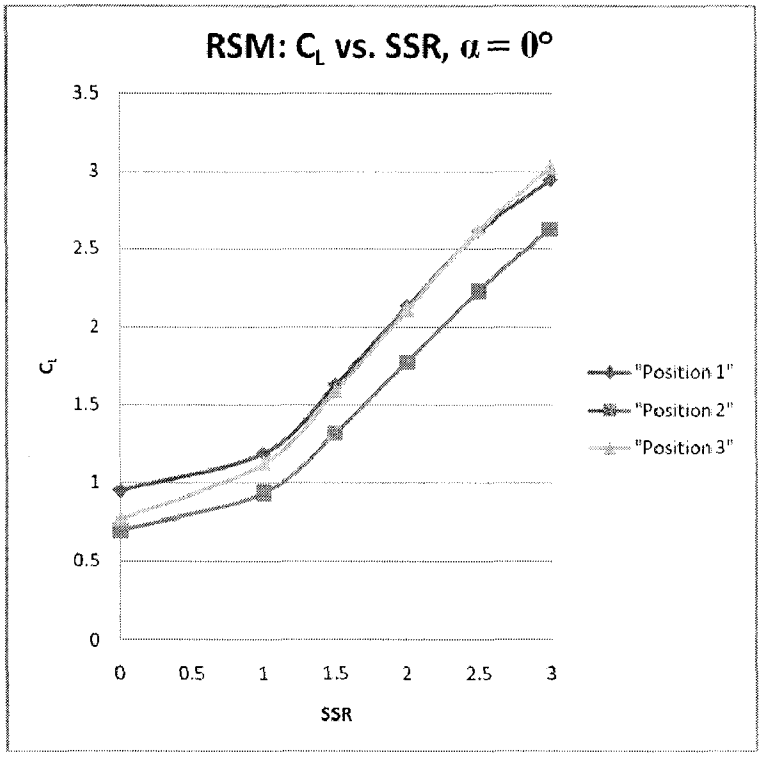

Figure 6-120. Lift vs. SSR curve plot, α = 0°.

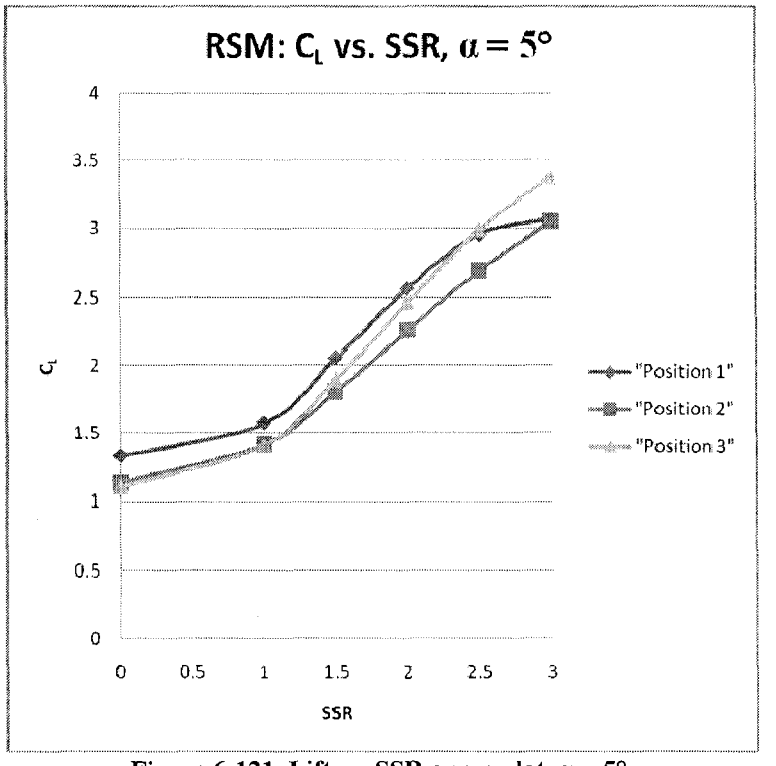

Figure 6-121. Lift vs. SSR curve plot, α = 5°.

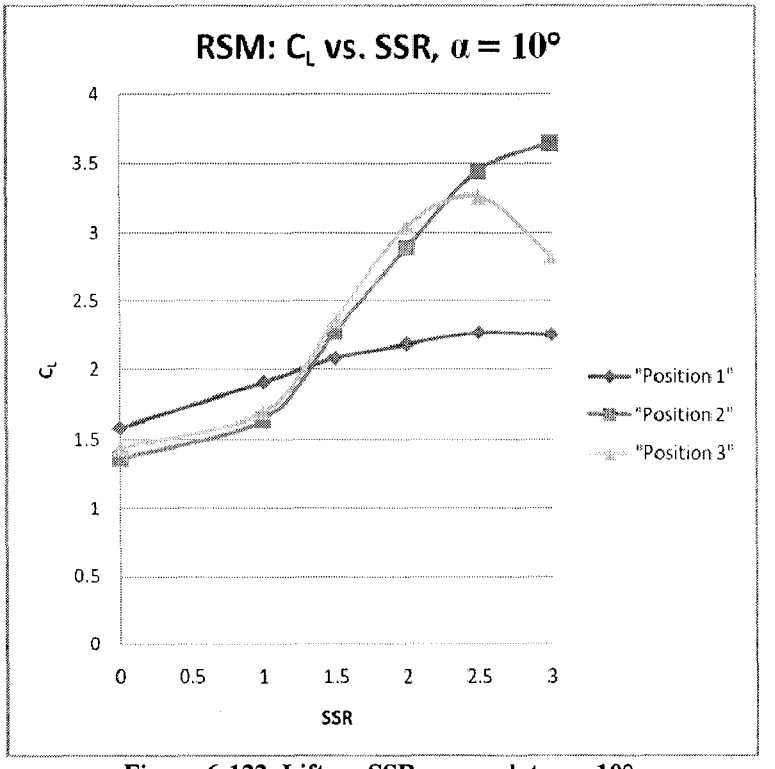

Figure 6-122. Lift vs. SSR curve plot, α = 10°.

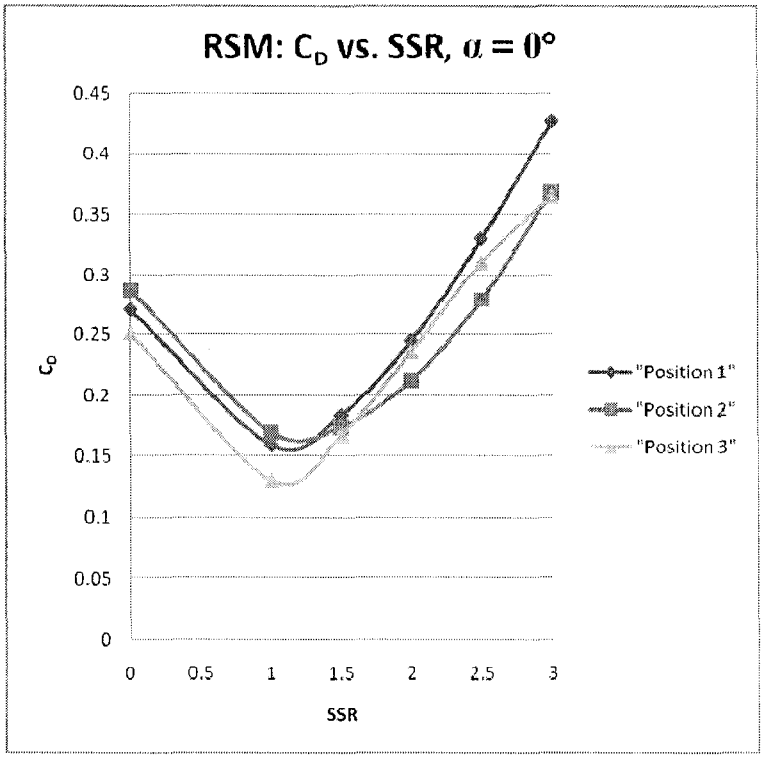

Figure 6-123. Drag vs. SSR curve plot, α = 0°.

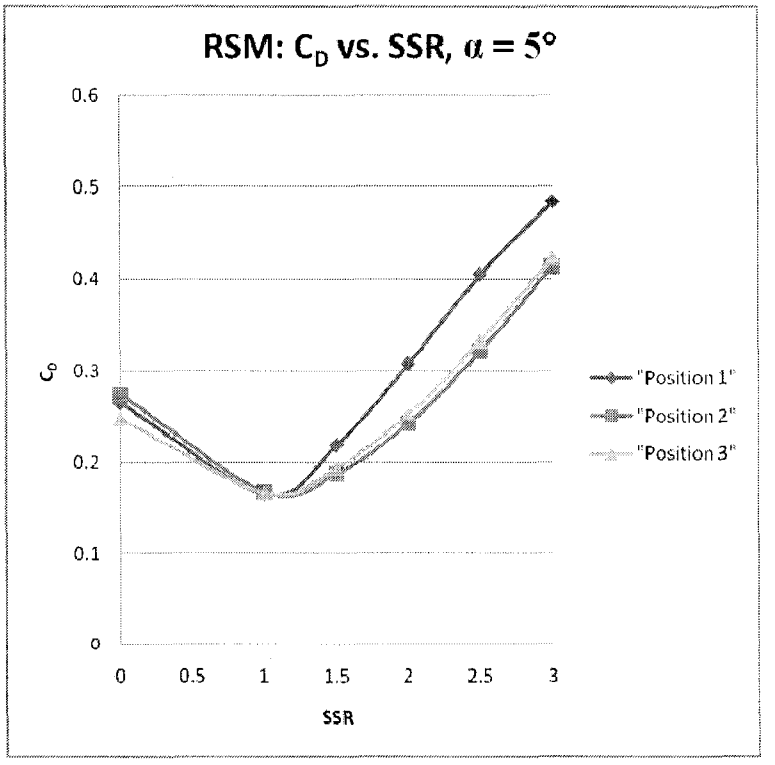

Figure 6-124. Drag vs. SSR curve plot, α = 5°.

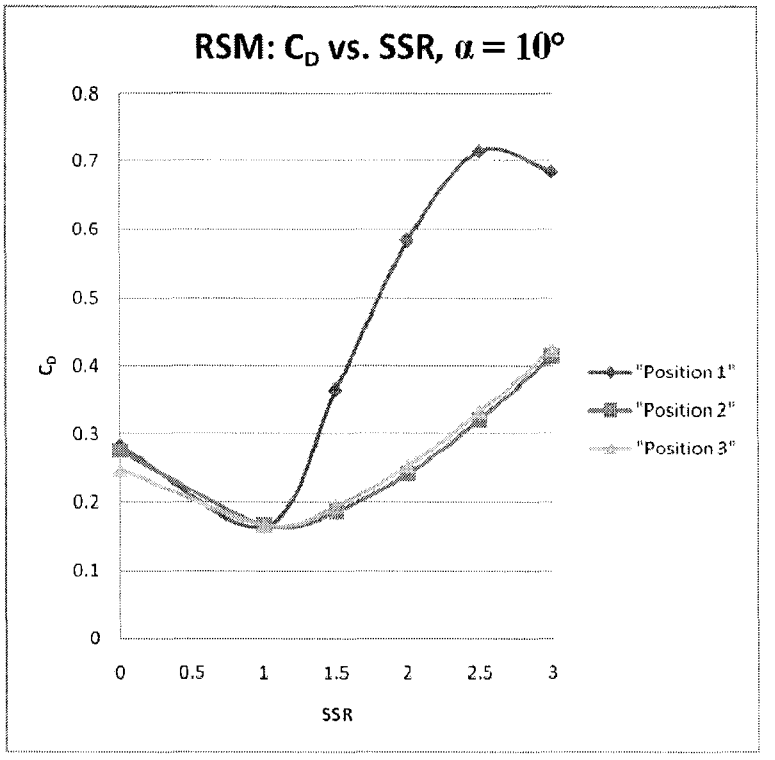

Figure 6-125. Drag vs. SSR curve plot, α = 10°.

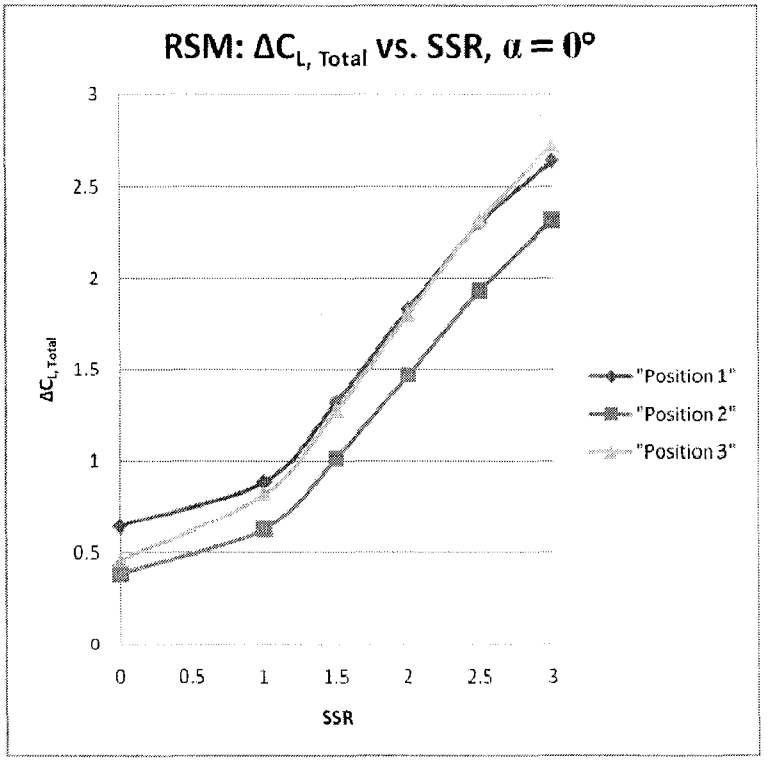

Figure 6-126. Lift increment vs. SSR curve plot, α = 0°.

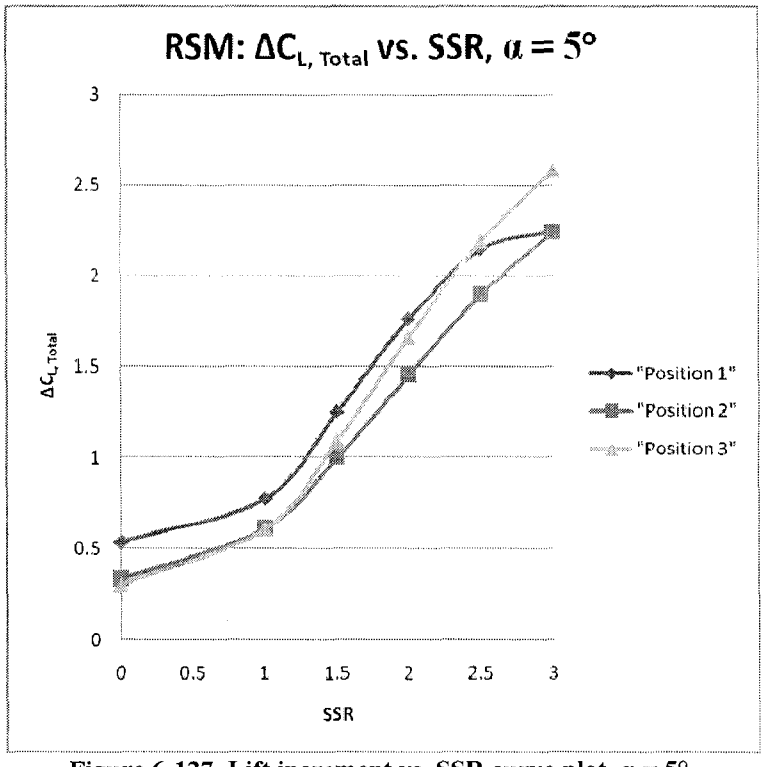

Figure 6-127. Lift increment vs. SSR curve plot, α = 5°.

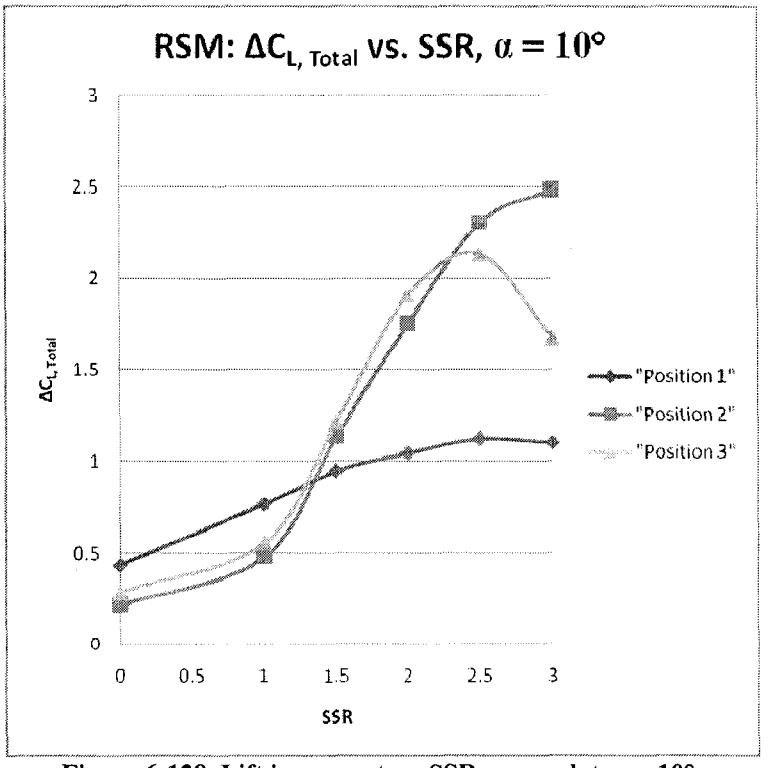

Figure 6-128. Lift increment vs. SSR curve plot, α = 10°.

Curve Plots Illustrating the Effect of α at Various "Positions"

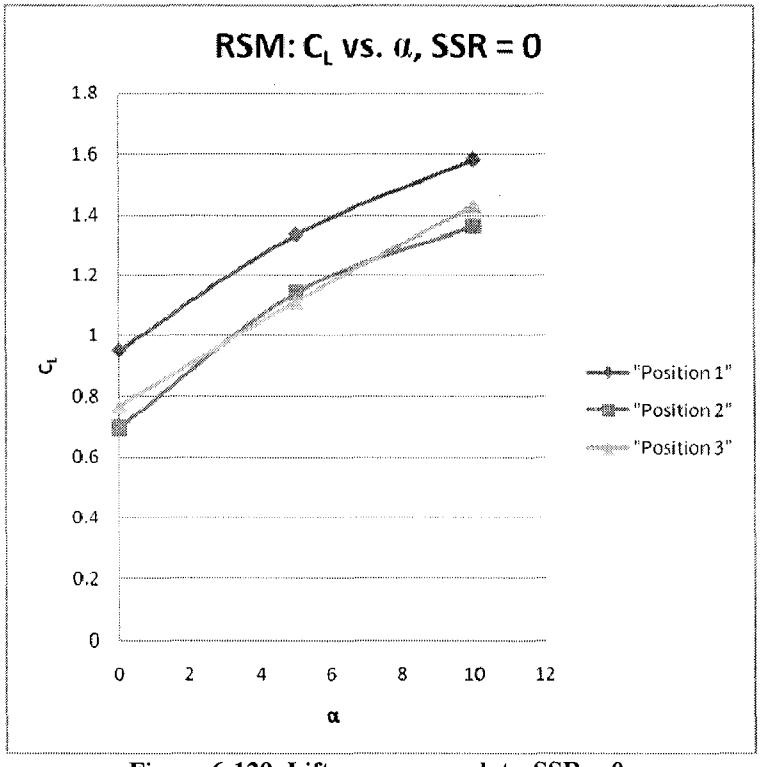

Figure 6-129. Lift vs. α curve plots, SSR = 0.

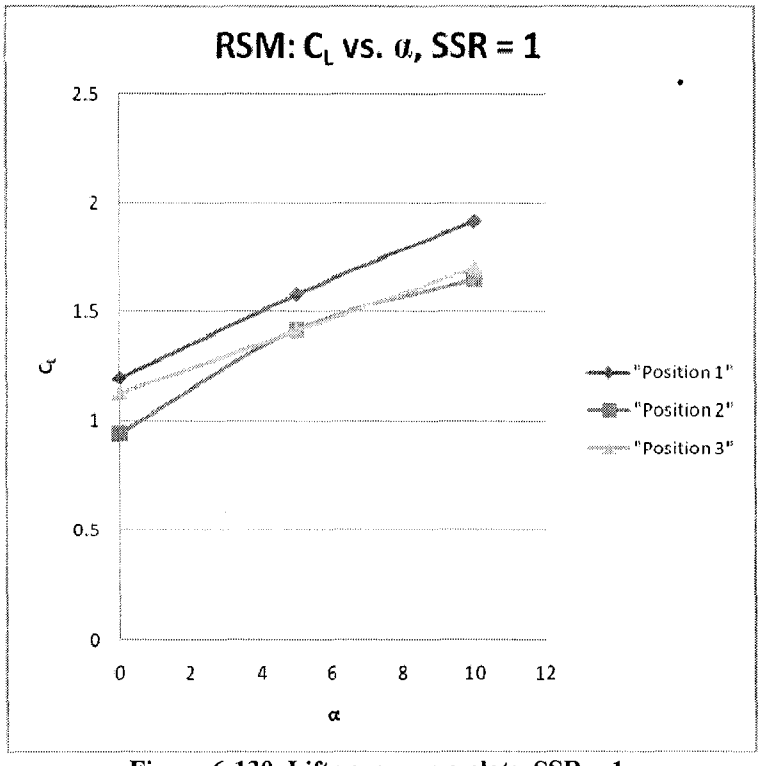

Figure 6-130. Lift vs. α curve plots, SSR = 1.

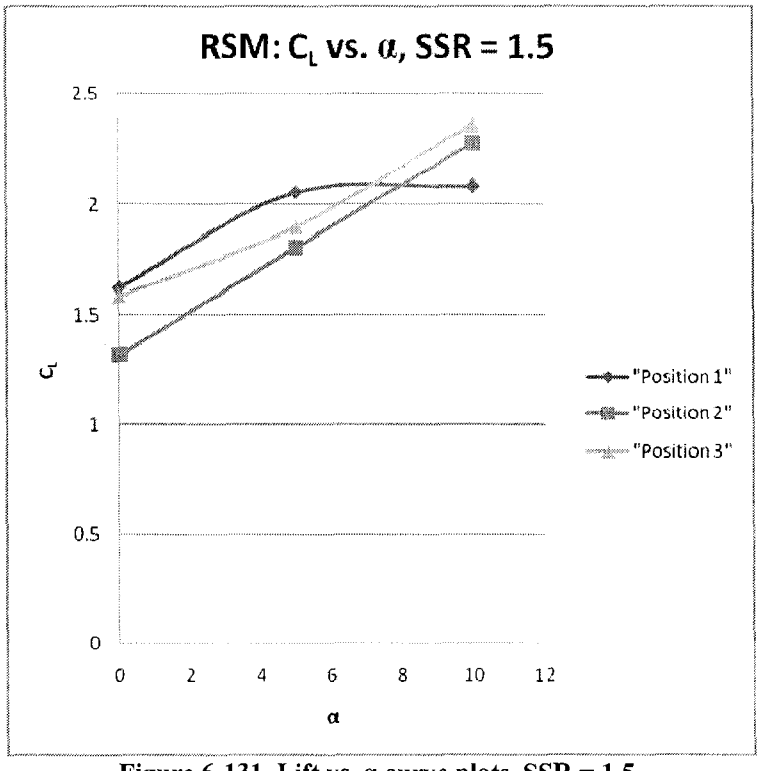

Figure 6-131. Lift vs. α curve plots, SSR = 1.5.

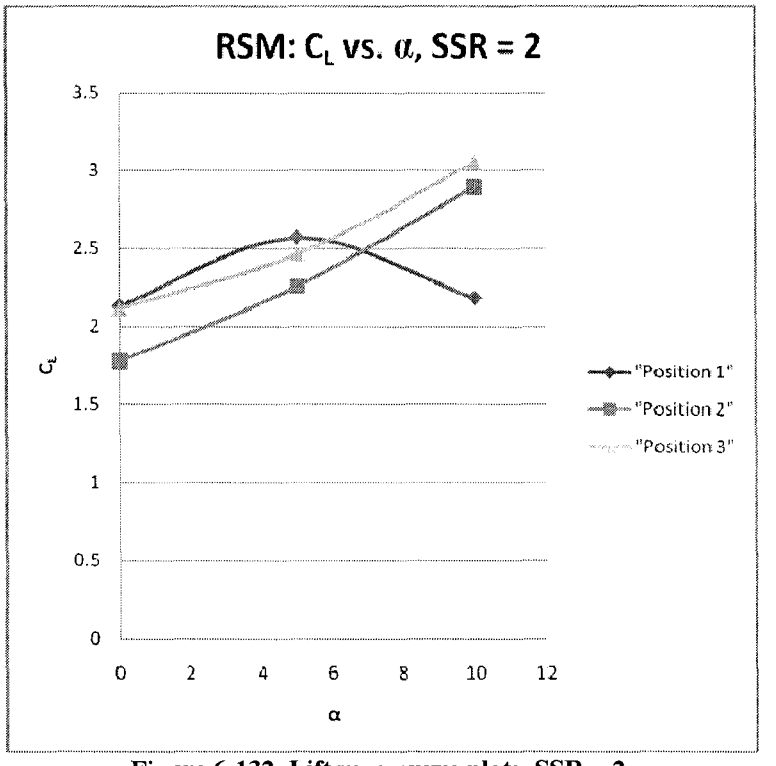

Figure 6-132. Lift vs. α curve plots, SSR = 2.

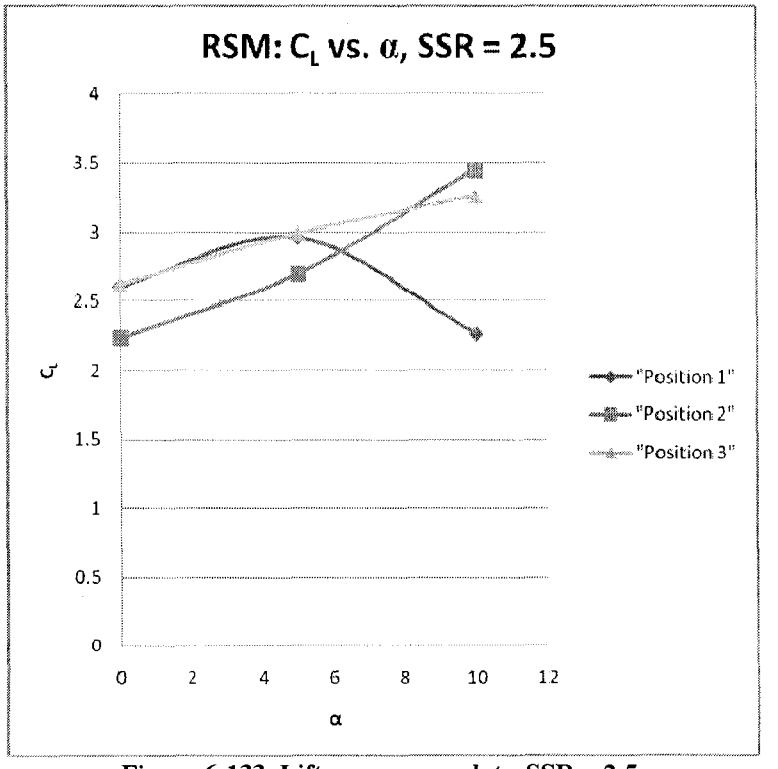

Figure 6-133. Lift vs. α curve plots, SSR = 2.5.

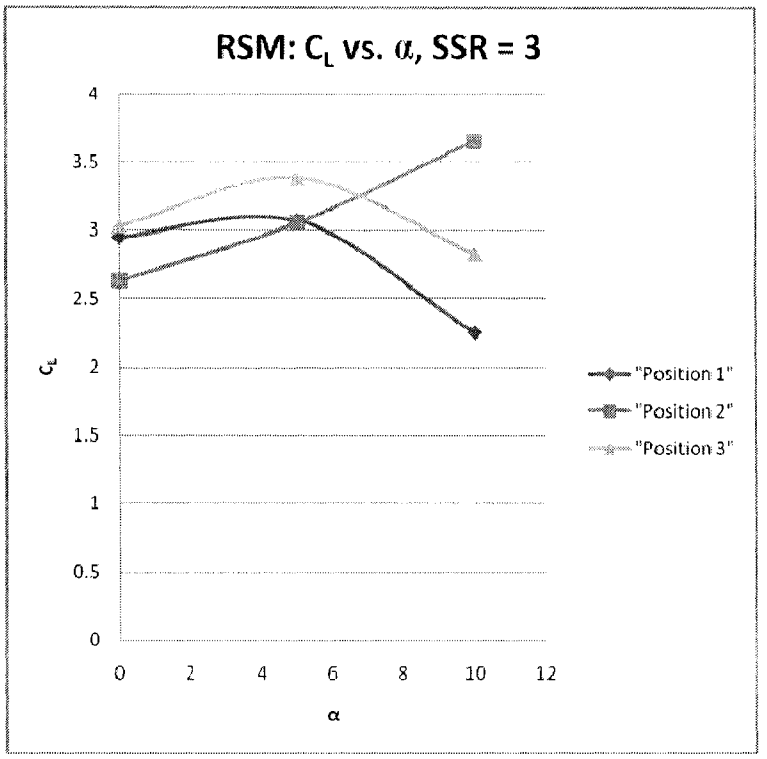

Figure 6-134. Lift vs. α curve plots, SSR = 3.

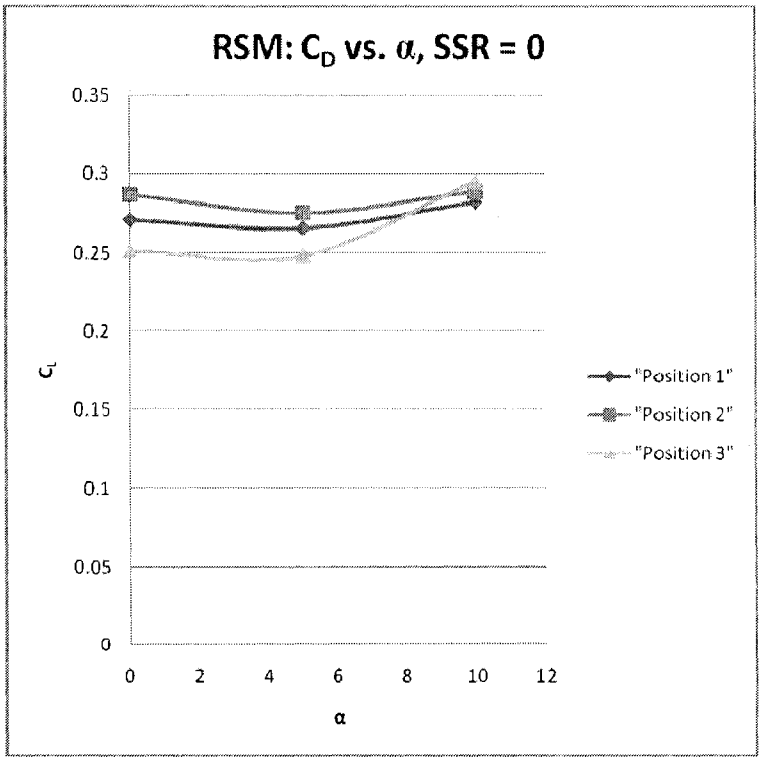

Figure 6-135. Drag vs. α curve plots, SSR = 0.

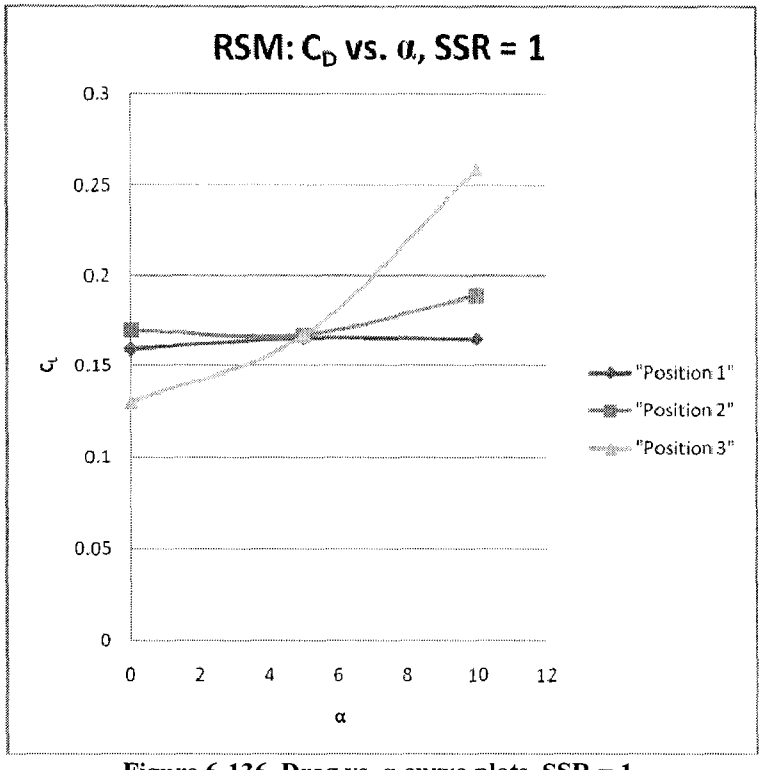

Figure 6-136. Drag vs. α curve plots, SSR = 1.

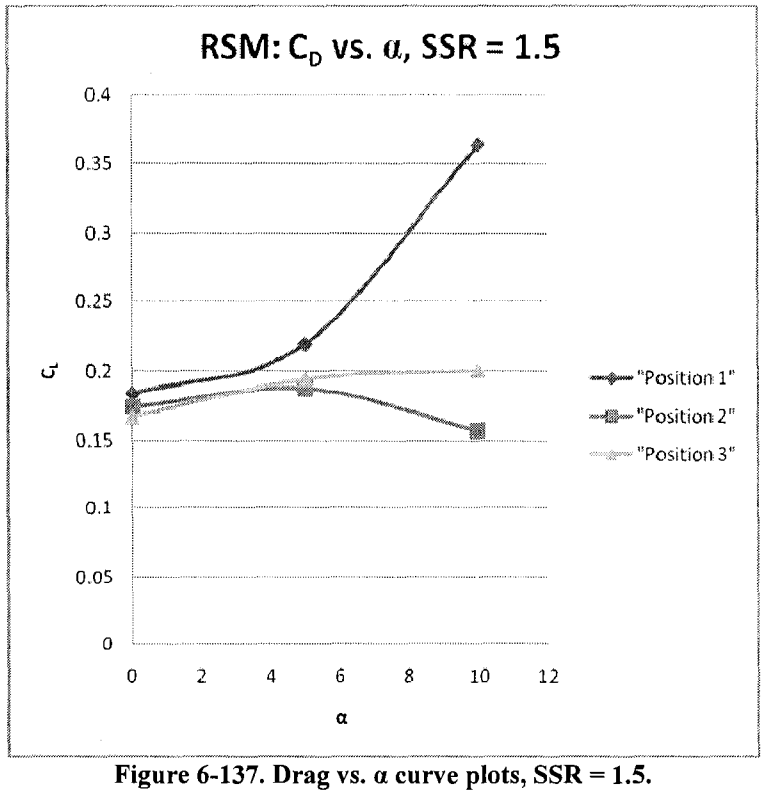

Figure 6-137. Drag vs. α curve plots, SSR = 1.5.

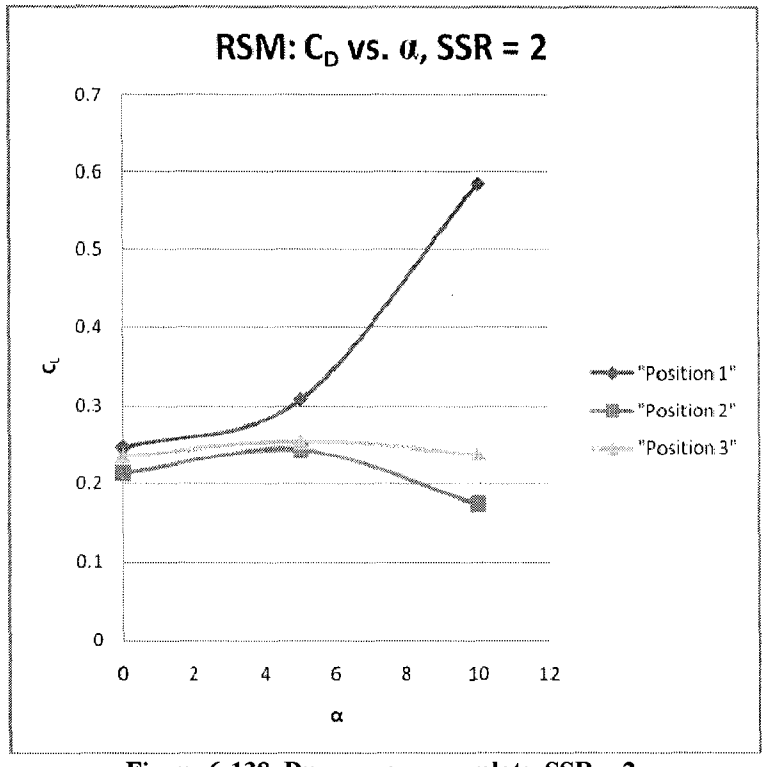

Figure 6-138. Drag vs. α curve plots, SSR = 2.

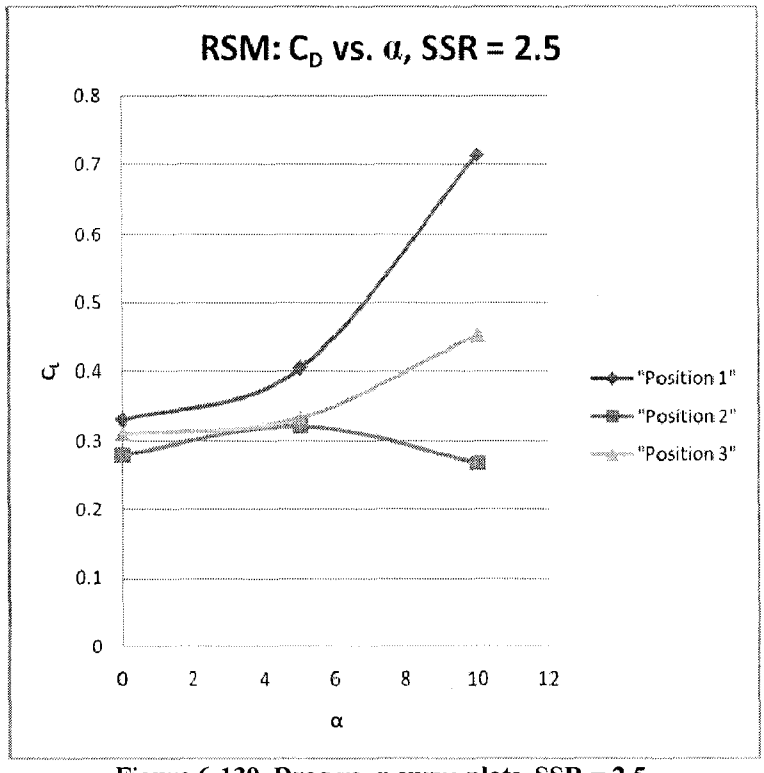

Figure 6-139. Drag vs. α curve plots, SSR = 2.5.

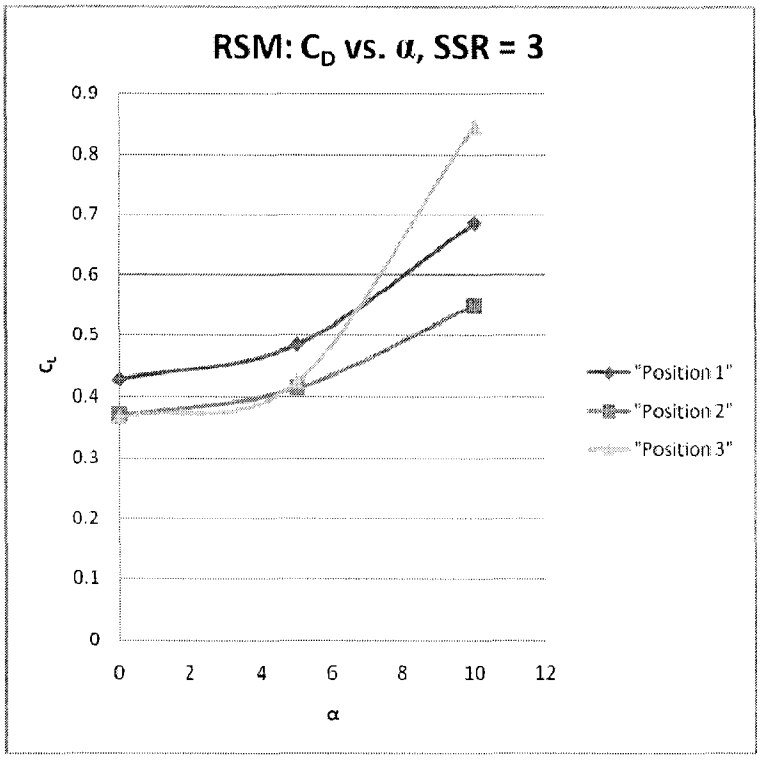

Figure 6-140. Drag vs. α curve plots, SSR = 3.

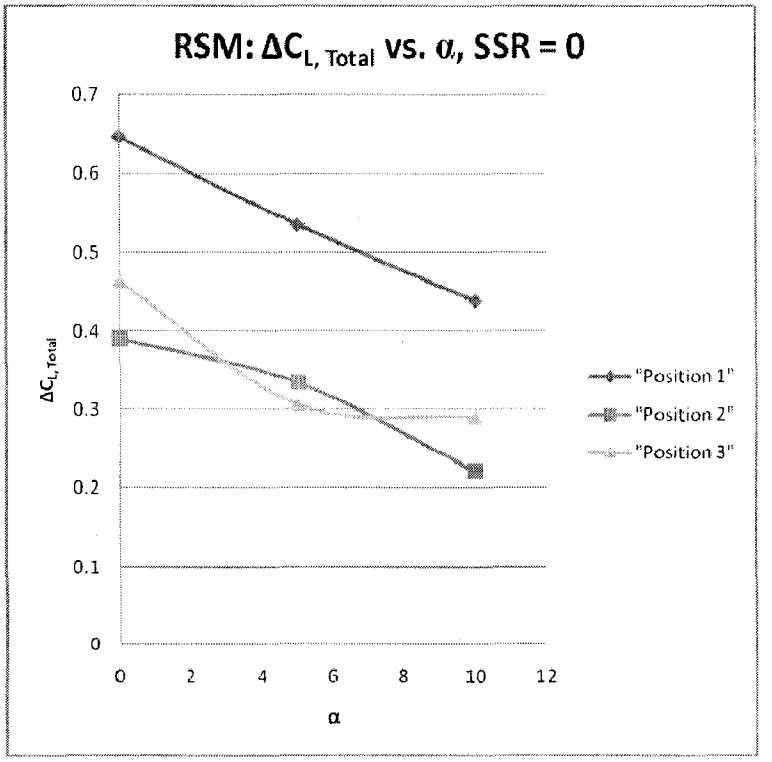

Figure 6-141. Lift increment vs. α curve plots, SSR = 0.

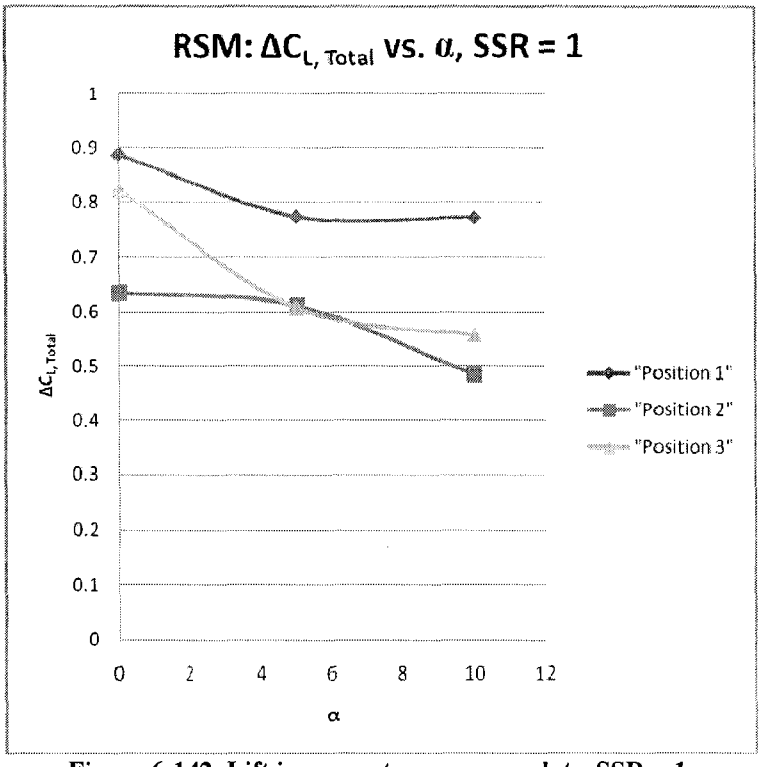

Figure 6-142. Lift increment vs. α curve plots, SSR = 1.

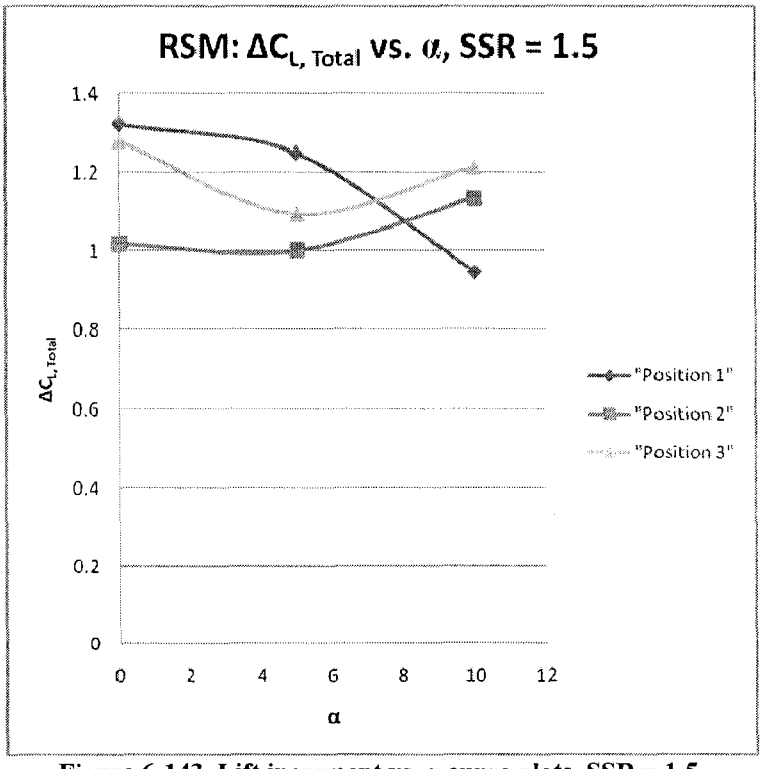

Figure 6-143. Lift increment vs. α curve plots, SSR = 1.5.

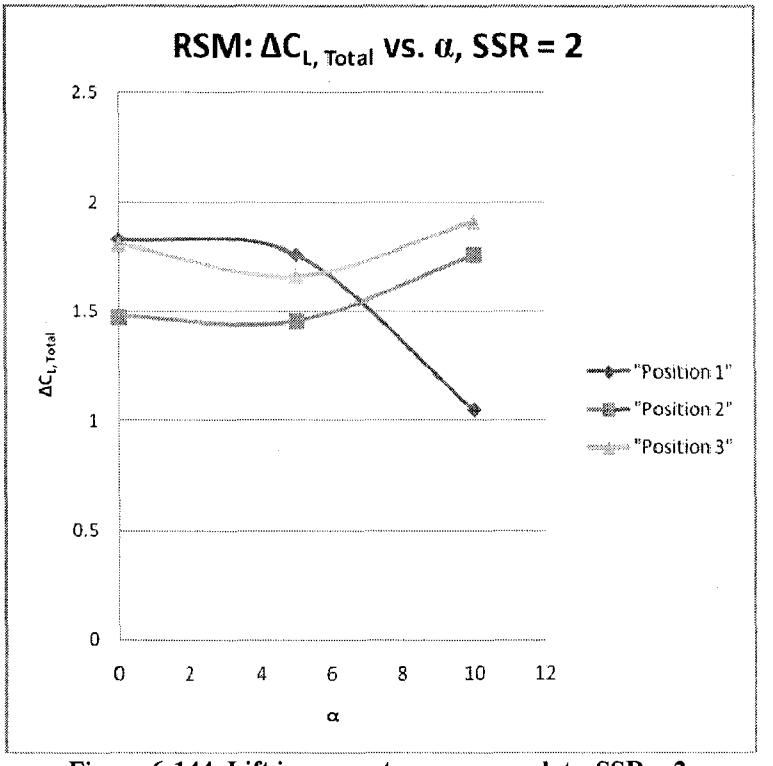

Figure 6-144. Lift increment vs. α curve plots, SSR = 2.

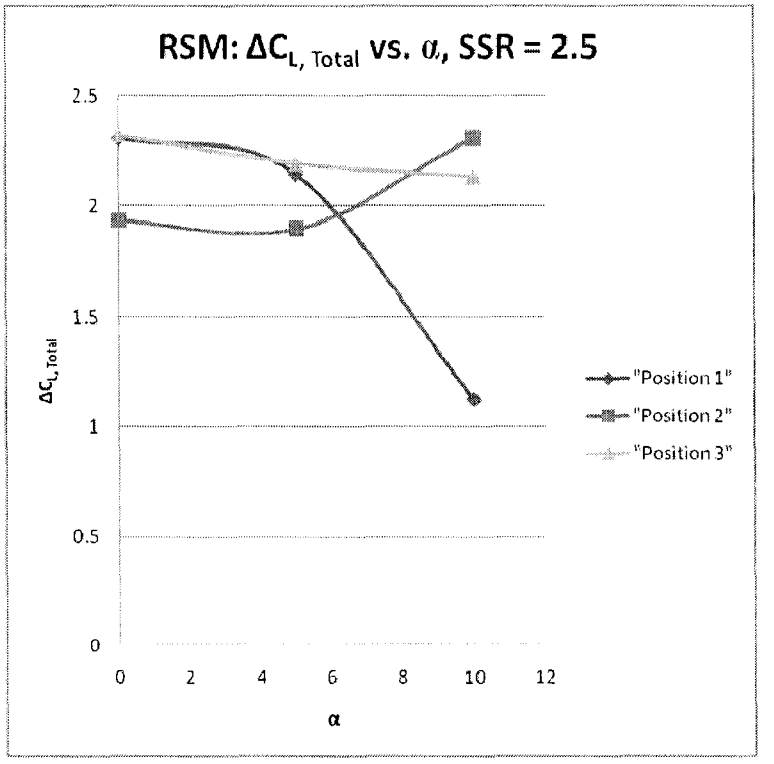

Figure 6-145. Lift increment vs. α curve plots, SSR = 2.5.

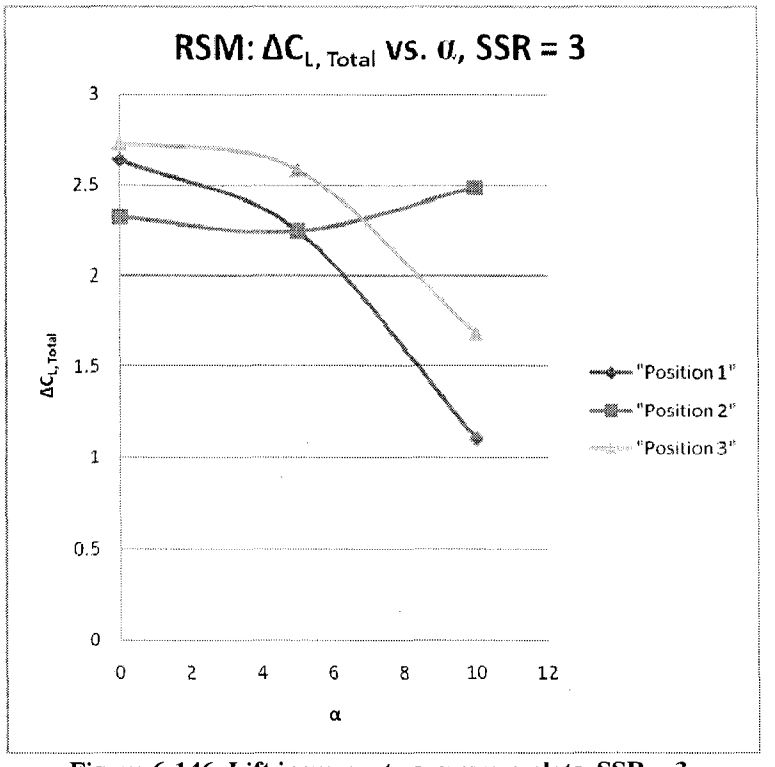

Figure 6-146. Lift increment vs. α curve plots, SSR = 3.

Development of the Polynomial Curve Net Method through an Optimization Study of Over-the-Wing Configurations of the Vortex Flap

During the work that produced the Vortex Flap, a number of other positions not detailed were also investigated. Following is a discussion of those positions, and the development of the optimization (RSM) methods which became an integral part of this dissertation. A presentation of this work and development follows.

Expanding the operating envelope of aircraft has been a primary pursuit of aerospace engineers since the advent of aviation as a human practice. However, the basic elements which are conducive to high-speed flight stand at odds with those essential for low-speed flight. For aircraft which must operate effectively in both regimes, means must be found to accommodate the disparate demands. For many decades, the search has been on for means to improve the low-speed performance of aircraft in a manner which sacrifices as little high-speed or other operational functionality as possible.

As the demand for higher operating speeds increased, variable-geometry wings were created to allow the wing shape to change in flight to accommodate the demands of each flight regime. In time, powered-lift, and even vertical-takeoff and landing aircraft became available and practical for certain missions, but still the desire to improve the basic, non-powered-lift, high-lift device continues.

It is with an eye out for such a high-lift device that it was decided to investigate the behavior and performance of a rotating cylinder placed with the major axis spanwise along an unswept wing. It was unknown where the cylinder should be placed with respect to the wing, and determining the best location or locations was a major objective of the investigation. An experimental study was devised and executed.

A great deal of data was collected from these tests; over 1,700 relevant combinations of parameters were tested measuring lift and drag. However, the nature of the testing provided data at only discrete locations, and the combinations of parameters were not directly comparable. What was needed was a continuous surface which could be searched for an optimal cylinder location as a function of the other parameters. Therefore, in order to 'search' the parameter space for an optimal cylinder location, the data will have to be approximated by a surface which can be searched. This surface will be generated from the data using an adaptation of Response Surface Methods (Box 1987) which employs a net of polynomial curves generated from data points to approximate a continuous surface.

Engineering Model

The model upon which this investigation is based, is a set of data points obtained during a wind tunnel investigation of a physical model in the Low-Speed Wind Tunnel at Washington University in Saint Louis. The tests were designed to approximate two dimensional flow, and were conducted over as wide a range of Reynolds number, Surface-Speed-Ratios (SSR or the ratio of the tangential velocity of the surface of the cylinder to the free stream velocity), airfoil angle of attack and cylinder position as was permitted by the physical limitations of the test apparatus.

The data was collected electronically; each test produced 2,000 data points collected over two seconds, and averaged to produce the lift and drag for each test. Some areas of the test space were examined more thoroughly than others.

Optimization Study

Given the broad scope of the original testing, for brevity this appendix will only address the optimization of lift for a selected subset of the data. In particular, only one angle of attack will be examined (0 degrees), only the flat plate will be included, and only tests placing the cylinder above the airfoil will be considered. In addition, the

data points selected will include only a restricted range of Reynolds number. This reduces the number of tests under consideration from around 1,700 to around 140.

Generating a multi-variable response surface based on discrete data is difficult. In order to make the problem more tractable, a method was developed which addresses the relationship between only two variables at a time. It is possible to extend this method beyond four variables, but that was as far as necessary for this problem.

Rather than generating a single comprehensive function which described the response surface, a net of polynomial curves derived from data points and interpolated 'data points' was used to generate the surface. A 'net' is an n-dimensioned grid comprised of curves which relate. The following method was implemented to generate the surface.

1. **Generate a list of n variables for which a relationship is sought.** The list should be as short as possible. For this investigation, a Buckingham Pi analysis was conducted to ensure that the minimum number of variables was considered. In this case, the list is Lift, SSR, cylinder horizontal position, and cylinder vertical position.
2. **Pick two variables.** In this case, for convenience, SSR and Lift were selected initially, but any two variables could have been selected first.

3. At each geometric point for which data is available, **fit an appropriate polynomial curve** which describes the relations of, in this case, Lift and SSR, using least squares method. Increase the order of polynomial until the fit is 'good' (generally > 0.9 is good). In other words, find the relationship of SSR and Lift while holding cylinder position fixed. A chart showing the positions available for this investigation as well as the polynomial curve fitting at one point are shown below (Figures 6-141 and 6-142).

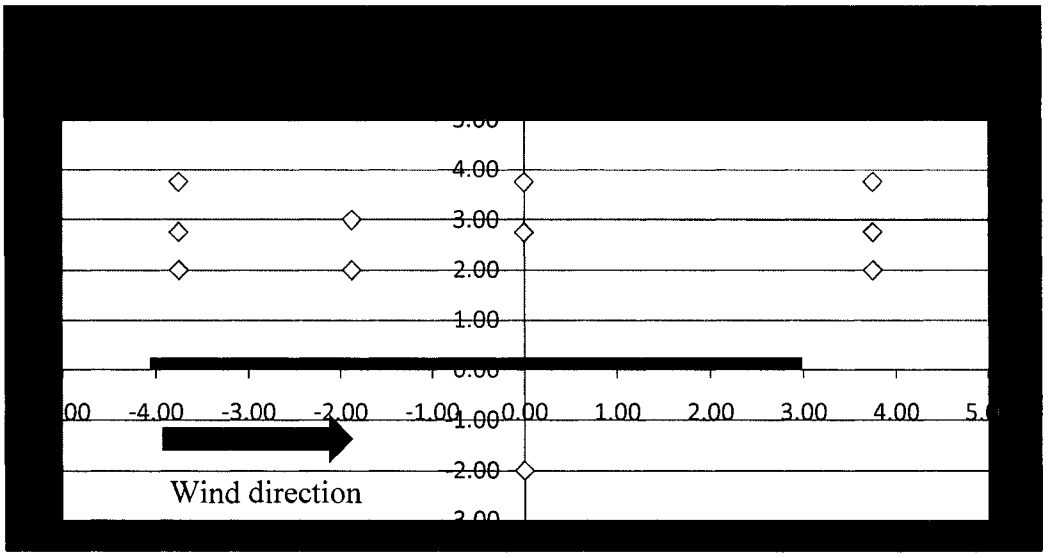

Figure 6-147. Cylinder positions tested.

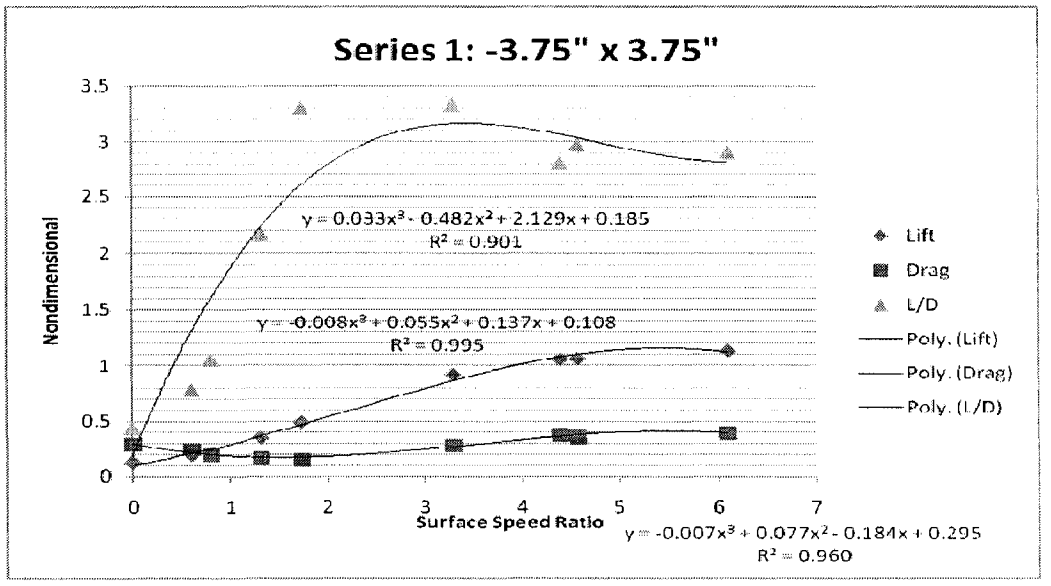

Figure 6-148. Lift vs. SSR.

4. Now the approximate polynomial description of the relationship can be used to **find the lift generated at any SSR within an appropriate range**, at every geometric point. Choose a convenient and reasonable set of SSR values to evaluate at each point for which a polynomial approximation has been generated.
5. At this point, having calculated the lift at convenient values of SSR at each point, the effect of cylinder position geometry can be investigated which holding SSR constant. **Fit polynomial curves to the relationship between Lift and vertical cylinder position**, holding SSR and cylinder horizontal position constant. Do this for all available values of SSR and horizontal

position. This is shown below for one horizontal position, and for all SSR simultaneously (Figure 6-143).

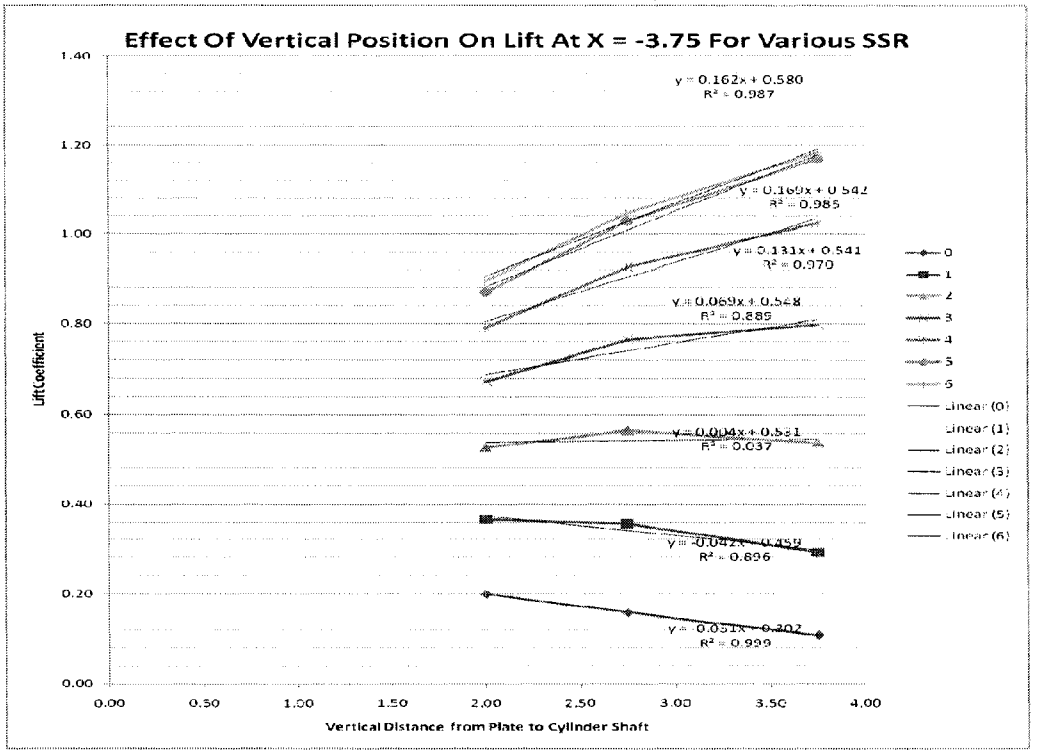

Figure 6-149. Lift vs. Vertical Position.

6. Now the approximate polynomial description of the relationship can be used to **find the lift generated at any vertical cylinder position within an appropriate range**. Choose a convenient and reasonable set of vertical cylinder position values to evaluate at each combination of SSR and horizontal position.
7. Having calculated the Lift generated at convenient vertical points and values of SSR, **fit polynomial curves to the relationship between Lift and horizontal position, holding SSR and vertical position fixed**. This is shown for one vertical position below (Figure 6-150).

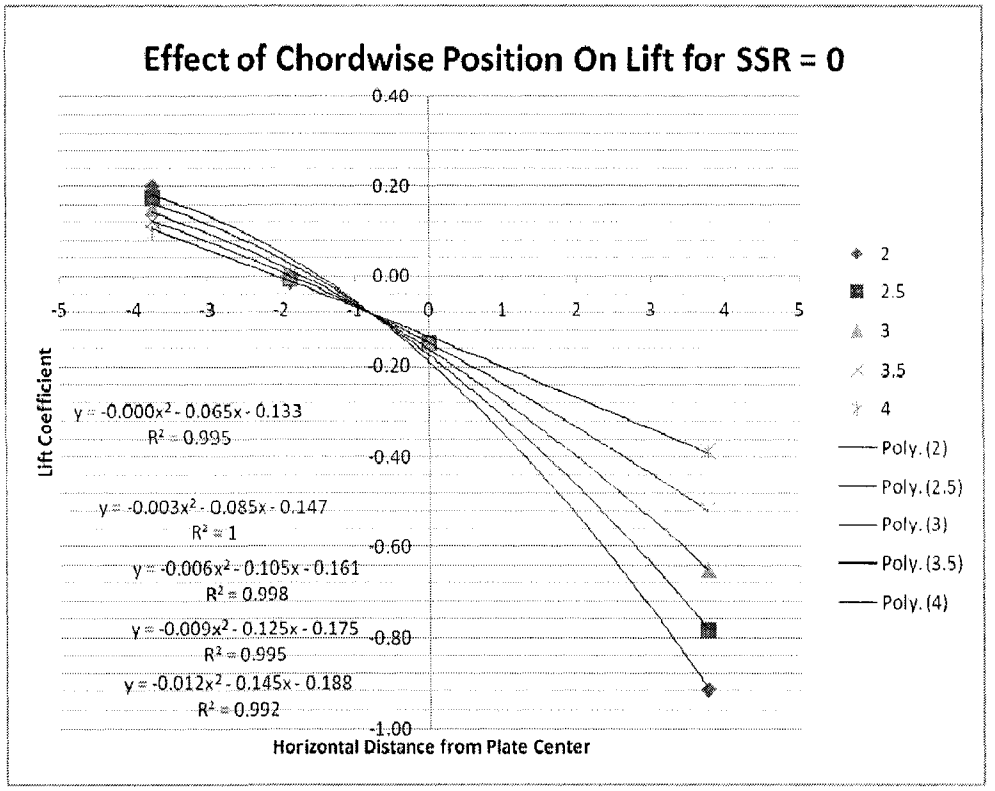

Figure 6-150. Lift vs. Horizontal (chordwise) position.

8. Having calculated the lift at convenient values of horizontal and vertical cylinder positions, and SSR, **a surface, or rather a mesh, can be generated** which describes the relationship between Lift, SSR, and cylinder position. For the sake of visualization, it is easiest to display surfaces of constant SSR across the range of cylinder geometry. The surface generated at an SSR of zero is displayed below.

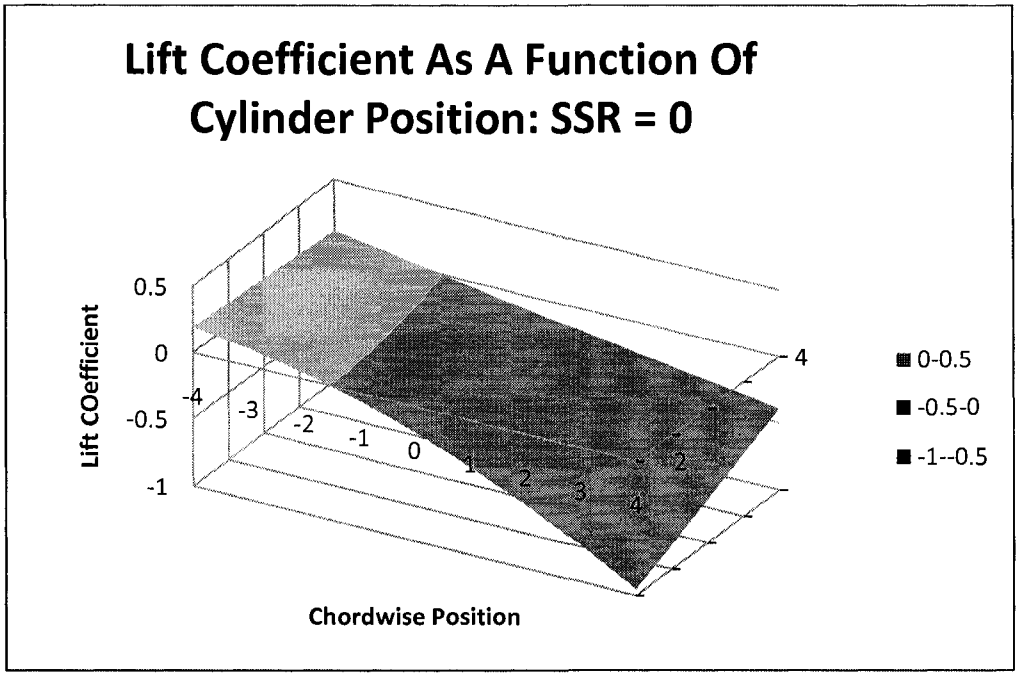

Figure 6-151. Surface generated for SSR = 0.

Results

Following are the surfaces generated for convenient integer values of SSR across the geometric range of cylinder position available. Note that any deviation from a lift coefficient (left vertical axis) of zero is due to the influence of the cylinder and it's rotation. The airfoil alone, at an angle of attack of zero, would produce no lift, positive or negative.

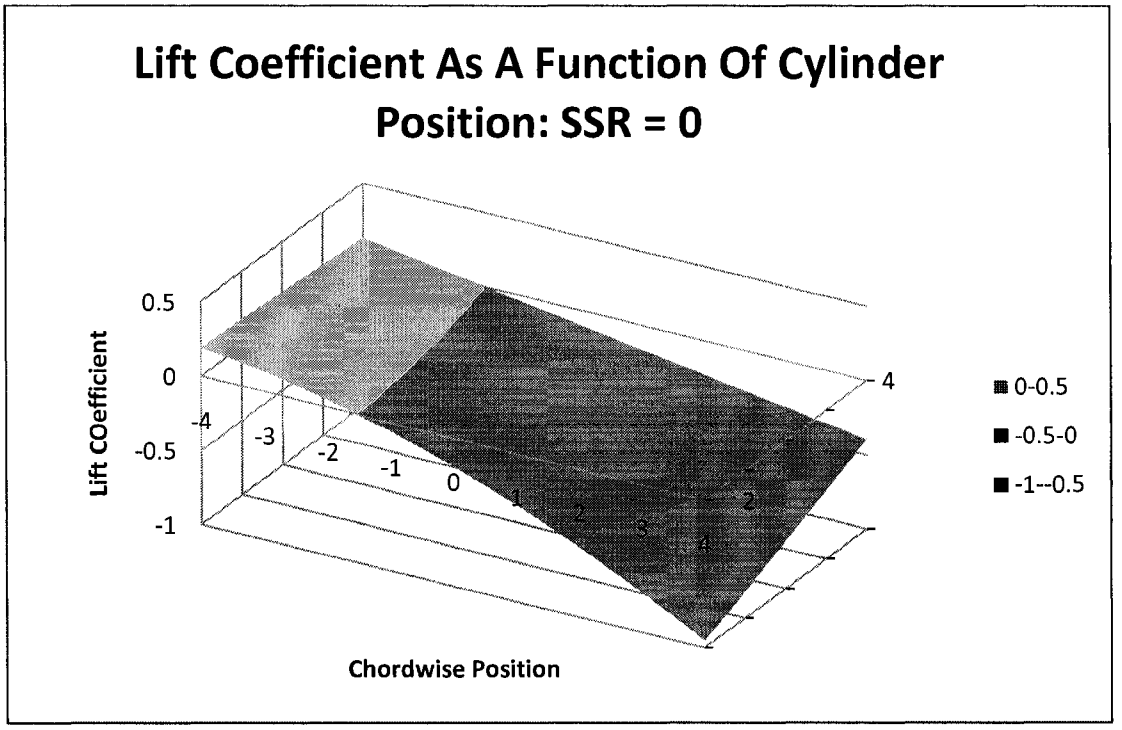

Figure 6-152. Surface generated for SSR = 0.

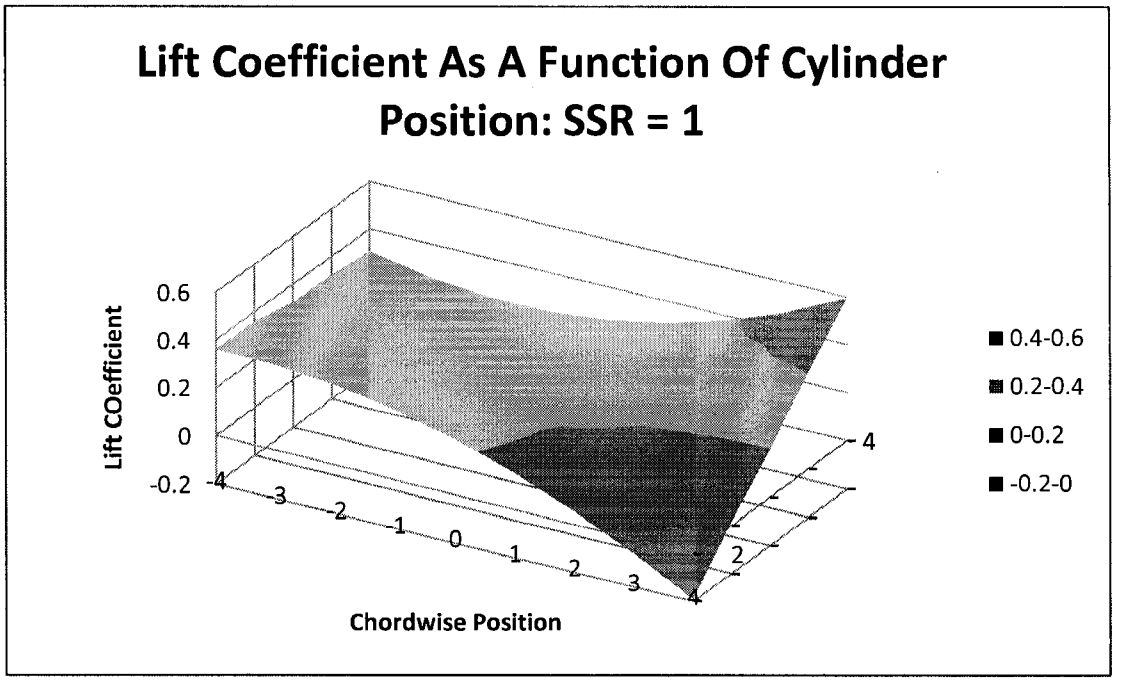

Figure 6-153. Surface generated for SSR = 1.

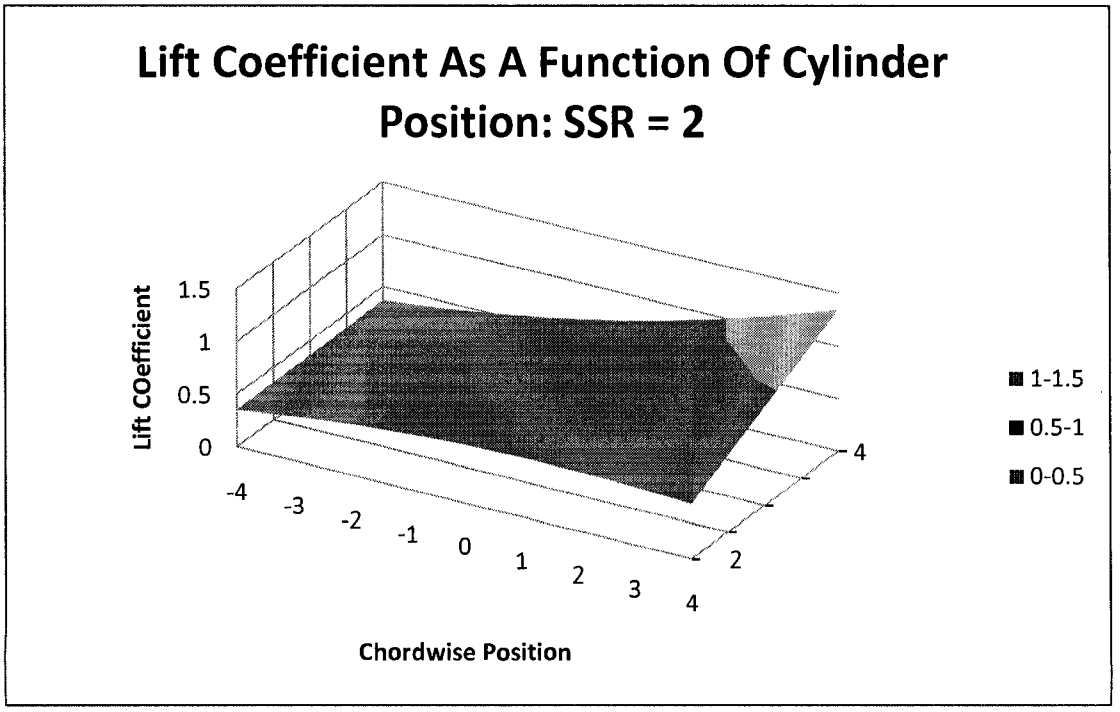

Figure 6-154. Surface generated for SSR = 2.

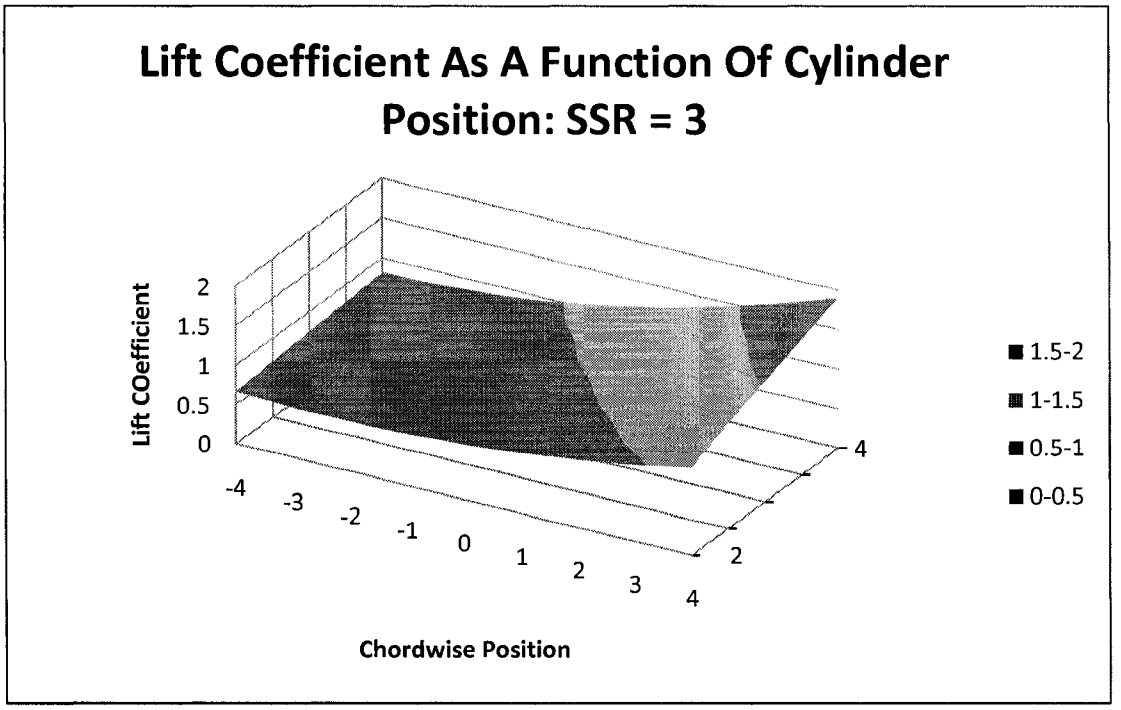

Figure 6-155. Surface generated by SSR = 3.

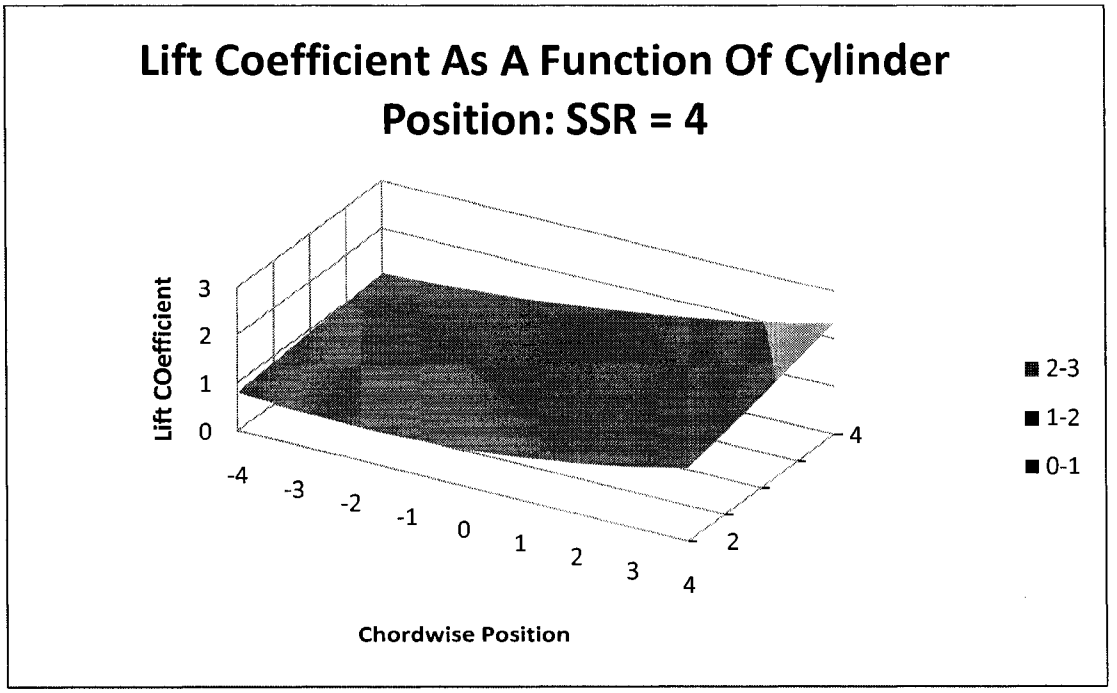

Figure 6-156. Surface generated at SSR = 4.

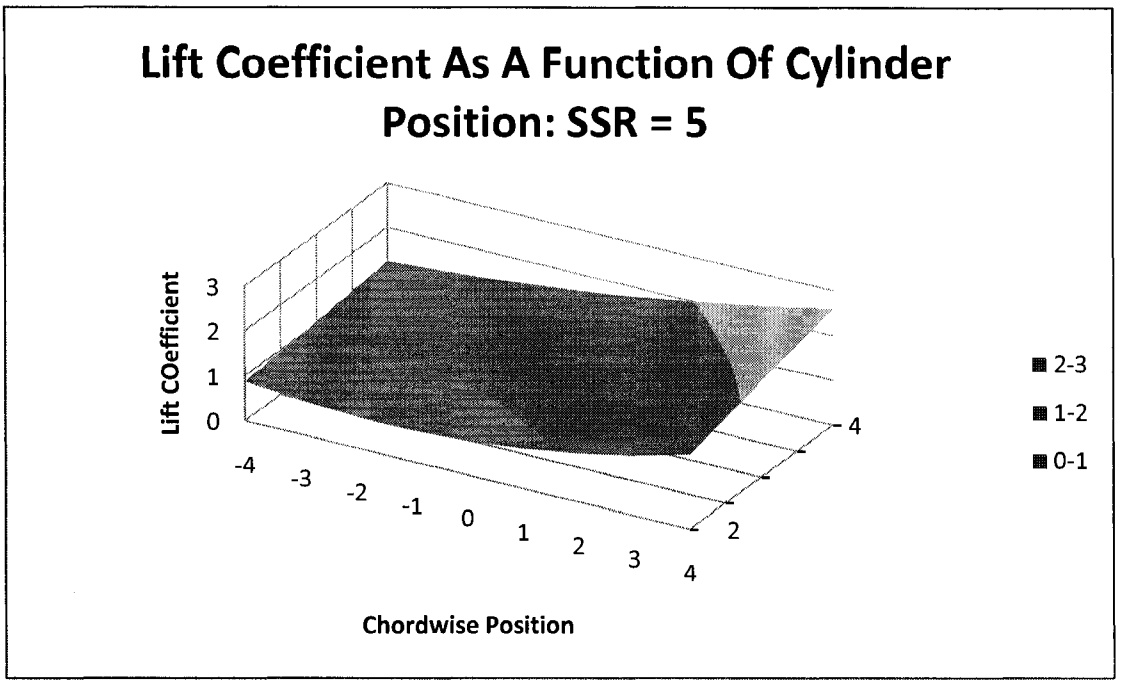

Figure 6-157. Surface generated at SSR = 5.

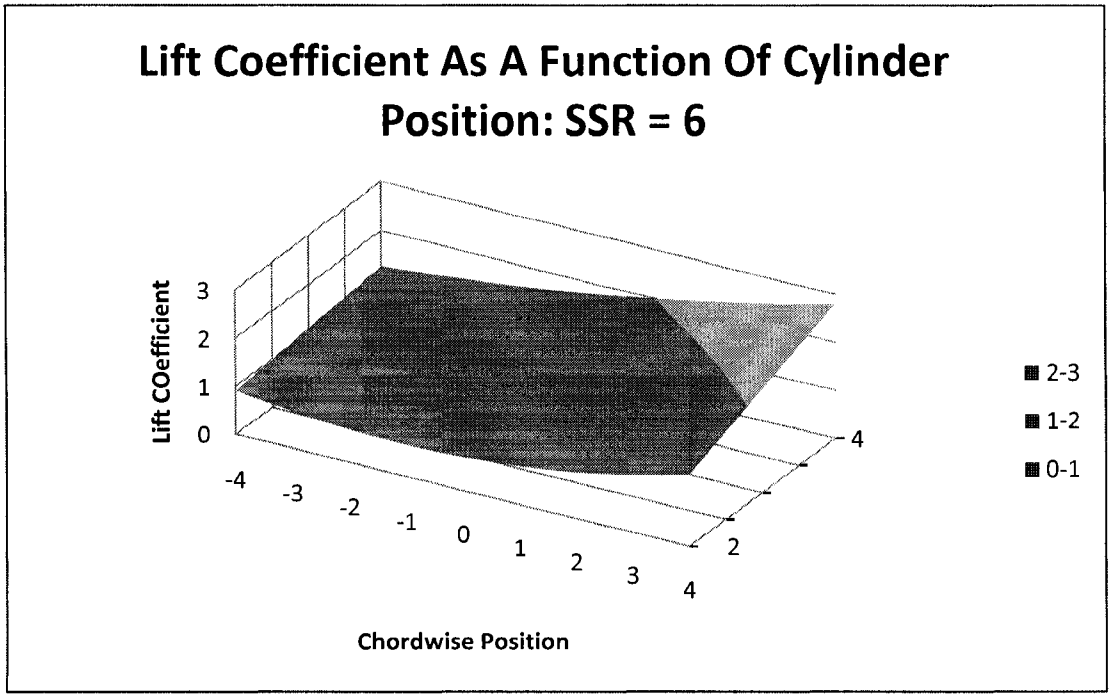

Figure 6-158. Surface generated by SSR = 6.

Conclusion

There are several counterintuitive trends evident in the surfaces above:

- At very low SSR, the cylinder has a beneficial effect if it is placed near the leading edge, and a strong lift-spoiling effect as it is moved toward the trailing edge.
- At moderate to high values of SSR, the cylinder becomes most effective in generating lift near the trailing edge and at larger vertical distances from the plate.

These are both interesting results, and suggest a direction for future experimental investigations. Of particular interest is the rate of increase near the edge of the surface above and at increasing vertical distance from the trailing edge.

There are two obvious and immediate extensions of this work. The first is to incorporate the full 1,500 data point set into the analysis. The second is to also produce surfaces for Drag, and L/D ratio. A more rigorous development and consideration of the polynomial curve net method might also be interesting, particularly if it could be shown to be a defensibly accurate and yet straightforward method for generating multidimensional response surfaces.

Appendix C- Wind Tunnel Data Corrections

Vortex Flap Data Comparison

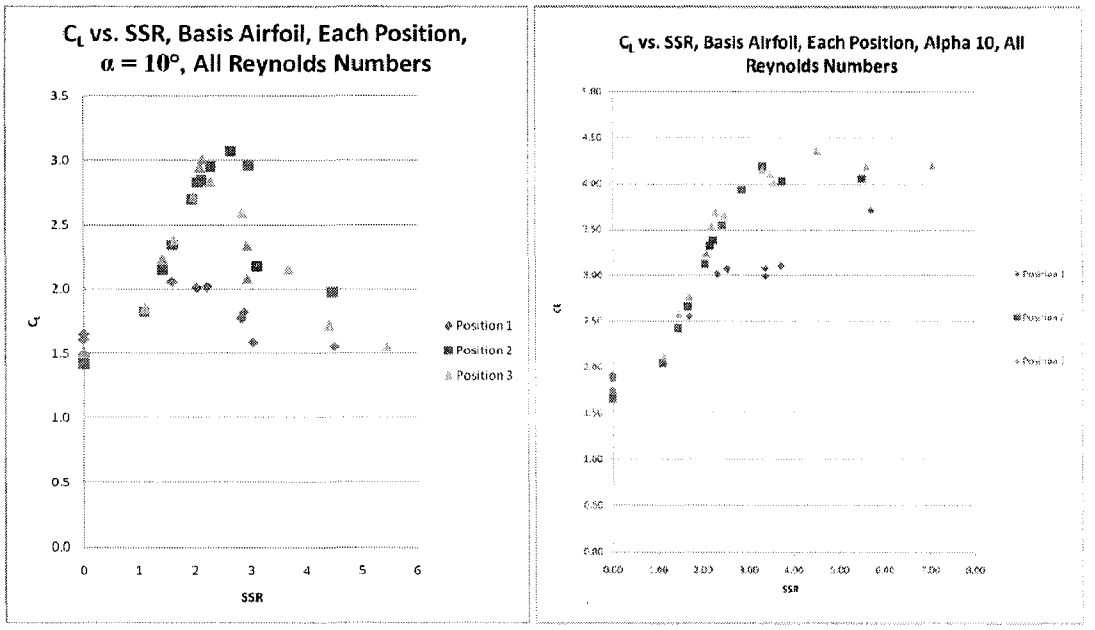

Figure 6-159. Corrected (left) and uncorrected (right) Lift vs. SSR graph.

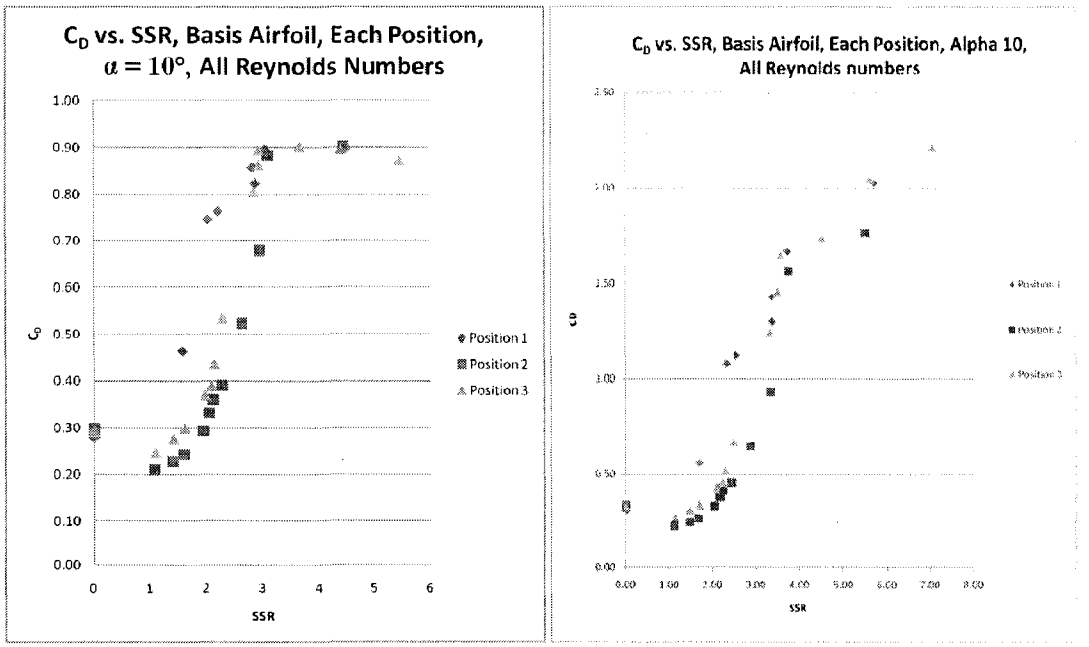

Figure 6-160. Corrected (left) and uncorrected (right) Drag vs. SSR graph.

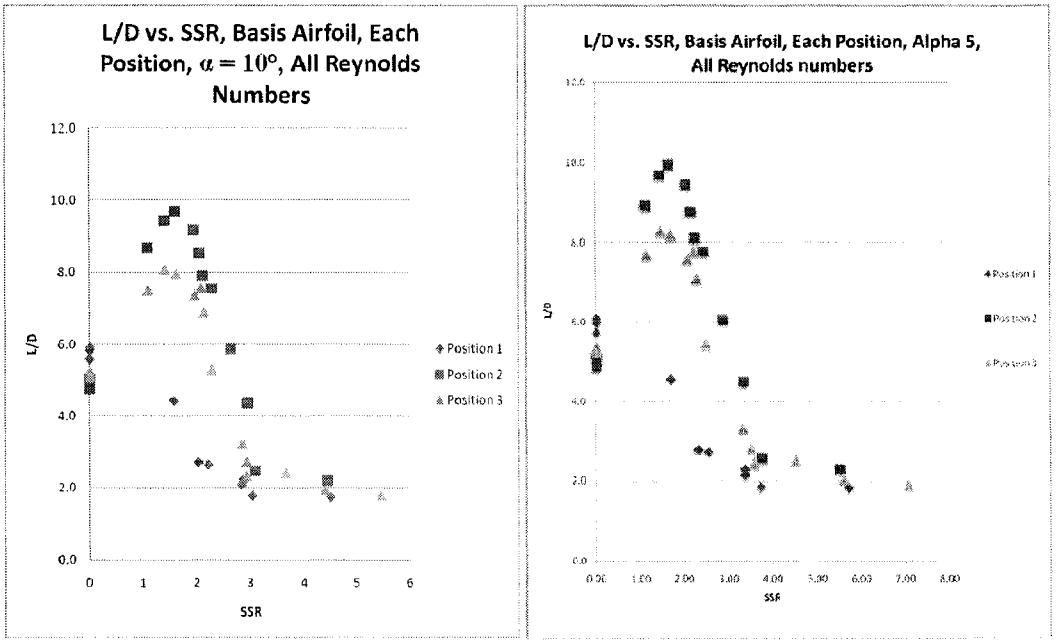

Figure 6-161. Corrected (left) and uncorrected (right) L/D vs. SSR graphs.

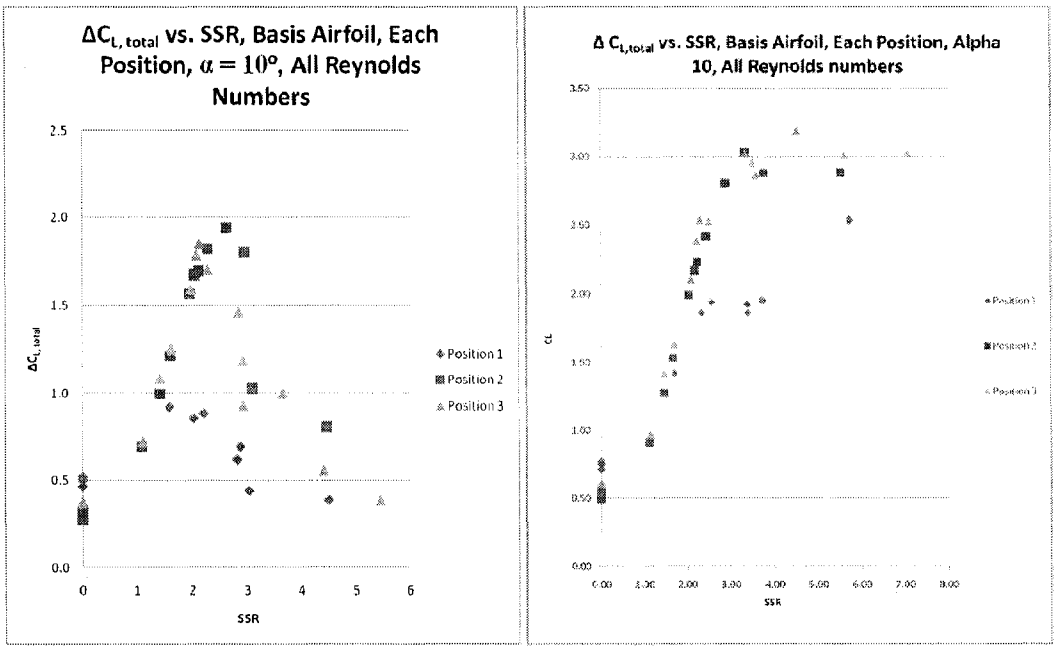

Figure 6-162. Corrected (left) and uncorrected (right) total lift increment graphs.

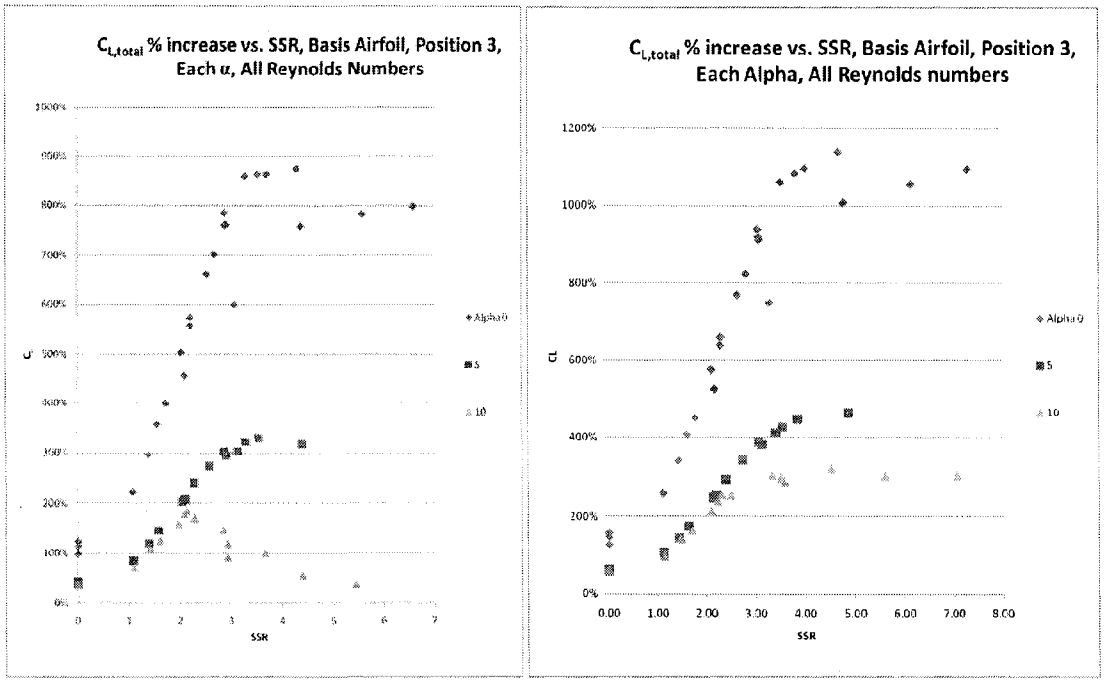

Figure 6-163. Corrected (left) and uncorrected (right) % lift increase vs. SSR graphs.

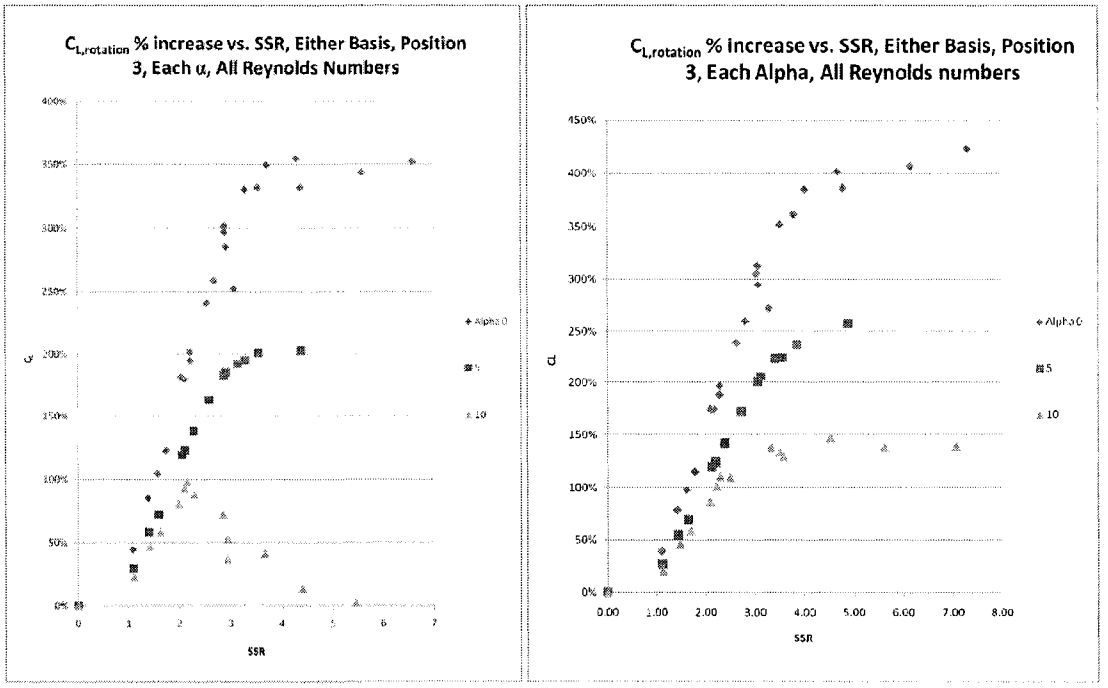

Figure 6-164. Corrected (left) and uncorrected (right) % lift increase vs. SSR graphs.

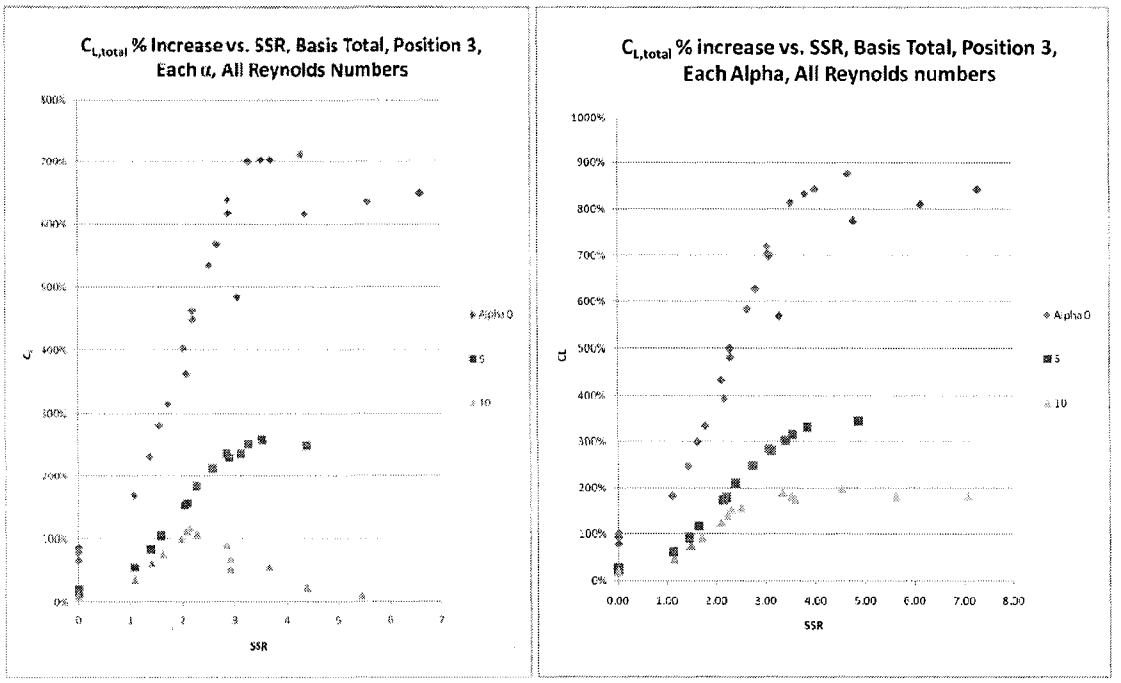

Figure 6-165. Corrected (left) and uncorrected (right) % increase in lift vs. SSR graphs.

Clark Y Airfoil Data Comparison

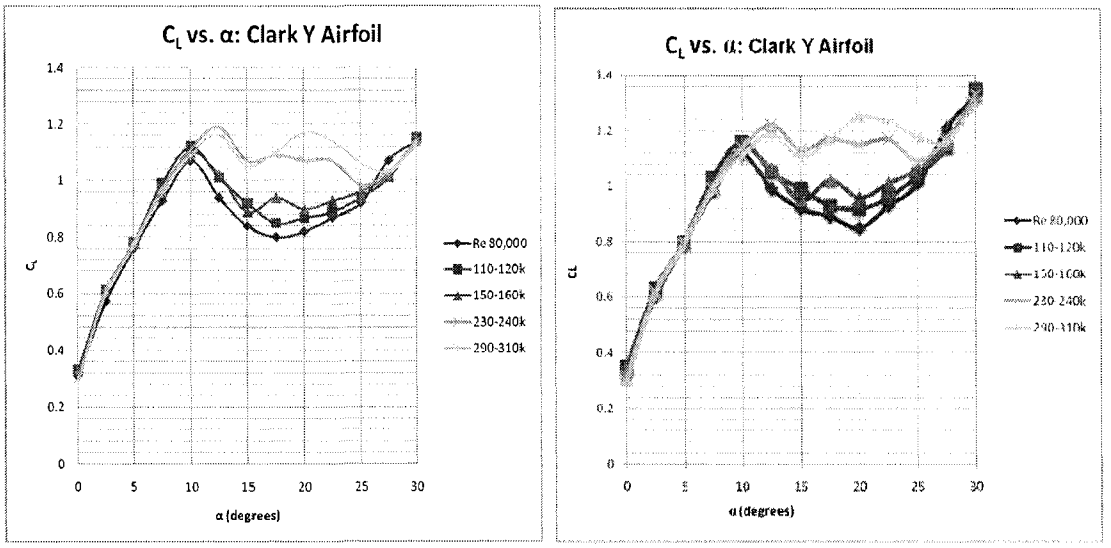

Figure 6-166. Correction (left) and uncorrected (right) lift coefficient vs. angle of attack.

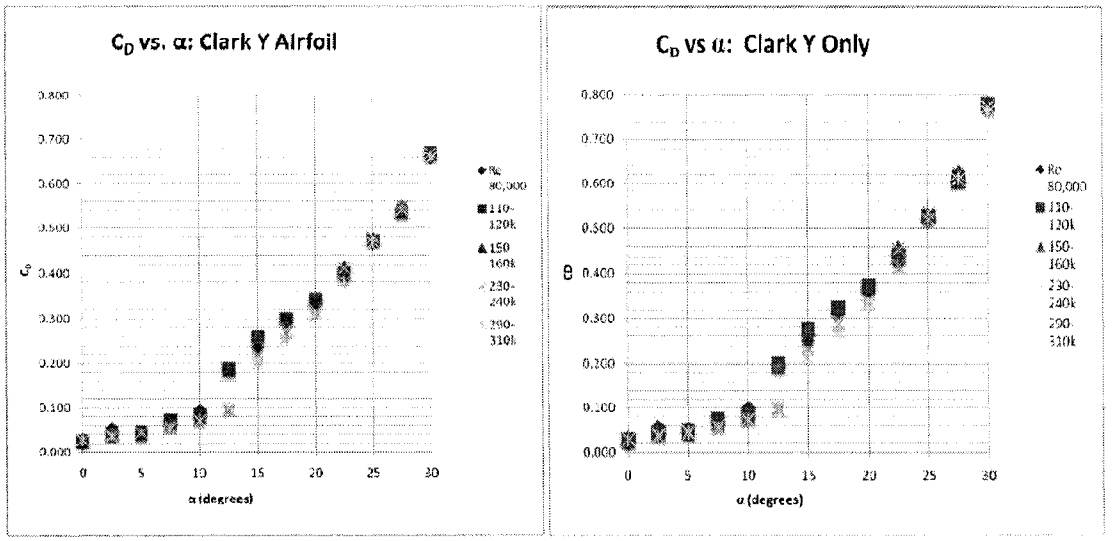

Figure 6-167. Corrected (left) and uncorrected (right) drag coefficients vs. angle of attack.

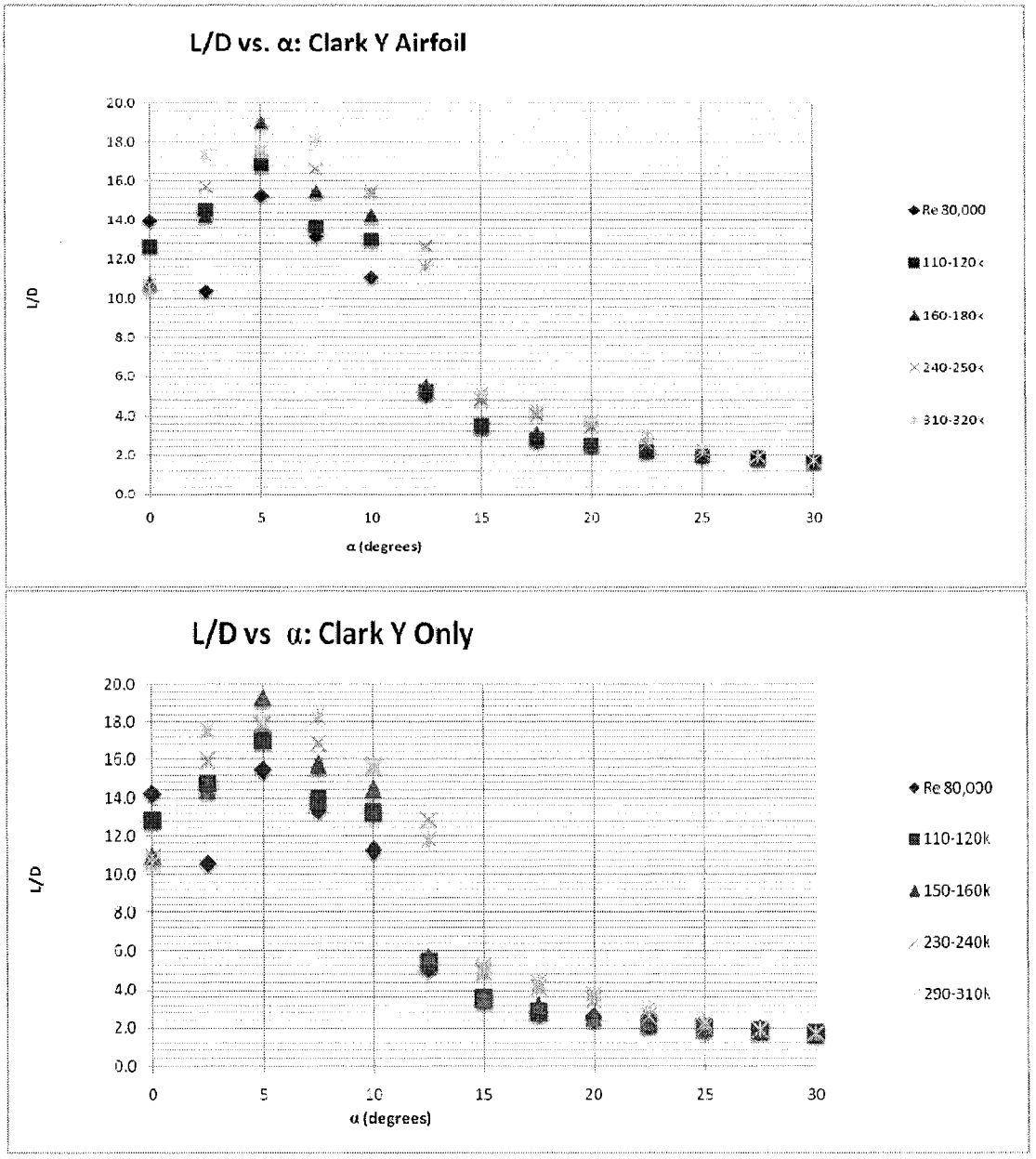

Figure 6-168. Corrected (top) and uncorrected (bottom) L/D vs. angle of attack.

Cylinder-only Data Comparison

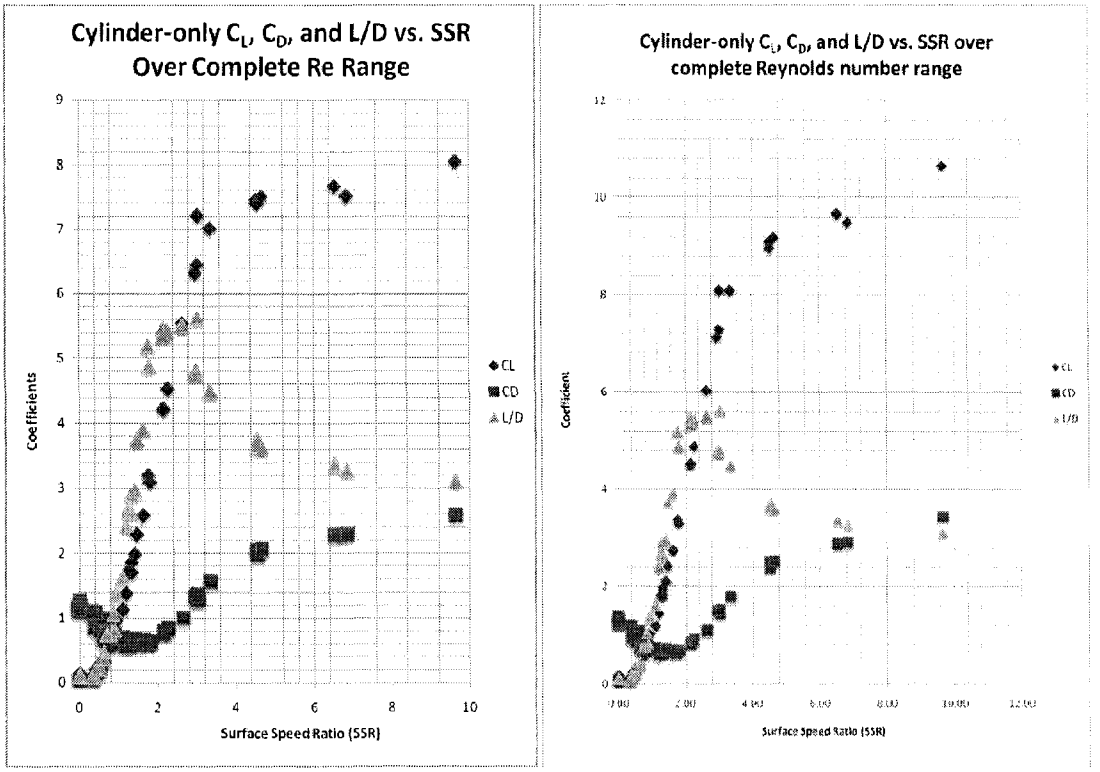

Figure 6-169. Corrected (left) and uncorrected (right) cylinder-only results.

Appendix D- Efficiency of Circulation Generation

The following is a graph of the actual circulation generated by the rotating cylinder used in this wind tunnel investigation as compared to the theoretical circulation generated (Currie 1974). The losses are attributed to counter-vorticity in the boundary layer and flow separation. That the efficiency would be so dependent on SSR and that it was relatively insensitive to Reynolds number was unexpected.

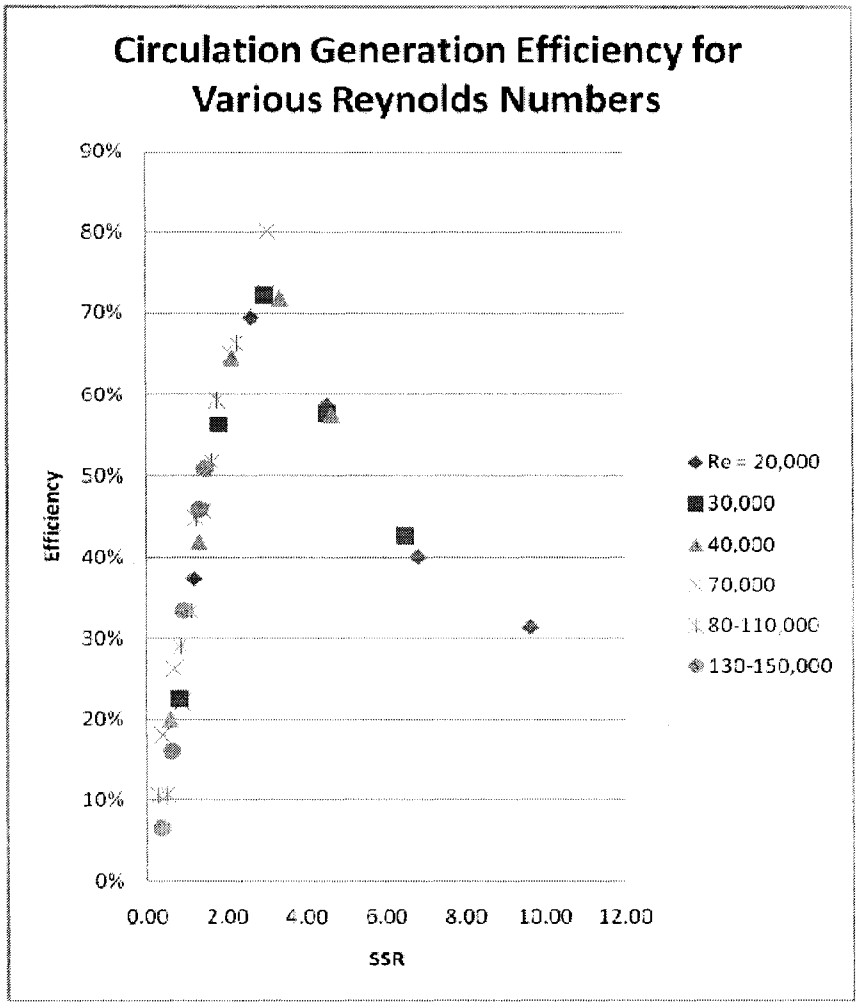

Figure 6-170. Efficiency of rotating cylinder as a generator of circulation, presented here as a function of SSR for various Reynolds numbers.

References

Abbott, I. H. and von Doenhoff, A. E., *Theory of Wing Sections Including a Summary of Airfoil Data,* General Publishing Company, Ltd., Toronto, 1959.

Achenbach, E., "Influence of surface roughness on the cross-flow around a circular cylinder," *Journal of Fluid Mechanics,* Vol. 46, Pt. 2, pp. 321-335, Cambridge University Press, Great Britain, 1971.

Ames, M. B. Jr., "Wind-Tunnel Investigation of Two Airfoils With 25-Percent-Chord Gwinn and Plain Flaps," NACA Technical Note No. 763, 1940.

Anderson, J. D., Jr., *A History of Aerodynamic and Its Impact on Flying Machine,* Cambridge University Press, New York, 1997.

Anderson, J. D., Jr., *Fundamentals of Aerodynamics*, 3rd ed., McGraw-Hill, Boston, 2001.

Apelt, C. J., and West, G. S., "The effects of wake splitter plates on bluff-body flow in the range $10^4 < R < 5 \times 10^4$. Part 2," *Journal of Fluid Mechanics,* Vol. 71 Pt. 1, pp. 145-160, Cambridge University Press, Great Britain, 1975

Apelt, C. J.,West, G. S., and Szewczyk, A. A., "The effects of wake splitter plates on the flow pat a circular cylinder in the range $10^4 < R < 5 \times 10^4$," *Journal of Fluid Mechanics,* Vol. 61 Pt. 1, pp. 187-198, Cambridge University Press, Great Britain, 1973.

Bandyopadhyay, P. R., Castano, J. M., Rice, J. Q., Philips, R. B., Nedderman, W. H., and Macy, W. K., "Low-Speed Maneuvering Hydrodynamics of Fish and Small Underwater Vehicles," *Transactions of the ASME,* Vol. 119, pp. 136 March 1997.

Baird, M. H. I., Wairegi, T. and Loo, H. J., "Velocity and Momentum of Vortex Rings in Relation to Formation Parameters." *The Canadian Journal of Chemical Engineering,* Vol. 55, February, 1977, pp. 19-26.

Barlow, J. B. and Rae, W. H. Jr., and Pope, A., *Low-Speed Wind Tunnel Testing,* 3rd ed., John Wiley & Sons, Inc., New York, 1999.

Bearman, P. W., "On vortex shedding from a circular cylinder in the critical Reynolds number regime," *Journal of Fluid Mechanics,* Vol. 1969, Pt. 3, pp. 577-595, Cambridge University Press, Great Britain, 1969.

Bearman, P. W., and Harvey, J. K., "Control of Circular Cylinder Flow bhe Use of Dimples," *AIAA Journal*, Vol. 31, No. 10, October 1993.

Bickley, W. G., The Influence of Vortices upon the Resistance experienced by Solids moving through a Liquid," *Proceedings of the Royal Society, London Series A.,* Vol. 119A, pp. 146-151, 1928.

Box, G. E. P., and Draper, N. R., *Empirical Model-Building and Response Surfaces,* John Wiley & Sons, Inc., New York, 1987.

Buerge, B. T., "The Design, Fabrication, and Testing of a High-Altitude Payload Return Glider," Master's Thesis, Department of Mechanical Engineering,Washington University in St. Louis, St. Louis, MO, 2005.

Cahill, J., "Summary of Section Data on Trailing-Edge High-Lift Devices," NACA Technical Report No. 938, 1949.

Calderon, A. Alvarez, "Aerodynamic System and Apparatus." US Patent # 3,092,354, 1960.

Chew, Y. T., Cheng, M. and Luo, S. C., "A numerical study of flow past a rotating circular cylinder using a hybrid vortex scheme," *Journal of Fluid Mechanics,* Vol. 299 pp. 35-71, Cambridge University Press, Great Britain, 1995.

Chow, C, and Chen, C, and Huang, M., "Trapping of a Free Vortex by Airfoils with Surface Suctions," *AIAA Journal*, Vol. 24, No. 8, pp. 1217-1218, 1986.

Cook, W. L. and Hickey, D. H., "Correlation of Low Speed Wind Tunnel and Flight Test Data for V/STOL Aircraft," NASA Technical Memorandum NASA-TM-X-62423, 1975.

Cox, J., "The Revolutionary Kasper Wing," *Soaring*, December, 1973.

Crabtree, L. F., "The Rotating Flap as a High-Lift Device," Aeronautical Research Council Current Paper No. 480, 1960.

Critzos, C. C., Heyson, H. H., and Boswinkle, R. W., Jr., "Aerodynamic Characteristics of NACA 0012 Airfoil Section at Angles of Attack from 0° to 180°," National Advisory Committee for Aeronautics Technical Note 3361, 1955.

Currie, I. G., *Fundamental Mechanics of Fluids,* McGraw-Hill, Inc., New York, 1974.

Deckert, W. H., Koenig, D. G. and Weiberg, J. A., "A Summary of Recent Large-Scale Research on High-Lift Devices," NASA SP-116, Conference on V/STOL & STOL Aircraft, pp. 63-79, 1966.

Diaz, F. Gabalda, J., Kawall, J. G., Keffer, J. F, and Giralt, F., "Vortex shedding from a spinning cylinder," *Physics of Fluids,* Vol. 126 No. 12 pp. 3454-3460, December 1983.

Dipankar, A., Sengupta, T. K., and Talla, S. B.,"Suppression of vortex shedding behind a circular cylinder by another control cylinder at low Reynolds numbers," *Journal of Fluid Mechanics,* Vol. 573, pp. 171-190, Cambridge University Press, United Kingdom, 2007.

Dierich, M., Gersten, K., and Schlottmann, F., "Turbulent flow around a rotating cylinder in a quiescent fluid," *Experiments in Fluids*, Vol. 25, 1998, pp. 455-460.

Fage, A. and Warsap, J. H., "The Effects of Turbulence and Surface Roughness on the Drag of a Circular Cylinder," ARC Reports and Memoranda No. 1283, 1930.

Finnaish, F. and Witherspoon, S., "Aerodynamic performance of an airfoil with step-induced vortex for lift augmentation," *Journal of Aerospace Engineering,* Vol. 11, No. 1, pp. 9-16, January 1998.

Filippone, A., *Flight Performance of Fixed and Rotary Wing Aircraft*, American Institute of Aeronautics and Astronautics, Inc., and Butterworth-Heinemann, an imprint of Elsevier, Great Britain, 2006.

Hoerner, S. F., *Fluid-Dynamic Drag - Practical Information on Aerodynamic Drag and Hydrodynamic Resistance,* published by the author, New York, 1992.

Hoerner, S. F. and Borst, H. V., *Fluid-Dynamic Lift*, 2nd ed., Mrs. Lisolette A. Hoerner, Bakersfield, CA, 1985.

Iversen, J. D., "Autorotating flat-plate wings: the effect of the moment of inertia, geometry and Reynolds number," *Journal of Fluid Mechanic,* Vol. 92, Part 2, pp. 327-348, Cambridge University Press, Great Britain, 1979.

Jacobs, E., "Airfoil Section Characteristics as Affected by Variations of the Reynolds Number," National Advisory Committee on Aeronautics Technical Report No. 586, 1939.

Jones, G. W. Jr., Cincotta, J. J., and Walker, R. W., "Aerodynamic Forces on a Stationary and Oscillating Circular Cylinder ant High Reynolds Number," NASA Technical Report No. R-300, 1969.

Jones, R. T., *Wing Theory*, Princeton University Press, Princeton, New Jersey, 1990.

Kohlman, D. L., *Introduction to V/STOL Airplanes*, Iowa State University Press, Ames, IA, 1981.

Kurpa, E. W., "A Wind Tunnel Investigation of the Kasper Vortex Concept," American Institute for Astronautics and Aerodynamics, Paper No. 77-310, 1977.

Li, F., and Aubry, N., "Feedback control of a flow past a cylinder bia transverse motion," *Physics of Fluids*, Vol. 15 No. 8, pp. 2163-2176, August 2003.

Liebeck, R. H., "Design of Subsonic Airfoils for High Lift," *Journal of Aircraft,* Vol. 15, No. 9, pp. 547-561, Sept. 1978.

Lim, H-C., and Lee, S-J., "Flow Control of Circular Cylinders with Longitudinal Grooved Surfaces," *AIAA Journal,* Vol. 40, No. 10, pp. 2027-2036, October 2002.

Loftin, L. K., Jr., "Quest for Performance: The Evolution of Modern Aircraft," NASA SP-468, 1985.

Lowry, J. G., "Wind-Tunnel Investigation of an NACA 23012 Airfoil with Several Arrangements of Slotted Flaps with Extended Lips," National Advisory Committee for Aeronautics, Technical Note No. 808, 1941.

Lugt, H. J., "Autorotation of an Elliptic Cylinder about an Axis Perpendicular to the Flow," Journal of Fluid Mechanics, Great Britain, 1979.

Lugt, H. J., and Ohring, S., "Rotating elliptic cylinders in a viscous fluid at rest or in a parallel stream," *Journal of Fluid Mechanics*, Vol. 79, part 1, pp. 127-156, Great Britain, 1977.

Maskell, E. C., "A Theory of the Blockage Effects on Bluff Bodies and Stalled Wings in a Closed Wind Tunnel," Aeronautical Research Council, Reports and Memoranda No. 3400, Great Britain, 1963.

Mittal, S. and Kumar, B., "Flow past a rotating cylinder," *Journal of Fluid Mechanics,* Vol. 476, pp. 303-334, Cambridge University Press, United Kingdom, 2003.

Modi, V. J., "Moving Surface Boundary-Layer Control: A Review," *Journal of Fluids and Structures*, Vol. 11, pp. 627-663, 1997.

Modi, V. J. and F. Mokhtarian, "Effect of Moving Surfaces on the Airfoil Boundary-Layer Control," *Journal of Aircraft*, Vol. 27, No. 1, January 1990.

Munson, B. R., Young, D. F., and Okiishi, T. H., *Fundamentals of Fluid Mechanics*, Third Edition Update, John Wiley & Sons, New York, 1998.

Munk, M., " The Aerodynamic Characteristics of Seven Frequently Used Wing Sections at Full Reynolds Number," National Advisory Committee for Aeronautics, Technical Report No. 233, 1927.

Omar, E., Zierten, T., Hahn, M., Szpiro, E., and Mahal, A., "Two-Dimensional Wind-Tunnel Tests of a NASA Supercritical Airfoil With Various High-Lift Systems," NASA Contractor Report NASA CR 2215, 1973.

Ou, Y. and Burns, J., "Optimal Control of Lift/Drag Ratio on a Rotating Cylinder," NASA Contractor Report 187586, 1991.

Oualli, H., Hanchi, S., Bouabdallah, A., and Askovic, R., "Experimental investigation of the flow around a radially vibrating circular cylinder," *Experiments in Fluids,* Vol. 27, pp. 789-801, 2004.

Parvin, Stephen, "MQ-8B Fire Scout," United States Navy Unmanned Air System Programs PMA-263, 2007.

Platt, R. C, "Aerodynamic Characteristics of a Wing with Fowler Flaps Including Flap Loads, Downwash, and Calculated Effect on Take-Off," NACA Technical Report No. 534, 1935.

Platt, R. C., "Aerodynamic Characteristics of Wings with Cambered External Airfoil Flaps, including Lateral Control with a Full Span Flap," NACA Technical Report No. 541, 1935.

Prandtl, L., "Application of the 'Magnus Effect' to the Wind Propulsion of Ships," NACA Technical Memorandum No. 367, 1926.

Raymer, D. P., *Aircraft Design: A Conceptual Approach*, 3rd ed., American Institute of Astronautics and Aeronautics, Inc., Reston, VA, 1999.

Reid, E. G., "Tests of Rotating Cylinders," National Advisory Committee for Aeronautics, Technical Note No. 209, 1924.

Roshko, A., "Experiments on the flow past a circular cylinder at very high Reynolds number," *Journal of Fluid Mechanics,* Vol. 10 pp 345-356, Cambridge University Press, Great Britain, 1961.

Roskam, J., *Airplane Design Part I: Preliminary Sizing of Airplanes,* Design, Analysis, and Research Corporation, Lawrence, KS, 2005.

Roskam, J., *Airplane Design Part II: Preliminary Configuration Design and Integration of the Propulsion System,* Design, Analysis, and Research Corporation, Lawrence, KS, 2004.

Roskam, J., *Airplane Design Part VI: Preliminary Calculation of Aerodynamic, Thrust and Power Characteristics,* Design, Analysis, and Research Corporation, Lawrence, KS, 2004.

Roskam, J., *Airplane Design Part VII: Determination of Stability, Control and Performance Characteristics: FAR and Military Requirements,* Design, Analysis, and Research Corporation, Lawrence, KS, 2006.

Rossow, V. J., "Lift Enhancement by an Externally Trapped Vortex," *Journal of Aircraft,* Vol. 15, No. 9, pp. 618-625, September 1978.

Rowe, F. J., *The Helio Courier Ultra C/STOL Aircraft, An Illustrated Developmental History*, McFarland & Company, Inc., Jefferson, North Carolina, 2006.

Saffman, P. G. and Sheffield, J. S., "Flow over a Wing with an Attached Free Vortex," *Studies in Applied Mathematics*, Vol. 57, pp. 107-117, 1977.

Saffman, P. G. and Tanveer, S., "Vortex Induced Lift on Two Dimensional Low Speed Wings," *Studies in Applied Mathematics*, pp. 65-78, 1984.

Schuldenfreid, M., "Wind-Tunnel Investigation of an NACA 23012 Airfoil with a Handley Page Slat and Two Flap Arrangements," National Advisory Committee for Aeronautics Wartime Report L-261, 1942.

Selig, M. S., and Donovan, J. F, and Fraser, D. B., *Airfoils at Low Speeds*, Soartech 8, H. A. Stokely, publisher, Virginia Beach, VA, 1989.

Silverstein, A., "Scale Effect On Clark Y Airfoil Characteristics From NACA Full-Scale Wind-Tunnel Tests," NACA Technical Report No. 502, 1935.

Skews, B. W., "Autorotation of Many-Sided Bodies in an Airstream," *Nature,* Vol. 352, 8 August 1991.

Simons, M., *Model Aircraft Aerodynamics*, 4th ed., Special Interest Model Books, Ltd., Poole, Dorset, England, 2002.

Smith, A. M. O., "Aerodynamics of High-Lift Airfoil Systems," *AGARD CP-102,* NATO Advisory Group on Aerospace Research and Development, 1972.

Smith, E. H., "Autorotating wings: an experimental investigation," *Journal of Fluid Mechanics,* Vol. 50, Part 3, pp. 513-534, Cambridge University Press, Great Britain, 1971.

Smith, H. C., *The Illustrated Guide to Aerodynamics,* 2nd ed., TAB Books, New York, 1992.

Sunderland, L. D., "What Happened to the Kasper Wing?," *Sport Aviation*, pp. 30-35, January 1976.

Taylor, J. W. R., *Jane's All the World's Aircraft, 1979-80*, Franklin Watts, Inc., New York, 1979.

Taylor, J. W. R., *Jane's All the World's Aircraft, 1961-62*, Sampson, Low, Marston & Co., London, 1961.

Theodorsen, T., and Regier, A., "Experiments on Drag of Revolving Disks, Cylinder, and Streamline Rods at High Speeds," NACA Technical Report No. 793, 1945.

Thom, A., "Blockage Corrections in a Closed High-speed Tunnel," Aeronautical Research Council, Reports and Memoranda No. 2003, 1943.

Tokumaru, P. T., and Dimotakis, P. E., "Rotary oscillation control of a cylinder wake," *Journal of Fluid Mechanics,* Vol. 224, pp 77-90, Cambridge University Press, Great Britain, 1991.

Tokumaru, P. T. and Dimotakis, P. E., "The lift of a cylinder executing rotary motions in a uniform flow," *Journal of Fluid Mechanics,* vol. 255, pp. 1-10, Cambridge University Press, Great Britain, 1993.

US Air Force, "Flight Manual USAF & Army Series U-10A U-10B U-10C Aircraft," WWW.FLIGHT-MANUALS-ON-CD.COM LTD, New Zealand, 2001.

US Navy, "RQ-8A and MQ-8B Fire Scout Unmanned Air Vehicle (UAV)," United States Navy Fact File, URL: http://www.navy.mil/navydata/fact_display.asp?cid=1100&tid=2150&ct=1 [cited 4 April 2008].

Walton, D. "A Brief Wind Tunnel Investigation of the Kasper Vortex Concept," *Soaring*, Vol. 38, pp. 26-27, November 1974.

Weiberg, J. A., "Takeoff and Landing Performance and Noise Measurements of a Deflected Slipstream STOL Airplane with Interconnected Propellers and Rotating Cylinder Flaps," NASA Technical Memorandum NASA TM-X-62,320, 1973.

Weick, Fred. The Aerodynamic Characteristics of a Model Wing Having a Split Flap Deflected Downward and Moved to the Rear. NACA Technical Note No. 422, 1932.

Wenzinger, C. J. and Harris, T. A., "Preliminary Wind-Tunnel Investigation of an NACA 23012 Airfoil with Various Arrangements of Venetian-Blind Flaps," , NACA Technical Report No. 689, 1940.

Wood, R. M. and Bauer, S. X. S, "Advanced Aerodynamic Control Effectors," NASA TM 1999-01-5619, 1999.

Woodward, D. S and Lean, D. E., "Where is High-Lift Today? – A Review of past UK Research Programmes," *AGARD-CP-515*, Specialized Printing Svcs. Ltd., Essex, Great Britain, 1993.

Zdravkovich, M. M., *Flow Around Circular Cylinders Vol. 1: Fundamentals*, Oxford University Press, New York, 1997.

Zdravkovich, M. M., *Flow Around Circular Cylinders Vol. 2: Applications*, Oxford University Press, New York, 2003.

Zdravkovich, M. M., "Review and Classification of Various Aerodynamic and Hydrodynamic Means for Suppressing Vortex Shedding," *Journal of Wind Engineering and Industrial Aerodynamics,* Vo. 7, pp. 145-189, 1981.

Ziada, S. Jebodhsingh, D., Weaver, D. S., Eisinger, F. L., "The effect of fins on vortex shedding from a cylinder in cross flow," *Journal of Fluids and Structures,* Vol. 21, pp 689-705, 2005.

Zhang, H. J., Huang, L., and Zhou, Y., "Aerodynamic loading on a cylinder behind an airfoil," *Experiments in Fluids*, Vol. 38, pp. 588-593, 2005.